NASA CONTRACTOR REPORT

NASA CR-2018

NASA CR-2018

THEORY AND DESIGN OF VARIABLE CONDUCTANCE HEAT PIPES

by B. D. Marcus

Prepared by
TRW SYSTEMS GROUP
Redondo Beach, Calif. 90278
for Ames Research Center

NATIONAL AERONAUTICS AND SPACE ADMINISTRATION • WASHINGTON, D. C. • APRIL 1972

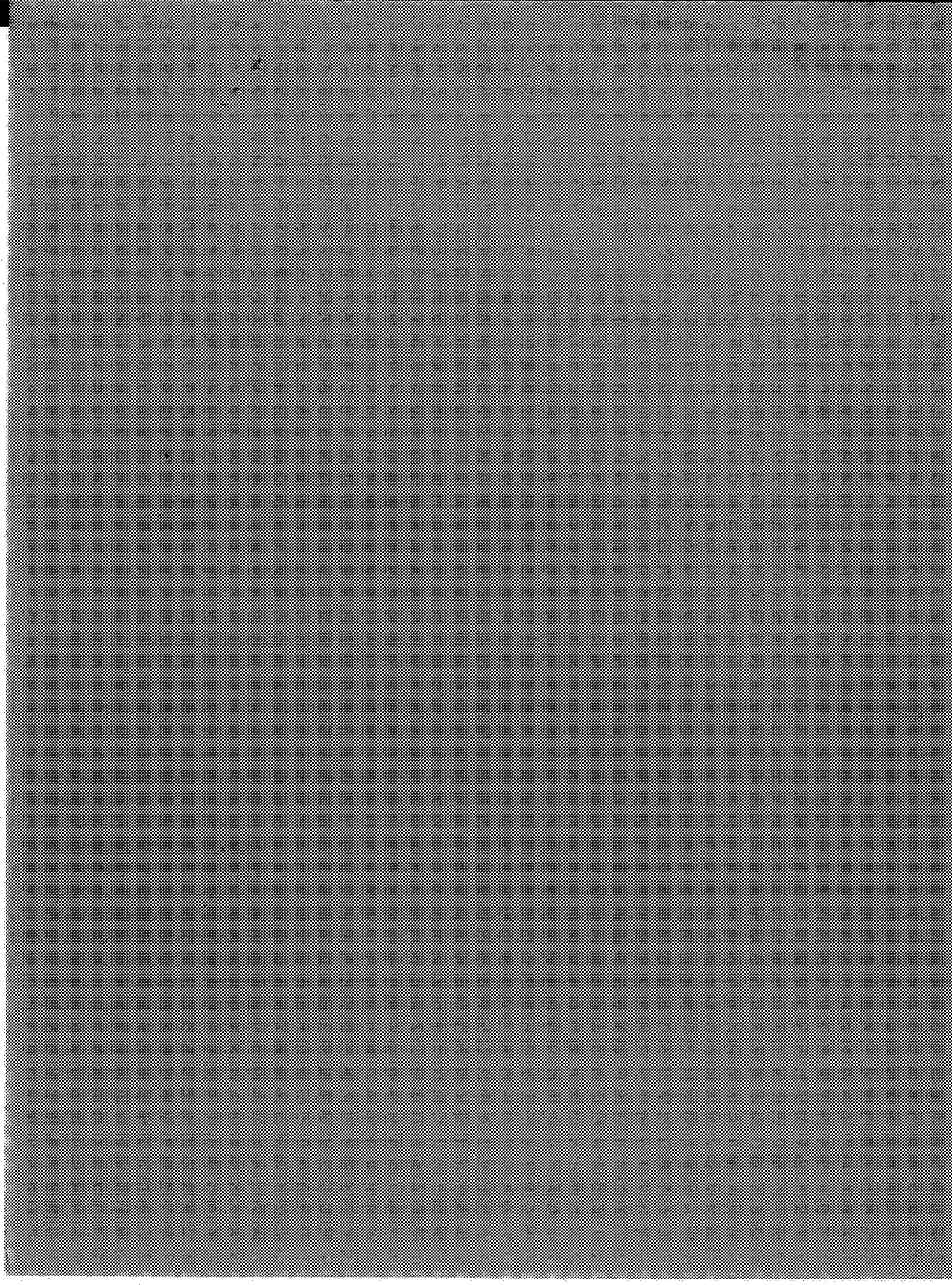

1. Report No.	2. Government Accession No.	3. Recipient's Catalog No.
NASA CR-2018		

4. Title and Subtitle	5. Report Date
"Theory and Design of Variable Conductance Heat Pipes"	April 1972
	6. Performing Organization Code

7. Author(s)	8. Performing Organization Report No.
B.D. Marcus	
	10. Work Unit No.

9. Performing Organization Name and Address	11. Contract or Grant No.
TRW Systems Group One Space Park Redondo Beach, Ca.	NAS 2-5503
	13. Type of Report and Period Covered

12. Sponsoring Agency Name and Address	
National Aeronautics & Space Administration Washington, D.C.	Contractor Report
	14. Sponsoring Agency Code

15. Supplementary Notes

16. Abstract

The report represents a comprehensive review and analysis of all aspects of heat pipe technology pertinent to the design of self-controlled, variable conductance devices for spacecraft thermal control. Subjects considered include hydrostatics, hydrodynamics, heat transfer into and out of the pipe, fluid selection, materials compatibility and variable conductance control techniques.

The report includes a selected bibliography of pertinent literature, analytical formulations of various models and theories describing variable conductance heat pipe behavior, and the results of numerous experiments on the steady state and transient performance of gas controlled variable conductance heat pipes. Also included is a discussion of VCHP design techniques.

17. Key Words (Suggested by Author(s))	18. Distribution Statement
Heat pipes; variable conductance heat pipes; capillary pumping, heat transfer, temperature control, spacecraft thermal control, change-of-Phase heat transfer	UNCLASSIFIED-UNLIMITED

19. Security Classif. (of this report)	20. Security Classif. (of this page)	21. No. of Pages	22. Price*
UNCLASSIFIED	UNCLASSIFIED	238	3.00

*For sale by the National Technical Information Service, Springfield, Virginia 22151

FOREWORD

The work described in this report was performed under NASA contract NAS 2-5503, "Design, Fabrication and Testing of a Variable Conductance Constant Temperature Heat Pipe". The contract is administered by Ames Research Center, Moffett Field, California, with Mr. J. P. Kirkpatrick serving as Technical Monitor.

The program is being conducted by TRW Systems Group of TRW, Inc., Redondo Beach, California, with Dr. Bruce D. Marcus serving as Program Manager and Principal Investigator. Major contributors to the effort include Mr. G. L. Fleischman and Professor D. K. Edwards.

TABLE OF CONTENTS

Table of Contents (Cont'd)

Table of Contents (Cont'd)

FIGURES

TABLES

1.0 INTRODUCTION

Heat pipe technology has advanced rapidly in the six years since Grover, et al, at Los Alamos, published their first paper [G1]. From the simple tube lined with a screen mesh, heat pipes are now being fabricated in many geometries with complex, multi-component capillary wick structures tailored to maximize their performance. Much work has been done to advance heat pipe hydrodynamics, heat transfer, materials compatibility and fabrication technology. However, one of the most important areas of endeavor has been in heat pipe control.

The heat pipe described by Grover is a completely passive device whose operating temperature automatically adjusts to the heat source and sink conditions so as to maintain conservation of energy. However, it was not long before investigators recognized the many potential applications of heat pipes which could be controlled, either actively or passively, to regulate temperatures. Numerous schemes have since been devised to accomplish this control, and many of these have been implemented. However, as is often the case in a rapidly advancing technology, the ability to accurately design and predict the performance of these devices had lagged the ability to build and operate them.

This program represents an effort to improve this situation through a comprehensive review and analysis of all aspects of heat pipe technology pertinent to the design of self-controlled, variable conductance, constant temperature devices for spacecraft thermal control. Subjects considered include hydrostatics, hydrodynamics, heat transfer into and out of the pipe, fluid selection, and materials compatibility, in addition to numerous variable conductance control techniques.

Most attention is given to passive gas-controlled heat pipes, be they cold or hot, wicked or non-wicked reservoir designs. However, for the sake of completeness, the report also deals briefly with active heated reservoir and feedback controlled systems since these will likely play an important role in spacecraft thermal control.

In addition, the subject matter includes discussions on other control schemes including (1) liquid flow control, (2) vapor flow control, and (3) the use of excess working fluid (rather than non-condensible gas) to effect condenser area variations.

This report presents the results of efforts to date in each of the areas mentioned. Since this is a continuing program, some of the material presented herein constitutes the current status of work in progress. In other cases, the work has been completed and the material presented serves to document these accomplishments.

In addition to the fundamental studies described, a major endeavor on this program was the design, fabrication and testing of prototype, qualification and flight units for the Ames Heat Pipe Experiment on board the OAO-C spacecraft. This experiment, which involves a functional internal reservoir gas controlled heat pipe, is currently scheduled for launch in May 1972. Although several fundamental studies, ancillary to the experiment, are presented in this report, the detailed documentation of this phase of the program is not. Instead, it constitutes a separate report; the "Ames Heat Pipe Experiment Description Document", to be issued shortly, and is the subject of reference [V6].

2.0 LITERATURE REVIEW

Judging by the remarkable growth rate of the literature, the heat pipe field has indeed attracted the interest of many workers in academia, industry and government. Whereas, in 1965, the pertinent literature numbered but a few documents, TRW's current heat pipe bibliography contains well over three hundred references.

As one task on this program, all of the identified and available literature was reviewed to select that information pertinent to the design of variable conductance heat pipes for spacecraft thermal control. The selective bibliography thus obtained is presented in Section 5.

Where possible, references have been cataloged as to their principal subject. These include:

- Hydrodynamics & Hydrostatics
- Heat Transfer
- Materials Compatibility
- Variable Conductance Techniques

Where references are too broad for inclusion in one of these categories, they have been listed under the "General" heading.

The specific literature of greatest importance to this program is identified throughout the body of this report where each of the pertinent subjects are discussed.

3.0 CONVENTIONAL HEAT PIPE THEORY

The theory of heat pipes has been developing for many years and is well documented in the literature (see Section 5). Consequently, it will not be developed again in its entirety within this report. Rather, a review of current theory is presented which provides a basis for the hydrodynamic and thermal design of variable conductance heat pipes. In those cases where new contributions to the theory have been made as a result of efforts on this program, detailed developments are presented.

3.1 Hydrodynamics

Because the heat pipe involves the circulation of a working fluid, certain pressure drops arise. In general, there will be viscous losses due to liquid flow in the wick or capillary structure, and viscous and inertial losses due to vapor flow in the core. In addition, there may be body forces which either aid or hinder circulation (e.g., acceleration fields due to gravity, rotation, rocket thrust, etc.). For steady-state operation of a heat pipe, a pressure head equal to the sum of these losses must be supplied by capillarity in the wick. This yields the following steady-state pressure balance, which must be satisfied between all points along the heat pipe.

$$\Delta P_c = \Delta P_\ell + \Delta P_v \pm \Delta P_b \tag{3-1}$$

$$\begin{bmatrix}\text{net}\\ \text{capillary}\\ \text{head}\end{bmatrix} = \begin{bmatrix}\text{liquid}\\ \text{pressure}\\ \text{drop}\end{bmatrix} + \begin{bmatrix}\text{vapor}\\ \text{pressure}\\ \text{drop}\end{bmatrix} \pm \begin{bmatrix}\text{body force}\\ \text{head}\\ \text{(if any)}\end{bmatrix}$$

3.1.1 Capillary Head

Of the terms in Eq. (3-1), the liquid and vapor pressure drops are functions of the circulation rate and increase with the heat transfer load on the device. On the other hand, the body force term is usually independent of load. Thus, to satisfy Eq. (3-1), the capillary head

must also increase with load in such a way as to match the losses incurred.

The capillary head in a saturated heat pipe wick arises as a dynamic phenomenon. It is due to the existence of a pressure difference across a curved liquid-vapor interface which is given by:

$$\Delta P_i = \sigma \left(\frac{1}{R_1} + \frac{1}{R_2} \right) \tag{3-2}$$

where:

ΔP_i - interfacial pressure difference

σ - surface tension

R_1, R_2 - two orthogonal radii of curvature of the interface

This pressure difference, which for concave menisci results in a depression of the liquid pressure with respect to the vapor, exists all along the heat pipe wick. In order to obtain a net capillary head, it is necessary for it to be greater at the evaporator than at the condenser. In a heat pipe under load, this is exactly what occurs due to changes in the interface curvatures. Vaporization of the liquid in the evaporator causes the menisci to recede into the wick resulting in a decrease in radii of curvature while condensation in the condenser has the opposite effect. Therefore, the capillary pressure is not constant. Capillary pumping is a passive phenomenon which automatically adjusts to meet the flow requirements--within limits.

The extremes of the interfacial pressure difference (Eq. 3-2) which can be generated along the wick depend on the wick pore geometry and the wetting angle between the liquid and wick material. The appropriate values for these extremes has been the subject of a good deal of heat pipe literature [H1, H2, H3, G2].

Class A Wicks:

In many wick structures, the maximum value of the interfacial pressure difference corresponds to the minimum possible values of R_1 and R_2. These might be referred to as "Class A" wicks. For cylindrical pores, which fall into this category, it is easily shown [G2] that this is given by:

$$\Delta P_{imax} = \frac{2\sigma\cos\psi}{r_p} \tag{3-3}$$

where:

ψ - wetting angle

r_p - actual pore radius

On the other hand, it seems to be generally accepted that, in a practical heat pipe, the liquid meniscus cannot exhibit a significant convex curvature. Thus, the maximum liquid pressure at any point along the wick surface cannot exceed the local static vapor core pressure. Consequently, the maximum net capillary head (ΔP_{cmax}) which can be generated between various points along a heat pipe is equal to ΔP_{imax}.

The capillary head, as given by Eq. (3-3), applies only to cylindrical pores, which is not characteristic of most class A heat pipe wicks. However, the form of this equation has been generally adapted for all such wicks by replacing the cylindrical pore radius (r_p) with an "effective" pore radius (r_{eA}) so calculated or measured as to render the equation applicable. Thus, in general:

$$\Delta P_{cmax} = \frac{2\sigma\cos\psi}{r_{eA}} \quad \text{(Class A wicks)} \tag{3-4a}$$

Class B Wicks:

It has been proposed [H3] that, for many heat pipe wicks, the maximum interfacial pressure difference which can be generated in the evaporator does not correspond to the minimum possible meniscus radii of curvature, but rather to the coalescence of adjacent menisci prior to the attaining

of a minimum surface free energy configuration. Under such circumstances, it is suggested that ΔP_{cmax} is independent of the wetting angle ψ. Thus, referring to these as "Class B" wicks, we have:

$$\Delta P_{cmax} = \frac{2\sigma}{r_{eB}} \qquad \text{(Class B wicks)} \qquad (3\text{-}4b)$$

For certain well-defined pore geometries, the effective pore radius can be analytically determined (see Section 4.1.1). However, in many cases (e.g., metal felts and foams, woven fabrics, sintered particles) this parameter must be experimentally measured.

There are several standard techniques utilized to make these measurements. These include, (1) measuring the height to which a wick will lift fluid against gravity [G3], (2) measuring the pressure difference required to break the menisci at the wick surface [H4], and (3) utilizing the hydrodynamic theory (to be discussed later) in conjunction with actual or simulated heat pipe performance measurements [H5].

Equations (3-4a) and (3-4b) presume a unique wick pore size. Thus, for completely isotropic wicks of uniform pore size, each of these measurement methods would yield the same result. However, this is usually not the case with heat pipe wicks, and thus the results differ. The rise test measures the smallest wick pores while the pressure test measures the largest wick pores. Since it is the largest pores which fail first in a heat pipe under load, the pressure test yields more realistic results. Most preferable, however, is the simulated or actual heat pipe test, for this measures the largest pores which are saturated at given operating conditions. Under certain conditions (e.g., operating against gravity) the largest pores of a wick with a pore size distribution can be desaturated at the evaporator without resulting in pipe failure. Instead the heat pipe continues to operate on the smaller pores, but with reduced capacity due to partial wick desaturation. This experimental technique is unique in that it allows measuring the effective pore size as a function of the body force head.

3.1.2 Liquid Pressure Drop

Liquid flow in heat pipe wicks is generally characterized by very low flow velocities and Reynolds numbers. Consequently, inertial effects can be neglected for steady-state operation, and the flow losses attributed only to viscous shear. Treating a cylindrical heat pipe (Fig. 3-1), with these assumptions, Cotter [H1] derived an expression for the liquid pressure gradient in the wick due to shear loss as follows:

$$\frac{dP_\ell}{dz} = + \frac{b\mu_\ell \dot{m}_\ell (z)}{A\rho_\ell \phi r_p^2} \tag{3-5}$$

where:

- μ_ℓ - liquid viscosity
- ρ_ℓ - liquid density
- $\dot{m}_\ell (z)$ - local axial mass flow rate
- A - wick cross sectional area
- ϕ - wick porosity
- b - tortuosity factor
- r_p - wick pore radius

Actually, as pointed out in reference [G4], Eq. (3-5) is a rigorous solution for flow in parallel circular capillaries of radius r_p when the tortuosity factor is set equal to 8. As with Eq. (3-3) for maximum capillary head, Eq. (3-5) has been generalized for all wick structures by setting r_p equal to the effective pore radius and including an empirical constant - b.

Again, the constant b can be calculated for certain well defined wick geometries, but in most cases must be measured. In fact, what is usually measured is the grouping $\frac{b}{\phi r_p^2}$.

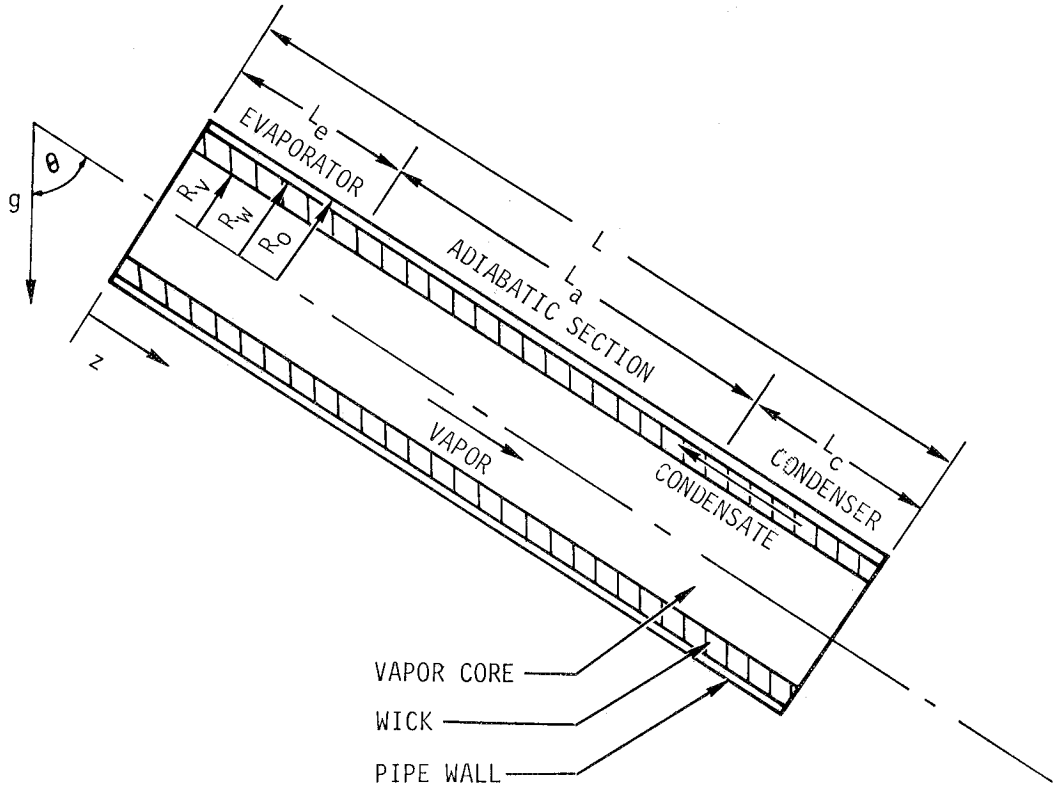

FIGURE 3-1. Schematic of Cylindrical Heat Pipe

Equation (3-5) is, in essence, a form of Darcy's Law for flow in porous media. Usually, Darcy's Law is expressed in terms of a permeability - K, which is a measure of the wick flow resistance.

$$\frac{dP_\ell}{dz} = + \frac{\mu_\ell \dot{m}_\ell (z)}{KA\rho_\ell} \tag{3-6}$$

Comparing Eqs. (3-5) and (3-6), it is seen that the grouping $\frac{b}{\phi r_p^2}$ is equivalent to the reciprocal of the permeability. Since both of these are usually empirically determined quantities, it seems preferable to use the more familiar form of the flow equation (Eq. 3-6). This is particularly true in that for many wicks (e.g., screens, metal felt), the pore geometry for axial flow is not the same as that for radial pumping. Thus, setting r_p in Eq. (3-5) equal to r_e as defined by Eq. (3-4) is somewhat misleading.

3.1.3 Vapor Pressure Drop

The vapor pressure drop in heat pipes is often considerably more difficult to calculate than that in the liquid, for in addition to viscous shear, the analysis must account for momentum effects and perhaps turbulent flow and compressibility. Complicating this analysis is the fact that mass addition in the evaporator and mass removal in the condenser can significantly alter the velocity profiles and, hence, the local pressure gradient.

In terms of heat pipes used for spacecraft thermal control, however, evaporation rates, condensation rates, and axial vapor velocities are usually relatively small. Under such circumstances laminar flow exists throughout the system, and the vapor pressure gradient can be approximated by the sum of two terms, that due to viscous shear and that due to momentum gradients in the evaporator and condenser. As discussed by Katsoff [G5], the gradient due to friction is given by:

$$\left(\frac{dP_v}{dz}\right)_f = -\frac{8\dot{m}_v(z)\mu_v}{\rho_v A_v R_v^2} \tag{3-7}$$

and the gradient due to momentum changes by:

$$\left(\frac{dP_v}{dz}\right)_m = -\frac{8\dot{m}_v(z)}{3\rho_v A_v^2}\frac{d\dot{m}_v(z)}{dz} \tag{3-8}$$

where:

$\dot{m}_v(z)$ - local mass flow rate
μ_v - vapor viscosity
ρ_v - vapor density
R_v - radius of vapor core
A_v - vapor core flow area

More rigorous treatments of the vapor pressure loss can be found in the literature [H1, H6, H7, H8, G4]. However, they yield very nearly the same expressions as given by Eq. (3-7) and (3-8), differing only slightly in the constant terms.

Since in spacecraft thermal control type heat pipes the vapor pressure loss is generally quite small, and often negligible, the equations presented here can be used with little error.

3.1.4 Body Force Head

The last term in the pressure balance equation (Eq. 3-1) is the pressure head due to body forces acting on the fluid - ΔP_b. Most frequently, body forces arise as a result of acceleration fields due to gravity, rotation, rocket thrust, etc. In these cases the body force head is dependent on the acceleration field, fluid density, heat pipe geometry and orientation, and is not dependent on the flow velocities. There do exist exceptions to this, such as electromagnetic body forces on a liquid metal flowing in a magnetic field gradient [H8], but this situation does not usually arise in spacecraft thermal control applications.

Furthermore, in all practical situations, the density of the vapor is very much lower than that of the liquid, so that body forces on the vapor can be neglected. Thus, for cases of interest in this program, the body force on the liquid is a vector quantity, independent of heat load, given by:

$$F_b = \rho_\ell \int \bar{g} dV \tag{3-9}$$

where:

$\bar{g}$ - acceleration field vector
dV - volume element

The fact that the body force is a vector quantity is of considerable significance. The cylindrical heat pipe theory presented here and in most of the literature is based on a one-dimensional hydrodynamic model. Thus, the contribution of body forces has typically been calculated by integrating the axial component of the body force along the length of the pipe [H1, G4].

$$\Delta P_{b_{\parallel}} = \int \frac{dP_b}{dz} = \pm \int \rho_\ell \, g\cos\theta \, dz \tag{3-10}$$

where:

$\Delta P_{b_{\parallel}}$ - axial component of body force head
g - magnitude of acceleration field
θ - angle of heat pipe axis with respect to acceleration field vector (see Fig. 1)
dz - elemental length

The component of the body force perpendicular to the pipe axis has usually been neglected. Integrated over the wick diameter - D_W this is given by:

$$\Delta P_{b_{\perp}} = D_W \rho_\ell \, g\sin\theta \tag{3-11}$$

Contrary to common practice, this component of the body force cannot be ignored. Clearly, in a spinning satellite, a high centrifugal field perpendicular to the pipe axis can render g in Eq. (3-11) so large as to completely dry the wick on one side of the heat pipe. However, even under less severe conditions, such as 1-g testing in the laboratory, the head corresponding to the pipe diameter can have a very significant effect. This is particularly true for the low surface tension fluids commonly used in spacecraft thermal control heat pipes (e.g., ammonia, methanol, freon).

This effect becomes clear when one considers the model shown in Fig. 3-2.

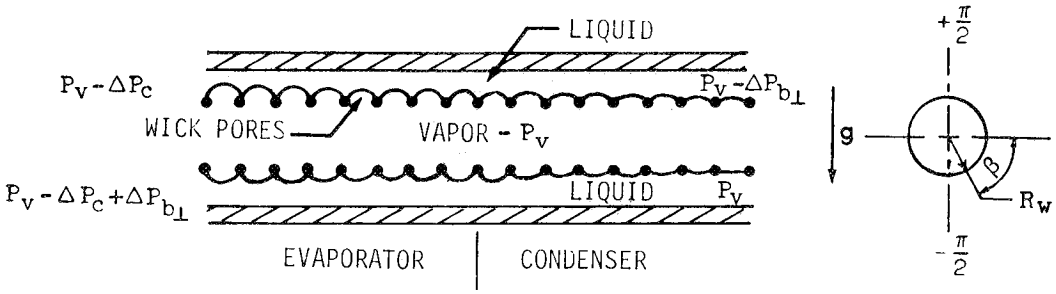

FIGURE 3-2. Hydrodynamic Model Showing Effect of Body Force Component Perpendicular to Heat Pipe Axis

The assumptions made are:

- The pipe is horizontal in a gravity field
- The vapor pressure loss is negligible*
- Liquid flow is in the axial direction only
- The wick is thin $(R_v \approx R_w)$

The figure shows a typical variation in pore menisci for a heat pipe operating under the assumed conditions. It was previously established that the maximum liquid pressure is equal to the local vapor core pressure - P_v and the minimum liquid pressure was equal to $P_v - \Delta P_c$ (Section 3.1.1).

The maximum liquid pressure (P_v) will exist at the end of the condenser along the bottom of the pipe ($\beta = -\frac{\pi}{2}$). Thus, the circumferential distribution of liquid pressure at this axial position is given by:

$$P_\ell(\beta)_c = P_v - \rho_\ell g(R_w + R_w \sin\beta) \tag{3-12}$$

where R_w is the wick radius.

At the top of the pipe, this yields $P_\ell = P_v - \Delta P_{b\perp}$. On the other hand, the minimum liquid pressure ($P_v - \Delta P_c$) will exist at the beginning of the evaporator along the top of the pipe. The circumferential distribution of pressure at this end is thus given by:

$$P_\ell(\beta)_e = (P_v - \Delta P_c) + \rho_\ell g(R_w - R_w \sin\beta) \tag{3-13}$$

At the bottom of the pipe, this yields $P_\ell = P_v - \Delta P_c + \Delta P_{b\perp}$.

Now, since liquid pumping is proportional to the axial gradient in liquid pressure, it is possible to obtain an averaged value of this parameter for the heat pipe by circumferentially averaging the quantity $[P_\ell(\beta)_c - P_\ell(\beta)_e]$. Thus, using symmetry to treat half the pipe,

---

*Vapor pressure losses do not change the results, but complicate the model.

$$\overline{\Delta P_\ell} = \frac{1}{\pi}\int_{-\frac{\pi}{2}}^{+\frac{\pi}{2}}\left[P_v - \rho_\ell g(R_w+R_w\sin\beta) - (P_v-\Delta P_c) - \rho_\ell g(R_w-R_w\sin\beta)\right] d\beta \qquad (3\text{-}14)$$

$$= \frac{1}{\pi}\int_{-\frac{\pi}{2}}^{+\frac{\pi}{2}}(\Delta P_c - 2\rho_\ell g\, R_w)\, d\beta$$

$$= \Delta P_c - 2\rho_\ell g\, R_w$$

Substituting the wick diameter - D_w for $2R_w$, we finally get:

$$\overline{\Delta P_\ell} = \Delta P_c - \rho_\ell g\, D_w = \Delta P_c - \Delta P_{b_\perp} \qquad (3\text{-}15)$$

Thus, it is seen that the available pumping head for a horizontal pipe is not ΔP_c, but that value reduced by the perpendicular body force head. In other words, the body force head to be used in the heat pipe pressure balance must include both the axial and perpendicular components. However, whereas the axial contribution can either aid or hinder performance, the perpendicular component is always a degrading factor. Thus, for a cylindrical heat pipe,

$$\left.\begin{aligned} \frac{dP_b}{dz} &= \pm\rho_\ell g\cos\theta \\ \text{but,}\quad \Delta P_b &= \rho_\ell g\left[D_w\sin\theta \pm\int\cos\theta\, dz\right] \end{aligned}\right\} \qquad (3\text{-}16)$$

3.1.5 Integrating the Flow Equations

In sections 3.1.1 through 3.1.4, equations were presented for each of the four elements making up the pressure balance equation (Eq. 1). These are summarized as follows:

Maximum Capillary Head:

$$\Delta P_{cmax} \begin{cases} \dfrac{2\sigma\cos\psi}{r_{eA}} & \text{(Class A wicks)} \\ \dfrac{2\sigma}{r_{eB}} & \text{(Class B wicks)} \end{cases} \tag{3-4}$$

Liquid Flow Loss:

$$\frac{dP_\ell}{dz} = \frac{\mu_\ell \dot{m}_\ell(z)}{KA\rho_\ell} \tag{3-6}$$

Vapor Pressure Loss:

Friction:

$$\left(\frac{dP_v}{dz}\right)_f = -\frac{8\dot{m}_v(z)\mu_v}{\rho_v A_v R_v^2} \tag{3-7}$$

Momentum:

$$\left(\frac{dP_v}{dz}\right)_m = -\frac{8\dot{m}_v(z)}{3\rho_v A_v^2}\,\frac{d\dot{m}_v(z)}{dz} \tag{3-8}$$

Body Force Head:

$$\frac{dP_b}{dz} = \pm\,\rho_\ell g\cos\theta$$

$$\Delta P_b = \rho_\ell g\left[D_w\sin\theta \pm \int\cos\theta\, dz\right] \tag{3-16}$$

These equations are generally applicable to all one-dimensional type heat pipes (tubes of any cross section) which operate in the temperature and heat load ranges applicable to spacecraft thermal control.* Also, since the loss equations are in differential form, there are no restrictions on the number of evaporator and condenser sections, the flux distribution along them, or axial changes in the wick system or pipe geometry.

*For other than circular cross sections, the hydraulic radius and an appropriate shape factor should be substituted for R_v in Eq. (3-7). Also, the required static pumping height for the liquid at $\theta = 90°$ should be substituted for D_w in Eq. (3-16).

To apply the equations to a particular heat pipe one simply integrates the loss terms over the pipe length. To accomplish this, however, several ancillary equations are required. First, continuity requires that, at any axial position - z, the vapor and liquid flow rates must be equal. Thus,

$$\dot{m}_\ell(z) = \dot{m}_v(z) \tag{3-17}$$

Second, neglecting axial wall conduction and sensible heat transport [H1, G2], the mass flow rate of change is related to the heat transfer rate per unit length as follows:

$$\frac{d\dot{m}(z)}{dz} = \frac{Q'}{\lambda} \tag{3-18}$$

where:

Q' - radial heat transfer rate per unit length

λ - latent heat of vaporization

For all but the simplest systems, integration of the flow losses is best performed numerically. However, one configuration, which is of significant practical importance, is readily solved analytically. This is the system shown on Fig. 3-1, consisting of a tube with single evaporator and condenser sections at the ends of the pipe, with or without an intervening adiabatic section. Also, the pipe geometry and wick are uniform axially as is the heat input and rejection over the evaporator and condenser respectively. Under such circumstances, the losses are given by [G4]:

$$\Delta P_\ell = \frac{Q\,(L + L_a)\,\mu_\ell}{2\pi K \rho_\ell \lambda (R_w^2 - R_v^2)}$$

$$\Delta P_v = \frac{4Q\,(L + L_a)\,\mu_v}{\pi \rho_v \lambda R_v^4} \tag{3-19}$$

$$\Delta P_b = \rho_\ell g \left[D_w \sin\theta + L\cos\theta\right]$$

where:

- Q - total axial heat transport
- L - total pipe length
- L_a - length of adiabatic section
- R_v - vapor core radius
- R_w - wick radius

3.1.6 Capillary Pumping Limit

The fact that there exists a maximum capillary head for any wick-fluid combination (Eq. 3-4) results in a hydrodynamic limit on heat pipe capacity. As mentioned previously, the capillary head must increase with the liquid and vapor pressure drops as the heat load (and hence the fluid circulation rate) increases. Since there exists a limit on the capillary head, there also exists a corresponding limit on the heat load if the pressure balance criterion (Eq. 3-1) is to be satisfied. This defines the capillary pumping limit.

In the general case, the capillary pumping limit is established for a given heat pipe by integrating the pressure drop equations along the pipe (as described in the last section) and comparing the sum of the losses at all points with the local maximum capillary head. Since the maximum capillary head and the body force head are usually not dependent on load, the capillary pumping limit criteria is most clearly defined by transposing Eq. (3-1), using ΔP_{cmax}, to read:

$$\Delta P_{cmax} - \Delta P_b \geq \Delta P_\ell + \Delta P_v \qquad (3\text{-}20)$$

In Eq. (3-20), only the terms on the right hand side are load dependent. Thus, the heat pipe operates below the capillary pumping limit as long as the inequality holds everywhere along the pipe. When the load increases so that the two sides of the equation are equal at any point along the pipe, the capillary pumping limit has been reached. Thus, to calculate the capillary pumping limit for a given heat pipe, the heat load is progressively increased until such an equality occurs. This is shown in Fig. 3-3 for a number of heat pipe configurations.

Fig. 3-3a represents a conventional heat pipe, with uniform heat transfer over the evaporator and condenser, operating against gravity. The pressure balance graph is drawn for the capillary pumping limit--that is, the sum of the liquid and vapor pressure drops just equals the maximum capillary head minus the body force head. In this case the failure point (shown as a dot) would occur on the top of the pipe at the beginning of the evaporator.

Fig. 3-3b depicts the same heat pipe operating in a gravity-aiding mode. Note that $\Delta P_{b_\perp}$ and $\Delta P_{b_\parallel}$ are now of opposite sign. The critical point on the pipe is still at the beginning of the evaporator, but failure occurs at a higher value of $\Delta P_\ell + \Delta P_v$, and thus at a higher heat load.

Fig. 3-3c depicts a situation where there are multiple evaporator and condenser sections along the heat pipe. This does not change the failure criterion. The capillary pumping limit still occurs at the heat load for which the equality in Eq. (3-20) is first reached at any point in the pipe. The fact that the liquid and vapor pressure curves are no longer monotonic functions is due to an assumed flow reversal situation along the pipe.

In Fig. 3-3c the failure point is still shown at the beginning of the evaporator. However, the situation often arises where the distribution of evaporator and condenser loads are such that failure occurs elsewhere along the pipe. This is shown in Fig. 3-3d. Note that in this case the vapor pressure loss curve does not start at the origin. Rather the lowest point along this curve is set equal to zero. This is consistent with the fact that the pressure balance equation must be satisfied at all points along the heat pipe.

Fig. 3-3e represents a heat pipe with an axial composite wick. The wick in the evaporator is presumed to have a smaller effective pore size and a higher flow resistance than the condenser wick. The vapor pressure loss curve is not affected by the wick variation but the liquid loss curve is, showing a discontinuity in slope at the wick juncture. More important,

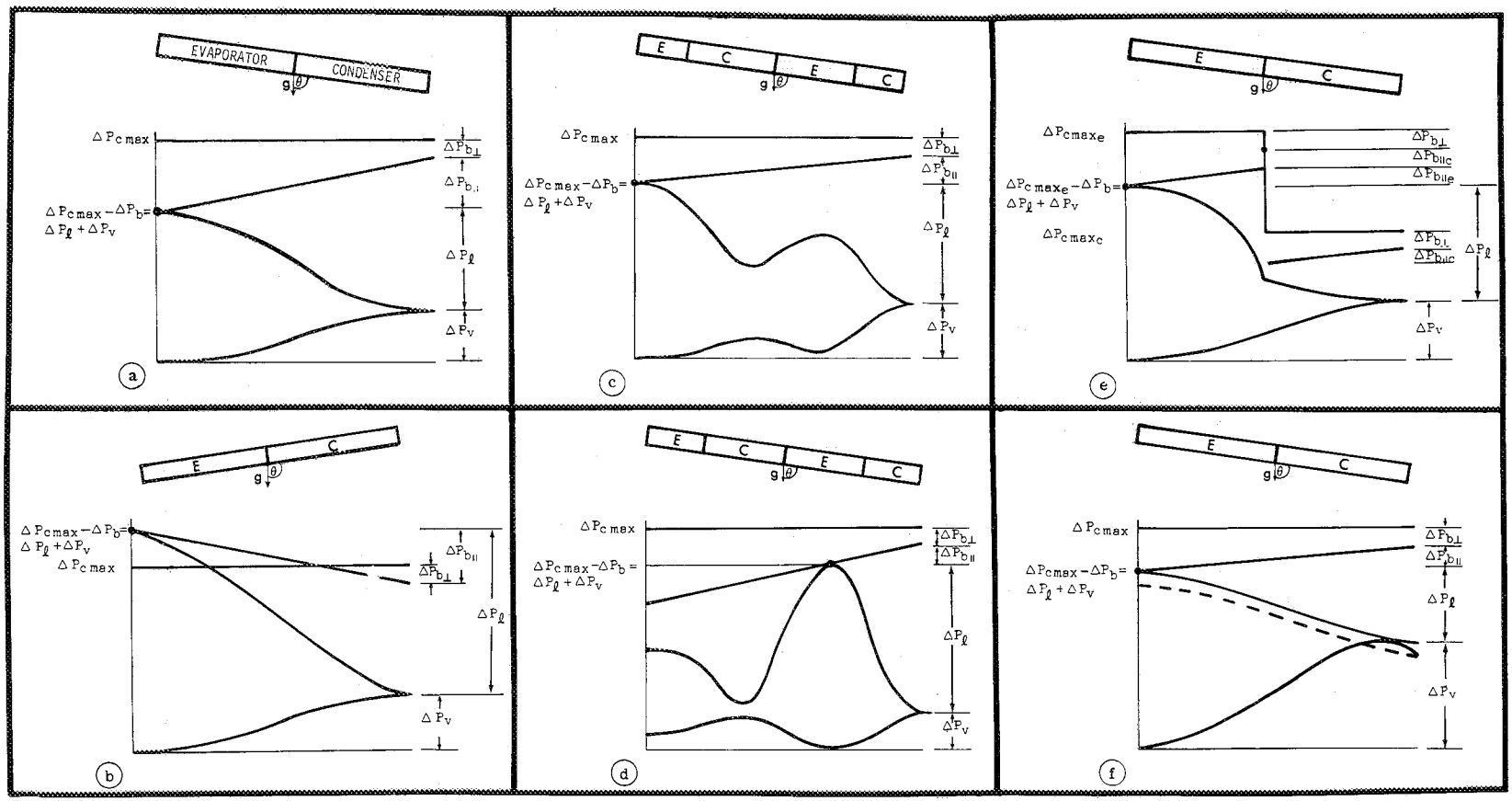

FIGURE 3-3. Capillary Pumping Limit Pressure Balance Graphs for Various Heat Pipe Configurations

the maximum capillary head is different in the two sections, giving rise to the pressure balance graph shown. Fig. 3-3e again shows the failure point at the beginning of the evaporator. However, it is clear that this could also occur at the beginning of the condenser if ΔP_{cmax} for the condenser where chosen a little lower. The object of using such composite wicks is, of course, to reduce the flow resistance in regions of the pipe where the sum of the flow losses is small, thus allowing higher circulation rates and heat loads. The simultaneous reduction in maximum capillary head within these regions can be tolerated (within limits) as shown in Fig. 3-3e.

Finally, Fig. 3-3f represents a case where the vapor flow is presumed high enough that the momentum pressure drop is significant (Eq. 3-8). Generally, for spacecraft thermal control heat pipes, the momentum drop is quite small; but for certain cases (very high loads at low operating pressure) it could be large enough so that recovery in the condenser leads to an extremum in the vapor loss curve as shown. Under such circumstances, the point of equal vapor and liquid pressure may no longer be at the end of the condenser as shown in Figs. 3-3a - e. This would yield the dashed line for $\Delta P_v + \Delta P_\ell$, which violates the requirement that the liquid be everywhere at a pressure equal to or lower than the local static vapor core pressure (sec. 3.1.1). Thus, the liquid loss curve must be elevated such that it is tangent to the vapor loss curve, and the point of tangency represents the position of equal liquid and vapor pressure. This phenomenon is discussed in more detail by Ernst [H2].

Note that this situation need not arise only as a result of momentum recovery. In the distributed source and sink case shown in Fig 3-3d, a slightly higher load on the interior condenser would result in tangency at the extremums of the loss curves rather than equality at the end of the pipe.

The six cases shown represent but a small number of possible situations. These cases were selected to demonstrate the pressure balance principle leading to a capillary pumping limit and the technique for calculating it. As stated earlier, the technique is generally applicable to heat pipes with any number of evaporator and condenser sections having arbitrary flux distributions along them, and can handle arbitrary axial variations in wicking or in pipe geometry.

Under certain simple configurations, numerical evaluation of the capillary pumping limit is not necessary. Thus, for the conventional heat pipe shown in Fig. 3-1, assuming uniform heat input and output, uniform wicking, and negligible momentum pressure drop, one can obtain a closed form analytical solution for this limit. To do this, one simply equates the maximum capillary head (Eq. 3-4) to the sum of the loss equations integrated over the entire length of the pipe (Eq. 3-19), yielding:

$$\left.\begin{matrix}\frac{2\sigma\cos\psi}{r_{eA}} \\ \frac{2\sigma}{r_{eB}}\end{matrix}\right\} = \Delta P_{cmax} = \frac{Q(L + L_a)\mu_\ell}{2\pi K\rho_\ell \lambda(R_w^2 - R_v^2)} + \frac{4Q(L + L_a)\mu_v}{\pi\rho_v\lambda R_v^4} + \rho_\ell g\left[D_w\sin\theta + L\cos\theta\right] \tag{3-21}$$

Solving for the maximum heat transport (capillary pumping limit) yields:

$$Q_{CL} = \frac{\pi\lambda}{(L + L_a)} \frac{\left[\Delta P_{cmax} - \rho_\ell g\,(D_w\sin\theta + L\cos\theta)\right]}{\left[\frac{\mu_\ell}{2K\rho_\ell(R_w^2 - R_v^2)} + \frac{4\mu_v}{\rho_v R_v^4}\right]} \tag{3-22}$$

3.1.7 Entrainment Limit

A phenomenon which can affect the capillary pumping limit, but is not included in Eq. (3-1), is liquid entrainment in the vapor. In a heat pipe, the vapor and liquid generally flow in opposite directions. Since they are in contact at the wick surface, this sets up a mutual drag at the vapor-liquid interface. If the relative velocity between the liquid and vapor becomes too great, the interface becomes unstable and droplets of liquid will be torn from the wick and entrained in the vapor. Since this liquid never reaches the evaporator, it cannot contribute to the heat transferred by the heat pipe. However, it does contribute to the liquid flow loss. Thus, the maximum axial heat transfer in the heat pipe is no longer equal to the maximum fluid circulation rate times the latent heat of vaporization, but is some lower value which defines the entrainment limit.

The conditions leading to entrainment are expressed in terms of the ratio of vapor inertial forces to liquid surface tension forces, called the Weber number:

$$We = \frac{\rho_v \bar{V}^2 z}{\sigma} \tag{3-23}$$

where:

ρ_v - vapor density
$\bar{V}$ - average vapor velocity
σ - liquid surface tension
z - characteristic dimension associated with liquid surface

At present, limited experimental data with screen wicks indicate that a Weber number of unity represents the entrainment condition when the characteristic dimension, z, is set approximately equal to the screen wire diameter [H9].* This suggests that by using finer mesh screens,

*Some authors argue that the wire-to-wire spacing is a more appropriate value for z [G4]. Additional experimentation is necessary to resolve this question.

entrainment can be inhibited--an hypothesis which has been verified at Los Alamos.

For wick structures that do not involve screens, any construction which reduces interaction between the vapor and liquid will serve to raise the entrainment limit. On the other hand, open wick structures such as axial grooves cut in the wall are particularly susceptible to the effects of vapor-liquid drag [G6].

When the Weber number is set equal to unity, the limiting axial heat flux corresponding to incipient entrainment is given by:

$$\frac{Q_e}{A_v} = \left[\frac{\rho_v \sigma \lambda^2}{z}\right]^{\frac{1}{2}} \qquad (3\text{-}24)$$

where:

$\frac{Q_e}{A_v}$ - maximum axial heat flux for incipient entrainment

A_v - vapor core flow area

λ - latent heat of vaporization

Using Eq. (3-24), the entrainment limit was calculated for water, ammonia and methanol; the primary fluids of interest in spacecraft thermal control. Calculations were performed for a series of characteristic lengths - z.

The results are presented on Figs. 3-4, 3-5 and 3-6 along with sonic flow limit curves (to be discussed later). The figures also include a table of standard screen meshes whose wire diameters equal the characteristic dimensions used in the calculations. Assuming the equivalence of wire diameter and characteristic dimension establishes the entrainment limit curves as those applicable to the corresponding

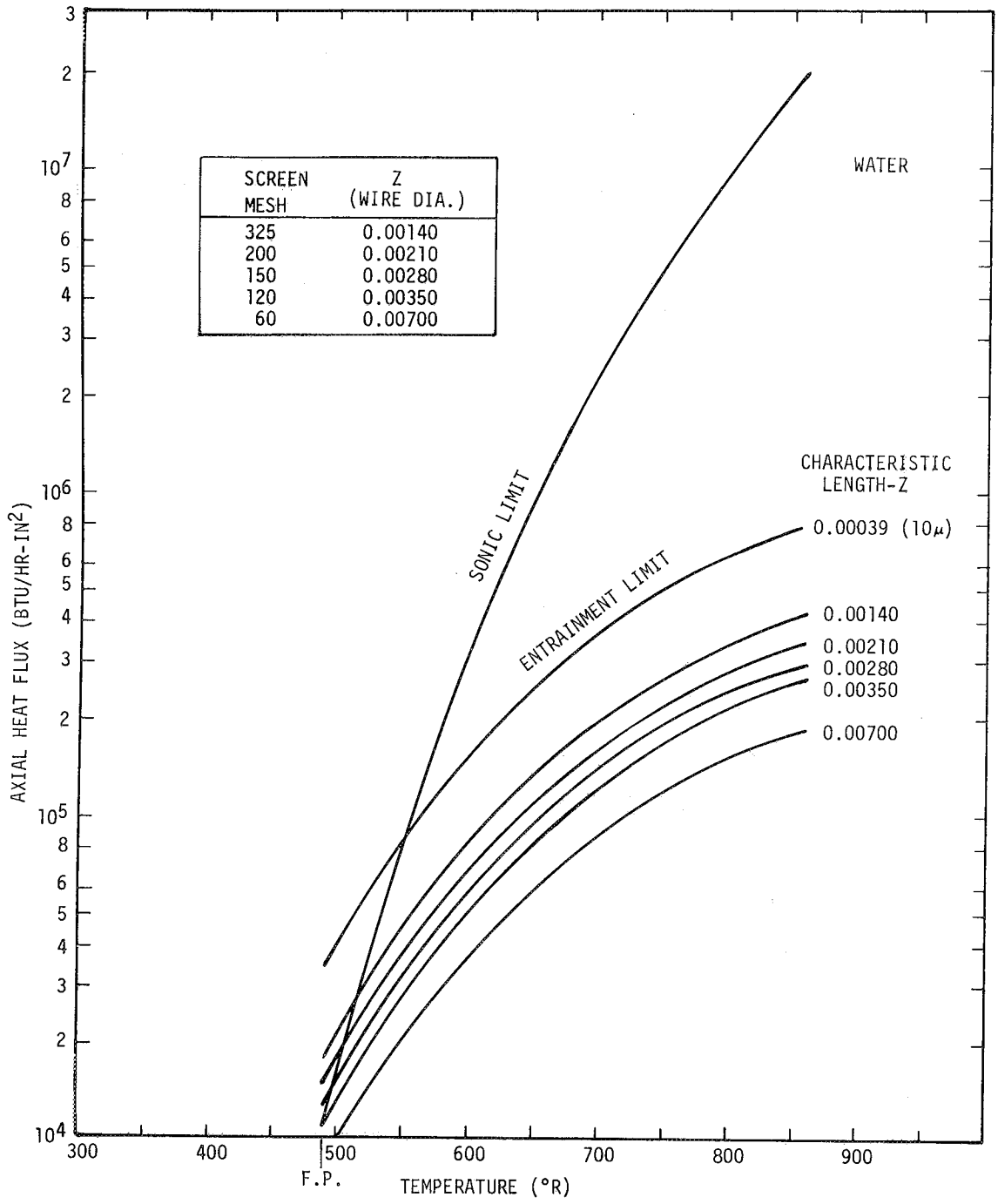

FIGURE 3-4. Estimated Heat Pipe Entrainment and Sonic Axial Heat Flux Limitations for Water

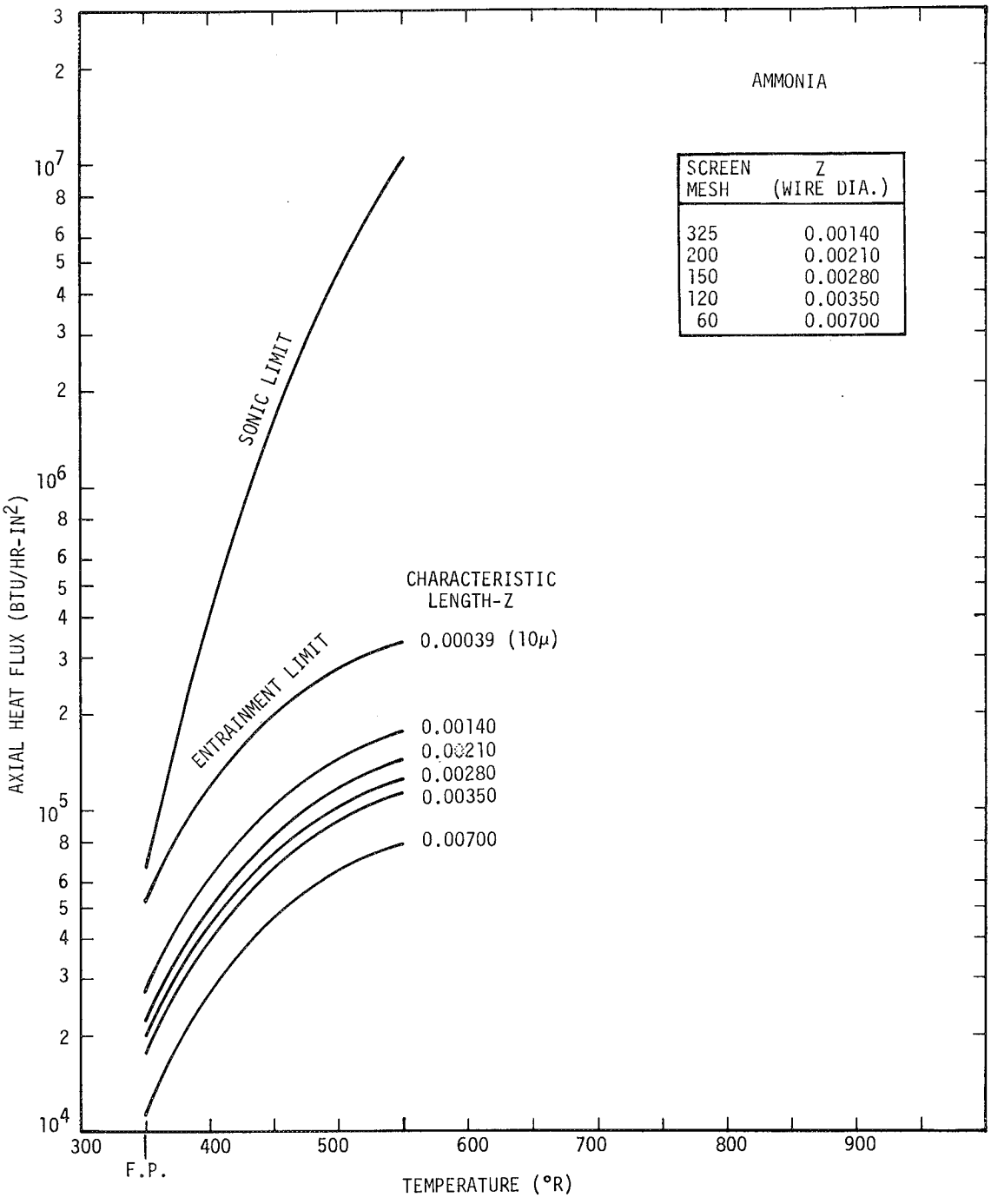

FIGURE 3-5. Estimated Heat Pipe Entrainment and Sonic Axial Heat Flux Limitations for Ammonia

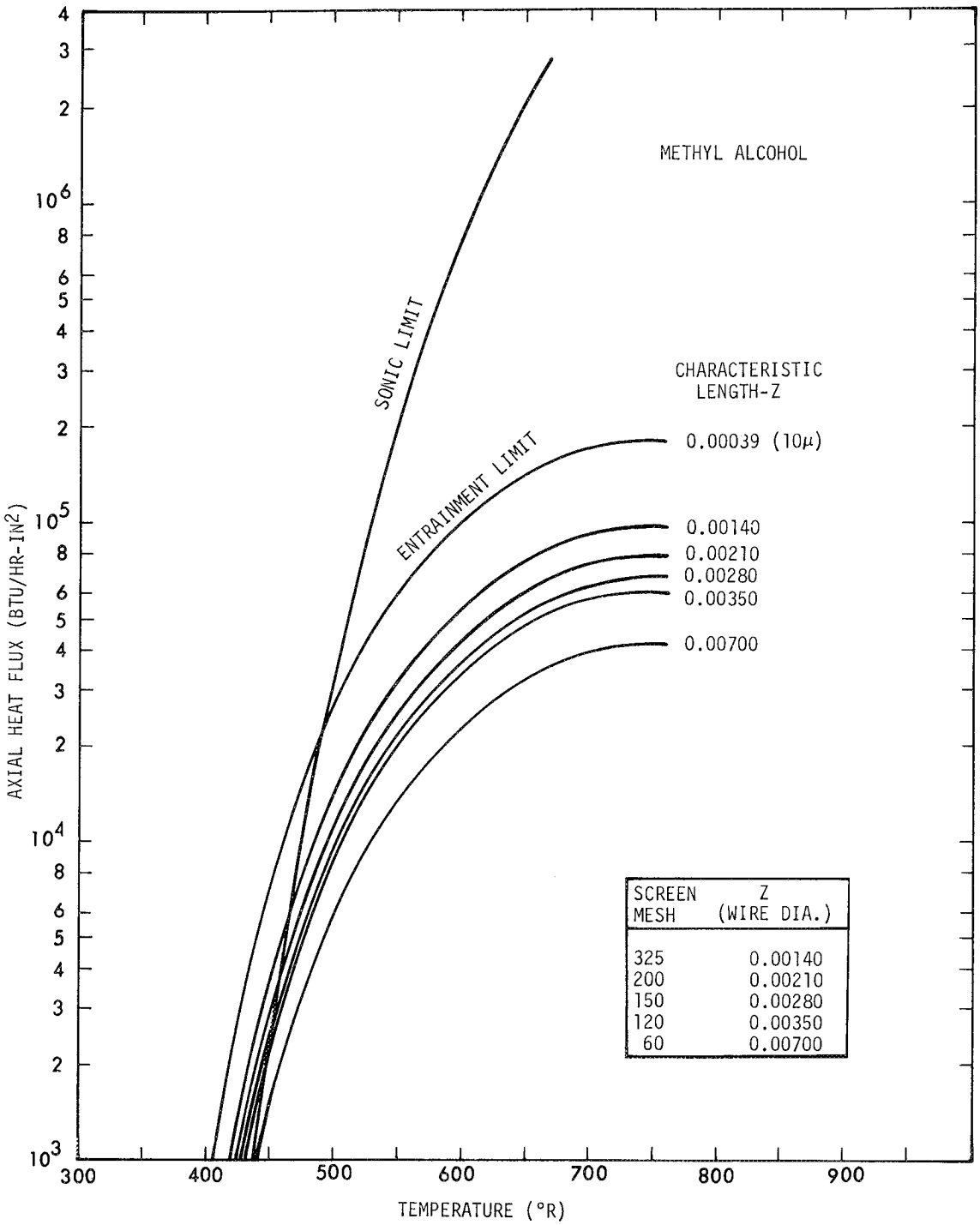

FIGURE 3-6. Estimated Heat Pipe Entrainment and Sonic Axial Heat Flux Limitations for Methyl Alcohol

screen mesh size. The curves are drawn in terms of z, however, and are valid whatever method is used to establish this value.

It was noted in the calculations that at high temperatures the surface tension decreases rapidly enough to result in a maximum in the curves. That is, the entrainment limit can actually decrease with increasing temperature. This is clearly seen from Eq. (3-24) since both σ and λ go to zero at the critical point.

3.1.8 Sonic Limit

It can be shown analytically [H10] that there is a correspondence between constant area flow in a heat pipe with mass addition (evaporator) and removal (condenser) and constant mass flow in a converging-diverging nozzle. The end of the evaporator section in the heat pipe corresponds to the throat of the nozzle. Consequently, just as there is a sonic (MACH 1) limitation on the flow velocity through a nozzle throat, there is a similar limit on the flow velocity at the heat pipe evaporator exit. For a given evaporator exit temperature and working fluid, this choked flow condition is a fundamental limitation on the axial heat flux capacity of the heat pipe. To increase the axial heat transfer capacity of the heat pipe, one must increase the vapor flow area.

The sonic limit is calculated by setting the vapor flow velocity equal to the sonic velocity in the continuity equation and multiplying by the latent heat of vaporization as follows:

$$\frac{Q_s}{A_v} = \lambda \rho_v V_s \qquad (3\text{-}25)$$

where:

$\frac{Q_s}{A_v}$ - axial heat flux at MACH 1 conditions

V_s - sonic velocity of vapor

Using Eq. (3-25), the sonic limit was calculated for water, ammonia and methanol. The results are presented on Figs. 3-4, 3-5 and 3-6 along with the entrainment limit curves. Note that over most of the temperature range of interest in spacecraft thermal control, the sonic limit on axial heat flux exceeds the entrainment limit. Furthermore, except at very low temperatures, both limits are quite high ($>10^4$ Btu/hr-in^2). Consequently, they are seldom encountered in the design of spacecraft thermal control heat pipes.*

When using Eq. (3-25) to calculate the sonic limit, the parameters must be evaluated at the local conditions where choking occurs (the exit of the evaporator). It is sometimes more convenient to calculate this limit in terms of conditions at the beginning of the evaporator. This can be done using an equation developed by Levy [H10]:

$$\frac{Q_s}{A_v} = \frac{\lambda \rho_v V_s}{\sqrt{2(k+1)}} \qquad (3\text{-}26)$$

where k = ratio of specific heats (C_p/C_v).

3.2 Heat Transfer

The fluid circulation phenomena discussed in the previous sections arise as a result of heat transfer into the heat pipe at the evaporator and out of it at the condenser. In most heat pipes this heat must be transferred through the pipe wall and saturated wick in both cases. Generally, these heat transfer processes are the major source of temperature drop in the heat pipe.**

*Except in the case of open axially grooved heat pipes where the vapor drag on the liquid can be appreciable.

**Temperature drops also arise due to the vapor flow losses along the pipe and to non-equilibrium at the vapor-liquid interfaces. However, these effects are relatively small unless the pipe operates under very high heat loads [H1, G2].

In many cases, the heat transfer process at the evaporator and condenser is by conduction in that the presence of the wick impedes convection. Thus, the temperature drop experienced in transferring heat into and out of the device is proportional to the local heat flux and wick-wall thickness, and inversely proportional to the effective thermal conductivity of the wall-wick-fluid composite.

3.2.1 Evaporator Heat Transfer - Boiling in the Wick

The fact that heat is transferred into the heat pipe through the wick gives rise to another limit on the heat pipe capacity. Frequently, liquid is vaporized only at the wick surface as a result of the heat conducted through the wick. However, the vapor at the wick surface is thermodynamically saturated. Consequently, the fluid within the wick at the evaporator is superheated by virtue of (1) the curvature of the menisci, and (2) the existing radial temperature gradient. The greatest superheat occurs at the interface of the wick and pipe wall. If this superheat becomes too large (it increases with the heat transfer rate), the fluid will begin to boil within the wick.

3.2.1.1 Nucleation Superheat

It is difficult to say just what level of liquid superheat must exist before nucleation (boiling) will begin at the pipe wall. However, using criteria similar to those which apply to nucleate boiling from planar surfaces, an estimate can be made. In this way, Marcus [G2] has shown that the critical evaporator superheat (temperature drop across the wick) is given by:

$$\Delta T_{crit} = \frac{T_{sat}}{J\lambda\rho_v}\left[\frac{2\sigma}{r_n} - \Delta P_c^*\right] \qquad (3\text{-}27)$$

where:

T_{sat} - saturation temperature of the fluid
J - mechanical equivalent of heat
r_n - effective radius of critical nucleation cavity
ΔP_c^* - maximum value of capillary head along the evaporator

Note that ΔP_c^* does not equal ΔP_{cmax} as given by Eq. (3-4) unless the heat pipe is operating at the capillary pumping limit. Rather, it is the maximum value of ΔP_c (as given by Eq. (3-1)) along the evaporator section(s) of the pipe.

Generally, all of the terms on the right hand side of Eq. (3-27) are known except r_n, which is a function of the boiling surface finish. To establish the appropriate value of r_n, one should first establish its value assuming cavities of all sizes were present on the surface, and then impose appropriate limits. This can be done using the nucleation theory of Rohsenow and Bergles [T1]. Their equation for r_n is:

$$r_n = \left[\frac{2\sigma T_{sat} k_\ell v_{\ell g}}{\lambda q''_r} \right]^{1/2} \tag{3-28}$$

where:

k_ℓ - thermal conductivity of liquid

$v_{\ell g}$ - difference in specific volumes of vapor and liquid

q''_r - radial heat flux into evaporator

The value of r_n given by Eq. (3-28) is the appropriate one to use in Eq. (3-27), assuming that cavities of such size exist on the surface and are potential nucleation sites.* On typical smooth surfaces, the largest potential nucleation sites have critical radii between 10^{-4} and 10^{-3} inches. Thus, Eq. (3-28) is appropriate if it predicts a smaller value of r_n but not if it predicts a larger value.

It is not clear that r_n is similarly bounded by 10^{-4} - 10^{-3} inches for wicked surfaces; but it is certainly bounded by the pore size of the wick (r_e in Eq. (3-4)). Thus, a conservative approach to establishing

---

*A potential nucleation site is a cavity which contains a pre-existing gaseous phase.

the critical superheat for nucleation is to use Eq. (3-28) for r_n as long as it predicts a value below the effective wick pore radius - r_e, and to use r_e otherwise.

This approach is actually very conservative for conventional heat pipe design, for it presumes the existence of nucleation sites containing a pre-existing gaseous phase. In the absence of such conditions, very much higher superheats are required for nucleation than those predicted by Eqs. (3-27) and (3-28). Thus, since a conventional heat pipe is very carefully processed to eliminate all foreign gases, one seldom observes nucleation at the superheat levels predicted in this way. For example, using ammonia as the working fluid with an operating temperature of 70°F, TRW has measured nucleation superheats of 7°F, compared with a maximum predicted value of 0.4°F (Eq. (3-27) with $r_n = 10^{-4}$ in.) [G7].

On the other hand, this program is primarily concerned with variable conductance heat pipes, in which control is frequently effected through the use of non-condensible gases. Under such circumstances, gases are abundantly present to promote nucleation and Eqs. (3-27) and (3-28) will apply. They are similarly applicable in cases where a non-condensible gas charge is introduced to aid start-up from a frozen state [G7, G8].

3.2.1.2 Maximum Heat Flux

The nucleation superheat predicted by Eqs. (3-27) and (3-28) represents the maximum temperature differential which can be sustained across the evaporator wick without nucleate boiling within the wick. The consequences of wick boiling depend on the nature of the wick used. In certain composite wicks, such as annular arteries or screen-covered grooves (to be discussed later), wick boiling clearly renders the heat pipe inoperative since the vapor cannot escape the wick. On the other hand, if the wick structure does permit the escape of vapor (e.g., a feltmetel wick, a packed bed wick), operation with boiling can be sustained.

In cases where the incipience of boiling represents heat pipe failure, heat must be conducted to the wick surface and the liquid vaporized there. Under these circumstances, the maximum pipe heat transfer (Boiling Limit) corresponds to the conduction heat flux into the evaporator which yields a wick temperature drop equal to ΔT_{crit} from Eq. (3-27). For cylindrical heat pipes such as that in Fig. 3-1, this is given by:

$$Q_{BL} = \frac{2\pi L_e k_{eff} \Delta T_{crit}}{\ell n \frac{R_w}{R_v}} \qquad (3\text{-}29)$$

where:

- Q_{BL} - boiling limit on pipe heat transport
- L_e - length of evaporator section
- ΔT_{crit} - nucleation superheat (Eq. 3-27)
- k_{eff} - effective thermal conductivity of saturated wick

For certain well defined wick structures the effective thermal conductivity of the saturated wick can be analytically calculated. However, as with the effective pore size (r_e), and permeability (K) of wicking materials, this must often be a measured quantity. Several investigators have dealt with this problem analytically and experimentally [T2, T3, T4], and a number of correlations exist for certain classes of wicks. However, considering the countless combinations of wick structures and fluids available, these correlations are of very limited usefulness.

Neglecting convection effects, it is relatively simple to show that the effective thermal conductivity of any saturated wick is bracketed by assuming either parallel or series conduction paths and weighting the solid and liquid conductivities on a void fraction basis. Thus:

$$\frac{k_s k_\ell}{\phi k_s + (1 - \phi) k_\ell} \leq k_{eff} \leq (1 - \phi) k_s + \phi k_\ell \qquad (3\text{-}30)$$

(series) (parallel)

Unfortunately, for the metallic wicks and non-metallic working fluids typical of spacecraft thermal control heat pipes, the bounds on k_{eff} given by Eq. (3-30) are very broad. If the wick design is such that nucleation represents heat pipe failure, conservative heat pipe design generally dictates that the lower bound (series case) be used. Thus, for conduction heat transfer, k_{eff} in Eq. (3-29) should be determined analytically, experimentally, or by correlation if possible; and if not, by the lower bound of Eq. (3-30).

In cases where the wick structure permits operation with internal vapor generation, the problem becomes much more complex. Under these circumstances, much higher evaporator heat fluxes can be tolerated than those predicted by Eq. (3-29) for conduction heat transfer. Still, there exists a maximum heat flux corresponding to the condition where vapor is generated within the wick at such a high rate that it cannot escape and forms an insulating layer which blankets the heat pipe wall. Although this failure mode is similar to the critical heat flux condition in pool boiling, it cannot be predicted using the pool boiling equations, for the presence of the wick alters both the vapor and liquid hydrodynamics.

Numerous investigators have studied the wick boiling phenomenon [G1, G3, H4, H11, H12, T5, T6, T7, T8, T9], and although there is still some controversy as to the phenomena involved, a theory is beginning to emerge for certain cases. For wicks with a pore size distribution (e.g., metal felt, sintered particles), the proposed mechanism is that once nucleation begins the liquid recedes into the wick such that, over the bulk of the evaporator wall, heat is conducted through a thin microlayer of liquid. The thickness of the liquid layer is hypothesized to be independent of the wick thickness but rather on the order of the fiber or particle size making up the wick. Thus, the theory suggests that, even with vapor generation internal to the wick, the heat transfer is by conduction through a fairly well defined liquid layer, and that the ebullition-induced mechanisms which characterize nucleate boiling are not significant. Such a model predicts a constant coefficient of

heat transfer for the "boiling" mode. This has been experimentally observed by Ferrel,et al [T9, T10] using packed sphere bed wicks, and also by workers at TRW using sintered particle wicks.

The maximum heat flux consistent with this model occurs when the pressure drop associated with vapor escape through the wick exceeds the ability of the available capillary forces to maintain the liquid film. Thus, the maximum heat flux is a function of the wick thickness whereas the coefficient of heat transfer is not. With this model Ferrel, et al [T9, T10] have been able to approximately predict maximum heat fluxes for packed sphere bed wicks.

Note that the theory described is limited to wicks with a pore size distribution and, in fact, has been seriously tested only for packed sphere bed wicks. Substantially different behavior has been observed for other wick types such as rolled screens [T8].

For a detailed discussion of wick boiling the reader is referred to the referenced literature. It is considered beyond the scope of this program--primarily because satisfactory predictive methods (either analytical or by correlation) do not yet exist. Furthermore, if a heat pipe operates with vapor generation internal to the wick, the hydrodynamic theory presented in Section 3.1 is no longer applicable. That theory is based upon laminar flow through fully saturated wicks. Liquid recession into the wick or vapor bubbles present within the wick will significantly alter the liquid flow in an as yet unpredictable way. Consequently, although it is certainly possible to operate heat pipes with wick boiling, it is not yet possible to predict their performance except by empirical means.

The application of heat pipes to spacecraft thermal control generally requires a predictive design capability, and thus it is recommended that such heat pipes be designed to avoid boiling altogether. This can be done using the nucleation criteria presented in the last section to

establish the maximum evaporator heat flux. Methods of achieving high radial heat fluxes without incurring nucleation will be discussed later in this report.

3.2.2 Condenser Heat Transfer

The heat transfer process at the condenser section of a heat pipe is a much simpler phenomenon than at the evaporator. Vapor is condensed at the wick surface and the latent heat of vaporization released is generally conducted through the wick to the pipe wall.* However, in this case, the conduction temperature drop results in subcooling of the liquid which is a stable situation. The condenser heat transfer is thus described by an equation similar to Eq. (3-29), but with no practical heat transfer limit on ΔT or Q.**

As with the evaporator case, techniques available for minimizing the condenser temperature drop will be discussed later in this report.

---

*Exceptions to this do exist, such as grooved wall condensers where the pipe wall is the wick.

**The limit on Q due to condenser flooding is actually a hydrodynamic limit, and that imposed by the kinetic rate of vapor arrival is so high that it can safely be neglected (except for some liquid metal pipes).

4.0 CONVENTIONAL HEAT PIPE DESIGN

The previous discussion dealt with the theory of conventional heat pipes from the hydrodynamic and heat transfer points of view. The theory of variable conductance heat pipes will be taken up in Research Report No. 2. This section deals with the application of the hydrodynamic and heat transfer theory to the design of heat pipes with reference to wick design, fluid selection, materials selection and heat pipe optimization.

In all but the simplest geometries, closed form solutions to the differential flow equations summarized in Section 3.1.5 are not available. Consequently, proper heat pipe design technique generally involves numerical analysis. All heat pipe design at TRW is accomplished with one of several digital computer programs which integrate the differential forms of the equations for the appropriate boundary conditions. These programs are outside the scope of this contract and will not be discussed here.

To illustrate the points to be made regarding the various design parameters, the closed form solution for the special case shown in Fig. 3-1 will be used as an example. This system consists of a tube with single evaporator and condenser sections at the ends of the pipe, with or without an intervening adiabatic section. The pipe geometry is assumed axially uniform as is the heat input and rejection.

4.1 Wick Design

The primary purpose of the heat pipe wick is to provide a capillary flow mechanism for liquid circulation. As such, it is clear from Eq. (4-1) that a "good" wick is one which generates a high capillary head while offering a minimal resistance to liquid flow. Furthermore, as discussed in Section 3.2, it is frequently the case that heat must be transferred through the saturated wick in both the evaporator and condenser sections. Thus, a "good" wick is also one which provides for this heat transfer with a minimum temperature drop.

4.1.1 Effective Pore Radii of Various Wicks

It was shown in Section 3.1.1 that the maximum capillary head is given by:

$$\Delta P_{cmax} = \frac{2\sigma\cos\psi}{r_{eA}} \qquad \text{(Class A wicks)} \qquad (3\text{-}4a)$$

$$\Delta P_{cmax} = \frac{2\sigma}{r_{eB}} \qquad \text{(Class B wicks)} \qquad (3\text{-}4b)$$

Thus, to maximize this quantity for a given fluid and material, one must minimize the effective pore radius r_{eA} or r_{eB}.

For certain well defined pore geometries, the effective pore radius can be determined analytically. Several examples, neglecting body force effects, are presented below.

Cylindrical holes:

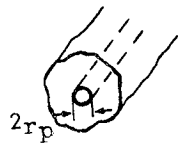

The isolated cylinder is the class A case for which Eq. (3-4a) was derived. Thus:

$$r_{eA} = r_p \quad \text{where } r_p \text{ is the actual pore radius.} \qquad (4\text{-}1)$$

Most wicks do not exhibit ideal cylindrical pores. However, one wick which approaches this--called the "parallel capillary channel" wick--has recently been developed [G9].

Rectangular grooves:

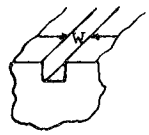

A popular wick geometry consists of axial grooves cut into the heat pipe wall. This is also a class A wick in that the lands between grooves separate adjacent menisci. As long as the groove depth is greater than half the groove width:

$r_{eA} = w$ where w is the groove width. (4-2)

Parallel wires:

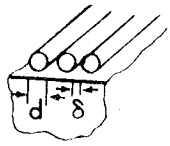

An interesting wick structure, first reported by Sweeney [H13], consists of a series of parallel wires spaced a given distance apart. This is similar to axial grooves but provides a re-entrant flow cavity. Thus, the ratio of capillary head to flow resistance will be higher than for the rectangular groove. This case will be developed in more detail to show the analytical method involved.

Using the model shown in Fig. 4-1, it is readily shown through a little geometry that the meniscus radius of curvature - R can be expressed in terms of the other variables as follows:

$$R = \frac{\frac{\delta}{2} + \frac{d}{2}(1 - \cos\beta)}{\cos(\beta - \psi)} \tag{4-3}$$

where:

- d - wire diameter
- δ - wire spacing
- R - meniscus radius of curvature
- ψ - wetting angle
- β - position in degrees around wire where liquid-vapor-solid contact exists

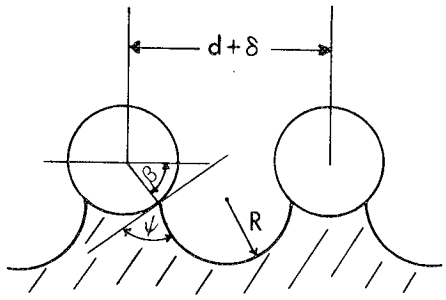

FIGURE 4-1. Capillary Model for Parallel Wire Wick

Assuming a class A wick and solving Eq. (3-4a) for r_{eA} by substituting Eq. (3-2) for ΔP_{cmax}, one sees that:

$$r_{eA} = \frac{2\cos\psi}{\left(\frac{1}{R_1} + \frac{1}{R_2}\right)_{max}} \tag{4-4}$$

For parallel wires (or axial grooves, etc.), one of the meniscus radii of curvature is infinite. Thus, Eq. (4-2) can be reduced to:

$$r_{eA} = 2\cos\psi\ R_{min} \tag{4-5}$$

where R_{min} is the minimum possible value for the meniscus curvature. For parallel wires R_{min} is the minimum value of R as given by Eq. (4-3).

Considering Eq. (4-3), it is immediately apparent that for zero wetting angle ($\psi = 0$), the minimum value of R is simply $\frac{\delta}{2}$, corresponding to $\beta = 0$. Thus, for $\psi = 0$, the effective pore radius is simply $r_{eA} = \delta$, which is similar to the result for straight-walled grooves. However, it is also apparent from Eq. (4-3) that this result does not hold for wetting angles other than zero. For this geometry it is possible for the meniscus to "roll around" the wire, altering the "effective" wire spacing. Thus, to solve the general case one must minimize Eq. (4-3) with respect to the angle β. Note that if a minimum exists in R for $\beta < 90°$ the maximum capillary head is determined by a minimum free energy condition and we indeed do have a class A wick. If no minimum exists for $\beta < 90°$ the meniscus will recede until adjacent menisci coalesce and we have a class B wick.

Differentiating Eq. (4-3) with respect to β, and setting $\partial R/\partial\beta$ equal to zero, one finds after a little algebra that the minimum R occurs when β satisfies the following equation:

$$\sin\ (\psi - \beta) = \frac{\sin\psi}{1 + \frac{\delta}{d}} \tag{4-6}$$

Since for wetting fluids $0 \leq \psi \leq 90°$, the right hand side of Eq. (4-6) is a positive number less than unity.

This, and the upper bound on ψ, limit the quantity $\psi-\beta$ to the first quadrant. Thus, the value of β at which R reaches a minimum is always equal to or less than ψ and is therefore $\leq 90°$; i.e., this is a class A wick.

We also see from Eq. (4-6) that the critical value of β is not generally zero, but varies with the wetting angle and the ratio δ/d. To determine r_{eA}, one must specify d, δ and ψ, solve Eq. (4-6) for β, solve Eq. (4-3) for R_{min}, and then determine r_{eA} from Eq. (4-5).

Fig. 4-2 shows the results of such computations for the general cases where $\delta = d$ and $\delta = 2d$. The effective pore radius is expressed in terms of the wire spacing: $r_{eA} = f\delta$, and the graph shows the variation in the factor f with the wetting angle.

As opposed to straight-walled grooves where the factor f is always unity, the parallel wire wick exhibits a decreasing value of f with increasing wetting angle. In other words, the ability of the meniscus to "roll around" the wires decreases the sensitivity of ΔP_{cmax} to the wetting angle.

Screen Mesh:

One of the most commonly used heat pipe wick materials is woven wire mesh. Although its popularity is in part due to precedent, it does offer certain features such as (1) a wide selection of readily available pore sizes, (2) ease of fabrication--especially of composite wick structures, and (3) low cost.

Wire mesh wicks are actually very complex and difficult to characterize. Their properties vary widely depending on whether single or multiple layers are used, how tightly adjacent layers contact each other,

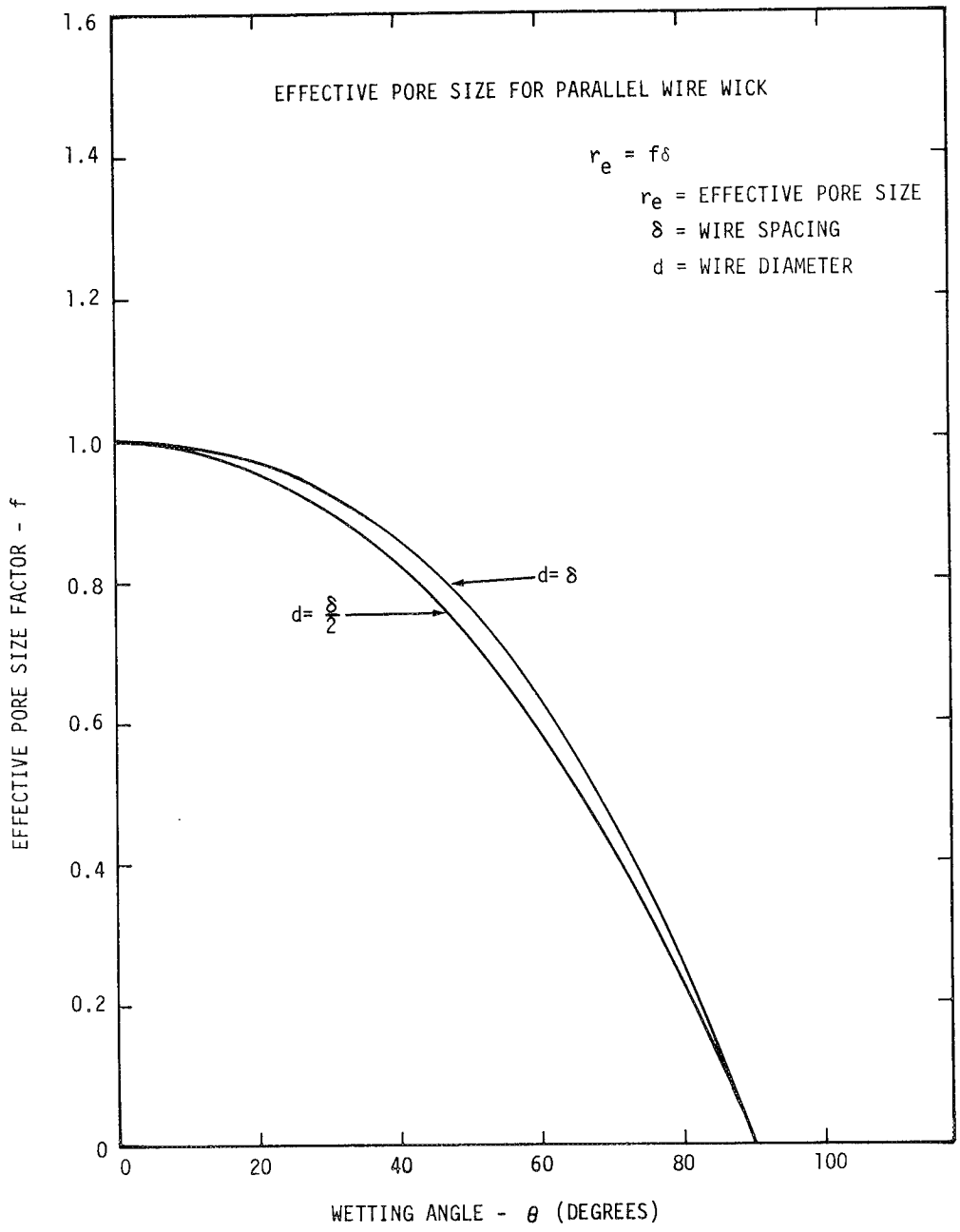

FIGURE 4-2. Effective Pore Size for Parallel Wire Wick

whether or not the evaporator end of the wick is sealed, etc. It will be assumed in this discussion that the wick layers are in close enough contact or that the evaporator end is sealed such that capillary pumping is limited by the mesh pores rather than the gaps between layers.

It might at first appear that a screen wick is similar to the parallel wire case just discussed. This, however, is not true by virtue of the multiple vs. single curvatures of the respective menisci. The meniscus formed in a screen pore is not a segment of a sphere but a complex geometry of varying curvature. To this author's knowledge, nobody has yet analytically studied the interfacial free energy of a screen pore meniscus to establish whether or not a minimum exists prior to coalescence of adjacent menisci. That is, it has not been analytically demonstrated whether screens represent a class A or class B wick.

Assuming a square mesh screen is a class B wick, Tien and Sun [H3] have shown that for single layers, the effective pore radius is given by:

$$r_{eB} = \frac{d + \delta}{2} \tag{4-7}$$

This formulation, which is independent of wetting angle, has successfully correlated the data of a number of investigators.

For multiple screen layers, Eq. (4-7) is no longer valid because of intermeshing between adjacent layers. No general correlation has been put forth for this case, but experience of several laboratories have shown that, in almost all cases,

$$\frac{\delta}{4} < r_e < \frac{\delta}{2} \tag{4-8}$$

Eq. (4-8) does not specify whether multi-layer screens represent class A or class B wicks. Insufficient data using multiple fluids with the same wick are available to reliably determine whether or not there exists a contact angle effect, and the uncertainty in the actual pore geometry

does not permit establishing whether measured capillary pressures correspond to minimum free energy menisci or menisci coalescence.

Because of the uncertainty in pore geometry of multi-layer screen wicks, and an observed irreproducibility depending on the degree of intermeshing, one should design these wicks conservatively. Thus, for single layer or loosely layered screen wicks, Eq. (4-7) is appropriate. For tightly wrapped multi-layer wicks, the upper bound of Eq. (4-8), assuming a class B wick ($r_{eB} = \frac{\delta}{2}$), will yield a conservative design.

Packed Sphere Beds, Metal Felts, Woven Cloths, etc.:

As with multi-layer screens, it has not yet been established whether materials in this category fall into class A or class B, or whether they vary depending on their microgeometry. This will have to await further study. However, from a design point of view, all of these materials exhibit behavior similar to the parallel wire wick in that, if they do suffer a class A limit, their dependence on wetting angle is much reduced by the ability of the menisci to "roll around" the fibers or particles. This, in addition to the fact that most fluid-material combinations exhibit very low wetting angles, allows the designer to neglect wetting angle effects and use Eq. (3-4b) for ΔP_{cmax}.

As opposed to cylindrical pores, grooves, single screen layers and parallel wires, materials of this type will have a distribution of pore sizes. Under such circumstances, the effective pore size varies with the level of wick saturation (the largest pores desaturate first). For cases where initial desaturation corresponds to heat pipe failure (e.g., a uniform wicked pipe with no boiling or body forces), the effective pore size is determined by the largest pores available. Under these circumstances, the literature [H3, T10, G10] suggests that:

For randomly packed sphere beds (a good approximation to sintered particle wicks):

$$r_{eB} = 0.41\ r_s \qquad (4\text{-}9)$$

where r_s is the sphere radii.

For fibrous wicks (e.g., metal felt):

$$r_{eB} = \frac{d + (32\ K/\phi)^{\frac{1}{2}}}{2} \tag{4-10}$$

where:

d is the fiber diameter

K is the permeability

Using Eqs. (4-7) for single layer screens, (4-9) for packed sphere beds, and (4-10) for metal felts, in conjunction with Eq. (3-4b) for ΔP_{cmax} in class B wicks, Tien and Sun [H3], have been able to correlate the data of numerous investigators on a single curve.

To summarize this discussion, it appears that there are two (at least) phenomena which give rise to a limit on pumping head, and thus which establish the effective pore size. One corresponds to the meniscus reaching a minimum free energy configuration (class A), and the other to the coalescence of adjacent menisci (class B). Wicks with isolated pores (e.g., parallel capillaries, grooves) are always of the class A type. Wicks with interconnecting pores may be either class A (parallel wires) or class B (single layer square mesh).

For well defined geometries it is often possible to analytically determine the failure mechanism and the effective pore size. For poorly defined geometries one must either empirically measure the appropriate effective pore size or, if available, use existing correlations.

Unfortunately, there exist very few correlations for r_e compared with the myriad of different wick materials and operating conditions (e.g., partial desaturation), and even those that exist are not as yet very well supported. Thus, measured wick property data is extremely

important to the heat pipe designer. A limited quantity of such data can be found in the open literature [H3, H4, H5, H11, H12, H14, T10, G3, G5, G11].

4.1.2 Permeability of Various Wicks

The permeability of a wick is an inverse measure of its flow resistance. Thus, a "good" wick has a high permeability.

As with the effective pore radius, it is possible to analytically determine the permeability of well defined capillary structures. The approach is to write an expression for the liquid pressure gradient--dP_ℓ/dz and equate it to Eq. (3-6) in order to solve for the permeability - K. Several examples follow for laminar flow.

Parallel Cylindrical Capillaries:

The pressure gradient for Poiseuille flow in a wick made up of cylindrical capillaries is given by:

$$\frac{dP_\ell}{dz} = \frac{8\mu_\ell \dot{m}_\ell(z)}{A\rho_\ell \phi r_p^2} \tag{4-11}$$

Equation (4-11), when combined with Eq. (3-6) yields:

$$K = \frac{\phi r_p^2}{8} \tag{4-12}$$

Axial Grooves, Parallel Wires, etc.:

Capillary structures consisting of grooves cut into the heat pipe wall or parallel wires laid against the wall can all be treated as a series of straight flow channels of various cross-section. Laminar flow solutions have been obtained for a large variety of flow cross-section shapes. These can all be reduced to a form similar to that for cylindrical channels which will yield approximate values for the liquid pressure gradient. Thus:

$$\frac{dP_\ell}{dz} = \frac{8\mu_\ell \dot{m}_\ell(z)}{A\rho_\ell \phi r_h^2} \cdot S \qquad (4\text{-}13)$$

where S is a shape factor dependent on the particular cross-sectional geometry, and r_h is the hydraulic radius, given by:*

$$r_h = \frac{2\ (\text{flow area})}{(\text{wetted perimeter})} = \frac{2A_F}{P_w} \qquad (4\text{-}14)$$

Values of the shape factor - S can be obtained from the literature for shapes whose laminar flow solutions are available [G12]. Typical values for heat pipe wicks range between 0.6 - 1.4. In the absence of a solution for a geometry similar to that of interest, one might simply use that for a circular duct; S = 1.0.

In Eq. (4-13) the product $A\phi$ is simply the total wick cross-sectional flow area, equal to the number of grooves (channels, etc.) multiplied by the flow area per groove. Unless the groove depth is large compared with its width, the curvature of the meniscus must be accounted for in computing A_F. Equation (4-13), when combined with Eq. (3-6) yields:

$$K = \frac{\phi r_h^2}{8S} \qquad (4\text{-}15)$$

Packed Sphere Beds (sintered particles):

The permeability of randomly packed sphere beds in the laminar flow regime is fairly well predicted by the Blake-Kozeny equation [G13]:

$$K = \frac{D_s^2 \phi^3}{150\ (1 - \phi)^2} \qquad (4\text{-}16)$$

---

*The use of the hydraulic radius for the characteristic dimension in Eq. (4-13) is somewhat arbitrary. The concept of the hydraulic radius is most useful in turbulent flow where it has been empirically demonstrated that it generally leads to a shape factor - S near unity. This is not true for laminar flow, as found in most heat pipes. However, using r_h is consistent with common practice, and in the absence of appropriate values for S, yields engineering estimates with S = 1.

where: D_s is the sphere diameter.

Metal Felts, Woven Cloths, etc.:

Wicks of this nature are difficult to treat analytically or by correlation. Tien and Sun [H3] argue that the permeability, porosity and effective pore diameter (for flow) are related in such materials as follows:

$$K = \frac{D_e^2 \phi}{32} \tag{4-17}$$

They also suggest that the effective pore size for flow is simply related to the effective pore size for capillary pumping (substituting D_e for $(32K/\phi)^{\frac{1}{2}}$ in Eq. (4-10). However, this assumes a class B wick, and even at that, has yet to be substantiated to any degree.

Thus, once again, measured wick property data are required to effectively design heat pipes with this type of wick. As with the effective pore size radius, a limited quantity of such data can be found in the open literature [H4, H5, H11, H12, T10, G3, G11].

Screen Mesh:

As mentioned earlier, the properties of screen mesh wicks vary widely depending on the degree of intermeshing between adjacent layers, etc. However, it is the case that loosely wrapped screen wicks have lower flow resistance than tightly wrapped or sintered wicks. Thus, using results for tightly wrapped wicks provides a conservative design approach.

Schmidt [G11] has presented a correlation for the pressure drop in wire mesh wicks based on experimental data for screens of 45 through 270 mesh. He was able to correlate all of his low Reynolds number data ($Re < 15$) with a modified form of the Blake-Kozeny equation as follows:

$$\frac{dP_\ell}{dz} = - \frac{\rho_\ell v_o^2}{D_p} \frac{(1 - \phi)}{\phi^3} \left(\frac{275}{Re} + 3.1 \right) \tag{4-18}$$

where the Reynolds number is defined as:

$$Re = \frac{D_p v_o \rho_\ell}{\mu_\ell} \left(\frac{1}{1 - \phi} \right) \tag{4-19}$$

and:

v_o - average liquid velocity

D_p - 1.5 times screen wire diameter

Equation (4-18) can be considerably simplified at little cost in accuracy if one drops the constant 3.1 as insignificant compared with 275/Re for small Re. With this assumption Eq. (4-18) can be equated with Darcy's Law for dP_ℓ/dz (Eq. (3-6)) to yield:

$$K = \frac{d^2}{122} \frac{\phi^3}{(1 - \phi)^2} \tag{4-20}$$

where d is the screen wire diameter. Also, an expression for the porosity of wire mesh wicks may easily be derived from the geometry of screens (neglecting intermeshing):

$$\phi = 1 - \frac{\pi F M d}{4} \tag{4-21}$$

where:

M - wires per inch

F - crimping factor* ($\approx$1.05)

Note that Eq. (4-20) is now identical to the Blake-Kozeny expression for permeability of packed beds (Eq. (4-16)) except for the empirical constant.

Equations (4-20) and (4-21) have been fairly successful at correlating data on screen wicks. Fig. 4-3 shows the data of several investigators compared with the predicted curve. The large quantity of data by

---

*The crimping factor accounts for the fact that screens are not simply crossed rods.

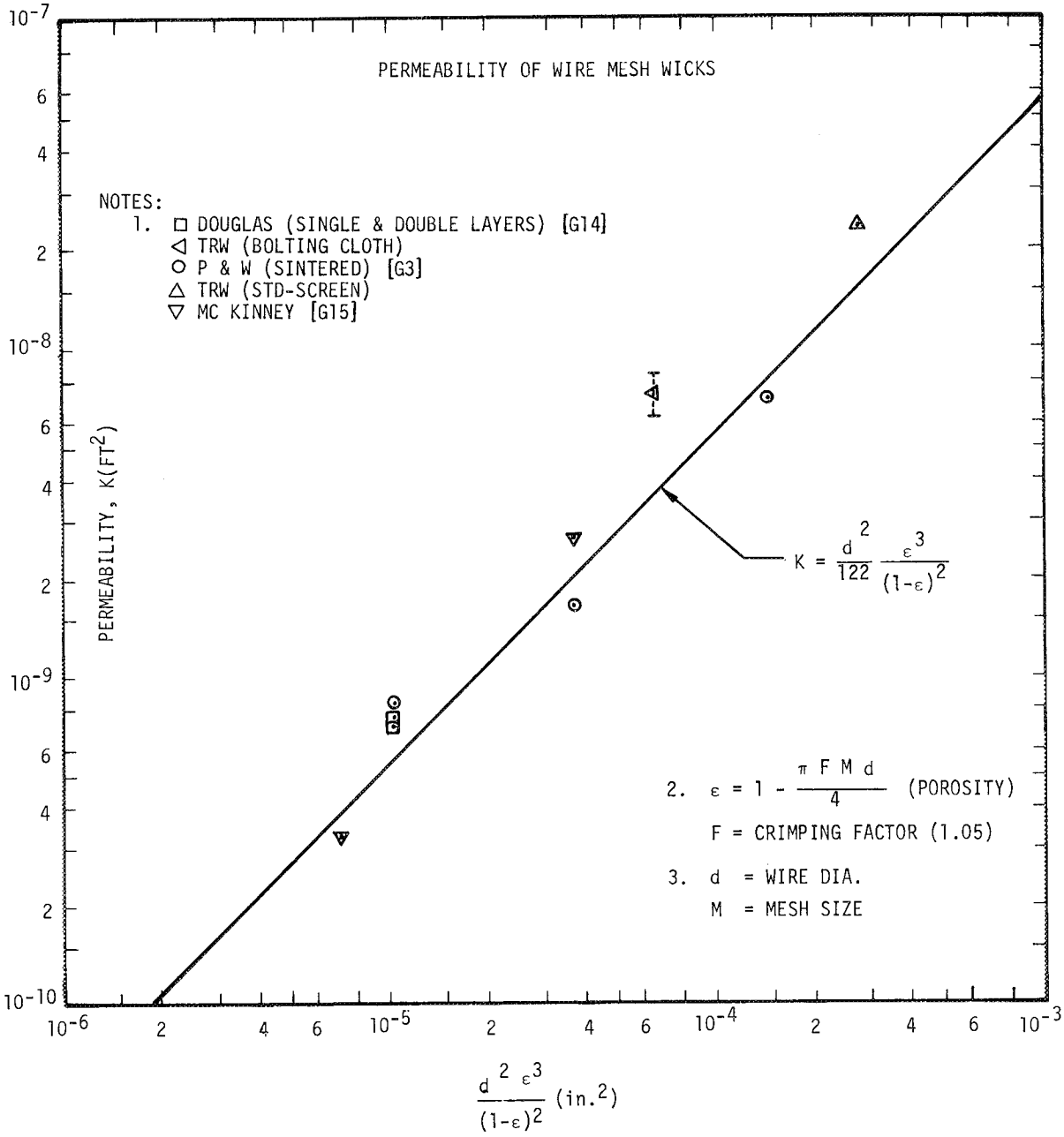

FIGURE 4-3. Permeability of Wire Mesh Wicks

Schmidt [G11] from which the equations were derived, and thus successfully correlate, is not shown.

4.1.3 Wick Optimization

It is always a desirable goal to design and build optimized heat pipes. Consequently, the heat pipe literature is full of heat pipe optimization analyses. Unfortunately, many of these analyses are not really pertinent--and some are actually incorrect. The basic difficulty here is in establishing the appropriate basis on which to perform the optimization. Depending on the application, the optimum heat pipe may be based on maximum hydrodynamic capacity, minimum temperature drop, minimum weight, minimum cost, maximum reliability, maximum life, maximum conductance ratio (for variable conductance pipes), etc. In practice, in designing a heat pipe for a particular application one must consider all of these criteria, weighted according to their relative importance, and perform trade-offs between them to arrive at an overall optimum design. Unfortunate as it may be, this does not generally reduce to the simple task of differentiating a single equation with respect to a single variable and setting the derivative equal to zero.

Hydrodynamic Criterion:

Not only is a simple extremizing procedure frequently inappropriate, it is sometimes misleading. For example, the heat pipe optimizing procedure most commonly seen in the literature [H1, G4] involves a hydrodynamic optimization. A pressure balance is written for the fluid cycle and extremized with respect to "the" appropriate capillary dimension of the wick (pore size). In this way, a relationship is derived for the optimum pore (groove, etc.) size which, when substituted in the pressure balance, leads to an optimum liquid/vapor flow area ratio and hence an optimum heat pipe based on hydrodynamic capacity.

In the first place, the equations derived in this manner are frequently misused, for most wicks (e.g., screen mesh, felt metal, foam metal,

woven fibers, etc.) are not truly homogeneous and isotropic, and therefore are not characterized by a single dimension (e.g., pore size). In other words, the porosity and tortuosity factors, which are treated as constants in this extremizing procedure, are themselves generally functions of the pore size. This functionality must be, and seldom is, included in the pressure balance before it is extremized with respect to the pore size. This can lead to a substantially different result for the optimum pore size than that generally seen in the literature for isotropic wicks.

These points can readily be illustrated by treating the case of wire mesh wicks. The pressure balance equation for the heat pipe shown in Fig. 3-1 at the capillary pumping limit was given by Eq. (3-21).

$$\left.\begin{matrix}\frac{2\sigma\cos\psi}{r_{eA}} \\ \frac{2\sigma}{r_{eB}}\end{matrix}\right\} = \Delta P_{cmax} = \frac{Q(L + L_a)\mu_\ell}{2\pi K\rho_\ell\lambda(R_w^2 - R_v^2)} + \frac{4Q(L + L_a)\mu_v}{\pi\rho_v\lambda R_v^4} + \rho_\ell g\left[D_w\sin\theta + L\cos\theta\right] \tag{3-21}$$

The procedure in hydrodynamically optimizing the wick is first to maximize the heat transport rate - Q with respect to the wick microstructure. For simplicity, we shall assume a zero degree wetting angle and the upper bound of Eq. (4-8) for r_e so that distinctions between class A and class B wicks disappear. Thus, the maximum capillary head is given by $\Delta P_{cmax} = 4\sigma/\delta$.

If one now substitutes Eq. (4-20) for K in Eq. (3-21), and Eq. (4-21) for ϕ in Eq. (4-20), the pressure balance equation can be re-written after some algebraic manipulation as follows:

$$\frac{4\sigma}{\delta} = \frac{Q(L + L_a)\mu_\ell}{2\pi\rho_\ell \lambda(R_w^2 - R_v^2)} \left\{ \frac{122\pi^2}{16} \frac{(FM)^2}{(1 - \frac{\pi FMd}{4})^3} \right\} + \frac{4Q(L + L_a)\mu_v}{\pi\rho_v \lambda R_v^4}$$

$$+ \rho_\ell g \left[D_w \sin\theta + L\cos\theta \right] \tag{4-22}$$

In extremizing with respect to the wick microstructure, many of the terms in Eq. (4-22) are constant. Thus, the equation can be simplified considerably by defining the following constant groupings:

$$A = \frac{(L+L_a)\mu_\ell}{2\pi\rho_\ell \lambda(R_w^2 - R_v^2)} \left(\frac{122\pi^2}{16} \right)$$

$$B = \frac{4\mu_v(L+L_a)}{\pi\rho_v \lambda R_v^4} \tag{4-23}$$

$$C = \rho_\ell g \left[D_w \sin\theta + L\cos\theta \right]$$

With these substitutions, and noting that $Md = 1 - M\delta$, Eq. (4-22) can be rearranged to yield:

$$Q = \frac{\frac{4\sigma}{\delta} - C}{\left[\frac{A(FM)^2}{(1 - \frac{\pi F}{4} + \frac{\pi FM\delta}{4})^3} + B \right]} \tag{4-24}$$

It is clear from Eq. (4-24) that the wick cannot be characterized by a single variable as is frequently assumed,* but depends on both M and δ (or d and δ since $Md = 1 - M\delta$). Thus, to properly optimize the wick, one must extremize Eq. (4-24) with respect to both of these variables to find the maximum Q in the three-dimensional (Q, M, δ) space. This extremizing procedure is algebraically very cumbersome and is best performed numerically.

---

*By assuming the porosity and tortuosity constant, the denominator is reduced to $\frac{A'}{\delta^2} + B$.

The wick optimization procedure for screens is substantially simplified if it can be assumed that the vapor pressure loss - ΔP_v is small compared with the other terms in the pressure balance equation. Experience has shown that this is frequently the case in the design of thermal control heat pipes which must be tested in a 1-g field.

If ΔP_v is small enough so that its variation with Q can be neglected in comparison with that of ΔP_ℓ, it can be treated as a constant in Eq. (4-22). Then the constant grouping B in Eq. (4-23) can be modified to include Q:

$$B' = \frac{4Q\mu_v(L + L_a)}{\pi\rho_v\lambda R_v^4} \tag{4-25}$$

The equivalent form of Eq. (4-24) now becomes:

$$Q = \frac{\frac{4\sigma}{\delta} - B' - C}{\frac{A(FM)^2}{(1 - \frac{\pi F}{4} + \frac{\pi FM\delta}{4})^3}} \tag{4-26}$$

This equation is much easier to extremize algebraically. Differentiating with respect to δ and setting the result equal to zero yields an optimum screen wire spacing for fixed M:

$$\delta_{opt} = \frac{4\sigma}{3(B'+C)} + 4\left[\frac{\sigma^2}{9(B'+C)^2} - \frac{(1 - \frac{\pi F}{4})}{3\pi FM(B'+C)}\right] \tag{4-27}$$

The wire spacing - δ_{opt}, as given by Eq. (4-27) yields a maximum value of Q for a given mesh. It is interesting to consider whether there similarly exists an optimum mesh size. Differentiating Eq. (4-26) with respect to M (holding δ constant) does yield an extremum, as follows:

$$M_{extremum} = \frac{8(1 - \frac{\pi F}{4})}{\pi F\delta} \tag{4-28}$$

However, if one examines the second derivative $(\partial^2 Q/\partial M^2)$, one finds it is positive at this value of M. On the other hand, the second derivative with respect to δ $(\partial^2 Q/\partial \delta^2)$ is negative at the extremum.

Thus, Eq. (4-28) does not yield an optimum value of M. Rather, the point in the (Q, δ, M) space defined by Eqs.(4-27) and (4-28) is a saddle point corresponding to a maximum in Q with respect to δ but a minimum in Q with respect to M.*

Examining Eq. (4-26) directly, in light of Eq. (4-27) for δ_{opt}, it can be shown that the required departure from the extremum of Eq. (4-28) is in the direction of increasing mesh size. One wants to use the highest mesh possible for a given wire spacing.

The design procedure for optimizing the wick thus reduces to the simultaneous solution of Eq. (4-27) which relates δ_{opt} to M and a table or graph of δ vs. M for available screen meshes. This procedure is shown on Fig. 4-4. The curve represents Eq. (4-27) showing a typical variation of δ_{opt} with M. The points on the graph represent δ, M couples for generally available screen mesh. The optimum wick corresponds to the screen of largest mesh size which falls on (or near) the curve.

Equation (4-27) for δ_{opt} was derived for the specific heat pipe shown in Fig. 3-1. However, it is easily generalized. If one replaces the constants $B' + C$ with ΔP_o and includes a safety factor - S defined by:

$$\Delta P_{cmax} = S\ (\Delta P_{\ell} + \Delta P_v \pm \Delta P_b) \qquad (4\text{-}29)$$

the equivalent form of Eq. (4-27) becomes:

---

*It is interesting to note that if Eq. (4-28) is substituted into Eq. (4-27), one finds that this saddle point corresponds to the condition where $\Delta P_{\ell} = \frac{1}{2} \Delta P_{cmax}$. This is the criteria suggested by Cotter [H1] for optimum wicks.

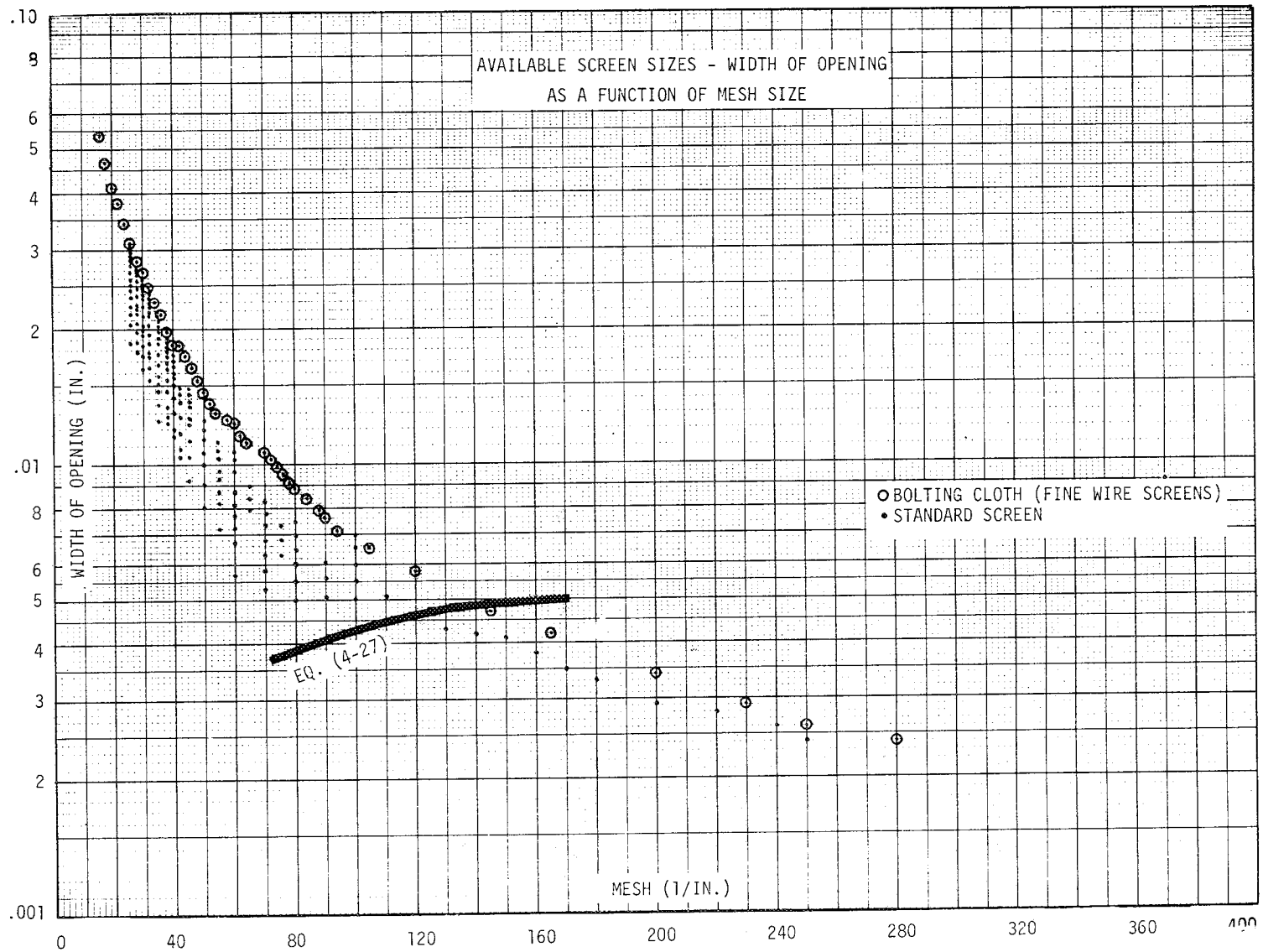

FIGURE 4-4. Wire Mesh Optimization Graph

$$\delta_{opt} = \frac{4\sigma}{3S\Delta P_o} + 4\left[\frac{\sigma^2}{9S^2\Delta P_o^2} - \frac{(1 - \frac{\pi F}{4})}{3\pi FSM\Delta P_o}\right] \qquad (4\text{-}30)$$

Equation (4-30) now allows optimizing the wick for a desired safety factor, which should always be considered in heat pipe design. Furthermore, the term ΔP_o now represents a generalized "loading" on the wick. In other words, the capillary head available for liquid pumping in the wick is given by:

$$\Delta P_{\ell avail} = \frac{\Delta P_{cmax}}{S} - \Delta P_o \qquad (4\text{-}31)$$

Thus, Eq. (4-30) can also be used for heat pipes with axial variations in wicking (hybrid wicks - see Fig. 3-3e). For example, if a pipe had a different wick in the evaporator than in the adiabatic section and condenser, ΔP_o would include the liquid pressure drop in the condenser and adiabatic section when optimizing the evaporator wick; i.e., $\Delta P_o = \Delta P_v + \Delta P_b + (\Delta P_\ell)_{cond + adiab.}$

Also, since Eq. (4-30) does not include specific wick dimensions, it can be used for wicks of any cross-sectional configuration; i.e., it is not limited to annular wicks as shown on Fig. 3-1.

Heat Transfer Criterion:

Even more important than avoiding the use of isotropic wick optimization procedures for non-isotropic wicks, one must exercise great care to assure that the optimization criterion used is the appropriate one.

For example, if one uses the appropriate procedure to obtain the optimum pore size, and then varies the wick thickness to alter the liquid/vapor flow area ratio, the resulting curve for maximum heat transfer vs. area ratio will appear as shown in Fig. 4-5a.

As seen in this figure, there will exist an optimum area ratio based on hydrodynamic considerations. For isotropic wicks under zero body force conditions, the vapor core should represent 2/3 of the total flow area. However, this is a strong function of the body force field.

One must recognize, however, that the hydrodynamic optimum may well correspond to an evaporator input heat flux which far exceeds the conduction heat transfer limit (i.e., there must exist internal vapor generation). Under such conditions, the equations that led to this optimum, which are based on Darcy flow through fully saturated wicks, are no longer applicable and the entire analysis is invalid. The generally utilized heat pipe hydrodynamic equations are only valid for fully saturated wicks and thus, for operation below the conduction heat transfer limit in the evaporator (see Sec. 3.2.1.2).

Of course, this conduction heat transfer limit is also a function of wick thickness (Eq. (3-29)) and can thus be superimposed on Fig. 4-5a to yield Fig. 4-5b. The hydrodynamic limit curve, based on flow in fully saturated wicks, is only valid to the left of the intersection between the two curves. For liquid metals this intersection usually falls to the right of the extremum and the hydrodynamic optimum wick, determined in this way, is appropriate. However, for ordinary fluids, the curves generally intersect to the left of the extremum. If the wick design is one that cannot sustain internal vapor generation, the optimum pipe corresponds to the intersection of the two curves. On the other hand, if the wick can sustain internal vapor generation, the optimum pipe would fall to the right of this intersection but Q_{max} will no longer be given by the hydrodynamic limit curve determined for saturated flow. Vapor generation within the wick will certainly impede liquid flow so that the actual hydrodynamic curve might appear as shown dotted in Fig. 4-5c. The actual shape of this curve cannot, at present, be determined by analytical means. This would require an ability to predict capillary flow in the presence of internal vapor generation. Although data for isolated cases and fluids are available, the results

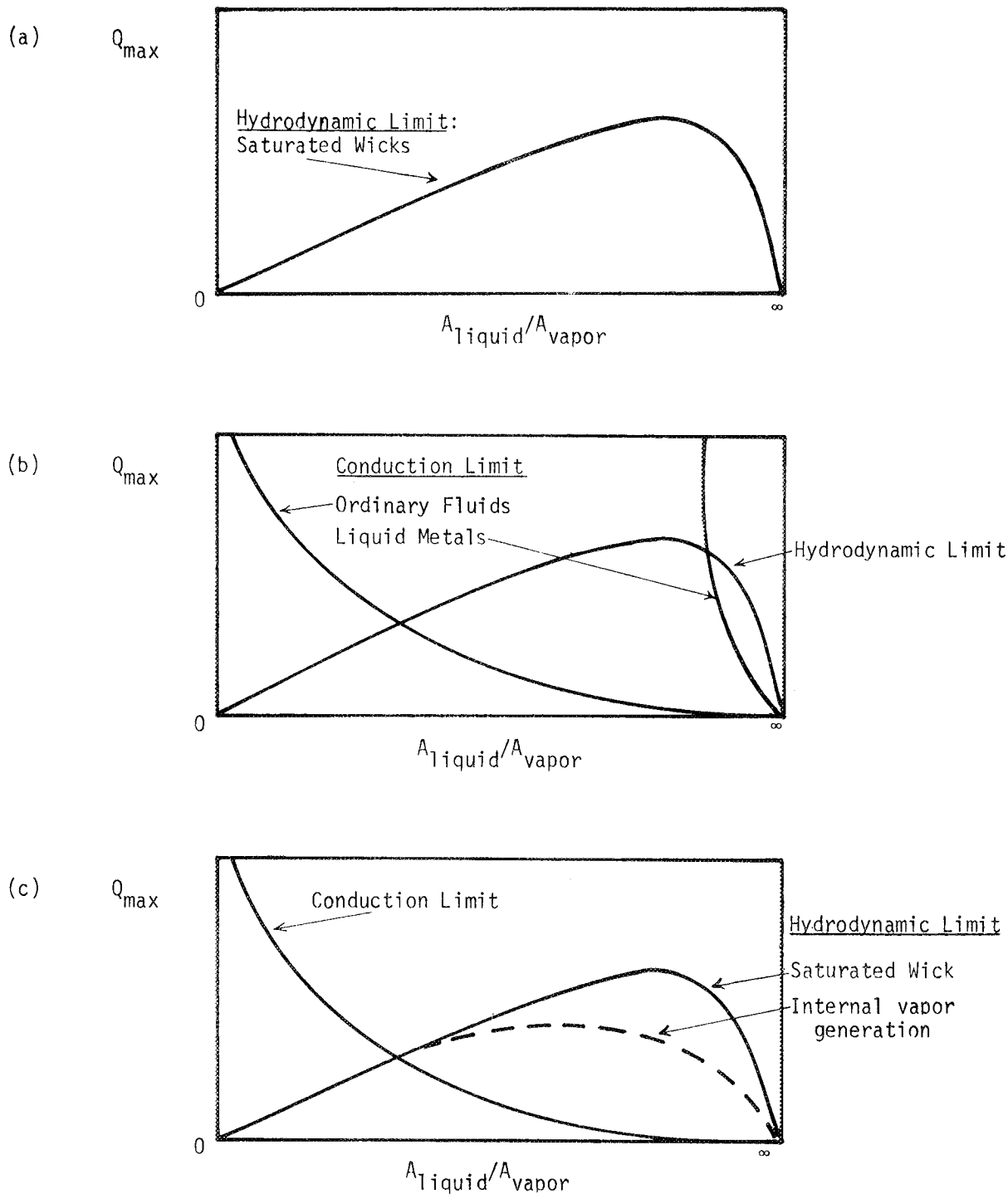

FIGURE 4-5. Heat Pipe Optimization

are not sufficient to enable the development of an empirical set of equations at this time.

The basic point to be gleaned from this discussion is that when optimizing heat pipes one must consider all pertinent phenomena and parameters. As seen, hydrodynamic optimization may violate heat transfer limits. It may also lead to heat pipes which are far from minimum weight, maximum conductance, etc. All such criteria must be considered in light of their relative importance when designing a heat pipe for a particular application.

4.1.4 Composite Wicks

It was seen in Sec. 4.1.1 that the maximum capillary head generated by a wick increases with decreasing pore size, which would suggest using wicks with small pores. On the other hand, it was seen in Sec. 4.1.2 that wick permeability increases with increasing pore size, which would suggest using wicks with large pores. Indeed, it is this diverse dependence on pore size which gives rise to an optimum pore size as discussed in Sec. 4.1.3.

A similar statement can be made regarding wick thickness. Increasing wick thickness decreases liquid flow resistance and thus raises heat pipe capacity. However, increasing wick thickness also increases the wick's thermal resistance and thus lowers heat pipe capacity by virtue of a lower maximum evaporator heat flux. This trade-off gives rise to an optimum wick thickness as discussed in Sec. 4.1.3.

Unfortunately, it is often the case that optimum heat pipes designed in this way are limited to low axial throughputs. This is especially true for spacecraft thermal control heat pipes which use relatively poor working fluids (compared with liquid metals). Furthermore, even for throughputs of only a few tens of watts, the temperature drop across the pipe can become excessive. Consequently, experience has shown that conventional designs with homogeneous wick-lined walls are inappropriate for high performance heat pipes.

The difficulty with such heat pipes arises because of the opposite dependence of key phenomena on the same variable. If the maximum capillary head and wick permeability were not dependent on the same (or related) pore size, it would be possible to make both large simultaneously. Similarly, if wick flow area and evaporator thermal resistance were not dependent on the same dimension, it would be possible to simultaneously increase the former and decrease the latter. In other words, one wants to de-couple capillary pumping from flow resistance in the wick, and axial wick hydrodynamics from radial heat transfer in the pipe. This has given rise to heat pipes with composite wicks.

Figure 4-6 shows four composite capillary structures which have been used in heat pipes to effect the de-coupling discussed above.

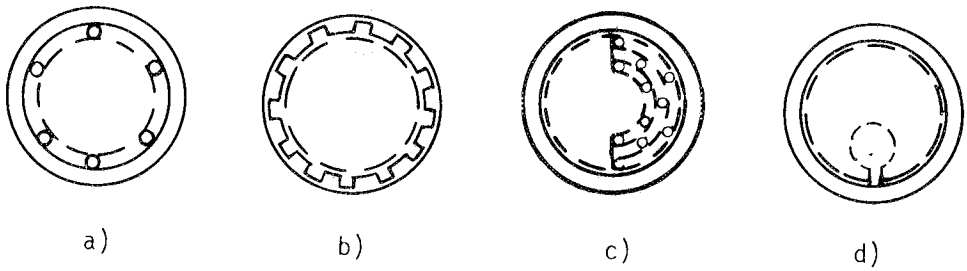

FIGURE 4-6. Composite Wick Heat Pipes

Configuration (a) represents a concentric annular artery formed by spacing a capillary surface (screen or otherwise) away from the tube wall with wires. In this way, a low axial flow resistance (high permeability) is obtained, corresponding to the resistance of the annular gap, while simultaneously achieving a high capillary pumping head representative of the pore size of the capillary surface. Thus, by departing from a homogeneous wick it is possible to de-couple the capillary head and wick permeability.

It should be noted that in this, and all other arterial wick structures, the local maximum capillary head is determined by the largest available pore or opening. Consequently, it is necessary that the capillary surface be sealed at the evaporator end and along its length to prevent any openings or holes that are larger than the pores of the wick material. The condenser end can be left open in cases where there doesn't exist any liquid-vapor pressure differential at that point (see Sec. 3.1.6).

The fact that the artery is sealed makes it particularly susceptible to internal boiling. If vapor is generated within an artery, its path of least resistance is to expand along the artery and cause it to empty of liquid. This, of course, eliminates the heat pipe's liquid pumping capability. Thus, great care must be exercised in design to assure that vapor does not form within or penetrate the artery.

This points up a drawback in the arterial design of configuration (a), for the heat must pass through the artery to reach the vapor-liquid interface for evaporation. Thus, the artery gap thickness is limited to that which causes a temperature drop sufficient to cause nucleation of vapor bubbles at the evaporator wall (within the artery). In other words, the axial hydrodynamics and radial heat transfer are still coupled through the wick thickness.

This situation is improved somewhat with configuration (b) which represents an axially grooved heat pipe wall with a cover layer of screen mesh or some other fine-pored material. Again, a low resistance axial flow path is provided by the grooves while the fine-pored cover provides a high capillary head. This system is less sensitive to the nucleation problem because almost all of the radial heat transfer is shunted through the metallic lands between the grooves and thus the superheat at the base of the grooves is not much higher than that at the groove-wick interface. There still will exist some liquid superheat in the grooves, the minimum corresponding to the temperature drop through the liquid-saturated wick covering both the grooves and lands. However,

this is rather insensitive to the grooves' depth and hence this wick structure does tend to de-couple the heat transfer (through the lands) from the hydrodynamics (through the grooves).

A deficiency of the grooved wall design is that one achieves large liquid flow areas at the expense of increased wall thickness, which can result in heavy heat pipes. Another geometry which accomplishes a similar heat transfer-hydrodynamic de-coupling with thin walled pipes is shown as configuration (c). In this case a thin wick lines the entire tube wall and a partial annular artery (or series of them) is placed asymmetrically along a portion of the wall. In this system, the portion of the pipe with the thin wick is utilized for heat transfer while the opposite side is used for fluid flow. This configuration permits considerable lattitude in liquid flow area without altering the pipe wall or the heat transfer path. Also, it allows for high perpendicular body force fields such as might be found on spinning spacecraft. The thin wick need only be sufficient to handle the circumferential flow to and from the artery. This allows for minimum heat conduction paths and hence small input and output temperature drops.

Configuration (d) represents a pedestal-type internal artery (or arteries) with a thin wick lining the tube wall. As with configurations (b) and (c), this geometry de-couples the heat transfer (through the thin wick) from the axial hydrodynamics (through the artery). However, a major advantage of this geometry is that the artery is removed from the heat input zone. Since the artery is surrounded by vapor, the fluid within it can be no hotter than saturation temperature. Consequently, since there exists no arterial superheat, there can be no arterial nucleation. Thus, a serious failure mode of arterial heat pipes is eliminated. One must only assure that no vapor generated at the wall penetrates the artery. For ordinary fluids this can readily be done by providing a very fine-pored wick layer to serve as a vapor barrier between the artery and the wall wick.

For moderate evaporator heat fluxes with ordinary fluids in conventional heat pipes, the circumferential wick in configurations (c) and (d) can usually be made thin enough to avoid nucleation, and with it the problem of controlling the vapor formed. However, in the case of variable conductance heat pipes which involve non-condensible gases, the superheat tolerance of the working fluids is much reduced (see Sec. 3.2.1.1). Under such circumstances it appears best to utilize a capillary structure for circumferential pumping which assures a non-boiling, surface evaporation heat transfer mode.

Very impressive results have been obtained along these lines [G6, G11] by replacing the wick lining the tube wall with a series of closely spaced circumferential grooves in the wall (actually, the wall can be internally threaded). Radial heat transfer in this case is almost exclusively through the metal lands between grooves. Conduction through the liquid is only through a very thin layer at the sides of the menisci (Fig. 4-7). In this way, the input temperature drop can be reduced to such small values that nucleation can generally be avoided even in the presence of non-condensible gases. Of course, the output temperature drop is similarly reduced, yielding a very high conductance heat pipe.

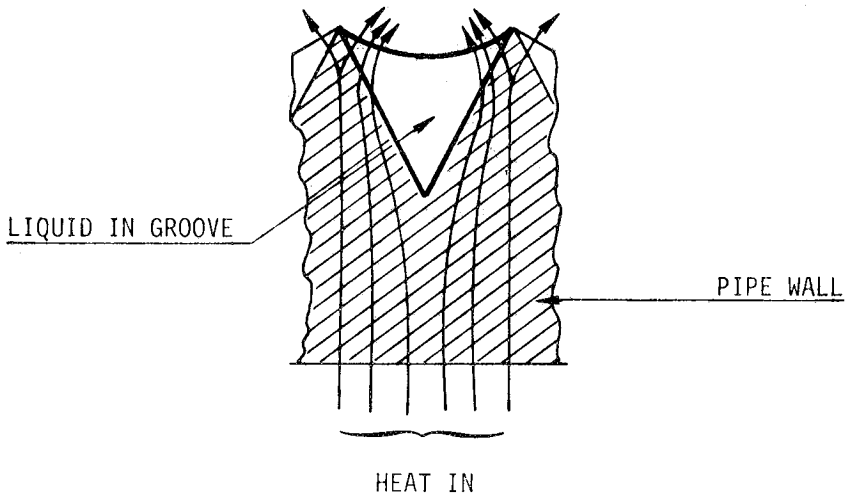

FIGURE 4-7. Heat Flow Path for a Circumferentially Grooved Heat Pipe

4.1.4.1 Designing Composite Wicks

The composite wick geometries shown in Fig. 4-6 represent but a small fraction of those which have been employed in heat pipe design. Many additional configurations are possible which serve the same primary purposes. These are:

(1) To de-couple flow resistance from capillary head
(2) To de-couple radial heat transfer from axial fluid flow

Depending on the requirements of a particular application, one might wish to design for either one or both of these criteria. Thus, for liquid metal pipes where radial heat transfer through the liquid poses no problem, the annular artery (Fig. 4-6a), which only accomplishes criterion (1), represents an excellent design.

Should an application arise which requires a heat pipe with a very low overall temperature drop but not a particularly high axial heat transport capacity, the best design might be based on criterion (2) alone. Such a design is shown in Fig. 4-8. The axial fluid flow is carried in a primary homogeneous wick, while the circumferential fluid flow and radial heat transfer are handled by circumferential grooves cut in the pipe wall. With such designs, the wick flow area can be increased without affecting the input or output temperature drop.

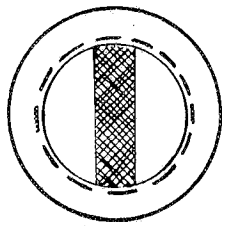

HOMOGENEOUS WICK/CIRCUMFERENTIAL GROOVES

FIGURE 4-8. Non-Arterial Composite Wick Design - Radial Heat Transfer De-coupled from Axial Liquid Flow

In many applications, however, the requirements call for both high axial heat transport capacity and low temperature drop. Since the working fluids suitable for spacecraft thermal control are characterized by low thermal conductivities, this often calls for a design which satisfies both criteria. One then requires arterial heat pipes such as those shown in Fig. 4-6b, c, d.

When designing homogeneous wick heat pipes of the class shown in Fig. 4-8, one uses the same design criteria discussed previously, with one important exception. Since the wick flow area can be varied without effecting the temperature drops, one can now optimize the homogeneous wick on hydrodynamic criteria alone. Boiling in the wick is no longer a factor (see Sec. 4.1.3).

When designing arterial heat pipes, however, the wick design criteria change. The purpose of arteries is to allow independent design of the capillary pumping head and the flow resistance. When the artery is completely filled with liquid the capillary head corresponds to the pore size of the material forming the artery while the flow resistance corresponds to the internal artery configuration. Since decreasing the pore size of the artery wall material does not alter the axial flow resistance, there is no longer an optimum pore size as discussed in Section 4.1.3. One wants to use the smallest pore size possible, consistent with (1) available materials, (2) fabricability, (3) pressure drop due to flow into or out of the artery itself, and (4) under certain circumstances, consideration of pore plugging due to erosion or mass transport.

The axial flow resistance of an artery is independent of the artery wall pores. It is determined solely by the internal artery dimensions (e.g., the gap sizes in Fig. 4-6a, c; the groove dimensions in Fig. 4-6b; the artery diameter in Fig. 4-6d). To decrease flow resistance one simply increases these dimensions.

In the absence of body forces (e.g., gravity, centrifugal force, etc.) there is no theoretical limit to the size of the artery other than the geometry of the heat pipe. However, if the pipe must operate in a body force field such as is required for 1-g testing, a constraint is added. It is true that an artery, once filled with liquid, will remain full under expulsive forces up to the maximum capillary head producible by the pores of the artery wall. However, should the artery be partially or fully depleted of liquid, it is necessary to design for automatic refill; i.e., the artery should be self-priming under the surface tension forces provided by its internal dimensions.

The self-priming requirement establishes a limit on the internal dimensions of an artery. For example, the gap of an annular artery (Fig. 4-6a) develops a capillary head given by:

$$\Delta P_{cmax} = \frac{2\sigma}{\delta} \cos\psi \tag{4-32}$$

where δ is the gap width.

For a horizontal heat pipe in a 1-g field, this artery will self-prime if ΔP_{cmax} exceeds the hydrostatic head of liquid corresponding to the pipe diameter.

$$\frac{2\sigma\cos\psi}{\delta} > \rho_\ell D_w \frac{g}{g_o} \tag{4-33}$$

Thus, the maximum gap size is given by:

$$\delta \leq \frac{2\sigma\cos\psi}{\rho_\ell D_w \, g/g_o} \tag{4-34}$$

From a practical point of view, the gap width must be designed smaller than that given by Eq. (4-34). One should always allow a safety factor for manufacturing tolerance. However, even more important in very long heat pipes, it may not be possible to test the pipe in a perfectly horizontal position. Any deviation from horizontal must be added to

the D_w term in Eq. (4-34), since the priming requirement of the liquid is from the lowest point in the system to the highest point within the artery.

In the annular artery heat pipe treated as an example, the self-priming requirement establishes the maximum size of the artery. This, however, does not limit the capacity of a heat pipe since multiple arteries can be used. Fig. 4-6c shows an example of a series of partial annular arteries stacked side by side. Each gap is sized to self-prime; but by placing several in parallel, a large flow capacity can be achieved. Similarly, the screen covered grooves of Fig. 4-6b actually represent a series of arteries where each of the grooves is sized to self-prime.

A final consideration regarding arterial priming is whether or not the artery must self-prime under load. The self-priming criteria previously discussed refer to the case where there is no heat transfer load on the heat pipe. However, it will often be the case in actual applications that it is not possible to completely remove the load on a heat pipe to allow self-priming in the event of arterial failure. For example, the artery of a spacecraft heat pipe may be drained of liquid during launch, and expected to self-prime when the spacecraft enters orbit. It may well be possible to provide reduced load conditions during this phase of the time-line, but it will seldom be possible to provide zero load conditions.

To establish the load under which an artery can self-prime, one uses a criterion similar to that for no-load priming except that the flow losses (pressure drops) are added to the relevant body forces when equated to the capillary head generated by the internal artery dimensions (<u>not</u> the artery wall). For example, Fig. 4-9 shows the self-priming capacity for a pedestal artery as a function of the artery diameter, using ammonia as a working fluid. It is interesting to note that, under 0-g conditions, the load under which the artery can self-prime continually increases with artery diameter, since the flow resistance decreases more

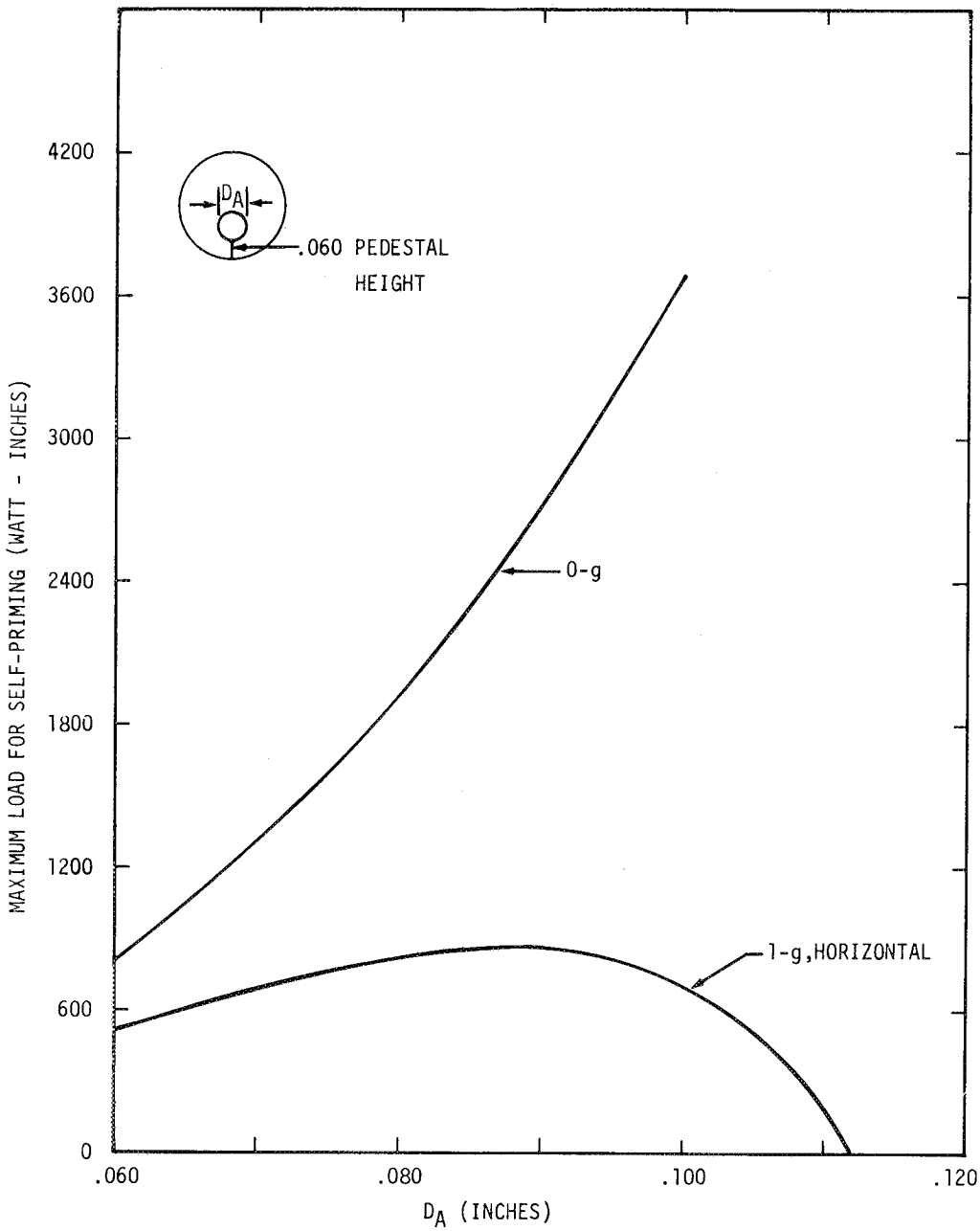

FIGURE 4-9. Self-Priming Capacity of Pedestal Artery Heat Pipe with Ammonia Working Fluid

rapidly ($\propto \frac{1}{D_A^4}$) than the capillary head ($\propto \frac{1}{D_A}$). On the other hand, for a horizontal pipe under 1-g conditions, an optimum artery size exists by virtue of the hydrostatic head which "comes off the top" of the available capillary head.

It should also be noted that the maximum load for self-priming also represents the capacity of the artery if the evaporator end were not sealed.

Although the heat transfer and hydrodynamic design of arterial pipes is fairly straight forward, arteries are characterized by several unique design and manufacturing problems.

As discussed earlier, the local maximum capillary head of a filled artery is determined by the largest available pore or opening. This requires careful fabrication of the artery to assure it is sealed along its length and at the evaporator end.

A more elusive problem is to assure that the artery is completely filled. If an artery contains bubbles, the maximum capillary head will not correspond to the pores of the artery wall but to the bubble radius. If the bubble locally fills the artery, this reduces to the capillary head of the artery itself. In either case, the pumping capability of the artery is very much reduced. (In the latter case, it is reduced to the self-priming capacity.)

There are several ways in which bubbles can be generated in an artery. As discussed previously, if the liquid in the artery is sufficiently superheated, nucleation of vapor bubbles is possible. Furthermore, even if boiling does not occur within the artery itself, boiling in close proximity could lead to vapor penetration.

It is also possible to generate arterial bubbles during initial fill or any subsequent repriming of the artery made necessary by liquid expulsion

due to vibration, shock, excessive tilting, excessive heat load, etc. If the artery walls are self-wetting, they are generally wetted before the interior fills, permitting bubbles to be trapped inside.

A third mechanism for generating arterial bubbles is peculiar to heat pipes which contain non-condensible gases, whether to aid in start-up from the frozen state or for use in gas-controlled variable conductance heat pipes. Under operating conditions, the non-condensible gas in such heat pipes is swept to the condenser end where it forms a gas plug. This gas plug acts as a diffusion barrier to the flowing vapor, causing the blocked region of the condenser to fall in temperature. Because the solubility of gases in liquids varies inversely with temperature, the axial temperature gradient caused by gas blockage represents a potential bubble forming mechanism within arteries. The gas dissolves in the liquid at the cold, gas-blocked region of the condenser. As the liquid flows back to the hot evaporator, part of the gas comes out of solution due to its decreased solubility at the higher temperature.

The formation of arterial bubbles would not represent a particularly serious problem if mechanisms existed for their rapid elimination under ordinary operating conditions. Unfortunately, this does not appear to be the case.

The fact that the artery is sealed everywhere* by a wetted wall makes physical expulsion usually impossible. By using a non-self-wetting artery wall (e.g., a single layer of screen), Bienert [G-16] has demonstrated that the artery wall can be locally dried by overheating, allowing bubbles to escape. However, this approach will often be unacceptable in actual applications in that it involves at least a temporary failure of the arterial system.

---

*Under conditions where one portion of the heat pipe always represents the condenser, the artery need not be sealed at that end.

If the bubbles cannot escape through the artery wall, the remaining removal mechanism is for them to collapse. Pure vapor bubbles will rapidly collapse within a uniform temperature, non-superheated liquid due to surface tension forces. However, if the liquid in the artery is superheated, vapor bubbles of sufficient size will grow and displace the liquid in that region.

Unfortunately, it is also possible to sustain relatively stable bubbles within a non-superheated artery if they contain non-condensible gas. Relatively small quantities of non-condensible gas within the bubbles can increase their internal total pressure (vapor pressure plus partial pressure of gas) sufficiently to stabilize them against the surface tension forces trying to collapse them. In an operating heat pipe, such bubbles can only collapse by the diffusion of the stabilizing non-condensible gas through the wetted artery wall into the vapor core. This is, however, a very slow process. Bienert [G16] reports typical collapse rates of elongated arterial bubbles on the order of $\sim 10^{-4}$ cm/sec.

In view of these bubble stability considerations, what can the heat pipe designer do to assure successful operation of arterial heat pipes? In the first place, it appears that fabricating the artery with non-self-wetting walls (e.g., a single layer of screen) avoids the problem of bubble entrapment during arterial priming. Second, one should design to avoid arterial superheat. If the hydrodynamic requirements permit, this can be assured by utilizing a "hybrid" wick design where the artery is constrained to the condenser and adiabatic section, and a homogeneous wick is utilized in the superheated evaporator section. This simultaneously avoids problems of nucleation within the artery and penetration of vapor due to boiling in close proximity to the artery. Also, it assures that pure vapor bubbles within the artery will collapse.

Finally, there remains the problem of eliminating gas-stabilized bubbles in heat pipes containing non-condensible gases. At this point, the only practical removal mechanism which has been identified is diffusion of

the stabilizing gas out of the artery through the wetted artery wall. Although this is indeed a slow process, the significance of the rate is only in comparison with the rate in which such bubbles are formed. If, through proper design, one avoids entrapment of bubbles during priming, and generation or penetration of bubbles due to boiling, the only apparent mechanism for bubble formation is that due to gas accumulation as a consequence of an existing temperature gradient combined with the inverse solubility of gas in the liquid. However, this is also a very slow process. Thus, the relevance of this problem is a question of relative rates of gas accumulation by virtue of solubility variations and gas removal by diffusion.

To the author's knowledge, this problem has not yet been treated analytically and thus no general statements can be made. There is, however, some limited experimental data available which indicate that, at least in certain cases, the gas removal rate by diffusion is sufficient to avoid gas accumulation in the artery. Long term successful operation of gas-loaded arterial heat pipes has been achieved at TRW for water-nitrogen with an annular artery (Fig. 4-6a) and methanol-nitrogen with an asymmetric artery (Fig. 4-6c). In addition, successful life tests of ammonia-helium systems with a pedestal artery (Fig. 4-6d) have been reported in the literature [G8].

4.2 Fluid Inventory

An important design consideration in the manufacture of all heat pipes is to determine the appropriate quantity of working fluid with which to fill the pipe. Excess fluid in a heat pipe is undesirable from two points of view. First, under 0-g conditions (and, in some cases, 1-g conditions) the constant flow of vapor from evaporator to condenser pumps the excess fluid to the condenser end, forming a liquid plug which "shuts off" that portion of the condenser which it fills. If the application calls for a short condenser length, this could be a critical factor. Second, excess fluid in a heat pipe can slosh within the vapor core, leading to undesirable effects on spacecraft dynamics.

On the other hand, a deficiency of working fluid is also undesirable. If the capillary structure is characterized by a single pore size (e.g., identical axial grooves), the fluid deficiency appears at the evaporator end leading to local dryout. The degree of dryout which can be tolerated depends on the particular application and how much axial conduction the pipe wall (or saddles, etc.) can provide.

If the heat pipe contains an artery, even a small fluid deficiency will prevent the artery from filling, leading to grossly reduced performance.

The most tolerant wick system with respect to underfill is a homogeneous wick with a pore size distribution (e.g., metal felt). In this case the fluid deficiency does not all appear at the end of the evaporator, but is spread among the larger pores all along the wick. The small pores in the evaporator continue to pump liquid.

Once again, however, the pumping capacity of the wick will be reduced. Because the wick is partially desaturated, the liquid flow area is reduced. To make matters worse, it is the largest pores (those of minimum flow resistance) which are unavailable for flow. Furthermore, the available capillary head is reduced because the maximum local liquid pressure need no longer be equal to the vapor core pressure (see Sec. 3.1.6). Instead it will be reduced by the capillary head corresponding to the largest pores which remain filled at the point of zero axial condenser flow.

We thus see that, qualitatively, homogeneous wicks can tolerate underfill but with reduced capacity. To analytically quantify the reduction in capacity requires detailed knowledge of the pore size distribution in the wick and the permeability as a function of desaturation. Since this information is generally not available for homogeneous wicks, it is currently necessary to determine the effects of underfill empirically for the particular wick involved.

4.2.1 Fluid Inventory Variations

According to the previous discussion, there are undesirable consequences of either over-filling or under-filling a heat pipe. Ideally, one should introduce just enough inventory to completely saturate the wick structure. Unfortunately, this is generally impossible in practical heat pipes. This is because both the liquid volume and the wick inventory requirements vary within a given heat pipe as a function of operating conditions. Several phenomena leading to this behavior are as follows:

- If a wick is saturated under no-load conditions, fluid will be expelled when the pipe is under load due to meniscus recession at the wick surface.
- If boiling occurs in the evaporator, fluid will be expelled by vapor within the wick.
- Homogeneous wicks with pore size distributions can partially desaturate when operated in a body force field (e.g., tilted against gravity).
- The liquid density, the vapor density and the void volume all vary with operating temperature, but not in proportion to each other. Consequently, 100% fill at one temperature corresponds to either over-fill or under-fill at other temperatures.

The relative importance of these phenomena depend on the type of wick structure used and the nature of the application. However, for space-craft thermal control heat pipes, the most troublesome source of volume variation is the last one. Fortunately, this problem can be handled analytically.

The following assumptions are made in the analysis:

(1) The pipe has a constant cross-section along its entire length.
(2) The wick is always fully saturated.

(3) The pipe is filled to 100% theoretical at temperature T_0.

(4) Thermal expansion or contraction of the wall and wick is negligible compared with liquid and vapor density variations. Calculations have shown that this is a very good assumption.

The basis of the analysis is that the mass of working fluid within the heat pipe is a constant. Thus,

$$m = \rho_\ell V_\ell + \rho_v V_v = \text{constant} \tag{4-35}$$

where:

- m - mass of working fluid
- ρ_ℓ - liquid density
- ρ_v - vapor density
- V_ℓ - liquid volume
- V_v - vapor volume

Using the subscript "0" for conditions when the pipe is filled, and the subscript "T" for operating conditions, Eq. (4-35) can be written:

$$(\rho_\ell V_\ell)_0 + (\rho_v V_v)_0 = (\rho_\ell V_\ell)_T + (\rho_\ell V_\ell)_T \tag{4-36}$$

Solving Eq. (4-36) for $V_{\ell T}$ yields:

$$V_{\ell T} = \frac{(\rho_\ell V_\ell)_0 + (\rho_v V_v)_0 - (\rho_v V_v)_T}{\rho_{\ell T}} \tag{4-37}$$

For uniform pipe cross-section and saturated wicks; and for the case of net liquid expansion:

$$\left.\begin{aligned} V_{\ell 0} &= \phi A_w L_p \\ V_{v0} &= A_v L_p \\ V_{vT} &= A_v (L_p - L_{ex}) \end{aligned}\right\} \tag{4-38}$$

where:

ϕ - wick porosity
A_w - wick cross-sectional area
A_v - vapor core cross-sectional area
L_p - length of pipe
L_{ex} - length of liquid slug in condenser due to net liquid expansion

Substituting Eq. (4-38) into Eq. (4-37) yields:

$$V_{\ell T} = \frac{\rho_{\ell 0}\phi A_w L_p + \rho_{v0} A_v L_p - \rho_v A_v (L_p - L_{ex})}{\rho_{\ell T}} \tag{4-39}$$

But, the length of the excess liquid slug in the condenser can also be expressed in terms of volumes, lengths and areas, as follows:

$$L_{ex} = \frac{V_{\ell T} - V_{\ell 0}}{A_v} = \frac{V_{\ell T} - \phi A_w L_p}{A_v} \tag{4-40}$$

Now substituting Eq. (4-39) for $V_{\ell T}$ in Eq. (4-40), and performing some algebra, one arrives at the following expression for L_{ex}/L_p, the length of the excess fluid slug ratioed to the pipe length.

$$\frac{L_{ex}}{L_p} = \frac{(\rho_{\ell 0} - \rho_{\ell T})\,\phi \frac{A_w}{A_v} + (\rho_{v0} - \rho_{vT})}{\rho_{\ell T} - \rho_{vT}} \tag{4-41}$$

Equation (4-41) is the desired result. It expresses the length of the excess fluid slug at any operating temperature as a function of the pipe geometry and the temperature at which it was filled to 100% of theoretical.

It is interesting to examine the behavior of this equation as a function of operating temperature. Fig. 4-10 shows this behavior for an ammonia heat pipe filled to 100% theoretical at 15°F. L_{ex}/L_p is plotted as a function of operating temperature with the geometrical grouping $\phi A_w/A_v$ as a parameter.

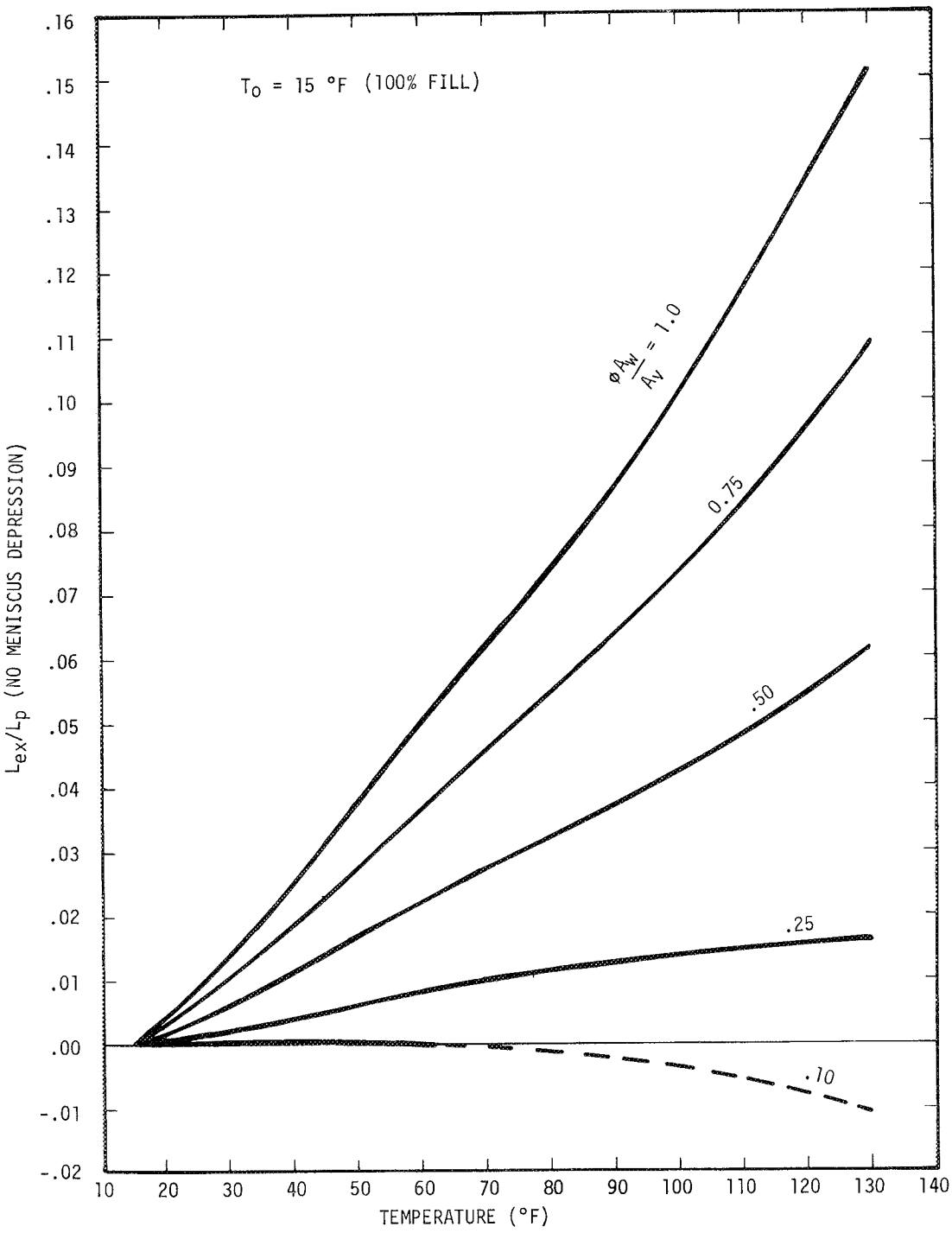

FIGURE 4-10. Liquid Volume Variation with Operating Temperature - Ammonia

As one would expect, the excess fluid slug, as a percent of pipe length, increases with the wick to vapor core area ratio. However, it is particularly interesting to note that L_{ex}/L_p does not necessarily increase with operating temperature. At low values of $\phi A_w/A_v$, L_{ex}/L_p can actually decrease with increasing T, and can even be negative.*

The reason for this behavior is that, although as temperature increases the liquid density decreases causing fluid expulsion, the vapor density also increases resulting in a conversion of liquid to vapor. If the liquid volume to vapor volume ratio is small enough ($\propto \phi A_w/A_v$), liquid to vapor conversion in greater than liquid expansion, and an increase in temperature results in a net decrease in liquid volume.

The critical value of $\phi A_w/A_v$ at which a change in operating temperature from T_0 to T results in no change in liquid volume can be deduced from Eq. (4-41) by setting L_e/L_p equal to zero. Thus,

$$\left(\phi \frac{A_w}{A_v}\right)_{L_{ex}=0} = - \frac{\rho_{v0} - \rho_{vT}}{\rho_{\ell 0} - \rho_{\ell T}} \tag{4-42}$$

The negative values of L_{ex}/L_p on Fig. 4-10 are, of course, not physically realistic, but correspond to the case of decreased liquid volume leading to wick desaturation. To obtain the percent desaturation for such cases, a similar analysis is performed in terms of a percent wick desaturation rather than L_{ex}.

The implications of these results depend, of course, on the type of wick system used. For example, heat pipes with arterial wicks generally have low values of the parameter $\phi A_w/A_v$. Thus, assuming a value of 0.1, an ammonia heat pipe which must operate above 60°F should be filled to 100% theoretical at the highest anticipated operating temperature, or else the artery would be partially empty and not function at that temperature.

---

*A negative L_{ex} is not a physical reality but corresponds to wick desaturation. More will be said about this later.

4.3 Excess Fluid Reservoirs

As discussed in the last section, it is not possible to fill a heat pipe such that it has 100% theoretical inventory under all operating conditions. However, as was also pointed out, both overfill and underfill conditions are undesirable. In fact, under certain circumstances, both conditions are intolerable. An example of such conditions would be a long, arterial heat pipe with a very short condenser. A fluid deficiency would result in failure of the artery while a fluid excess might block the condenser to an intolerable degree.

Under such circumstances, one can incorporate a capillary excess fluid reservoir in the wicking system. This concept, developed for the Ames Heat Pipe Experiment on this contract, is simply an additional capillary structure placed within the heat pipe to act as a "sponge". The pore size of the reservoir must be larger than any of those in the primary wick structure (including arteries) such that it does not draw liquid from the wick unless it is fully saturated. However, it will draw liquid from the tube itself, and thus prevents build-up of a liquid slug at the condenser end.

By using a capillary excess fluid reservoir, the pipe can be filled to 100% theoretical under minimum fluid volume and maximum wick saturation conditions. The reservoir volume should be sized to hold the maximum fluid excess generated by the anticipated variation in operating conditions. In this way, all fluid volume variations are taken up by the capillary reservoir. The primary wicks remain saturated and a condenser liquid slug is prevented under all operating conditions.

One must, however, use care in the sizing and placement of such "sponges" in the heat pipe. The simplicity of the concept under static conditions can lead to improper design, for the device must operate under dynamic conditions. Thus, the maximum capillary head generated by the excess fluid reservoir must not simply be larger than that of the vapor core, but must exceed the local liquid pressure depression in the wick. If not, the reservoir could not pump liquid from a slug at the end of the condenser.

Analytically, this criterion can be expressed as follows:

$$(\Delta P_{cmax})_{reservoir} > \left[\Delta P_{\ell} + \Delta P_{v} + \Delta P_{b}\right]_{(Z)_{res}}^{(Z)_{P_{\ell}}} = P_{v} \qquad (4\text{-}43)$$

where the bracket represents the integrated pressure losses from the position of the excess fluid reservoir to the point where the liquid and vapor static pressures are equal.

Graphically, this criterion is shown on Fig. 4-11 for a heat pipe operating in the absence of body forces (e.g., 0-g). Figure 4-11 represents a pressure balance curve similar to those discussed in Sec. 3.1.6. The bracketed terms on the right hand side of Eq. (4-43) are represented by the vertical distance between the ΔP_{v} and ΔP_{ℓ} curves.

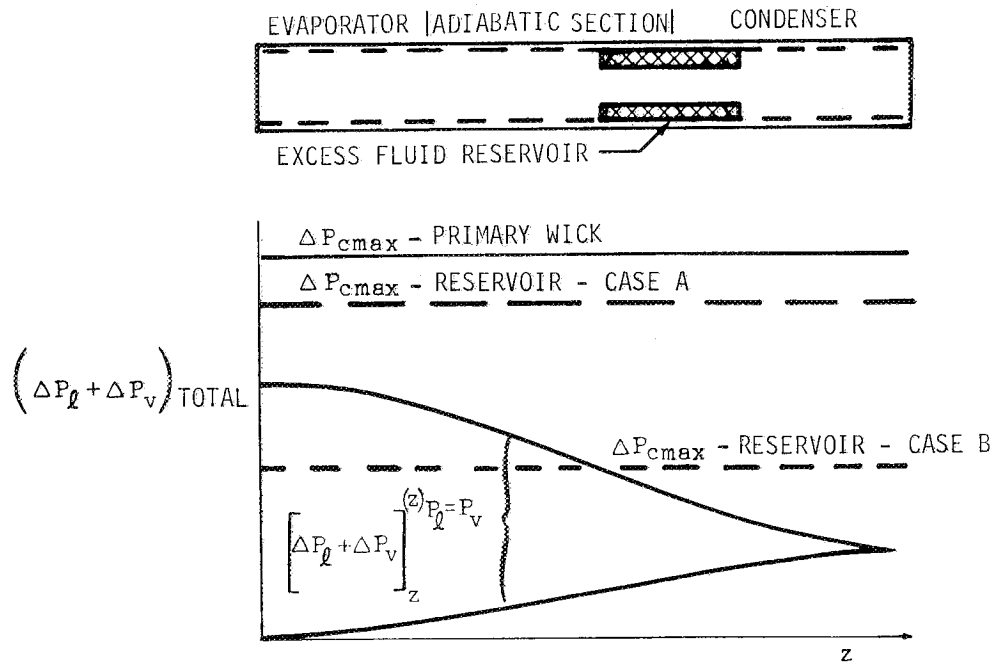

FIGURE 4-11. Pressure Balance Criterion for Locating Excess Fluid Reservoir

Thus, if $(\Delta P_{cmax})_{res}$ is greater than $\Delta P_{\ell} + \Delta P_{v}$ everywhere in the pipe, the excess fluid reservoir can be placed anywhere in the system (e.g., case A). On the other hand, if $(\Delta P_{cmax})_{res}$ is not greater than $\Delta P_{\ell} + \Delta P_{v}$ at all points (e.g., case B), the excess fluid reservoir must be placed in a region where this criterion does hold; i.e., to the right of the point where $\Delta P_{\ell} + \Delta P_{v} = (\Delta P_{cmax})_{res}$.

4.4 Working Fluid

The selection of the appropriate working fluid for a given application is based on many considerations. These include:

(a) operating temperature range
(b) heat transfer requirements
(c) expected body-force field (e.g., 0-g, 1-g, etc.)
(d) tolerance of wick structure to boiling
(e) type of heat pipe (conventional or variable conductance)
(f) special requirements
(g) materials compatibility and stability

Brief discussions of these considerations follow.

4.4.1 Operating Temperature Range

Clearly, a heat pipe cannot be operated below the freezing point or above the thermodynamic critical point of its working fluid. Thus, the first criteria for selection of a fluid is that these two thermodynamic conditions bracket the required operating temperature range.

These conditions, however, actually represent lower and upper bounds which are seldom approached. Most often, the low end of a given fluid's operating temperature range is established by adverse vapor dynamics (sonic limit, entrainment limit, or simply excessive ΔP_{v}) due to low vapor densities and corresponding high vapor velocities. The high end of the temperature range is frequently set by the mechanical aspects of containing the fluid vapor pressure.

4.4.2 Heat Transfer Requirements

The axial heat transport requirement can have a major impact on the choice of working fluid. Different fluids will yield different capillary pumping limits for the same wick structure. Thus, the case can easily arise where a simple homogeneous wick design can be substituted for a complex arterial wick design by the choice of fluid.

To determine the best fluid for a given application, one must theoretically examine optimal designs for each fluid by integrating the loss equations to determine their respective capillary pumping limit (see Sec. 3.1.6). Sometimes this is actually necessary since, in the general case, there is no simple grouping of fluid properties which serves as a basis for selection. There do, however, exist such groupings for special cases which at least provide some general guidelines. Thus, for a heat pipe operating in the absence of body forces and for which the vapor pressure drop is negligible, the capillary pumping limit can be shown to be proportional to the grouping $(\sigma\rho_\ell\lambda/\mu_\ell)$, sometimes referred to as the "liquid transport factor" or "0-g figure of merit". Figure 4-12 shows the liquid transport factor for the principal fluids of interest in spacecraft thermal control as a function of operating temperature. Additional curves for many other fluids can be found in the literature [G4, G14, G17].

Although this grouping applies to the special case of negligible body forces and vapor pressure drop, those conditions do pertain to many spacecraft thermal control applications so that this is a valid basis of comparison for such heat pipes. However, as mentioned previously, it is not of general value. As Joy [G4] has shown, the presence of even small body forces (e.g., acceleration fields) can render this basis of comparison invalid for cryogenic fluids.

4.4.3 Expected Body-Force Field

As pointed out in the last section, the presence of body forces can have a major impact on the relative performance of various fluids. This situation is due to two phenomena: (1) the body force head is

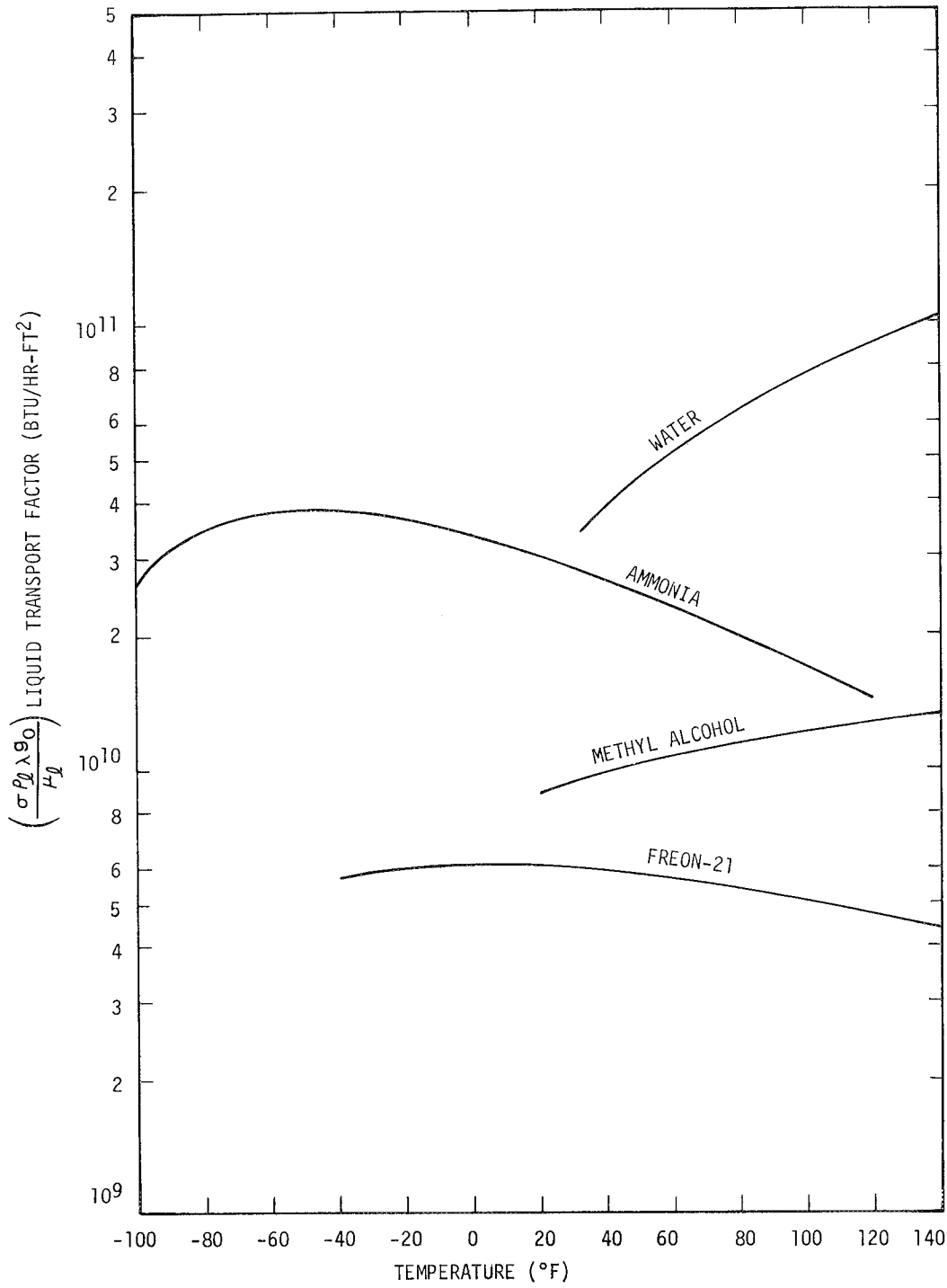

FIGURE 4-12. Liquid Transport Factor for Heat Pipe Working Fluids

subtracted from the maximum capillary head in establishing the pumping head available to overcome flow losses, and (2) the body force head must be overcome by surface tension effects in order to prime arteries, etc.

Since, in both cases, the problem is one of surface tension forces working against body forces, the ratio of these forces represents a basis of fluid comparison. In terms of fluid properties, this ratio is proportional to the grouping (σ/ρ_ℓ). Thus, to minimize adverse body-force effects, one should select a fluid with a high value of this parameter. Fig. 4-13 shows the variation in (σ/ρ_ℓ) with operating temperature for the principal spacecraft thermal control fluids.

4.4.4 Tolerance of Wick Structure to Boiling

In the last two sections, fluids were compared on the basis of their hydrodynamic and hydrostatic properties. However, as has been emphasized in this report, one must also consider radial heat transfer in the evaporator, especially if boiling would seriously degrade hydrodynamic performance (e.g., nucleation with arteries). The criteria for nucleation were discussed in Section 3.2.1.1. Assuming the critical radius (r_n) in Eq. (3-27) for the critical superheat is equal to the wick pore size, the pertinent fluid property grouping for superheat tolerance is $(\sigma/\lambda\rho_v)$. Multiplying this grouping by the thermal conductivity of the liquid yields a measure of the fluids' radial heat transfer tolerance with respect to nucleation. Fig. 4-14 shows the variation of this parameter $(k\sigma/\lambda\rho_v J)$ with operating temperature for the principal spacecraft thermal control fluids.

4.4.5 Conventional or Variable Conductance Heat Pipe

The fluid selection criteria discussed so far apply to all heat pipes. However, if one is designing variable conductance heat pipes, additional criteria may be involved, depending on the control scheme. Thus, heat pipes which employ vapor throttling as a control mechanism require low pressure working fluids. Similarly, the non-condensible

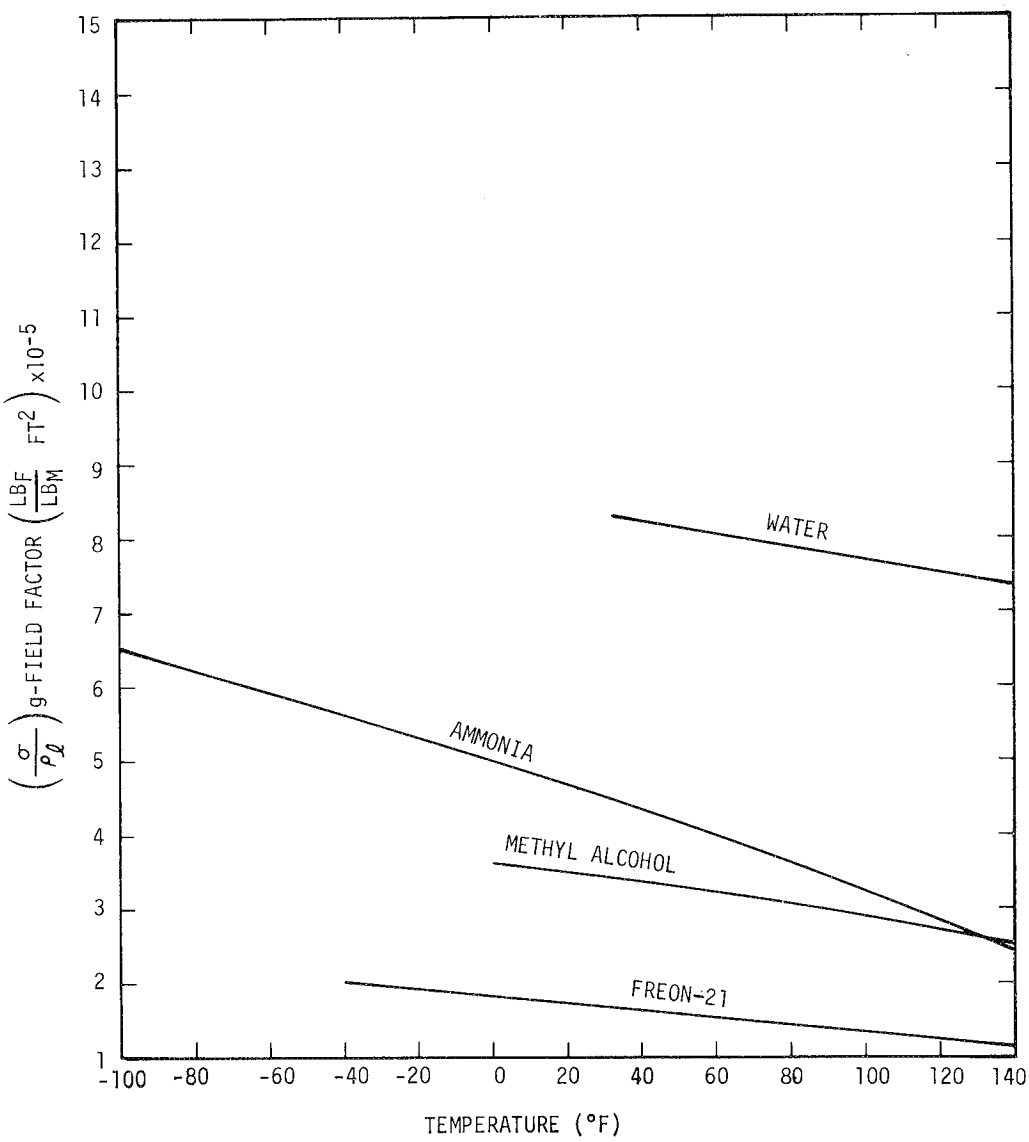

FIGURE 4-13. g-Field Figure of Merit for Heat Pipe Working Fluids

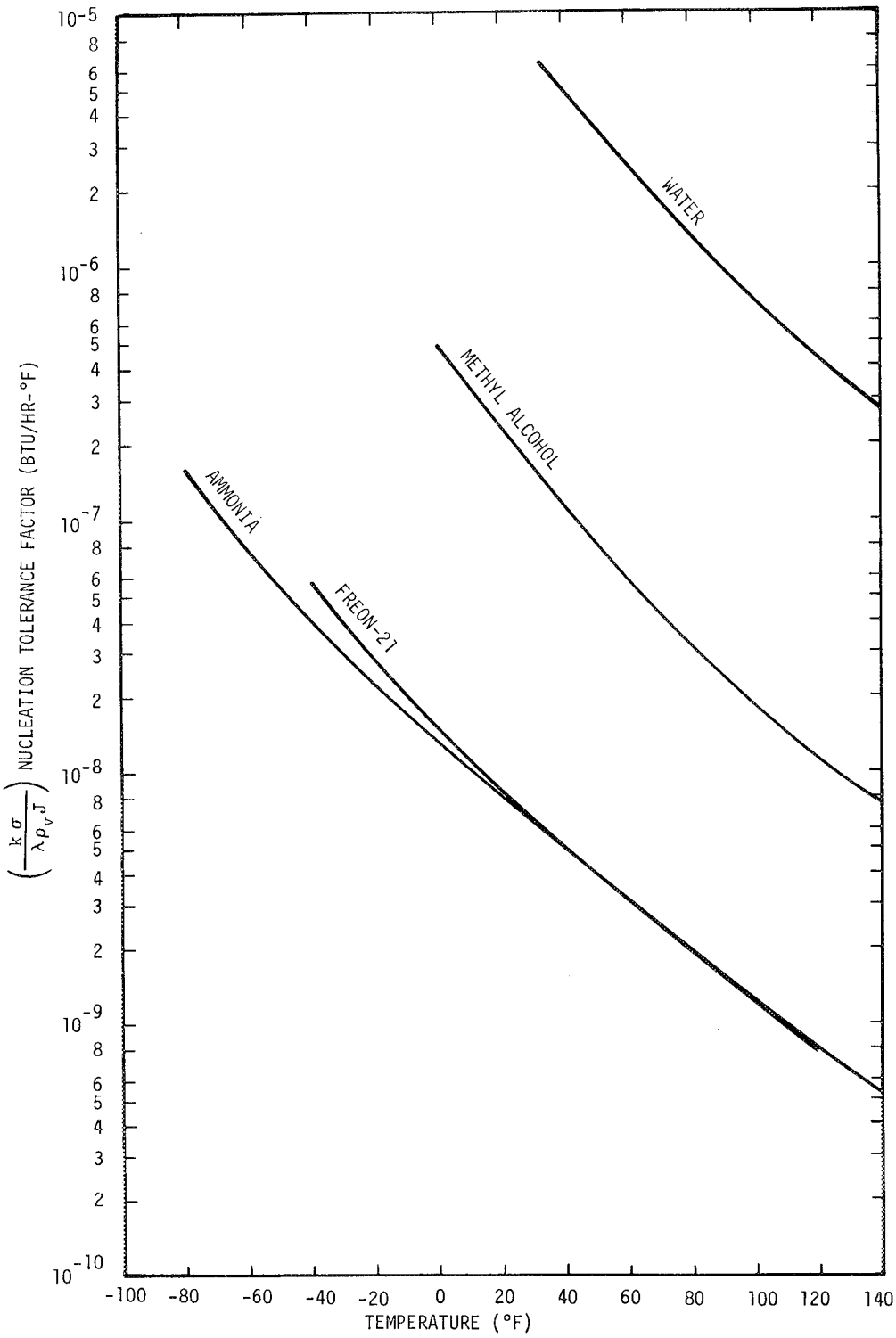

FIGURE 4-14. Nucleation Tolerance Parameter for Heat Pipe Working Fluids

gas control scheme provides additional selection criteria based on the slope of the vapor pressure curve.

The fluid property requirements imposed by the various variable conductance control schemes will be dealt with in Research Report No. 2.

4.4.6 Special Requirements

In addition to properties which affect the thermodynamic and hydrodynamic performance of heat pipes, there are other factors which can impose severe constraints on fluid selection for particular applications. For example:

- Many applications wherein the heat pipe concept is integrated into the packaging of electronic equipment will require the use of dielectric working fluids.
- Applications of heat pipes on-board manned spacecraft or aircraft may require the use of non-toxic and/or non-flammable working fluids.

4.4.7 Materials Compatibility and Stability

A major factor in selection of working fluids is their stability and compatibility with other materials in the heat pipe system. Certain low temperature heat pipes, of the type applicable to spacecraft thermal control, are subject to continuous performance degradation as a result of (1) chemical reaction or decomposition of the working fluid, or (2) corrosion or erosion of the container and wick.

Chemical reaction or decomposition of the working fluid may result in non-condensible gas evolution (e.g., H_2, N_2, O_2). A specific example of this is the hydrolysis of water yielding hydrogen gas when one attempts to build a water-aluminum heat pipe. In an ordinary heat pipe all non-condensible gas is swept to the condenser end, forming a diffusion barrier to vapor flow and effectively reducing the available condenser area. In gas controlled, variable conductance heat pipes, the generation of

additional non-condensible gas raises the operating temperature of the heat pipe above design conditions. Similar effects can result from a change in the chemical composition of the working fluid by virtue of a change in its vapor pressure as a function of temperature.

Corrosion and erosion of the container and wick can be manifested as a change in the wetting angle of the working fluid as well as the permeability, porosity, or capillary pore size of the wick. Solid precipitates resulting from corrosion and erosion are transported by the flowing liquid to the evaporator region where they are deposited when the liquid vaporizes. This leads to an increased resistance to fluid flow in the evaporator, resulting in a decrease in the heat transport capacity of the heat pipe.

At this point in time, there does not appear to exist any generally satisfactory way to predict stability or compatibility under arbitrary operational conditions. Consequently, faced with the need for such information, many heat pipe laboratories have run extensive test programs to empirically establish stable materials combinations and processing variables.

A widely used approach to compatibility testing is to employ actual heat pipe hardware and monitor the rate of gas generation with time. As mentioned previously, non-condensible gas generated within a heat pipe collects at the end of the condenser, blocking vapor flow and causing a local temperature drop (see Fig. 4-15). Thus, by monitoring the temperature distribution along an operating heat pipe, one has a measure of gas build-up as it actually affects performance. Note that the tests should be run with the condenser elevated above the evaporator to avoid artifacts due to fluid puddling.

Several such compatibility tests were performed on this contract as part of the development program leading to the Ames Heat Pipe Experiment on the OAO-C spacecraft. Control range considerations for this variable

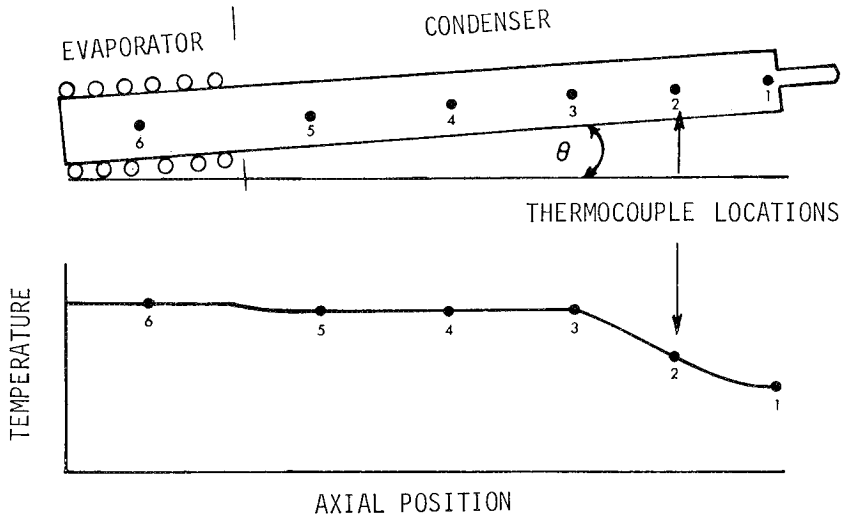

FIGURE 4-15. Schematic Diagram of Gas Generation Compatibility Test

conductance heat pipe led to the choice of methanol as the working fluid and stainless steel as the wick and container material. Because the heat pipe was to operate at 65 $\pm$5°F the internal pressure would be quite low ($\sim$2 psia) and the pipe would thus be very sensitive to even small quantities of gas generation.

Four 304 stainless steel/methanol heat pipes were fabricated utilizing different surface and fluid preparation techniques. After ultrasonically cleaning all parts in various solvents and firing all parts in dry hydrogen at 1200°C, two of the pipes were vacuum fired at 1100°C for two hours and two were oxidized in air at 500°C for one hour. The methanol used in all cases was spectrophotometric grade. However, in two pipes the fluid was used as received while, in the second two, it was specially dried by passing it through dried molecular sieve. The following material/fluid matrix was thus established.

No. 100 Vacuum fired S.S. Specially dried methanol	No 101 Vacuum fired S.S. As received methanol
No. 102 Oxidized S.S. Specially dried methanol	No. 103 Oxidized S.S. As received methanol

The four heat pipes were placed on continuing life test at 105° ±5°F and the temperature profiles recorded periodically. A typical result is shown on Fig. 4-16 where the temperature difference between thermocouples 1 and 5 (see Fig. 4-15) is plotted as a function of time. After 2200 hours with no apparent gas generation (except in H.P. No. 102*), the operating temperature was raised to 145 ±10°F and the test continued. At this point, over 7000 hours of test data have been accumulated without evidence of any gas generation in pipe nos. 100, 101 and 103, nor additional gas generation in pipe no. 102 following apparent cracking of the methanol during an accidental high temperature excursion.

Although these test results can only be reliably applied to the fabrication of heat pipes using precisely the same processing techniques and operating at similar temperatures, they do provide the guideline that methanol/stainless steel is an acceptable combination. Many similar

*After 1300 hours of testing with no gas generation, pipe no. 102 experienced a severe overheat and heater burnout due to a malfunction in equipment. After installation of a new heater, the pipe exhibited about 8°F temperature gradient suggesting gas generation by cracking of the methanol. This temperature difference has remained constant in 6000 hours of additional testing, supporting the thesis that this was a decomposition rather than a corrosion type phenomenon. Unfortunately, the maximum temperature reached by the heat pipe during this excursion is not known.

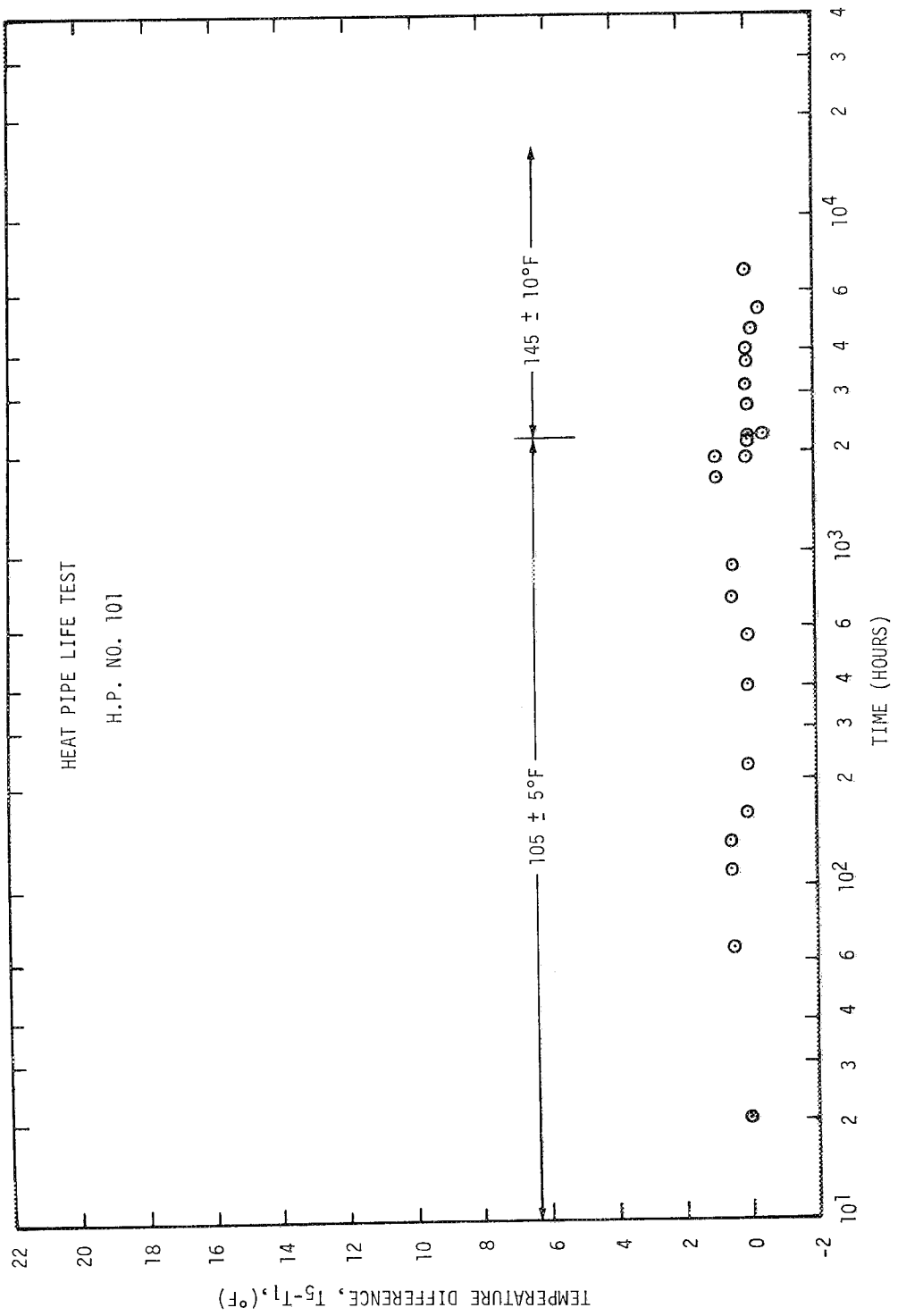

FIGURE 4-16. Compatibility Test Results - Heat Pipe No. 101

experiments have been performed by workers in the field, and although most of this work has not yet reached the open literature, enough has been reported to at least provide similar guidelines for most fluid/material combinations of interest in spacecraft thermal control.

Table 4-1 is a compilation of much of the available literature on this subject [M1, M2, M3, G7, G8, G17, G18]. The table indicates combinations of fluids and materials of construction which have been reported to be compatible or not on the basis of non-condensible gas generation. Of course, even in those cases listed as compatible, considerable attention must be given to cleanliness of the materials and purity of the working fluids to achieve satisfactory performance.

TABLE 4-1. Heat Pipe Materials Compatibility Matrix

Aluminum	Stainless Steel	Copper	Nickel	Working Fluid
○	●–○	●	●–○	Water
●	●	–	●	Ammonia
○	●	●	●	Methanol
–	●	●	–	Acetone
●	–	–	–	Freon-21
●	–	–	–	Freon-11
●	–	–	–	Freon-113

● Long term compatibility demonstrated in heat pipes
○ Incompatible - generation of non-condensible gas
●–○ Compatibility demonstrated in heat pipes, but very sensitive to passivation and processing techniques
– No heat pipe data found in literature

4.4.8 Summary

As is apparent from the previous discussion, the choice of working fluid depends very much on the requirements of the particular application. For the operating temperature range of interest in spacecraft thermal control, the four best working fluids are water, ammonia, methanol and Freon-21. In Table 4-2, these four fluids are ranked in terms of the various criteria discussed.

It would appear from the table that, from most points of view, water is the best fluid. In certain cases it will be. However, the high freezing point of water and its low vapor pressure at relevant temperatures limits its use to the high end of the thermal control range.

From a hydrodynamic point of view, ammonia is the next best fluid. Because this fluid is compatible with aluminum, it also allows for light weight heat pipes. It has very little superheat tolerance, however, and care must be used to avoid designs which are very sensitive to boiling, especially if the pipe contains non-condensible gases.

In the event that ammonia's toxicity is unacceptable, methanol and Freon-21 are alternatives. Methanol is the superior fluid thermodynamically, but its incompatibility with aluminum is a drawback, and it is still toxic. It is much less toxic than ammonia, however, and its sub-atmospheric vapor pressure at temperatures of interest prevents the expulsion of vapor into a controlled atmosphere (manned spacecraft) in the event of pipe failure.

If the application calls for a variable conductance heat pipe, additional fluid selection criteria are involved. These will be discussed in Research Report No. 2.

TABLE 4-2. Potential Heat Pipe Working Fluids for Spacecraft Thermal Control

	(Ranking at 70°F)			
	Water	Ammonia	Methanol	Freon-21
Liquid transport factor ($\sigma\rho_\ell\lambda/\mu_\ell$)	1	2	3	4
g-field operation (σ/ρ_ℓ)	1	2	3	4
Superheat tolerance ($\sigma/\lambda\rho_v$)	1	4	2	3
Toxicity	1	4	3	2
Flammability	1	2	4	3
Materials compatibility	3	1	2	?

5.0 HEAT PIPE CONTROL TECHNIQUES

The conventional heat pipe consists of a sealed, wicked vessel containing only an appropriate quantity of working fluid and possessing no moving parts. If the fluid inventory is sufficient but not excessive, such a heat pipe will tend to transport heat at nearly isothermal conditions. However, it does not have any particular operating temperature.* Instead, it automatically adjusts its temperature to match the heat source and sink conditions so as to maintain conservation of energy.

There are many potential heat pipe applications, however, in which a specific operating temperature range is desired along certain portions of the pipe, in spite of variations in the source and sink conditions. In those cases, it becomes necessary to actively or passively control the heat pipe so that it maintains the desired temperature range.

Similarly, there exist numerous potential applications where one wishes the heat pipe to operate as (1) a thermal switch, or (2) a diode. In both cases, the objective is for the heat pipe to operate either as a thermal insulator or an effective heat conductor, depending on either a reference temperature (thermal switch) or the direction of the thermal gradient (diode). Again, it is necessary to introduce an active or passive control feature to effect this behavior.

This report deals primarily with control techniques leading to variable conductance heat pipes which control the evaporator or source temperature. However, several of the techniques studied exhibit thermal switching or diode behavior under certain circumstances.

---

*For a given working fluid, the operating temperature range is theoretically bounded by the freezing and critical points, and is usually more restrictively bounded by considerations pertaining to minimum and maximum tolerable vapor pressures.

Three fundamental approaches to controlling heat pipes have been examined: (1) liquid flow control, (2) vapor flow control, and (3) condenser flooding using non-condensible gases or excess working fluid. Each of these control techniques deal with the operation of the heat pipe itself. One can also, of course, control the heat pipe thermal system externally; say, by varying the specific thermal resistance (resistance per unit area) between the heat source and evaporator or between the condenser and heat sink. However, such thermal control techniques are outside the scope of this study.

The following paragraphs briefly describe the three device-oriented approaches to heat pipe control. Each will be dealt with in greater depth later in this report.

5.1 Liquid Flow Control

The liquid flow control technique involves interrupting or impeding the condensate return in the wick. With reference to the evaporator section of the heat pipe, the effective heat transfer area is that portion of the pipe which contains liquid for evaporation. If the evaporator wick suffers a partial dryout, the available area for efficient input heat transfer, and hence the heat pipe conductance, is reduced.

If the heat source is a dissipative one (e.g., heat generation in electronic equipment), incipient dryout of the wick represents a hydrodynamic failure mode (capillary pumping limit) for, in the absence of a parallel heat transfer path, it leads to thermal runaway of the dry portion of the evaporator. However, if the heat source is represented by a temperature boundary condition (e.g., heat exchanger), partial evaporator dryout simply results in reduced heat transfer into the pipe.

Thus, for dissipative heat sources, liquid flow control is limited to providing "on-off" control; i.e., thermal-switching. However, for fixed temperature sources, continuous modulation of the heat pipe conductance is possible by varying the wick flow resistance.

5.2 Vapor Flow Control

Vapor flow control refers to the interruption or throttling of the vapor flow between the evaporator or condenser sections of the heat pipe. This gives rise to a pressure difference between the two regions and, with it, a corresponding temperature difference; hence, a variable conductance.

If the vapor flow path is interrupted, the evaporator temperature and pressure can increase until the pressure differential across the pipe exceeds the "bubble point" pressure of the wick/fluid combination, when the vapor will "blow through" the wick. In this manner one achieves on-off operation similar to liquid flow interruption.

On the other hand, if the vapor flow is only throttled, one can continuously control the evaporator-condenser temperature differential. But the range of control is substantially limited by the fact that the evaporator-condenser pressure differential must not exceed the bubble point pressure of the wick/fluid combination.

5.3 Condenser Flooding Using Non-Condensible Gas

This technique refers to the well-known "gas-load" heat pipe. Whenever a heat pipe contains a non-condensible gas in addition to its primary working fluid, its ability to transfer heat is altered significantly from that of a conventional device. During operation of such a heat pipe, vapor flows from the evaporator to the condenser region. As a consequence, any non-condensible gas present in the vapor is swept along and, since it does not condense, accumulates at the condenser end forming a gas plug. This gas plug represents a diffusion barrier to the flowing vapor and very nearly "shuts off" that portion of the condenser which it fills. Consequently, by varying the length of this gas plug, one varies the active condenser area and, hence, the heat transfer from the system.

5.4 Condenser Flooding Using Excess Working Fluid

This approach is analagous to the "gas-load" heat pipe except that excess liquid is used to very the active condenser area rather than non-condensible gas.

6.0 VARIABLE CONDUCTANCE THROUGH THE USE OF NON-CONDENSIBLE GASES

The technique of using non-condensible gas to flood the condenser and vary its effective area has commanded the greatest effort on this program, and will be dealt with first.

As mentioned previously, the underlying principle of non-condensible gas control is the formation of a gas plug at the condenser end of the pipe which acts as a diffusion barrier to the flowing vapor. This gas plug tends to "shut-off" that portion of the condenser which it fills, leading to an axial temperature gradient along the heat pipe as shown on Fig. 6.1. By varying the length of this gas plug, one varies the active condenser area and, hence, the heat rejection properties of the system.

A feature which makes non-condensible gas control particularly attractive is that the basic heat pipe (Fig. 6-1) accomplishes this variation in condenser area passively. By introducing a fixed mass of gas into the system shown, it occupies a certain portion of the condenser section, depending on the operating temperature of the pipe's active region and the environmental conditions. If the operating temperature increases, the vapor pressure of the working fluid increases. This compresses the non-condensible gas into a smaller volume, thus providing a greater active condenser area. On the other hand, if the operating temperature falls, the vapor pressure of the working fluid falls and the fixed mass of gas expands to a greater volume, thus blocking a larger portion of the condenser. The net effect is to provide a passively controlled variable condenser area which increases or decreases with the heat pipe temperature. As a consequence, this reduces the temperature response of the active zone to variations in the heat input rate or environmental (sink) conditions.

6.1 Flat-Front Theory: Mathematical Model

A great deal of insight into the behavior of gas-controlled heat pipes can be obtained from a rather simple mathematical model of the system. Consider the model shown in Fig. 6-2, and allow the following assumptions:

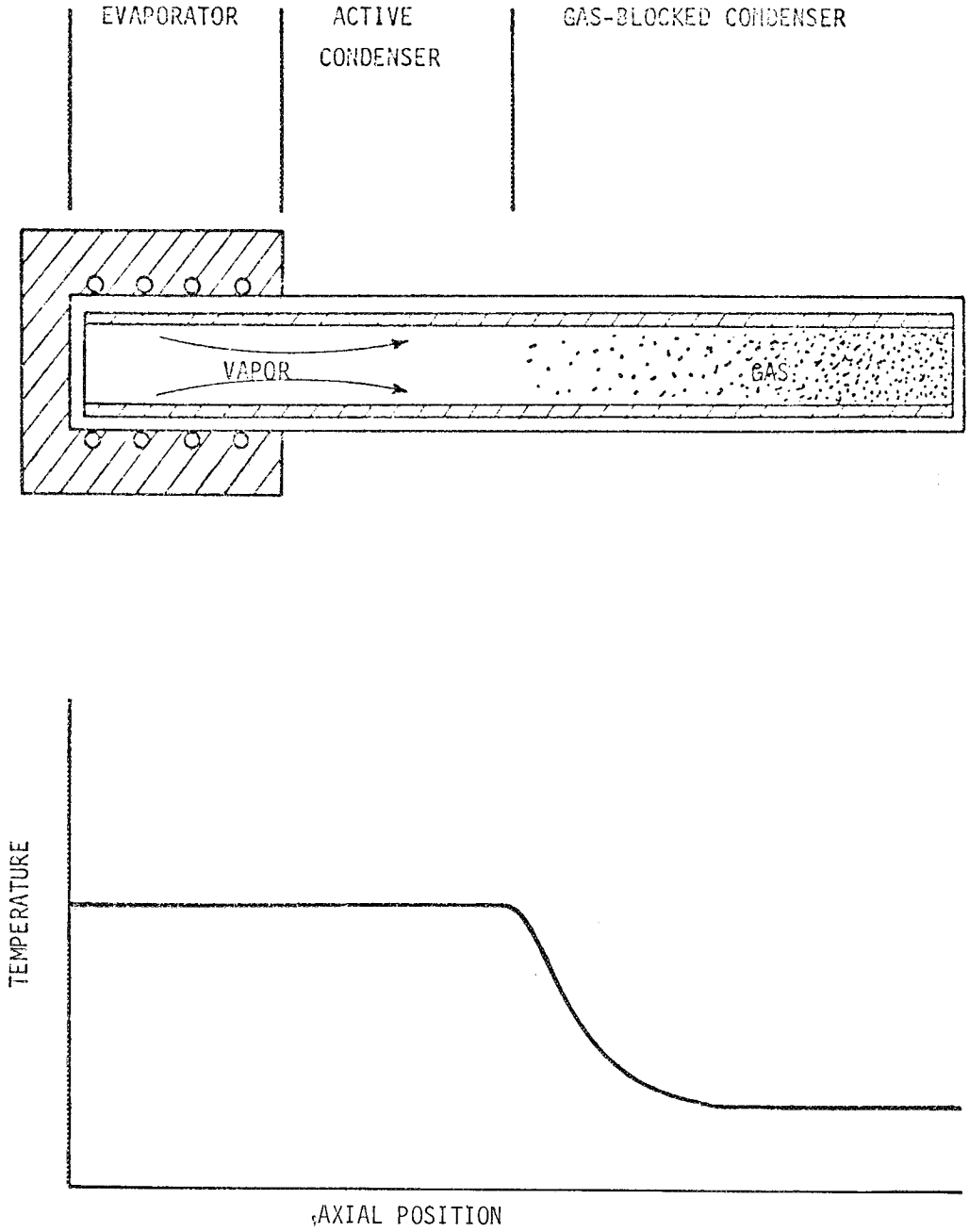

FIGURE 6-1. Schematic Diagram and Temperature Distribution of a Gas Loaded Heat Pipe

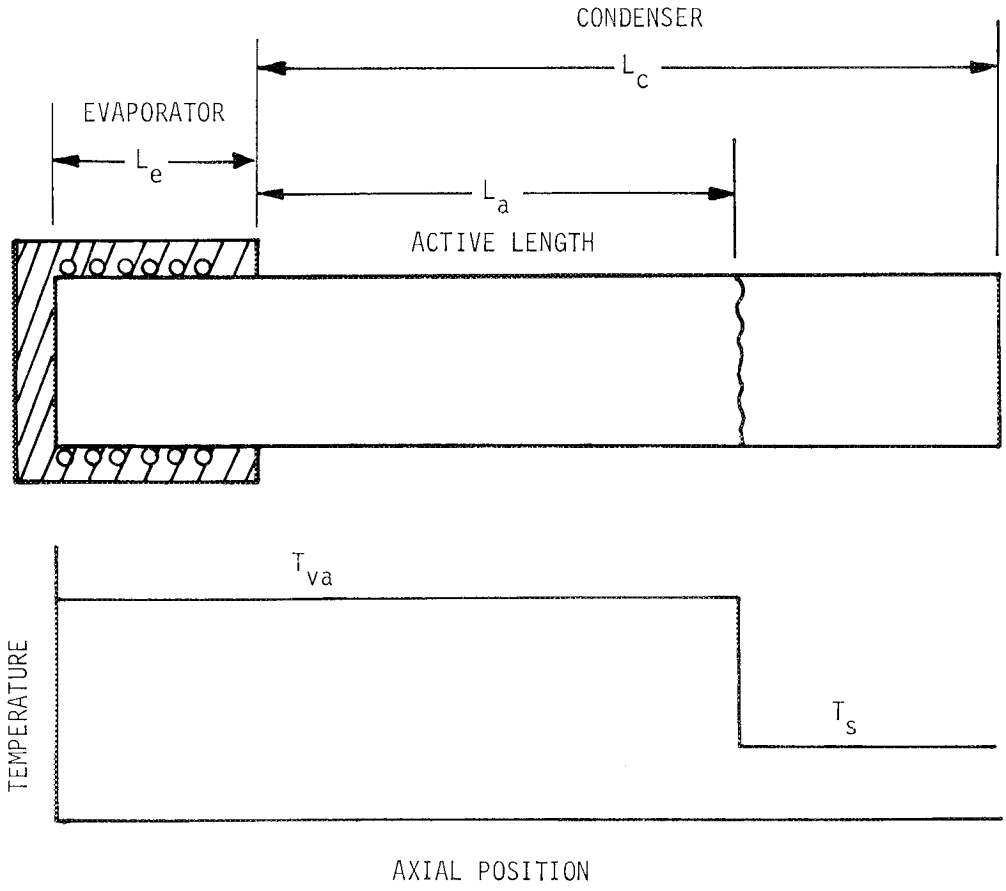

FIGURE 6-2. Definition of an Analytical Model for a Gas Loaded Heat Pipe

- Steady-state conditions prevail
- The interface between the active and shut-off portions of the pipe is very sharp
- Axial conduction can be neglected
- For small temperature variations, heat transfer per unit area from the vapor to the sink at the condenser is proportional to the temperature difference between the vapor and the sink
- The total pressure is uniform throughout the pipe (vapor flow losses are negligible)
- The vapor-gas mixture is ideal

With these assumptions, one can write a simple equation for heat transfer from the condenser, as follows:*

$$Q = hA' L_a (T_{va} - T_s) \qquad (6\text{-}1)$$

where:

Q - heat transfer rate
h - heat transfer coefficient
A' - heat rejection area per unit length of condenser
L_a - active length of condenser
T_{va} - vapor temperature in active zone
T_s - sink temperature

To determine an expression for the active condenser length, one invokes the requirement that the molar non-condensible gas inventory for a given heat pipe remains constant for all operating conditions. For an ideal gas mixture, the molar gas inventory for an element of pipe volume is simply:

---

*In many spacecraft thermal control applications, Eq. (6-1) does not adequately describe condenser heat transfer. A more general equation, accounting for radiation to and from condenser fins, is presented later in this report (section 6.3.1). However, Eq. (6-1) is much simpler to work with and will suffice to demonstrate the principles of the flat front theory.

$$dn = \frac{P_g}{R_u T_g} dV \qquad (6\text{-}2)$$

where:

dn - number of moles of gas in the volume element dV

P_g - partial pressure of gas in dV

T_g - temperature of gas in dV

R_u - universal gas constant

Thus, for any given operating condition, one can obtain an expression for the total molar gas inventory in the heat pipe by integrating Eq. (6-2) over its volume. For the flat-front model of Fig. 6-2, this integral reduces to a single term for the inactive portion of the condenser:*

$$n = \frac{P_g (L_c - L_a) A_v}{R_u T_g} \qquad (6\text{-}3)$$

where:

A_v - vapor core cross-sectional area

L_c - total condenser length

Within the gas-blocked region of the condenser, the gas and liquid are at the sink temperature and hence there exists a partial pressure of vapor within this region equal to the liquid vapor pressure at T_s:

$$\text{Thus: } \left.\begin{aligned} P_g &= P_{va} - P_{vs} \\ T_g &= T_s \end{aligned}\right\} \qquad (6\text{-}4)$$

where:

P_{va} - vapor pressure at T_{va} (total pressure)

P_{vs} - vapor pressure at T_s

*There is assumed to be no gas in the active portion of the heat pipe.

Substituting Eq. (6-4) into (6-3), solving for the active condenser length - L_a, and then substituting for L_a in Eq. (6-1) yields the following operating characteristic:

$$Q = hA' (T_{va}-T_s) \left[L_c - \frac{nR_u T_s}{A_v (P_{va}-P_{vs})} \right] \qquad (6\text{-}5)$$

Equation (6-5) describes the heat transfer characteristics of the simple gas-loaded heat pipe. It will be shown later that the "flat-front" analysis used in its derivation is somewhat inaccurate because it neglects axial conduction and diffusion. However, the errors are quantitative rather than qualitative, and this simple model does permit preliminary design analysis and identifies most key design parameters.

6.1.1 Effect of Working Fluid: Fixed Sink Conditions

The key element in Eq. (6-5) is the term in brackets which represents the active condenser length, and which when multiplied by hA' yields the heat pipe conductance.

The objective of the device is to maintain a nearly constant temperature over the active portion of the pipe in spite of substantial variations in power throughput or environmental conditions. Thus, the active condenser length should ideally be a very strong function of the operating temperature.

From Eq. (6-5) we see that the variation in active length with operating temperature - T_{va} occurs by virtue of changes in the corresponding fluid vapor pressure - P_{va}. The fluid properties also enter the equation in the term P_{vs}, which is the vapor pressure at the sink temperature - T_s. However, if we postulate fixed sink conditions (constant T_s), the only fluid parameter which varies is P_{va}.

This provides a criterion for the selection of the working fluid. Greater control sensitivity can be achieved using fluids which undergo large relative vapor pressure changes $\frac{\Delta P_{va}}{P_{va}}$ with temperature; i.e., large values of $\frac{d(\ln P_{va})}{dT_{va}}$.

If one uses the Clausius-Clapeyron relationship to approximate the vapor pressure curve for small variations in temperature, it is easily shown that:

$$\frac{d(\ln P_{va})}{dT_{va}} = \frac{\lambda M}{R_u T_{va}^2} \qquad (6\text{-}6)$$

where:

λ - latent heat of vaporization

M - molecular weight

R_u - universal gas constant

Thus, Eq. (6-6) suggests that the grouping $\frac{\lambda M}{R_u}$ represents a "Gas Control Sensitivity Factor", useful in ranking various potential working fluids. Fig. 6-3 shows the variations in this factor with operating temperature for the principal fluids of interest in spacecraft thermal control.

6.1.2 Effect of Variations in Sink Temperature

The environmental conditions or effective sink temperature influences Eq. (6-5) in three ways. It alters the heat rejection temperature potential ($T_{va} - T_s$) so that a change in active condenser length is necessary to maintain a given heat transfer rate - Q.

It also enters the second term in brackets where, for the flat-front model, T_s establishes the temperature of the "shut-off" portion of the condenser. The T_s in the numerator of this term represents the gas temperature. Since the volume occupied by the gas depends on its temperature as well as its partial pressure (through the perfect gas law), one would expect the gas temperature to effect the gas blocked length, as indicated in Eq. (6-5).

Finally, it enters the equation as P_{vs} - the vapor pressure of the working fluid at T_s. Within the gas blocked portion of the condenser there always exists a partial pressure of vapor, which is a function of the local temperature. This vapor, in essence, acts as additional gas inventory since it must displace its equivalent in non-condensible gas. In other words, even though one introduces a fixed inventory of non-condensible gas in the pipe, the "effective gas inventory" is not fixed but varies

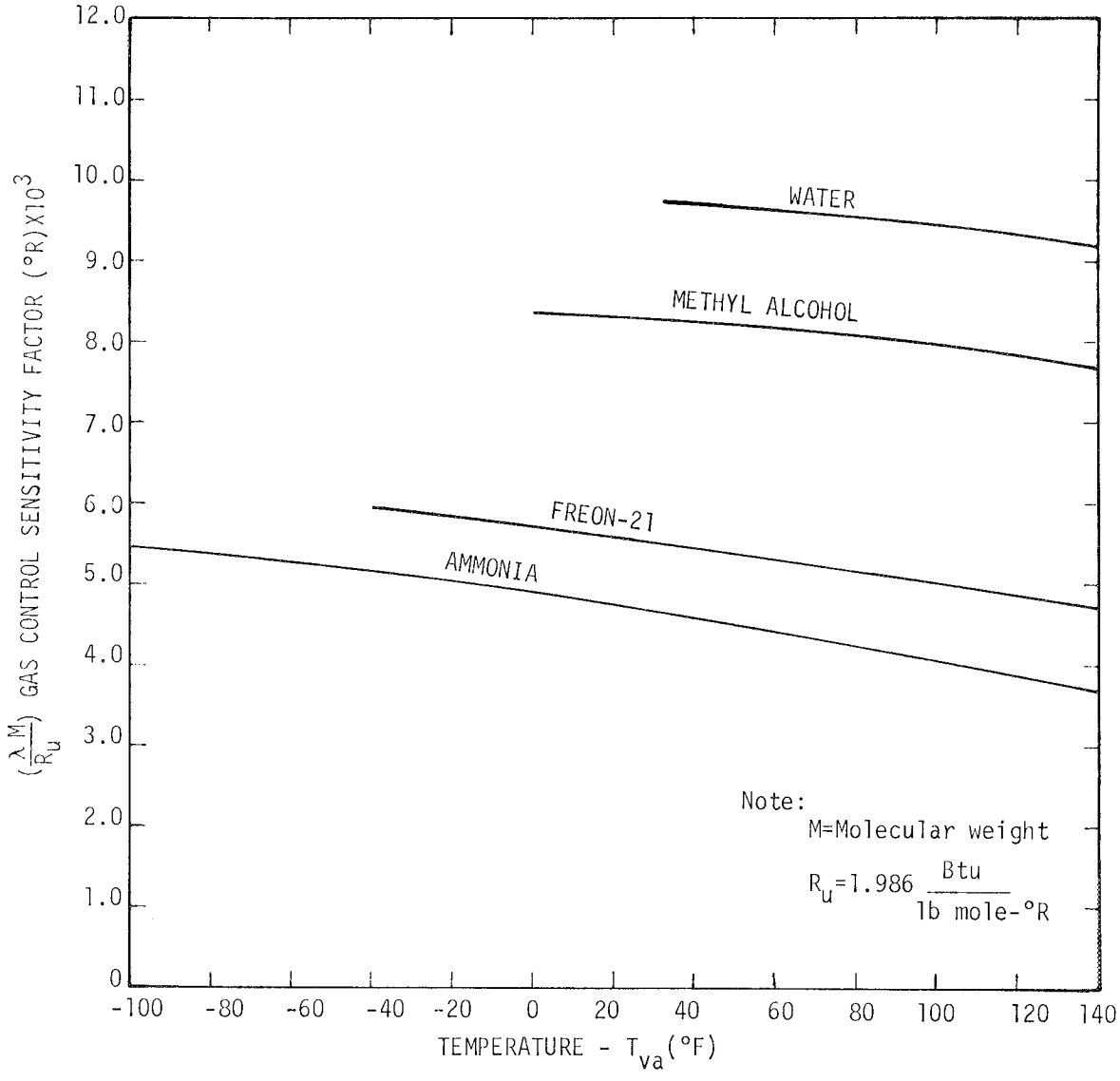

FIGURE 6-3. Gas Control Sensitivity Factor for Heat Pipe Working Fluids

with sink temperature through its control of the partial pressure of vapor in the gas (plus vapor) blocked region.

If one examines Eq. (6-5) for the effect of a change in T_s - say an increase - we see the following.

(1) Since $(T_{va} - T_s)$ decreases, the active length (term in brackets) must <u>increase</u> to maintain a constant heat rejection - Q.

(2) But, the increase in gas temperature tends to increase the second term within brackets which acts to <u>decrease</u> the active condenser length.

(3) Also, the increase in P_{vs} will decrease the term $(P_{va} - P_{vs})$ and thus, again tends to increase the second term within brackets and <u>decrease</u> the active condenser length.

Thus, all three effects of an increase in T_s are additive; i.e., they are non-compensating, and their summary effect is to maximize the increase in T_{va} (and P_{va}) necessary to provide the <u>increase</u> in active condenser length which will maintain a constant heat rejection rate - Q.

These phenomena; i.e., the adverse effects of sink temperature variations on control sensitivity, represent the most severe constraints on the application of gas-controlled heat pipes to spacecraft thermal control. As such, a great deal of effort has gone into the development of techniques and designs to overcome them. These will be discussed in considerable detail later in this report.

6.1.3 <u>Effect of Working Fluid: Variable Sink Conditions</u>

It was shown in Sec. 6.1.1 that, to maximize control sensitivity for fixed sink conditions, one should utilize a working fluid with a large slope in its vapor pressure (P_{va}, T_{va}) curve at the operating temperature.

However, we have seen in the last section that, when the sink conditions vary, the fluid properties enter the characteristic equation not only as P_{va}, but also as P_{vs} - the vapor pressure at the sink temperature. Since

variations in P_{vs} were shown to adversely affect control, one clearly wishes to minimize this effect.

One approach to this end is to prudently select the working fluid. Since P_{vs} enters Eq. (6-5) only as a subtractive term in $(P_{va} - P_{vs})$, the effects of variations in P_{vs} are minimal when the absolute value of the variation $-\left(\int_{T_{smin}}^{T_{smax}} P_{vs}\right)$ is small compared with P_{va}. In terms of the working fluid, this criteria will be met for fluids with small values of the ratio $\frac{P_{vs}}{P_{va}}$. Fig. 6-4 shows the variation in P_{vs}/P_{va} with T_s for the principal fluids of interest at a fixed value of T_{va} = 70°F.*

As might be expected, the ranking between fluids is the same as for control sensitivity with fixed sink conditions (Fig 6-3) since it is based on a related criterion.

In addition to ranking various working fluids, Fig. 6-4 also graphically demonstrates a significant point with respect to the effects of vapor in the gas blocked region. The problem is only significant when the sink temperature approaches the operating temperature. For applications where the maximum sink temperature is far below the operating temperature, the P_{vs} term in Eq. (6-5) becomes negligibly small.

6.1.4 Gas Reservoirs

It has been emphasized in past discussion that to achieve high control sensitivity, the active condenser length should be a very strong function of the operating temperature. This, in turn, requires that L_a be a strong function of the system total pressure - P_{va}. Since motion

---

*Although the magnitudes of P_{vs}/P_{va} change with the selection of T_{va}, the relationship between fluids does not. The selection of 70°F for the figure is consistent with typical operating temperatures for spacecraft thermal control.

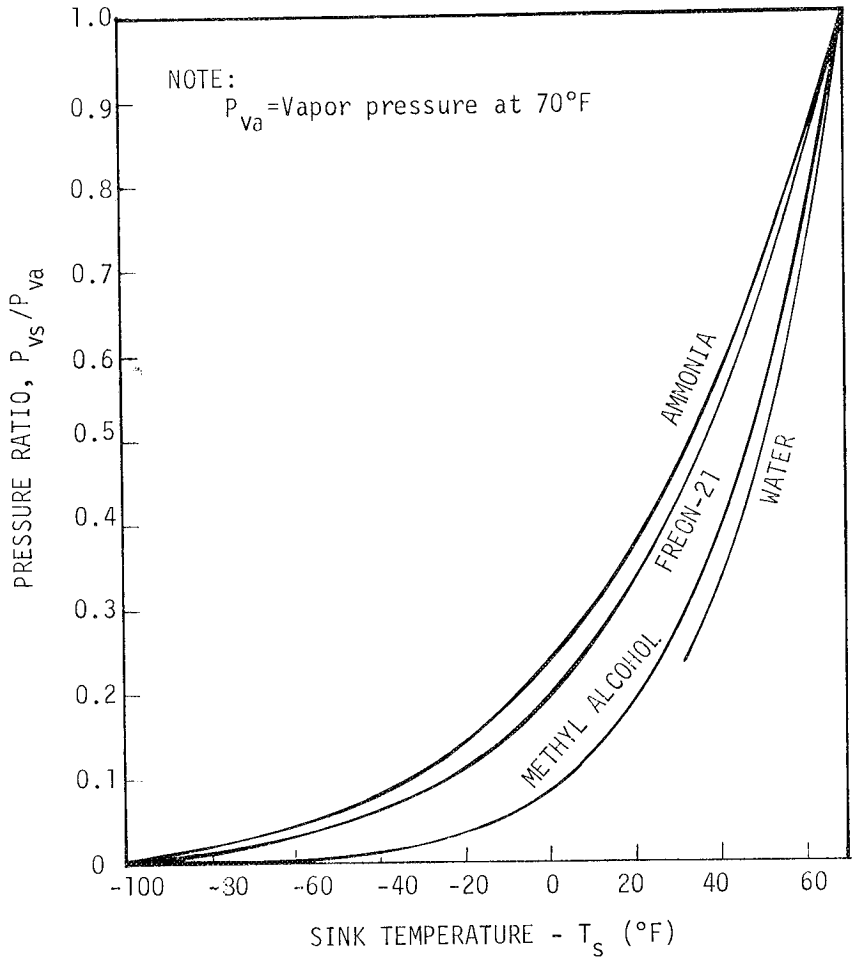

FIGURE 6-4. Sink Temperature to Operating Temperature Vapor Pressure Ratios for Heat Pipe Working Fluids

of the vapor-gas interface reflects compression of the gas inventory, it follows that to maximize the sensitivity of L_a to P_{va} one wishes to minimize the relative compression of gas $(\frac{\Delta V_{gas}}{V_{gas}})$ necessary to move the interface. A convenient method for accomplishing this is to provide a large gas storage volume outside the range of vapor-gas interface travel; i.e., a gas reservoir.

6.1.4.1 Wicked Reservoir, $T_R = T_s$

The simplest approach to providing a gas reservoir on a gas-controlled heat pipe is shown schematically on Fig. 6-5. A relatively large storage volume is added to the end of the condenser section into and out of which the gas can flow.

Assuming that the reservoir is internally wicked and in equilibrium with the same environment as the gas-blocked portion of the condenser, the appropriate flat-front temperature distribution is also shown on Fig. 6-5.

To derive the appropriate characteristic equation for this system, one follows the same procedure as in Sec. 6.1, but the integral of the molar gas inventory (Eq. 6-2) over the system volume now yields two terms.

For both the reservoir and inactive portion of the condenser:

$$\left.\begin{aligned} T_g &= T_s \\ P_g &= P_{va} - P_{vs} \end{aligned}\right\} \qquad (6\text{-}7)$$

Thus, the molar gas inventory is given by:

$$n = \int \frac{P_g dV}{R_u T_g} = \frac{(P_{va} - P_{vs})}{R_u T_s} \left[A_v (L_c - L_a) + V_R\right] \qquad (6\text{-}8)$$

where V_R - reservoir volume.

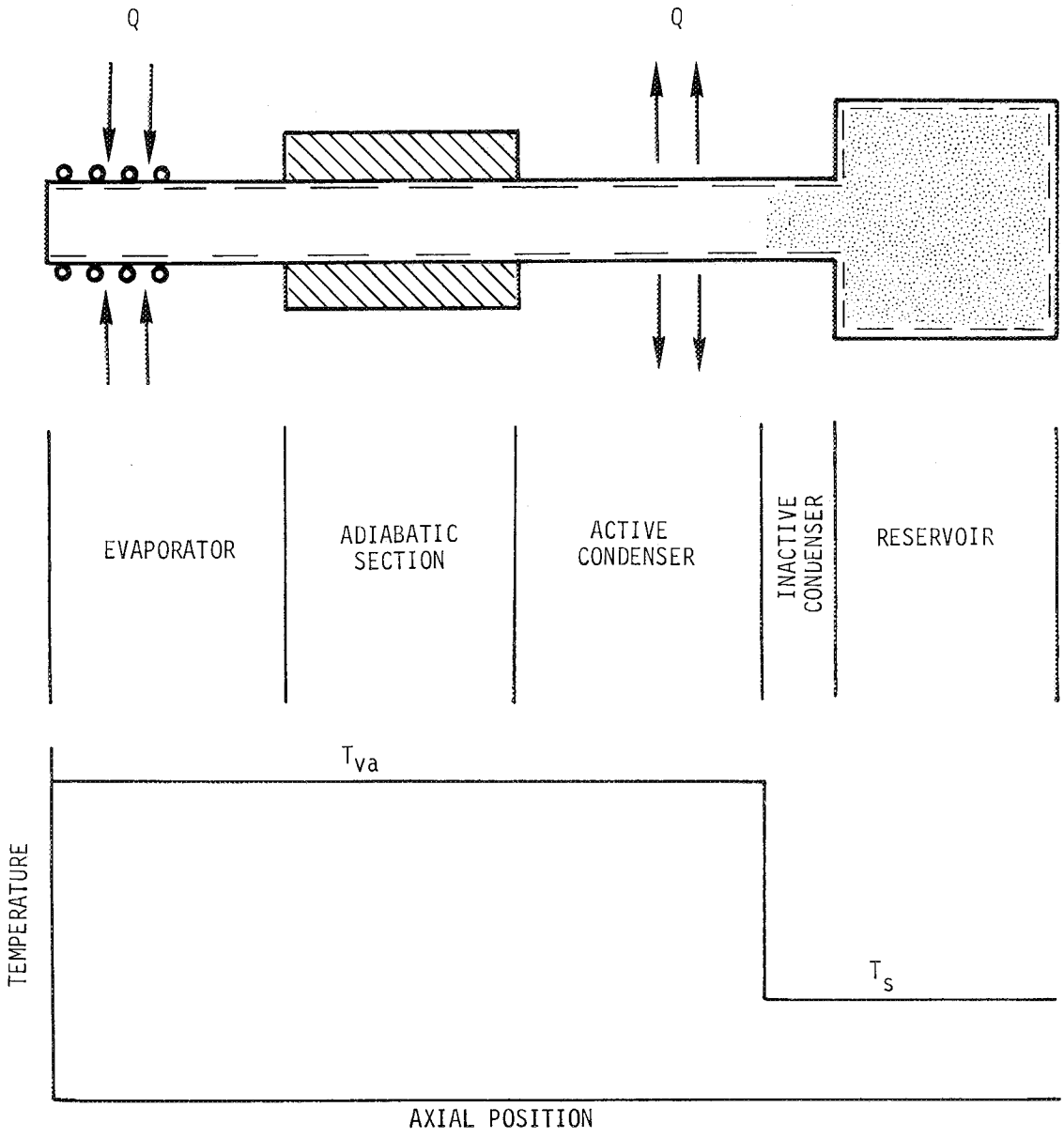

FIGURE 6-5. Schematic Diagram and Flat-Front Temperature Distribution of a Cold Wicked Reservoir Gas Controlled Heat Pipe

Solving Eq. (6-8) for the active length - L_a, and substituting into Eq. (6-1) now yields the following characteristic equation.

$$Q = hA' \ (T_{va}-T_s) \left[L_c + \frac{V_R}{A_v} - \frac{n \ R_u T_s}{A_v \ (P_{va}-P_{vs})}\right] \qquad (6\text{-}9)$$

Comparing this result with Eq. (6-5), we see that the effect of the reservoir is simply to add the term V_R/A_v to those in brackets. The effect of the reservoir volume may not be immediately obvious from this equation, but with a little more analysis its effect will be clearer and the equation generalized.

The term in brackets again represents the active condenser length. For given sink conditions, the control range of the heat pipe corresponds to a variation in active length from zero to the total condenser length - L_c. Thus, when $L_a = L_c$, the heat pipe is rejecting maximum heat (Q_{max}) <u>within its control range</u>,* and the operating temperature is at the maximum end of the range (T_{vamax}). Under these circumstances, Eq. (6-9) reduces to:

$$Q_{max} = hA' \ (T_{vamax} - T_s) \ L_c \qquad (6\text{-}10)$$

Equation (6-10) can now be used to normalize Eq. (6-9) and make it more general. Thus:

$$\frac{Q}{Q_{max}} = \frac{(T_{va}-T_s)}{(T_{vamax}-T_s)} \left[1 + \frac{V_R}{L_c A_v} - \frac{n \ R_u T_s}{L_c A_v \ (P_{va}-P_{vs})}\right] \qquad (6\text{-}11)$$

Recognizing that the product $L_c A_v$ is simply the vapor core condenser volume - V_c, and re-arranging terms, one can cast Eq. (6-11) into a more convenient form as follows:

*Both Q and T_{va} can be increased beyond this point but the variable conductance range has been exhausted and the pipe behaves as an ordinary heat pipe with conductance $hA' L_c$.

$$\frac{T_{va}-T_s}{T_{vamax}-T_s} = \frac{Q}{Q_{max}} \left[\frac{V_c/V_R}{1 + \frac{V_c}{V_R} - \frac{n R_u T_s}{V_R (P_{va}-P_{vs})}} \right] \qquad (6\text{-}12)$$

Equation (6-12) is a generalized expression for the sensitivity of cold reservoir heat pipes as shown in Fig. 6-5. By normalizing with respect to conditions at the maximum end of the control range, it is now independent of the external geometry (A') or coefficient of heat transfer (h).

The effect of the reservoir volume is now more apparent. V_R enters the equation in two ways; as $\frac{n}{V_R}$ and as $\frac{V_c}{V_R}$. The term $\frac{n}{V_R}$ establishes the set point temperature (T_{vamax}) at which the heat pipe will operate for given sink conditions - T_s. Larger gas reservoirs, of course, require larger molar gas inventories to achieve a given pressure in the system. The term V_c/V_R, the ratio of condenser void to reservoir volumes, influences the control sensitivity. Eq. (6-12) shows that, as this ratio grows small (large reservoirs), the bracketed term becomes a progressively stronger function of P_{va} and hence the control sensitivity increases; i.e., variation in T_{va} with Q is decreased.

The quantitative effect of the ratio V_c/V_R (or V_R/V_c as is more commonly used) depends on the working fluid, sink temperature, and set point (T_{vamax}). However, a typical example for spacecraft thermal control applications is shown on Fig. 6-6.

The improvement in control sensitivity with reservoir volume is obvious. (An increment of 0.1 on the ordinate represents 17.5°F). However, it is also obvious that as V_R increases, one reaches a point of diminishing returns. More will be said on this later when discussing design techniques.

6.1.4.2 Wicked Reservoir, $T_R \neq T_s$

The system described in the last section presumed that the reservoir was in thermal equilibrium with the same environment as the

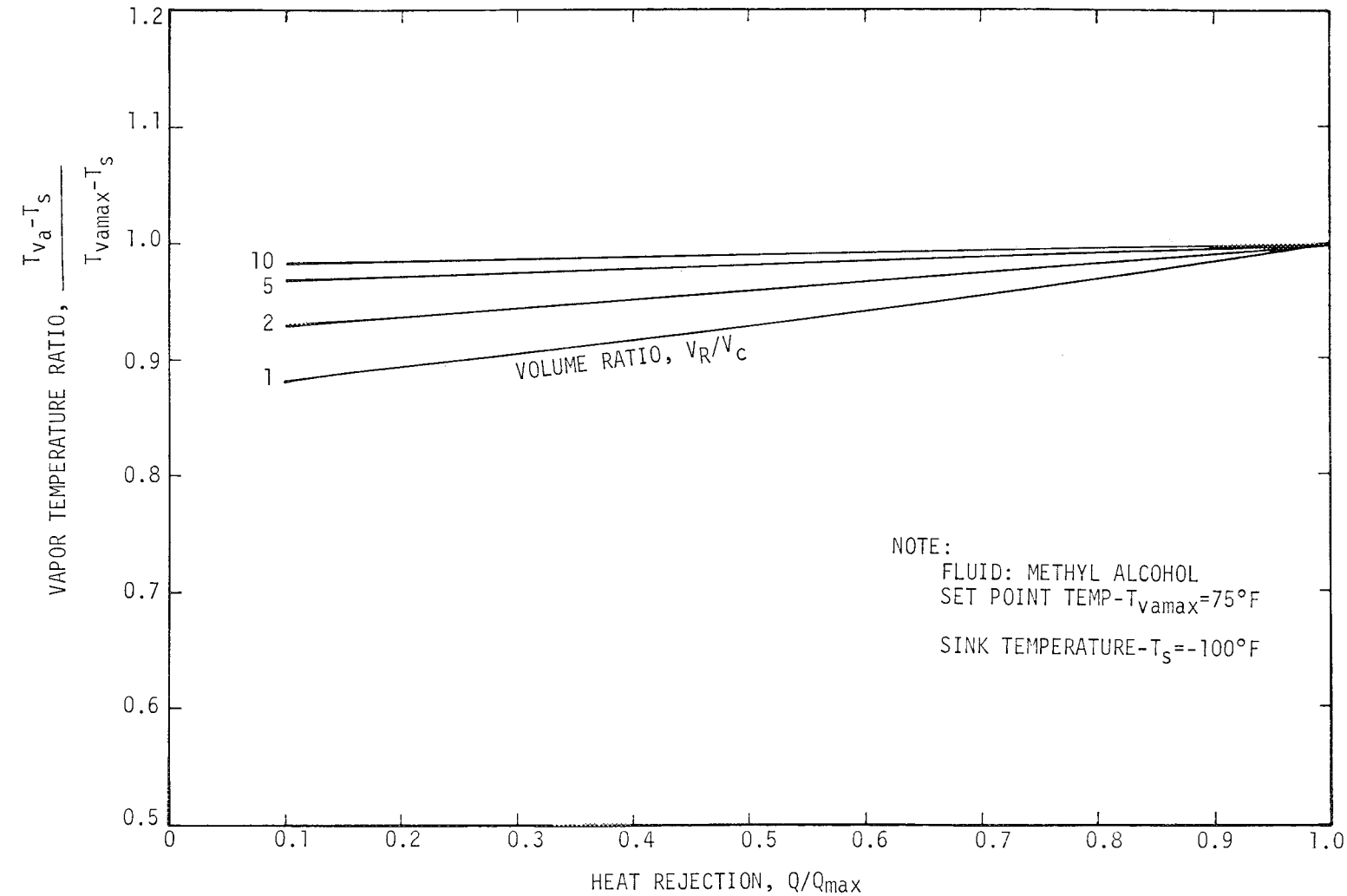

FIGURE 6-6. Effect of Reservoir to Condenser Volume Ratio on Control Sensitivity

gas-blocked portion of the condenser, and both were at the sink temperature - T_s. This is indeed a realistic case and led to a simple characteristic equation for purposes of examining the effect of the reservoir volume. However, there are many applications of gas-controlled heat pipes where the reservoir temperature is other than that of the gas-blocked condenser zone. As discussed in section 6.1.2, a serious constraint on control is introduced by variations in environmental conditions, both by virtue of changes in gas temperature and the partial pressure of vapor in the gas-blocked zone. The introduction of a gas-reservoir, which is in effect an extension of the gas-blocked zone, amplifies this problem in the same way as it amplifies control sensitivity. Thus, for situations in which the sink conditions vary widely, causing a serious loss in control, it may be preferred to position or control the reservoir so that its temperature fluctuates less.

The characteristic equation for this more general case is determined in the same way as before, but now:

for the inactive portion of the condenser:

$$T_g = T_s$$

$$P_g = P_{va} - P_{vs}$$

and, for the reservoir:

$$T_g = T_R$$

$$P_g = P_{va} - P_{vR}$$

where: T_R - reservoir temperature.

Following the procedure described in section 6.1:

$$n = \int \frac{P_g dV}{R_u T_g} = \frac{(P_{va}-P_{vs})}{R_u T_s} (L_c-L_a) A_v + \frac{(P_{va}-P_{vR})}{R_u T_R} V_R \qquad (6\text{-}13)$$

$$L_a = L_c - \frac{R_u T_s}{A_v (P_{va} - P_{vs})} \left[n - \frac{V_R}{R_u T_R} (P_{va} - P_{vR}) \right] \qquad (6\text{-}14)$$

$$Q = hA' (T_{va} - T_s) \left[L_c + \frac{V_R}{A_v} \cdot \frac{T_s}{T_R} \cdot \frac{(P_{va} - P_{vR})}{(P_{va} - P_{vs})} - \frac{n R_u T_s}{A_v (P_{va} - P_{vs})} \right] \qquad (6\text{-}15)$$

Comparing this generalized characteristic equation with Eq. (6-9) for $T_R = T_s$, we see the effect of $T_R \neq T_s$ is to multiply the $\frac{V_R}{A_v}$ term by $\frac{T_s}{T_R} \cdot \frac{(P_{va} - P_{vR})}{(P_{va} - P_{vs})}$ which, of course, reduces to unity when $T_R = T_s$.

In the last section, it was shown that large values of V_R/V_c improve control sensitivity. Since, for a given condenser length - L_c, $V_R/V_c \propto V_R/A_v$, it is apparent that it is this second term in brackets which reflects the reservoir influence. To maximize sensitivity, one wishes to maximize this term.

It is clear that:

$$\frac{T_s}{T_R} \frac{(P_{va} - P_{vR})}{(P_{va} - P_{vs})} \begin{cases} < 1 \text{ when } T_R > T_s \\ = 1 \text{ when } T_R = T_s \\ > 1 \text{ when } T_R < T_s \end{cases} \qquad (6\text{-}16)$$

Thus, for a given reservoir size - V_R, and condenser sink temperature - T_s, control sensitivity $\frac{\partial Q}{\partial T_{va}}$ is increased when $T_R < T_s$ and decreased when $T_R > T_s$.

However, the purpose of decoupling the reservoir from the condenser sink conditions ($T_R \neq T_s$) is not so much to alter control sensitivity as to minimize the effect of sink temperature fluctuations.

Equation (6-15) clearly shows this effect. For fixed T_R (and hence P_{vR}), variations in T_s have a proportional effect on both the second and third terms in brackets. Since these terms are of opposite sign, the effects are compensating. When T_R equals and varies with T_s, the second term in brackets reduces to V_R/A_v and this compensation is eliminated.

Thus, we see that holding the reservoir temperature constant decreases the sensitivity of the system to sink temperature variations. Preferably, one wants to hold T_R constant at a lower temperature than T_s, for this would also increase control sensitivity ($\frac{\partial Q}{\partial T_{va}}$). However, in spacecraft thermal control applications, this may not often be possible. In most cases, condenser heat rejection is by radiation to space, and a natural reservoir environment which is both colder and fluctuates less than the effective sink temperature is simply not available. Also, actively cooling the reservoir by refrigeration is generally not practical.

Consequently, the most promising approach to reservoir temperature control is to place it in a relatively constant temperature warm environment (inside the spacecraft) or to thermostatically heat it. However, for the wicked reservoirs under discussion, one must be sure that the reservoir temperature is well below that of the evaporator (T_{va}). As T_R approaches T_{va}, the term (P_{va}-P_{vR}) grows smaller and the effect of the reservoir in providing control sensitivity (the second term within brackets in Eq. (6-15) is diminished. If $T_R = T_{va}$, the vapor pressure in the reservoir equals the total pressure in the pipe (P_{va}) and the reservoir is no longer available to store any gas. If $T_R > T_{va}$, the heat pipe actually reverses and the reservoir not only cannot store gas, but it becomes the evaporator.

6.1.4.3 Non-Wicked Reservoir

In the previous section, it was shown that reservoir temperature control can de-sensitize a gas-controlled heat pipe from sink temperature variations. It was also pointed out that, from a practical point of view, one must usually control the reservoir temperature above the range in sink temperature, but that for wicked reservoirs T_R must be kept well below the evaporator operating temperature (T_{va}), for as T_R approaches T_{va} the reservoir rapidly becomes ineffective as a gas storage volume. The reason for this difficulty is that, for wicked reservoirs, the partial pressure of vapor within the reservoir - P_{vR} corresponds to the reservoir temperature - T_R.

Temperature control of wicked reservoirs is the most generally effective method of minimizing the effects of sink temperature variations, since it controls both the gas temperature and partial pressure of vapor within the reservoir. However, for spacecraft applications, it will usually require thermostatically controlled reservoir heaters.* This eliminates one of the major features of the simple gas-controlled heat pipe; i.e., passive operation. The inclusion of heaters involves both a power requirement and an inherent loss in system reliability.

A compromise solution which still yields a passive system is to simply eliminate the reservoir wick, as shown schematically on Fig. 6-7.

By removing the wick from the reservoir, its partial pressure of vapor no longer corresponds to its temperature since it contains no liquid.** Instead, the presence of working fluid vapor in the reservoir is established by diffusion to and from the closest point at which liquid does exist; i.e., the reservoir entrance.

The potential for vapor diffusion is the difference in vapor concentration between the reservoir and its entrance. Thus, at equilibrium, the concentration of vapor within the reservoir will equal that at its entrance.*** Assuming an ideal gas-vapor mixture and a uniform total pressure, the mole fraction and partial pressure of vapor are proportional. Thus, the partial pressure of vapor in the reservoir will correspond not to its own temperature, but to the temperature at the reservoir entrance. For the assumptions of the flat-front model, this is equal to the sink temperature - T_s.

---

* Usually, placing the reservoir within a stable temperature portion of the spacecraft will not permit it to operate at a temperature far enough below T_{va}.

** T_R must be higher than T_s to prevent vapor from condensing in the reservoir.

***Neglecting thermal diffusion.

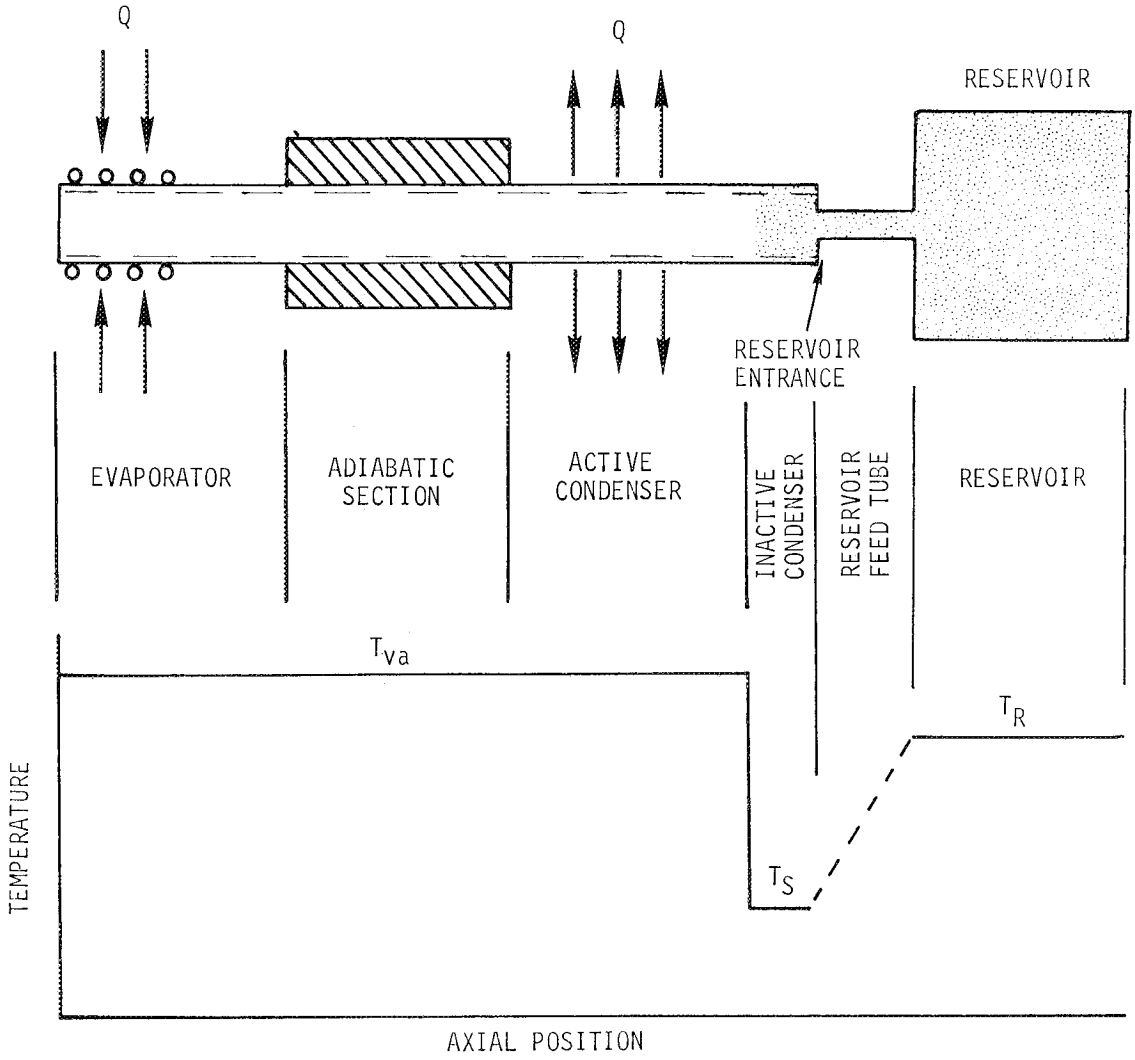

FIGURE 6-7. Schematic Diagram and Flat-Front Temperature Distribution of a Hot Non-Wicked Reservoir Gas Controlled Heat Pipe

The effect of removing the reservoir wick on the characteristic equation is simply to replace the term P_{vR} with P_{vs}.* Equation (6-15) then reduces to:

$$Q = hA\ (T_{va}-T_s)\left[L_c + \frac{V_R}{A_v}\frac{T_s}{T_R} - \frac{nR_uT_s}{A_v(P_{va}-P_{vs})}\right] \qquad (6\text{-}17)$$

As with the controlled temperature wicked reservoir system, controlling the temperature of a non-wicked reservoir minimizes the effect of sink variations on the gas temperature.** However, as opposed to the former system, the latter still suffers variations in the partial pressure of vapor within the reservoir (P_{vs}) with variations in T_s. Thus, it is less subject to variations in T_s than an uncontrolled wicked reservoir pipe where $T_R = T_s$, but more so than a controlled temperature wicked reservoir system where T_R is fixed.

Note, however, that partial vapor pressure variations within the reservoir are only problematic when P_{vs} is significant with respect to P_{va}. If $P_{vs}/P_{va} << 1$ over the entire range of T_s, then P_{vs} can be dropped from Eq. (6-17), and the controlled-temperature non-wicked reservoir offers the ultimate in insensitivity to sink conditions. This situation prevails when the sink temperature range is well below the operating temperature, and depends on the working fluid as shown in Fig. 6-4.

A major advantage of the non-wicked reservoir over the wicked system is that the reservoir temperature need not be much lower than the evaporator temperature, since the reservoir vapor pressure is not a function of T_R. In fact, T_R can be equal to or even higher than T_{va}. Because of this, it is now a simple matter to provide close reservoir temperature control independent of the surroundings and without the use of heaters and

---

* If one neglects the volume of the small reservoir feed tube between the condenser and reservoir.

**Variations in T_s effect only the gas in the blocked portion of the condenser, not that in the reservoir.

thermostats. This is achieved by thermally coupling the reservoir directly to the evaporator, either in contact with it or actually within it, as shown schematically in Fig. 6-8.

A significant disadvantage of the non-wicked reservoir heat pipe is that working fluid vapor enters or leaves the reservoir by mass diffusion through the control gas. Mass diffusion is a rather slow process and, under certain circumstances, this can seriously retard the heat pipe's transient response characteristics. This will be taken up in more detail later in the section on transient behavior (section 6.4.2).

6.1.4.3.1 Thermal Diffusion

In deriving the characteristic equation (6-17) for non-wicked reservoir heat pipes, it was assumed that the partial pressure of vapor is uniform throughout the reservoir. However, there exists a phenomenon wherein a mixture of gases at constant pressure tends to separate due to a temperature gradient. This is called thermal diffusion.

This phenomenon is of potential significance in non-wicked reservoir heat pipes for these are precisely the conditions in the reservoir feed tube. This tube, at uniform and essentially constant pressure, has one end at the reservoir temperature and the other end at the sink temperature. This should lead to a thermal diffusion effect, causing a concentration gradient across the tube. Under most circumstances the lighter gas moves to the hot end. This phenomenon will alter the equilibrium partial pressure of vapor in the reservoir, causing it to be other than the vapor pressure at the effective sink temperature. Fortunately, thermal diffusion is generally a weak phenomenon and, other than to demonstrate this, it can generally be neglected.

The equilibrium variation in concentration between two ends of the reservoir feed tube under a temperature gradient is given by:

$$x_{vR} - x_{vs} = -k_{\overline{T}} \ln \frac{T_R}{T_s} \qquad (6\text{-}18)$$

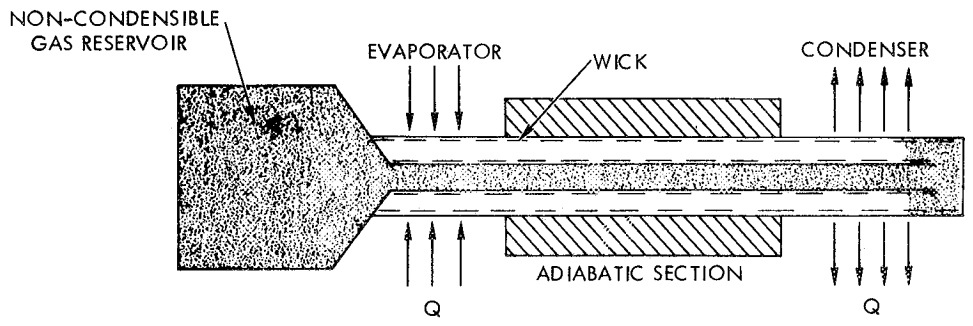

a) Thermally Coupled Reservoir

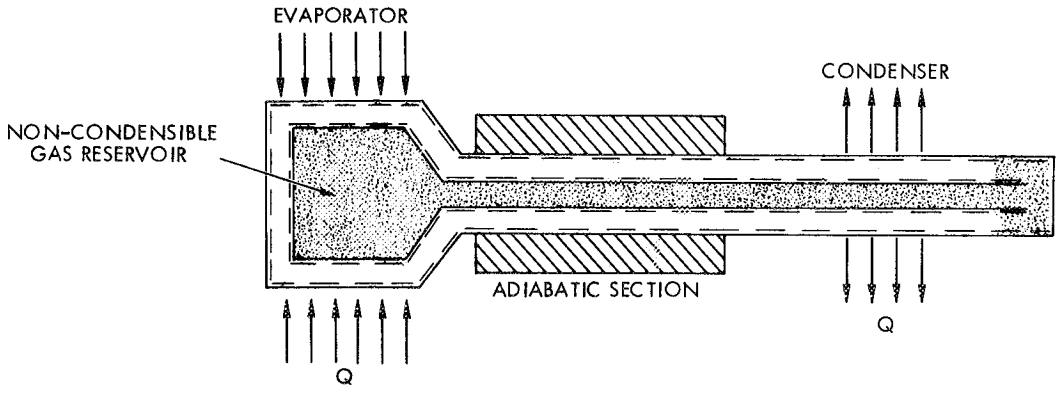

b) Internal Reservoir

FIGURE 6-8. Schematic Diagrams of Hot Non-Wicked Reservoir Heat Pipes with Reservoir - Evaporator Thermal Coupling

where:

x_{vR}, x_{vs} - mole fraction of vapor at the reservoir and condenser ends of the feed tube

k_T - thermal diffusion coefficient

The thermal diffusion coefficient varies between about 0.01 and 0.1 for most gas pairs, depending in large part on the molecular weights of the two species and the difference between them.

For typical temperature differentials across the reservoir feed tube in spacecraft thermal control applications (say T_R = 70°F and T_s = -100°F), Eq. (6-18) yields $0.004 \leq \Delta x_v \leq 0.04$ for the mole fraction of the vapor. Since, for ideal gases, the partial pressure and mole fraction are proportional ($P_v = x_v P_{tot}$), these results indicate that the thermal diffusion effect may diminish the partial pressure of vapor in the reservoir by 0.4 to 4 percent of the total pressure. This represents a relatively small effect, particularly if the lower end of the range is applicable. This is most likely the case when one provides a close match in molecular weights between the working fluid and control gas. In any case, by choosing a control gas of lower molecular weight than the working fluid, the effect works to one's advantage by helping keep vapor out of the gas reservoir.

6.1.5 Effect of Condenser Geometry

The characteristic equations also provide insight into the effects of condenser geometry, both internal and external, on control sensitivity.

The effects of internal geometry are most easily seen from the equations in normalized form; e.g., Eq. (6-12). In discussing Eq. (6-12), it was shown that control sensitivity increases with the reservoir to condenser volume ratio - V_R/V_c. This ratio can be made large by using large reservoirs. However, one can alternatively design for small condenser volume. This can be accomplished either by utilizing short condensers or by minimizing the vapor core cross-sectional area - A_v.

External to the pipe, the characteristic equations (6-5, 6-9, etc.) show that to minimize the variation of T_{va} with Q, the external conductance

per unit length of condenser - hA' should be high. By using extended surfaces (e.g., fins) to increase the heat rejection area per unit length - A', and designing for high values of the effective coefficient of heat transfer - h, one minimizes the change in active length required to accommodate changes in heat rejection - Q.* This, in turn, minimizes the variations in T_{va} necessary to accomplish the required motion of the interface.

6.1.6 Sizing the Gas Reservoir with the Flat-Front Model

The characteristic equations derived with the flat-front model can be used to establish the reservoir volume requirements for a given application. To accomplish this, one writes the characteristic equation for the two operating extremes; i.e., the full-on condenser at maximum thermal boundary conditions and the full-off condenser at minimum thermal boundary conditions, without specifying the reservoir volume or gas inventory. These expressions are then solved simultaneously for the molar gas inventory and reservoir volume, other parameters being specified.

To demonstrate the procedure, the special case of a wicked reservoir with $T_R = T_s$ will be treated. Also, it will be assumed that the extremes of heat rejection - Q, correspond to the extremes of condenser active length: $0 \leq L_a \leq L_c$. Under such conditions (see Sec. 6.1.4.1):

$$Q_{max} = hA' (T_{vamax} - T_{smax}) L_c \tag{6-19a}$$

$$Q_{min} = 0 \tag{6-19b}$$

Writing the characteristic equation (Eq. 6-9) for both extremes now yields

$$Q_{max} = hA' (T_{vamax} - T_{smax}) \left[L_c + \frac{V_R}{A_v} - \frac{nR_u T_{smax}}{A_v (P_{vamax} - P_{vsmax})} \right] \tag{6-20a}$$

---

*For a given total conductance requirement ($hA' L_c$), maximizing hA' and minimizing L_c are equivalent.

$$Q_{min} = hA'(T_{vamin} - T_{smin})\left[L_c + \frac{V_R}{A_v} - \frac{nR_u T_{smin}}{A_v(P_{vamin}-P_{vsmin})}\right] \qquad (6\text{-}20b)$$

Equating (6-19) to (6-20) for Q_{max} and Q_{min}, and performing some algebra yields:

$$\frac{V_R}{A_v} - \frac{nR_u T_{smax}}{A_v(P_{vamax}-P_{vsmax})} = 0 \qquad (6\text{-}21)$$

$$L_c + \frac{V_R}{A_v} - \frac{nR_u T_{smin}}{A_v(P_{vamin}-P_{vsmin})} = 0 \qquad (6\text{-}22)$$

One now solves both Eqs. (6-21) and (6-22) for the molar gas inventory - n, and since this is invariant, equates the two expressions, leading to:

$$\frac{V_R}{A_v} \cdot \frac{A_v(P_{vamax}-P_{vsmax})}{R_u T_{smax}} = n = \left(L_c + \frac{V_R}{A_v}\right)\frac{A_v(P_{vamin}-P_{vsmin})}{R_u T_{smin}} \qquad (6\text{-}23)$$

Performing some additional algebra, and substituting $V_c = L_c A_v$, finally yields a simple expression for the condenser to reservoir volume ratio:

$$\frac{V_c}{V_R} = \left[\frac{P_{vamax}-P_{vsmax}}{P_{vamin}-P_{vsmin}} \cdot \frac{T_{smin}}{T_{smax}} - 1\right] \qquad (6\text{-}24)$$

Eq. (6-24) was derived for the special case of a wicked reservoir with $T_R = T_s$, and $0 \leq L_a \leq L_c$. Similar procedures yield equivalent expressions for more general cases, although the algebra is more cumbersome. Thus, for the general wicked reservoir case, where $T_R \neq T_s$, $Q_{min} \neq 0$, and $L_a \neq L_c$ at Q_{max}, T_{smax} and T_{Rmax}, one can show that:

$$\frac{V_R}{V_c} = \frac{\xi_1 - \xi_2}{\xi_3} \qquad (6\text{-}25)$$

where:

$$\xi_1 = \left[1 - \frac{Q_{min}}{L_c\, hA' (T_{vamin}-T_{smin})}\right]\left[\frac{P_{vamin}-P_{vsmin}}{T_{smin}}\right]$$

$$\xi_2 = \left[1 - \frac{Q_{max}}{L_c\, hA' (T_{vamax}-T_{smax})}\right]\left[\frac{P_{vamax}-P_{vsmax}}{T_{smax}}\right]$$

$$\xi_3 = \left[\frac{P_{vamax}-P_{vRmax}}{T_{Rmax}} - \frac{P_{vamin}-P_{vRmin}}{T_{Rmin}}\right]$$

For non-wicked reservoir heat pipes, the generalized equation for V_R/V_c is given by a modified version of Eq. (6-25), where P_{vsmax} is substituted for P_{vRmax} and P_{vsmin} is substituted for P_{vRmin}. For the special case where the reservoir is coupled to the evaporator ($T_R = T_{va}$), and $0 \leq L_a \leq L_c$ for $0 = Q_{min} \leq Q \leq Q_{max} = hA' L_c (T_{vamax}-T_{smax})$, the equivalent form of Eq. (6-24) becomes:

$$\frac{V_c}{V_R} = \left[\frac{P_{vamax}-P_{vsmax}}{P_{vamin}-P_{vsmin}} \cdot \frac{T_{smin}}{T_{vamax}} - \frac{T_{smin}}{T_{vamin}}\right] \qquad (6\text{-}26)$$

Equations (6-24) and (6-26) are particularly useful expressions. They yield the required reservoir to condenser volume ratios in terms of the anticipated variation in sink temperature and the desired control range.* Although they are special cases of the generalized equation (6-25), they are quite realistic. Hot non-wicked reservoirs will often be coupled to the evaporator as a stable temperature zone, and cold wicked reservoirs will frequently see the same environment as the condenser. The assumption of full condenser utilization ($0 \leq L_a \leq L_c$) is certainly a desirable design goal.

---

*T_{vamin} and T_{vamax} establish P_{vamin} and P_{vamax}.

Thus, these equations yield a simple, convenient method for performing parametric analyses on how the working fluid, sink conditions, and required control range impact the reservoir volume requirements (V_R/V_c). They also provide a convenient basis for comparing hot-non-wicked and cold-wicked designs.*

As an example, Fig. 6-9 presents the results of such calculations for a typical spacecraft thermal control application. Eqs. (6-24) and (6-26) have been solved for V_R/V_c where:

$$T_{va} = 70 \pm \frac{\Delta T_{va}}{2} \quad °F$$

$$-156°F \leq T_s \leq -44°F$$

The curves show the required V_R/V_c to achieve a given control range - ΔT_{va} for methanol in both hot and cold reservoir systems, and for ammonia in a hot reservoir system.

As is apparent, methanol allows much closer control than does ammonia for the hot reservoir system. This is true for cold reservoir systems as well, and is actually a reflection of the fluid vapor pressure characteristics discussed in sections 6.1.1 and 6.1.3.

It is also apparent that, for a given fluid (e.g., methanol), the hot non-wicked reservoir allows much closer control than a cold-wicked reservoir. This, of course, is due to stabilization of the gas temperature, as discussed in Sec. 6.1.4.3. It is true for passively controlled heat pipes regardless of the fluid used.

---

*By using procedures similar to those which yielded Eqs. (6-24) and (6-26), equivalent expressions can be derived for any gas-controlled heat pipe configuration; including wicked or non-wicked reservoirs, controlled or "floating" temperature reservoirs, multi-section condensers (cold traps, gas-blocked adiabatic sections), etc.

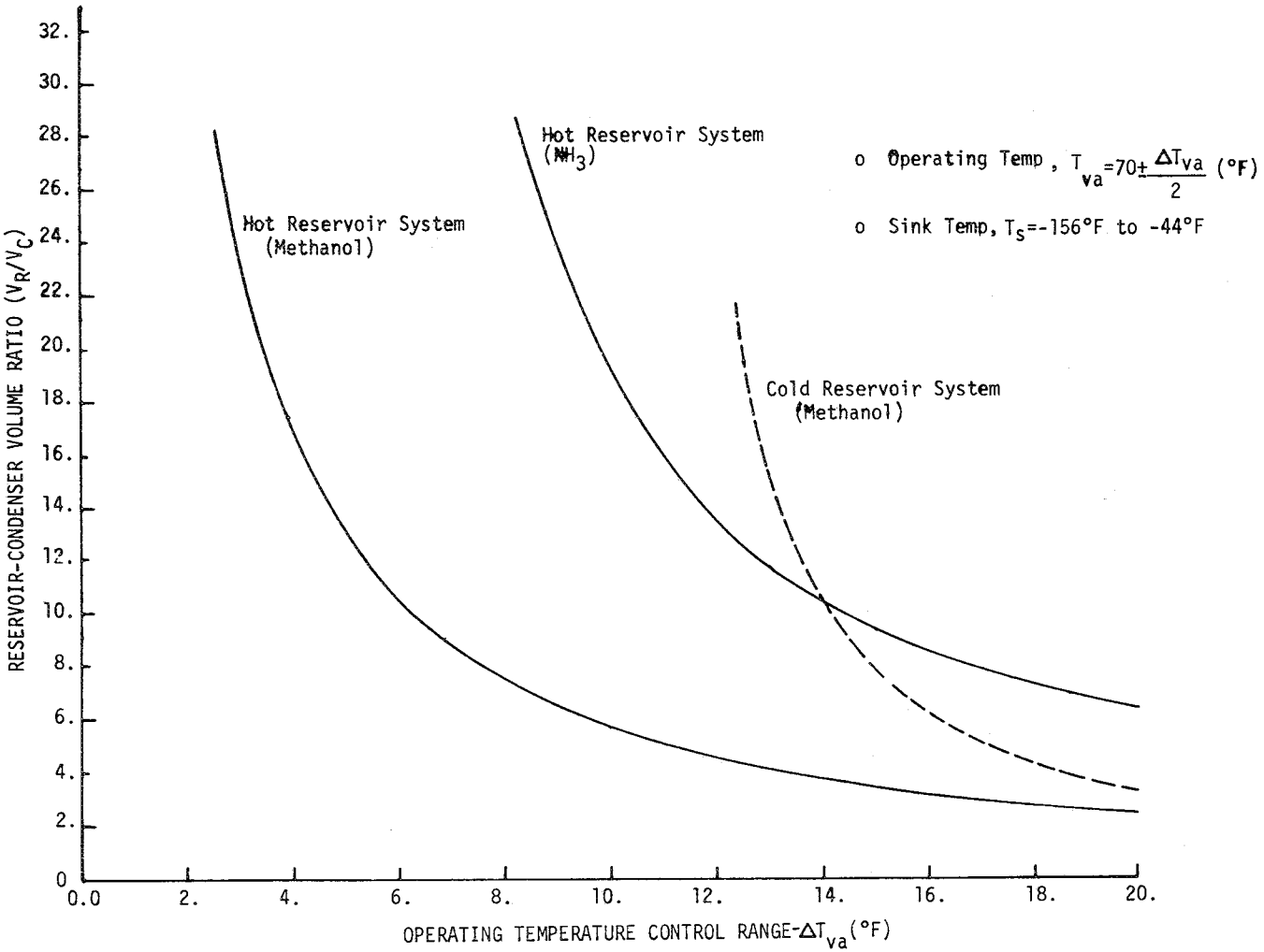

FIGURE 6-9. Reservoir Volume Requirements vs. Temperature Control Range

The quantitative results shown in Fig. 6-9 are not general, but apply only for the nominal evaporator temperature (70°F) and range in sink conditions ($-156 \leq T_s \leq -44$°F) specified. However, the qualitative conclusions are generally correct.

The effect of sink temperature variations was qualitatively discussed in sec. 6.1.2. Quantitatively, the magnitude of these effects can be seen by example in Fig. 6-10. Here, the hot and cold reservoir volume requirements are shown for several typical spacecraft ranges of effective sink temperature, where the fluid is methanol and the pipe is nominally set to operate at 70°F. Again, one sees that the hot, non-wicked reservoir design offers substantially better control than the cold, wicked reservoir. However, one also sees that it is much less sensitive to variations in sink temperature.

6.1.7 Limitations on Control with Passive Systems

Figures 6-9 and 6-10 point up an important fact with regard to the limits of temperature control possible with passive gas-controlled heat pipes. Variations in the effective sink temperature provide a lower bound to the control range regardless of how large one makes the reservoir.

For fixed sink conditions, Eq. (6-12) shows that as V_c/V_R approaches zero (infinitely large reservoir), temperature control becomes perfect; i.e., T_{va} does not vary at all with changes in Q. However, for varying sink conditions, the curves of Fig. 6-9 and 6-10 show that ΔT_{va} approaches finite positive limits as $V_R/V_c \to \infty$.

The magnitudes of these limits are, of course, a function of the working fluid, nominal operating temperature (T_{va}), and the particular range in sink temperature involved. It is a relatively simple matter to calculate the limit for any given set of conditions with the theory already presented.

6.1.8 Variable Set-Point Heat Pipes

The devices previously described will serve to maintain the operating temperature of the heat pipe within a narrow range around a set point

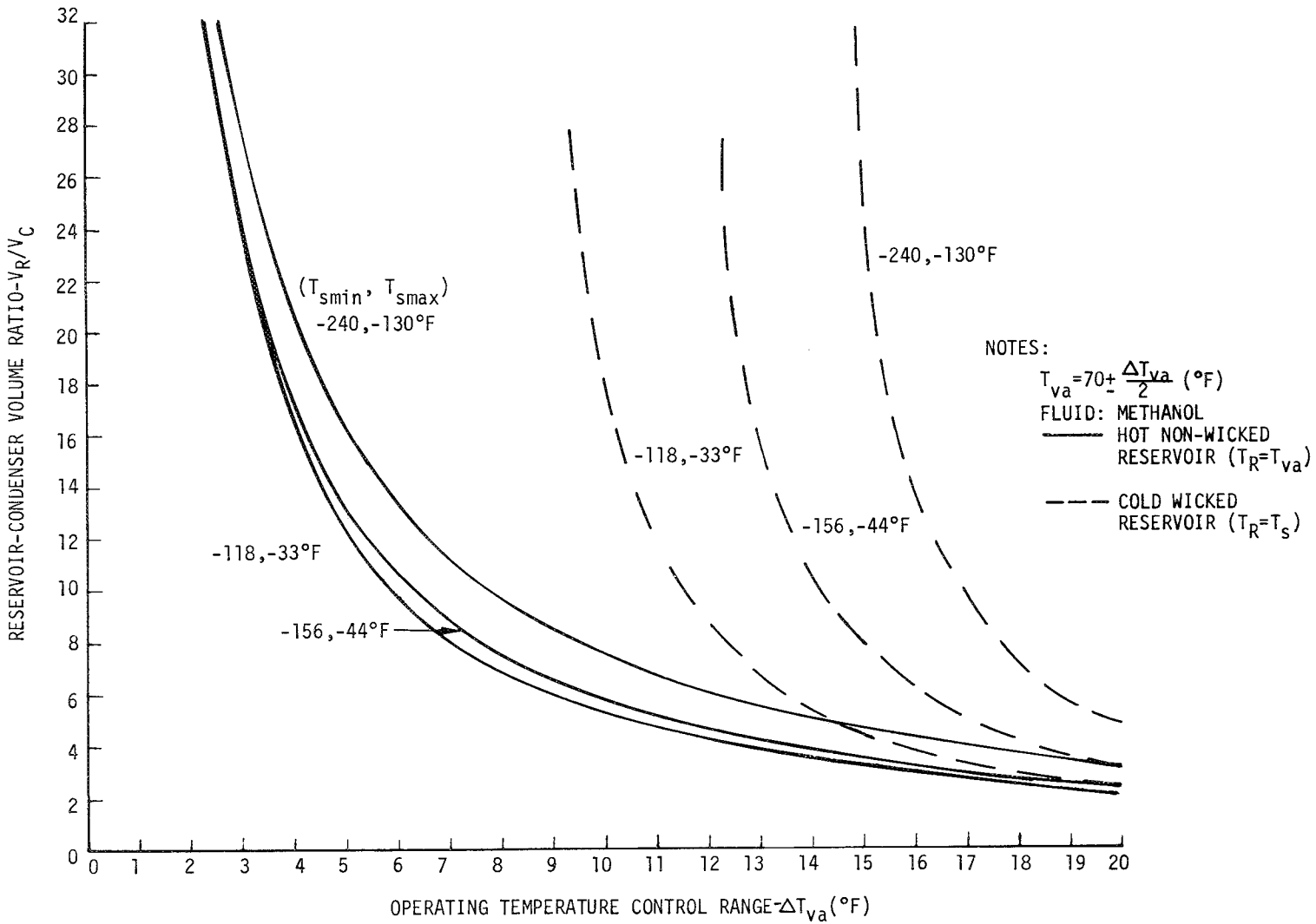

FIGURE 6-10. Reservoir Volume Requirements vs. Temperature Control Range

determined by the gas inventory. From the various characteristic equations derived, one sees that the set point depends on the quantity - n of non-condensible gas in the system. Thus, the operating temperature can be raised or lowered by adding or removing gas. This, however, would require a complex metering system to precisely control the gas and working fluid inventories.

Another approach to obtaining a variable set point is to keep the gas inventory constant and vary the system volume. Thus, by making the gas reservoir a controllable bellows (or piston, etc.), one can have a sealed system and still vary the operating temperature at will. This is shown on Figure 6-11.

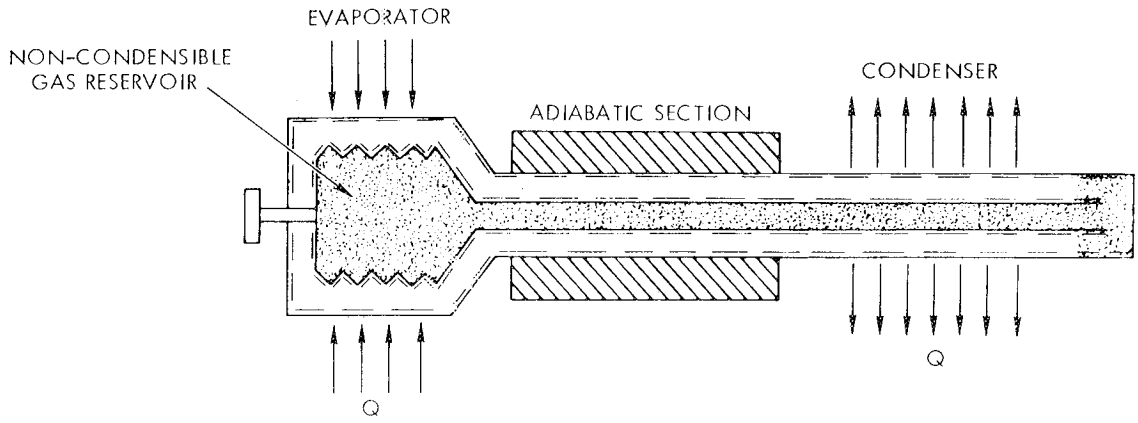

FIGURE 6-11. Schematic Diagram of a Variable Reservoir Volume Gas Controlled Heat Pipe

In Fig. 6-11 the variable volume reservoir is shown internal to the evaporator. It is also possible to use an external variable volume reservoir [V12]. However, in that case there will exist a pressure differential across the reservoir wall which varies with changes in internal or external pressure. A considerable increase in system complexity is involved to prevent variations in this pressure differential from altering the reservoir volume. When the reservoir is placed within the heat pipe, the total pressure within it equals that surrounding it. Thus, this problem is eliminated.

The appropriate characteristic equation for the internal, non-wicked reservoir heat pipe shown in Fig. 6-11 is Eq. (6-17) with T_{va} substituted for T_R.

$$Q = hA'(T_{va}-T_s)\left[L_c + \frac{V_R}{A_v}\frac{T_s}{T_{va}} - \frac{nR_u T_s}{A_v(P_{va}-P_{vs})}\right] \qquad (6\text{-}27)$$

In Eq. (6-27), altering the bellows volume changes V_R in the brackets causing a change in T_{va}. However, this is not an equivalent approach to set point control as varying the gas inventory - n. As shown previously, the control sensitivity is a strong function of the volume ratio V_c/V_R. Thus, varying the reservoir volume changes the control sensitivity as well as the set point. This is quantitatively shown on Fig. 6-12, which plots the functional dependence of T_{va} (T_s is assumed constant) on input power for both variable volume and fixed volume internal reservoir heat pipes. The solid lines represent the fixed volume case (V_R) and show the control sensitivity for five different gas inventories (n') yielding maximum control temperatures (full-on condition) of 20, 40, 60, 80 and 100°F. The dotted lines represent the fixed inventory (n), variable volume case and show the control sensitivity for five reservoir volumes (V_R') which yield the same maximum control temperatures. The two cases are normalized to the 20°F curve. That is, it is assumed that the variable volume pipe has been designed so that, at maximum reservoir volume, it operates with a maximum control temperature of 20°F, and that its volume and gas inventory equal that of the fixed volume pipe at the same temperature setting.

The curves clearly show that as the set point temperature is increased (increasing n or decreasing V_R) the control sensitivity of the variable volume pipe is seriously degraded with respect to the fixed volume - variable inventory pipe.

Thus, although the variable volume pipe offers a much simpler approach to varying the operating temperature than varying the gas inventory, it does so at considerable expense in control sensitivity at high operating temperature.

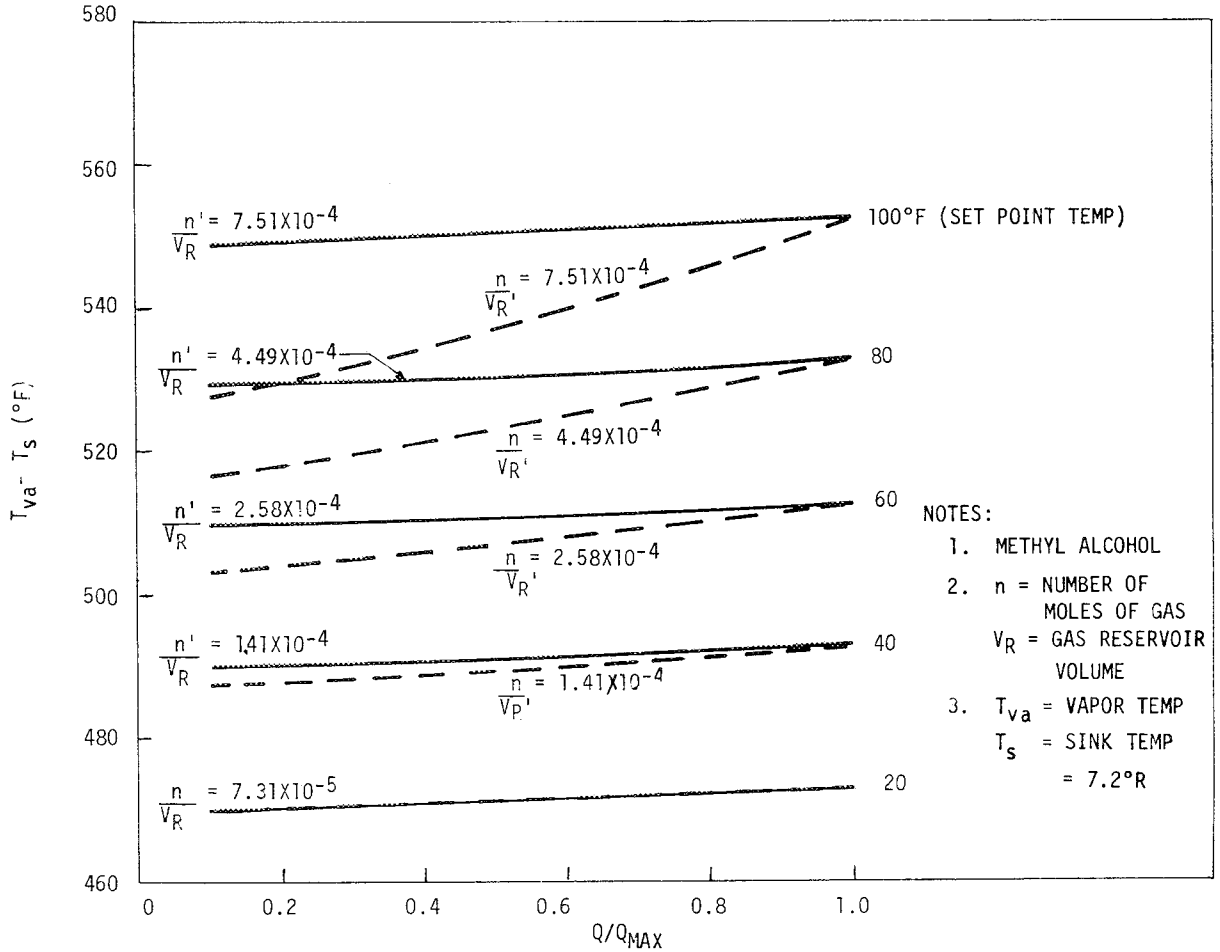

FIGURE 6-12. Comparison of Gas Inventory vs. Reservoir Volume Set Point Control

Still another approach to set point control is to control the reservoir temperature. In sec. 6.1.4.2, reservoir temperature control was discussed as a means of improving control sensitivity by minimizing reservoir temperature fluctuations. However, it can be used as well to vary the nominal operating temperature of a given pipe.

In this case, of course, the reservoir must be external to the heat pipe and its temperature independently controlled, as shown in Fig. 6-13. Two operational modes exist, depending on whether or not the reservoir is wicked.

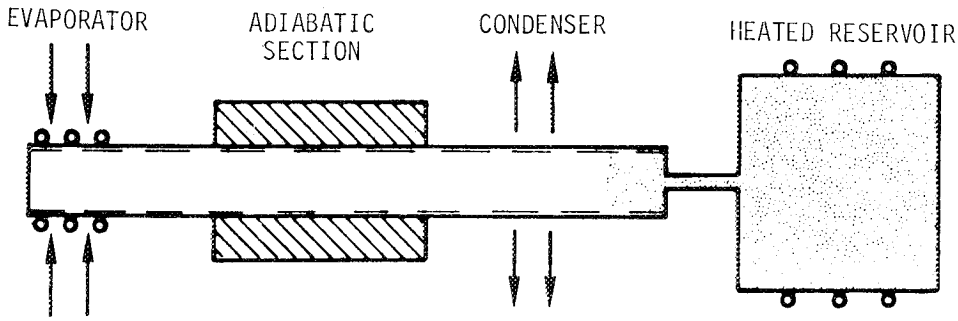

FIGURE 6-13. Schematic Diagram of a Heated Reservoir Gas Controlled Heat Pipe

If the reservoir is not wicked, control of the reservoir temperature provides set point control through variations in the gas temperature. Analytically, the effect is to vary the term T_R in the appropriate characteristic equation (6-17). This is essentially equivalent to varying the reservoir volume - V_R, which appears in the same term within brackets. Hence, it is clear that this approach to set point control suffers a loss in control sensitivity of equal magnitude as the variable reservoir volume approach.

The only constraint on reservoir temperature is that it always be above the temperature at the reservoir entrance, or else vapor would diffuse

into it, condense, and be lost to the system. However, it should be noted that to achieve a wide range in set point control, very large variations in gas temperature are required. For example, from Fig. 6-12 we see that to vary the set point from 60°F to 80°F required nearly halving the reservoir volume. The equivalent for this system would be doubling the absolute reservoir temperature, which would place it hundreds of degrees above the operating temperature of the pipe. This, of course, is a serious limitation for spacecraft thermal control applications.

If the reservoir is wicked, set point control is provided through variations in both the gas temperature and the partial pressure of vapor within it. Analytically, both T_R and P_{vR} vary in Eq. (6-15). In this case, the reservoir has a maximum rather than a minimum temperature constraint. As discussed in Sec. 6.1.4.2, it must operate below T_{va} or the pipe switches and the reservoir becomes the evaporator. It was also shown that, as T_R approaches T_{va}, the control sensitivity provided by the reservoir $(\frac{\partial Q}{\partial T_{va}})$ is diminished. In fact, the rate of loss in control sensitivity with increasing T_R is greater than with a non-wicked reservoir because of the added influence of changes in P_{vR} within Eq. (6-15).

On the other hand, as T_R approaches T_{va}, this same dependence on P_{vR} amplifies the set point sensitivity $(\frac{\partial T_{va}}{\partial T_R})$ and reduces the variations in T_R necessary to effect changes in the nominal set point.

The result is that, from a practical point of view, the wicked system offers a substantially wider set point control range for a reasonable range in reservoir temperature than the non-wicked system.

To summarize this discussion, the nominal operating temperature of a gas-controlled heat pipe is established by the molar gas inventory. The most direct approach to altering this set point temperature is to alter the gas inventory. However, this becomes complex in a practical sense. Alternative approaches to set point control include varying the reservoir volume or temperature. In either case, increasing the set point temperature

(by decreasing V_R or increasing T_R) involves a loss in control sensitivity $(\frac{\partial Q}{\partial T_{va}})$.

From a practical point of view, variable reservoir volume control maintains the passive nature of the gas-controlled heat pipe, but is mechanically complex. If thermostatically controlled reservoir heaters are acceptable, wicked reservoir systems offer wider set point control ranges than non-wicked reservoir systems.

6.1.9 Feedback Controlled Heat Pipes

All of the previously discussed gas-controlled heat pipes operate on the thermodynamic feedback mechanism inherent in the differing pressure-temperature characteristics between a saturated working fluid and a non-condensible gas. This thermodynamic feedback mechanism operates internal to the heat pipe and serves to maintain the evaporator vapor temperature close to a nominal set point value.

However, it has been shown that under conditions of varying sink temperature, there exist definite limits as to the degree of control possible. In certain cases, these may be insufficient. Also, in many applications, control of T_{va} is not the desired end. For example, one might wish to control the evaporator surface temperature or the temperature of a heat dissipating source mounted on it. If the thermal resistance through the pipe wall and wick, or between the heat source and pipe is appreciable, variations in heat input may yield intolerable fluctuations in temperature of the controlled element even if T_{va} remained absolutely constant.

Under such circumstances, one can employ a "feedback controlled heat pipe". This nomenclature simply refers to the inclusion of an external feedback control loop which is referenced to the temperature at the point of interest (e.g., heat source) and which controls the heat pipe operating temperature. The mechanism by which the heat pipe operating temperature can be controlled can be any of those previously discussed in section 6.1.8 on set-point control. Thus, one can arrange to control the gas inventory, the reservoir volume, or the reservoir temperature such that

the reference point (e.g., source temperature) is maintained at any desired value.

The most attractive of these schemes is to utilize temperature control of a wicked reservoir in conjunction with an electronic (or thermostatic) control circuit, referenced to the source temperature, which controls the power to the reservoir so as to maintain the source at a preset temperature. Such a system is shown schematically in Fig. 6-14.

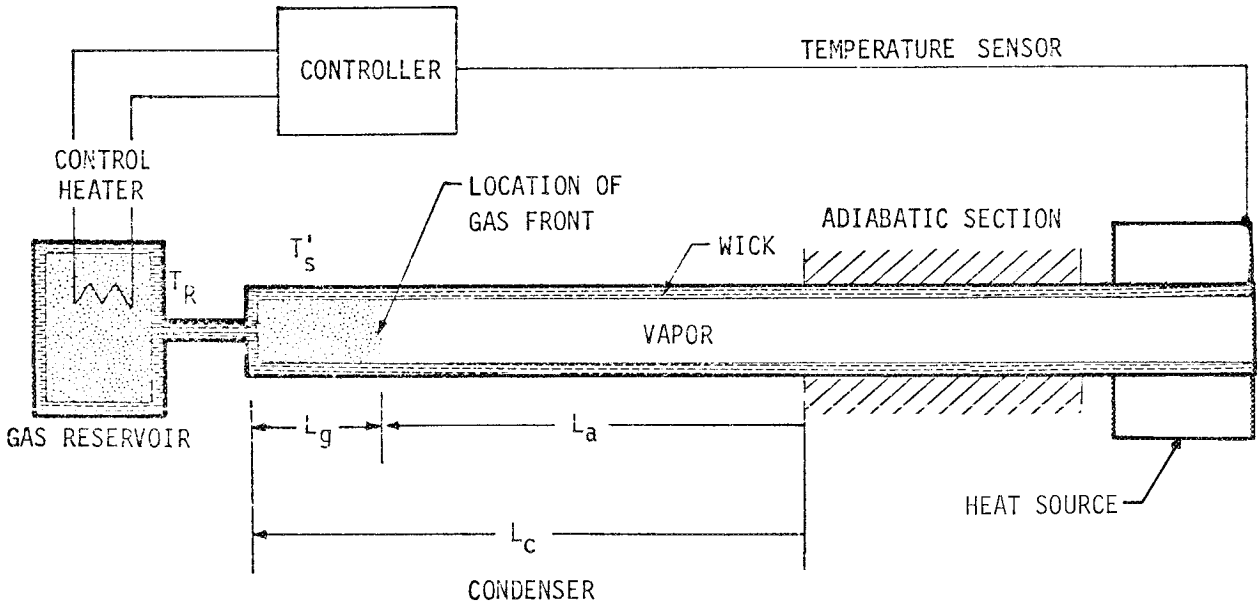

FIGURE 6-14. Schematic Diagram of a Heated Gas Reservoir Feedback Controlled Heat Pipe.

The controller is set such that when the temperature of the heat source falls below a reference value, the heater power is increased. This causes the reservoir temperature to increase, and with it, P_{vR}. The increase in P_{vR} displaces gas from the reservoir, thereby blocking more of the condenser. This in turn raises the evaporator temperature - T_{va}, and with it, the temperature of the heat source. An increase in source temperature causes the opposite sequence of events.

Note that this system actually permits a lowering of heat pipe evaporator temperature with increasing heat input (a negative value of $\frac{\partial T_{va}}{\partial Q}$). With passive systems, $\frac{\partial T_{va}}{\partial Q}$ is always positive, and approaches zero only as V_R/V_c approaches infinity. Thus, the active feedback control system inherently permits closer temperature control of the source than do passive systems. However, as with passive systems, the degree of control possible again depends on the nominal operating temperature, working fluid, and range in effective sink temperature.

Since this system is fundamentally a wicked reservoir heat pipe with $T_R \neq T_s$, the characteristic equation derived in Sec. 6.1.4.2 (Eq. 6-15) still applies. In this case T_R is not fixed, and this additional variable complicates parametric analysis. However, it still holds true that the maximum reservoir temperature must remain equal to or lower than T_{va}, or the reservoir becomes the evaporator.

Basically, rather than permit reservoir gas and vapor pressure variations to degrade controllability, this system actually employs such variations to provide the desired control. This results in an interesting variation from passive control systems. Better control can generally be achieved using working fluids with high values of P_{vR}/P_{va} as T_R decreases from T_{va}. Thus, whereas Fig. 6-4 showed methanol to be superior to ammonia for passive systems, ammonia is superior to methanol for heated wicked reservoir feedback systems.

Further information on the steady-state behavior of feedback controlled heat pipes can be found in the literature (V7, V8, V11). TRW Systems'

work in this area is not related to this program and the limited discussion presented in this report is included for completeness only.

6.2 Accuracy of the Flat-Front Theory

6.2.1 Potential Limitations

The flat-front model was built on several assumptions which were listed in Sec. 6.1. Of particular importance, the model assumes that the interface between the active and inactive portions of the condenser is very sharp, and that axial conduction in the pipe wall (and any attached fins) is negligible. Thus, the model presumes that the temperature in the "shut-off" portion of the condenser is everywhere equal to the effective sink temperature - T_s.

These assumptions are, of course, not realistic. If one considers a typical gas-loaded condenser profile (Fig. 6-15), it is clear that axial conduction and diffusion tend to spread the vapor-gas front. Defining the active condenser length as that portion at temperature - T_{va}, one sees that the flat-front model underestimates both the average gas temperature and the partial pressure of vapor within the gas-blocked zone. This should cause an actual heat pipe to operate at a higher temperature than predicted by the theory.

Furthermore, under conditions of high condenser utilization, the diffuse vapor-gas front causes the temperature at the end of the condenser to rise above the sink temperature ($T_{s'} > T_s$). For non-wicked reservoir heat pipes, where the partial pressure of vapor within the reservoir is established by the temperature at the end of the condenser, such non-fully-developed fronts result in higher reservoir vapor pressures than predicted by the theory. Again, this should cause the flat-front theory to predict lower operating temperatures than those actually achieved.

6.2.2 Experimental Verification of Flat-Front Theory

6.2.2.1 Experimental Measurements

It has been qualitatively argued that neglecting axial conduction and diffusion in the flat-front model would cause it to underestimate the heat pipe operating temperature.

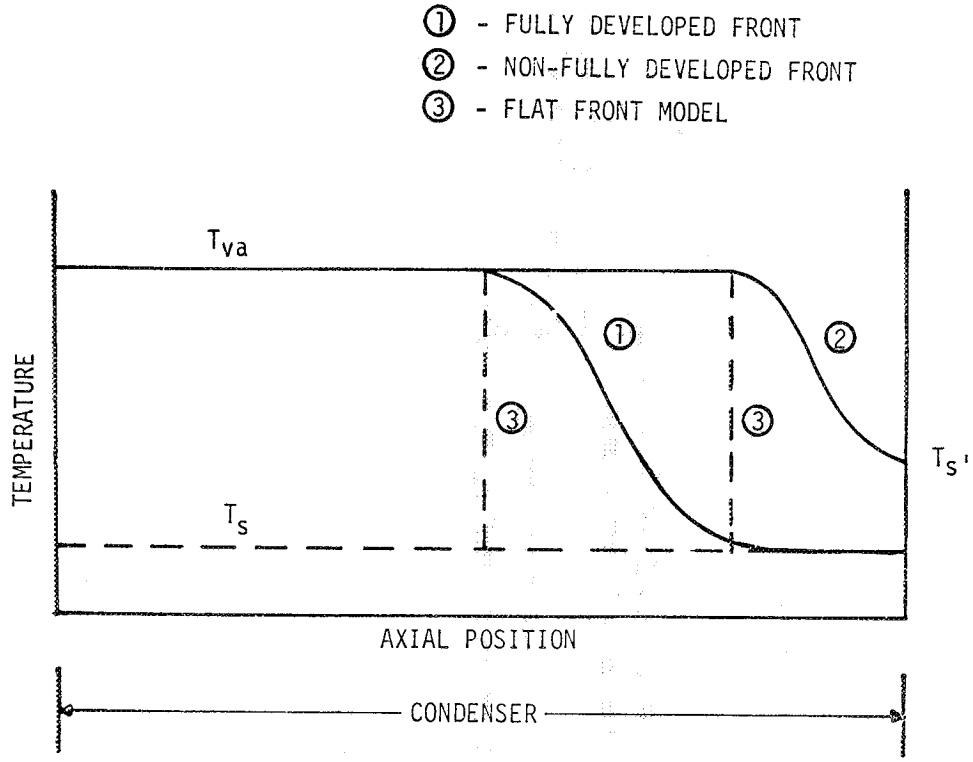

FIGURE 6-15. Temperature Profiles Along Gas Loaded Heat Pipes

In order to demonstrate this effect, experimental measurements were made with a non-wicked hot reservoir heat pipe. A schematic of the experimental heat pipe, which utilized an internal gas reservoir, is shown in Fig. 6-16. The design details are presented in Table 6-1. The pipe was instrumented with twelve thermocouples along its length and a pressure transducer attached to the fill tube. Heat was supplied by resistance wire wrapped around the pipe and insulated. The pipe dissipated heat by natural convection and radiation to ambient.

Figure 6-17 presents steady-state temperature profiles measured at various input power levels. The data were taken by altering the input power and allowing the system to operate until all temperatures and the total pressure measurement were constant for a period of one hour.

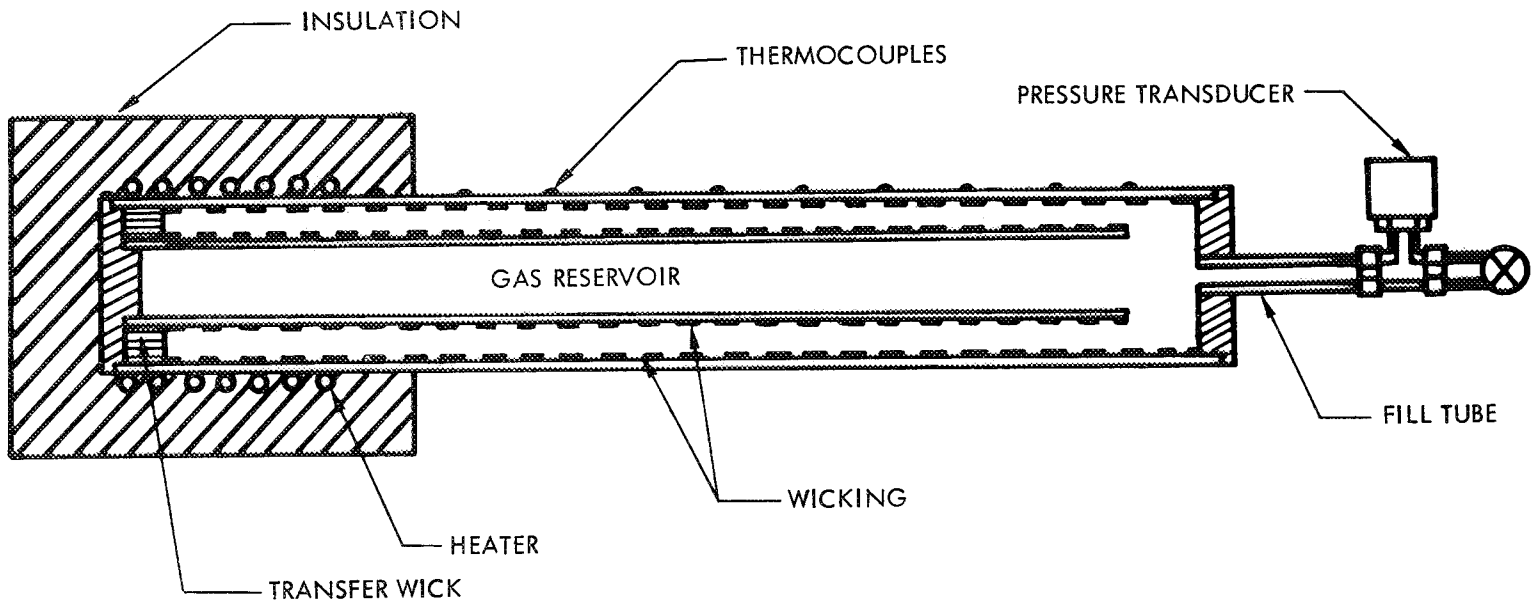

FIGURE 6-16. Schematic Diagram of Experimental Hot Reservoir Heat Pipe

TABLE 6-1
HEAT PIPE DESIGN DETAILS

Working Fluid:	Methanol	
Inert Gas:	Nitrogen at 10 psia	
Pipe:	Material:	Stainless steel
	Inside Diameter:	0.800 in.
	Outside Diameter:	0.8750 in.
	Length:	23 in.
End Plates:	Material:	Stainless steel
	Thickness:	0.125 in.
Gas Reservoir:	Material:	Stainless steel
	Inside Diameter:	0.490 in.
	Outside Diameter:	0.5625 in.
	Length:	21.875 in.
Wicking:	Material:	94 mesh 304 stainless steel screen
	Description:	2 wraps on heat pipe I.D.
		1 wrap on gas reservoir O.D.
		Multi-wrap transfer wick at end of evaporator

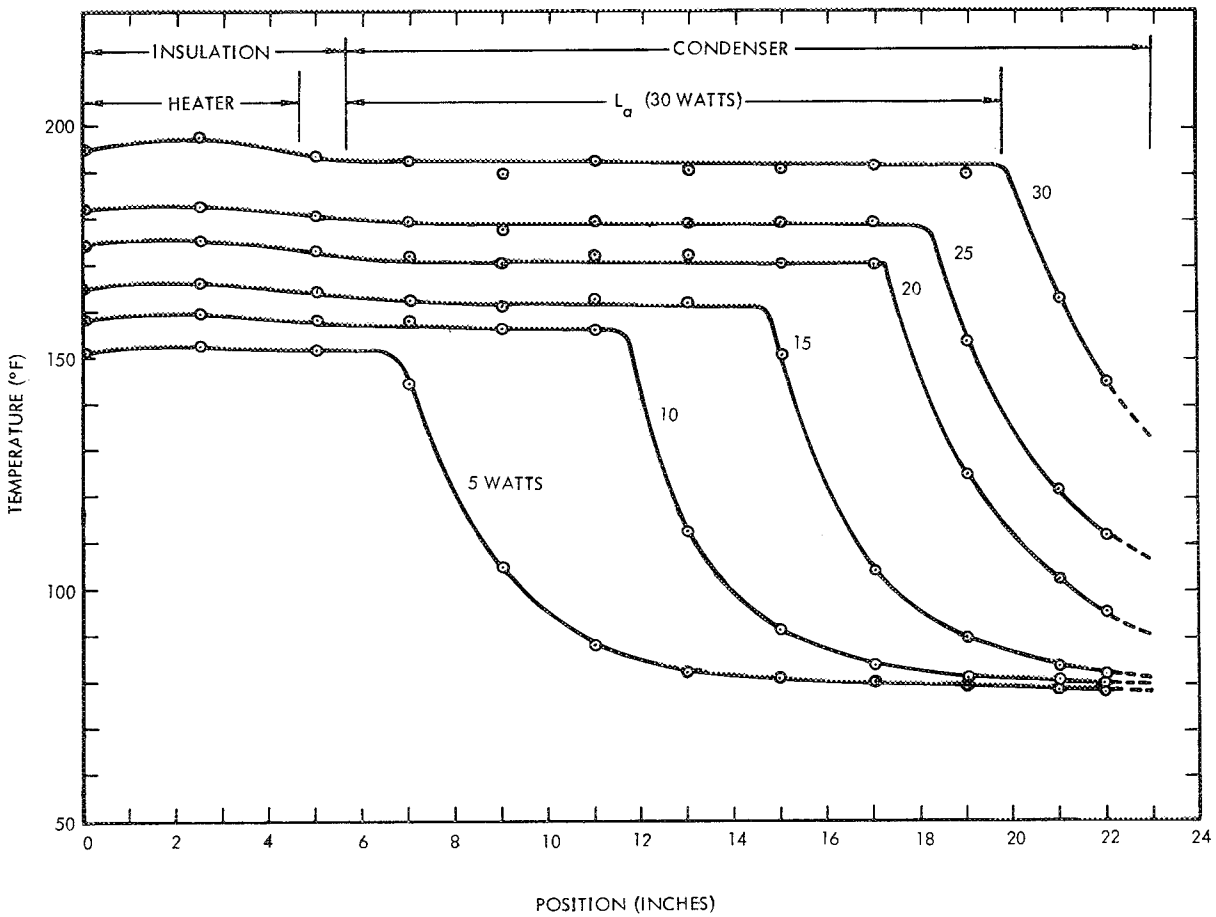

FIGURE 6-17. Steady State Temperature Distributions

6.2.2.2 Flat-Front Theory Predictions

The experimental heat pipe does not exactly fall into any of the categories previously discussed. This is because the reservoir is not at a uniform temperature, but exhibits an axial gradient along its length. However, assuming that (1) radial heat transfer within the pipe is sufficiently good to assure that the axial temperature profile along the reservoir is the same as that along the pipe wall, and (2) thermal diffusion is negligible compared with ordinary mass diffusion, the appropriate characteristic equation can be derived with the same techniques as used before.

Using the analytical model shown on Fig. 6-18:

within the inactive portion of the condenser and reservoir:

$$\left.\begin{aligned} P_g &= P_{va} - P_{vs} \\ T_g &= T_s \end{aligned}\right\} \qquad (6\text{-}28)$$

within the active portion of the reservoir:

$$\left.\begin{aligned} P_g &= P_{va} - P_{vs} \\ T_g &= T_{va} \end{aligned}\right\} \qquad (6\text{-}29)$$

Summing the molar inventory of gas in the pipe now yields:

$$n = \sum \frac{P_g\, dV_g}{R_u T_g} = \left(\frac{P_{va}-P_{vs}}{R_u T_s}\right)\left[A_p\ (L_c - L_a)\right] + \left(\frac{P_{va}-P_{vs}}{R_u T_{va}}\right)\left[A_R\ (L_e + L_a)\right] \qquad (6\text{-}30)$$

where:

V_p - total void volume of pipe
L_e - length of insulated evaporator section
A_p - internal cross-sectional area of pipe envelope
A_R - internal cross-sectional area of reservoir

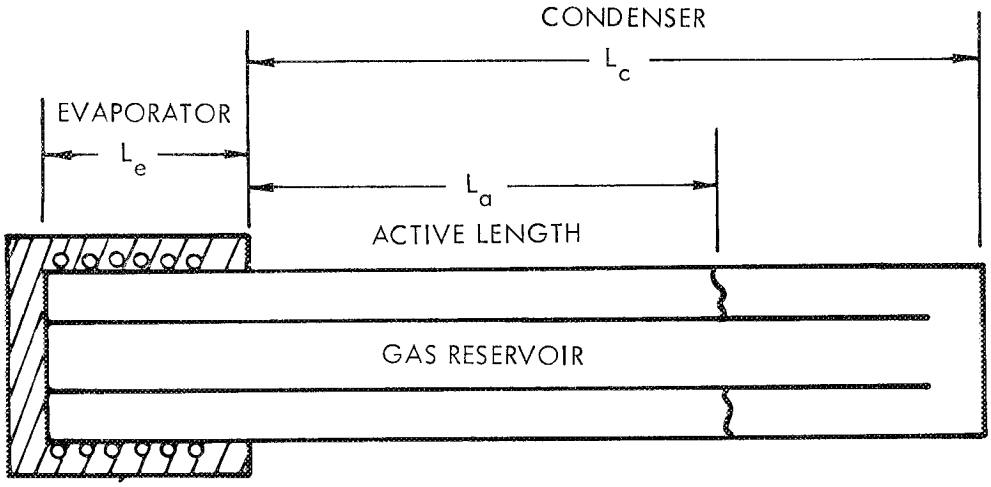

FIGURE 6-18. Definition of Analytical Model for Experimental Hot Reservoir Heat Pipe.

Solving Eq. (6-30) for L_a, and performing a little algebra yields:

$$L_a = \frac{\frac{V_p}{T_s} - \frac{nR_u}{(P_{va}-P_{vs})}}{\frac{A_p}{T_s} - \frac{A_R}{T_{va}}} - L_e \qquad (6\text{-}31)$$

One can now substitute Eq. (6-31) into Eq. (6-1) to obtain a characteristic heat transfer equation as before. However, because the coefficient of heat transfer - h is itself a function of T_{va}, it is preferable to eliminate this variable when comparing predicted and measured results.

Since Eq. (6-31) provides an expression for the active length - L_a which can be directly measured from the temperature profiles of Fig. 6-17, one actually need carry the analysis no further. However, the comparison of data and predictions can be visualized more clearly if the active length is normalized with respect to the total condenser length - L_c. Thus, dividing Eq. (6-31) by L_c yields an expression which represents the

fraction of condenser which is active, and which should theoretically vary between zero and one.

$$0 \leq \frac{L_a}{L_c} = \left[\frac{\frac{V_p}{T_s} - \frac{nR_u}{(P_{va}-P_{vs})}}{\frac{L_c A_p}{T_s} - \frac{L_c A_R}{T_{va}}} - \frac{L_e}{L_c} \right] \leq 1 \qquad (6\text{-}32)$$

6.2.2.3 Comparison of Predicted and Measured Results

One can now compare the measured results for L_a/L_c from Fig. 6-17 with Eq. (6-32), all of whose terms are known or measured with reasonable accuracy. The results of this comparison are shown in Fig. 6-19 (solid lines), which presents predicted and measured operating pressure (P_{va}) and temperature (T_{va}) as a function of L_a/L_c. Apparently, the model is fairly good at low values of L_a/L_c but is in serious error as L_a/L_c approaches unity.

If one examines Fig. 6-17, it is clear that the major drawbacks in the theoretical model discussed earlier are indeed significant. The fact that the transition length from T_{va} to T_s is not zero but substantial means that the average values assumed for the gas temperature in Eq. (6-32) are appreciably too low. This causes Eq. (6-32) to underestimate the operating temperature for all values of L_a/L_c, but particularly for values near zero where the gas-front zone is longest and the total system pressure is lowest. More important at high values of L_a/L_c is the fact that axial conduction causes the temperature at the reservoir entrance to rise well before the full-on region reaches it. Consequently, the partial pressure of vapor in the reservoir becomes substantially higher than the vapor pressure corresponding to T_s, causing a displacement of gas, and thus a further rise in pressure and temperature of the system above those predicted by Eq. (6-32). This effect becomes very significant as L_a/L_c approaches unity.

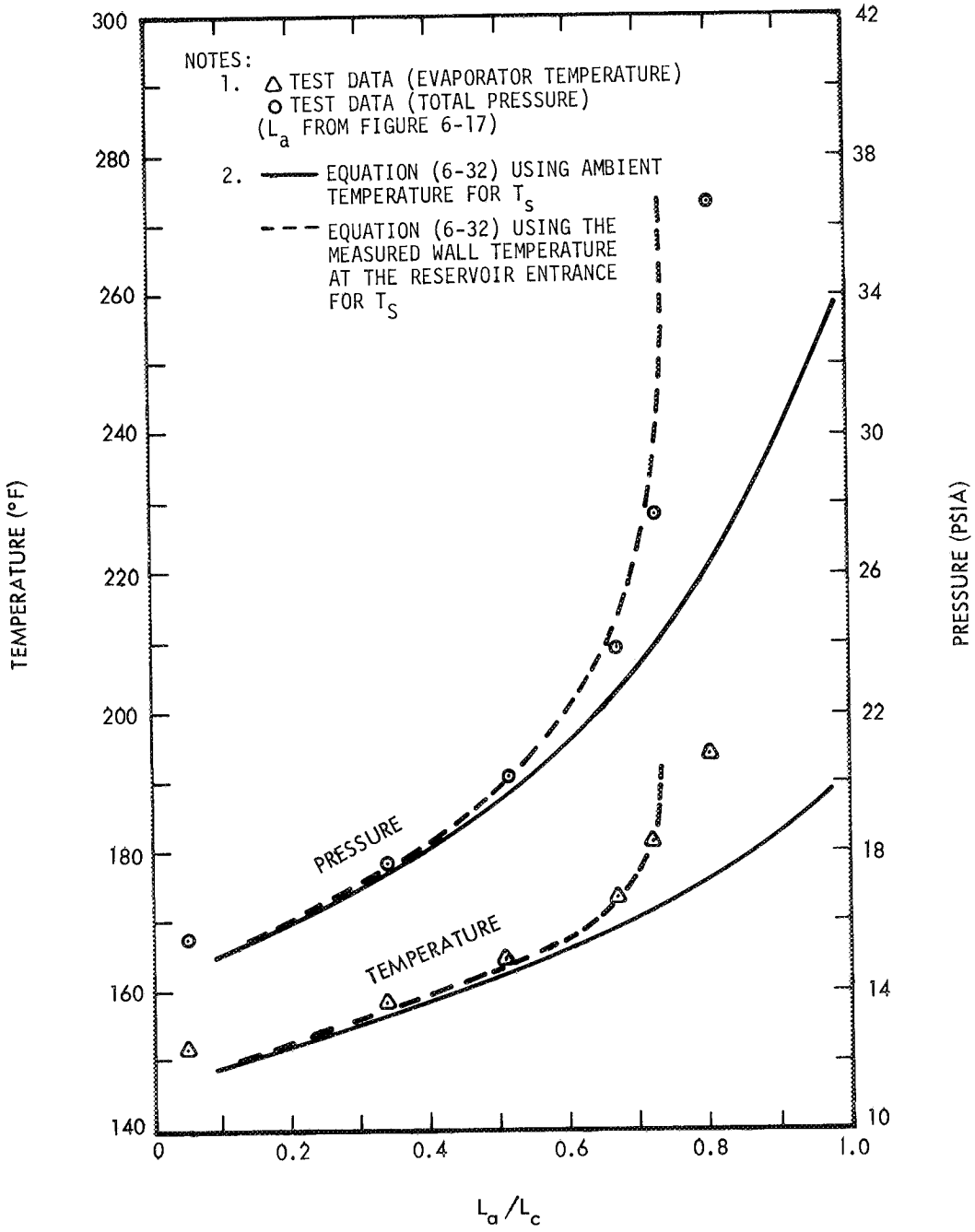

FIGURE 6-19. Steady State Evaporator Temperature and Pressure vs. Active Condenser Length. Comparison of Experimental Data with Theory.

That this is actually the dominant cause of the discrepancy between theory and data is also shown in Fig. 6-19, by the dotted lines. These curves also represent Eq. (6-32) but the measured wall temperature at the reservoir entrance ($T_{s'}$) has been substituted for T_s (and $P_{vs'}$ for P_{vs}) within the brackets. With this substitution, Eq. (6-32) much more closely correlates the data at the higher values of L_a/L_c. Precise agreement is not expected since these measured wall temperatures do not precisely control the vapor pressure conditions at the reservoir entrance. They do not account for radial wick resistance, cooling effects of the end cap and fill tube, or variations in axial temperature distribution between the reservoir tube and pipe wall.

6.2.3 Summary

The previous section shows the relative merits and inadequacies of the flat-front theory when applied to a non-wicked reservoir heat pipe. To bring the theory more closely into line with observed behavior, one must account for the actual temperature and pressure profiles at the vapor-gas interface. This will be dealt with in the next section.

However, it should be noted that the non-wicked reservoir heat pipe is the most severe test of the theory. The largest discrepancies between predicted and measured results corresponded to non-fully developed vapor-gas fronts ($T_{s'} > T_s$), where the theory involved serious underestimates of the partial pressure of vapor within the reservoir. In the case of wicked reservoir heat pipes, the reservoir vapor pressure depends on the reservoir temperature - not $T_{s'}$. By designing the heat pipe so that T_R is relatively de-coupled from $T_{s'}$, the flat-front theory will yield better results for high values of L_a/L_c than those obtained with the system tested.

6.3 Diffuse-Front Theory

As shown in the last section, the "flat-front" model is inconsistent with experimental observations which show that the decrease in vapor concentration and the corresponding increase in gas concentration occur smoothly over an appreciable length of the heat pipe; i.e., the vapor-gas front is diffuse. As a consequence, the flat-front theory does not predict

performance very well, particularly in the case of non-wicked reservoirs near "full-on" condenser conditions.

Furthermore, by neglecting the diffuse nature of the vapor-gas front, the flat front model does not permit accurate calculation of the axial "heat leak" when the condenser is filled with gas (when $L_a = 0$).

Finally, the flat front model yields no information on the rate of vapor diffusion into the gas-blocked zone of the condenser. This can be particularly important when the effective sink temperature is below the melting point of the working fluid and a portion of the gas-blocked region is frozen. Under such circumstances, there is a continuous diffusion of vapor into the sub-freezing zone where the vapor freezes and is lost to the system. If appreciable, this can eventually lead either to a deficiency of liquid in the pipe, or the local plugging up of the condenser vapor core with frozen fluid. In the former case, the pipe may suffer a hydrodynamic failure, particularly if it employs an arterial wick structure (which cannot operate in a partially de-saturated mode). In the latter case, the reservoir becomes isolated from the condenser, and the pipe loses its temperature control capability.

In view of these limitations in the flat-front theory, an analysis was performed for gas-loaded heat pipes which includes (1) simultaneous radiation and convection from a finned condenser, (2) axial conduction in the walls, fins and wicks, (3) binary mass diffusion between the vapor and gas, and (4) an approximate treatment of radial wick resistance which is accurate for high conductance wicks (e.g., circumferentially grooved walls).

6.3.1 Analytical Formulation

The condensing section of the pipe is assumed to reject heat by radiation and convection from a fin of perimeter P with an effectiveness η as shown in Fig. 6-20. The net heat loss from a length of condenser dz is thus taken to be

$$dQ = \left[\varepsilon\sigma T_w^4 + h(T_w - T_f) - q_{abs}\right] \eta P dz \qquad (6\text{-}33)$$

where ε is total hemispherical emittance, σ the Stefan-Boltzmann constant, T_w the wall temperature, h the convective heat transfer coefficient, if any, T_f the external fluid temperature, and q_{abs} is the power absorbed per unit area from the surrounds, αH in the case of irradiation H onto the condenser surface of absorptance α. For simplicity all parameters are taken to be constants.

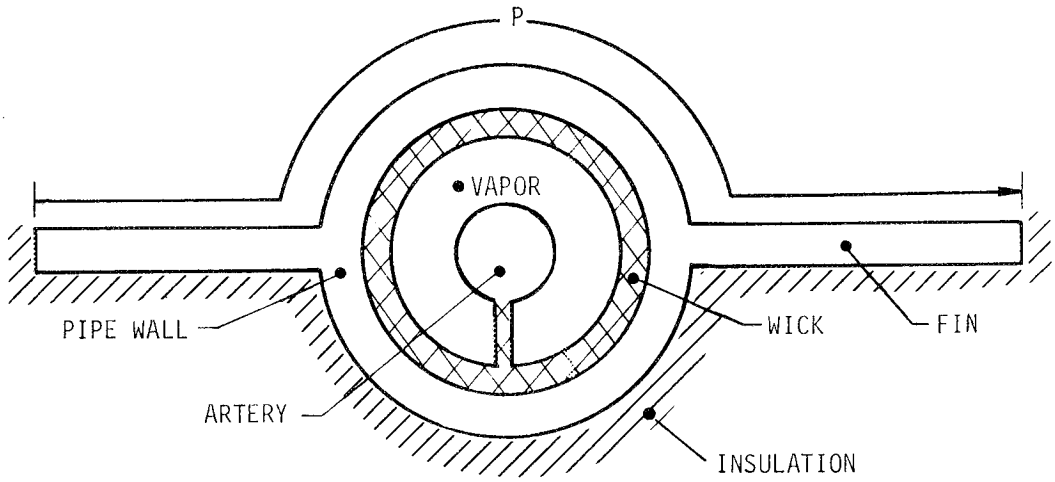

FIGURE 6-20. Cross-section of Condenser: Diffuse-Front Model

In the usual heat pipe application the difference between the wick-vapor interface temperature T_i and the condenser wall temperature T_w is small compared to absolute temperature level. For this reason Eq. (6-33) is written in a linearized form

$$dQ = Sdz\ (T_w - T_s) \tag{6-34}$$

where

$$S(z) = \left[4\varepsilon\sigma T_i^{\,3} + h\right] \eta P \tag{6-35}$$

and

$$T_s(z) = \frac{3\varepsilon\sigma T_i^{\,4} + q_{abs} + hT_f}{4\varepsilon\sigma T_i^{\,3} + h} \tag{6-36}$$

We adopt the unusual sign convention that the power Q is measured in the negative z direction. Then Fourier's law is written without the usual negative sign. Heat flows into an element of pipe dz long at z+dz and out at z by axial conduction. Heat also flows across the wick by conduction at the rate

$$\frac{2\pi k_e dz}{\ell n \frac{D_i+2\delta}{D_i}} (T_i-T_w) = Kdz\ (T_i-T_w) \qquad (6\text{-}37)$$

where k_e is the equivalent thermal conductivity of the liquid-filled wick, D_i the inside diameter of the wick, and δ the wick thickness. Equation (6-37) defines K. The heat balance on an element of condenser is then

$$C \frac{d^2T_w}{dz^2} + K(T_i-T_w) - S(T_w-T_s) = 0 \qquad (6\text{-}38)$$

where C is the axial conductivity-area product for the condenser cross-section,

$$C = \sum_{n=1}^{N} k_n A_{c,n} \qquad (6\text{-}39)$$

In Eq. (6-39) k_n is the effective axial conductivity, allowing for slots or other anisotropies, and $A_{c,n}$ the cross-sectional area of the nth element in the pipe. These elements may include the pipe wall, the wick and any arteries, and the fin wall, as shown in Fig. 6-20. Even if the wick artery is not in intimate thermal contact with the condenser wall, its axial conductance is included in Eq. (6-39), because the temperature gradient in it tends to follow dT_i/dz which in turn tends to follow dT_w/dz, when K is large compared to S.

The wick interface temperature T_i is the saturation temperature for the partial pressure of the vapor above the interface, since the net condensation rate is far from the absolute rate of condensation. Other simplifying assumptions introduced, which are reasonable for most applications, are negligible vapor side pressure loss and a simple vapor pressure law derived from the Clausius-Clapeyron relation. The mole fraction of the non-condensible at the interface x_i and the interface temperature T_i are then related in the following way

$$x_i = 1 - \exp\left[-(\lambda/RT_{ev})(T_{ev}/T_i - 1)\right] \tag{6-40a}$$

$$T_i = \frac{T_{ev}}{1 + \frac{RT_{ev}}{\lambda} \ell n \frac{1}{1-x_i}} = \frac{T_{ev}}{1 + \frac{T_{ev}}{T_o} \ell n \frac{1}{1-x_i}} \tag{6-40b}$$

Conservation of non-condensible gas requires that the diffusion plus convection in the tube sum to zero,

$$-c\mathcal{D}\frac{dx_s}{dz} - cVx_b = 0 \tag{6-41}$$

where c is the molar concentration, $\mathcal{D}$ the diffusion coefficient for the non-condensible diffusing in the vapor, x_s the spatial or area-weighted average mole fraction, V the mole average velocity, and x_b the bulk (area-velocity weighted) average. At least in the region of the condenser which is gas-controlled, the radial velocity rates will be sufficiently low so that the bulk, spatial, and wall values of mole fraction of non-condensible will be nearly the same. This assumption is made for the entire condenser so that the subscripts i, s, and b on x will be dropped in what follows.

To obtain an equation having the grouping $\dot{m} = cVA_vM$, the condensible flow rate, Eq. (6-41) is multiplied by A_vM, where M is the molecular weight of the condensible working fluid. In addition, the dependent variable is transformed from mole fraction x to ϕ by introducing

$$\phi = \ell n \frac{1}{x}, \qquad x = e^{-\phi} \tag{6-42}$$

Equation (6-41) then becomes

$$A_vM\mathcal{D}\frac{d\phi}{dz} + \dot{m} = 0 \tag{6-43}$$

Conservation of mass shows that increase in mass flow rate with distance from the end of the condenser is equal to the condensation rate which in turn is equal to the product of wick conductance and temperature difference across the wick divided by the latent heat of vaporization or sublimation.

$$\frac{d\dot{m}}{dz} = K(T_i - T_w)/\lambda \tag{6-44}$$

Equations (6-38), (6-43) and (6-44) form a set of three simultaneous differential equations in three unknowns: T_w, ϕ, and $\dot{m}$. The temperature T_i is related to ϕ through the highly non-linear relations, Eqs. (6-42) and (6-40). The coefficient S defined by Eq. (6-35) is also non-linear. An explicit energy equation for the liquid or vapor is not written, because subcooling of liquid in the wick and superheating of the vapor in the pipe are not considered to be key physical phenomena, and are neglected in the present treatment. Equations (6-44) and (6-38) will give an entirely correct energy balance when x_i, x_s, and x_b are identical, the wick resistance small, and no freezing occurs.

A boundary condition on (6-38), (6-43) and (6-44) is taken to be

$$\dot{m} = 0 \text{ at } z = 0 \tag{6-45}$$

In addition, either one of two conditions may be prescribed: a total heat rate rejected

$$Q = \int_0^{L_c} S(T_w - T_s)dz \tag{6-46a}$$

or a total number of moles of non-condensible present

$$n = A_v \int_0^{L_c} \left[P_{gi}(T_i(z))/R_u T_i \right] dz \tag{6-46b}$$

In computing n a more accurate vapor pressure law than Eq. (6-40) is required. An exponential of a polynomial in the reciprocal of T_i is used.

Strictly speaking, since Eq. (6-38) is second order, two more conditions must be specified, such as a zero CdT_w/dz at $z = 0$ and $z = L_c$. However, by assuming high radial wick conductance, T_w is close to the wick interface temperature - T_i, and the first and second derivatives of T_w and T_i with respect to z can be assumed equal, respectively. It will be shown that this approximation reduces the set of equations to two first order ones so that Eq. (6-45) and (6-46) are sufficient. The condition on CdT_w/dz is met at $z = 0$, and at $z = L_c$ it is met in practical effect when

the evaporator is purged of gas. The approximation regarding the derivatives of T_w and T_i is, of course, exact when the wick resistance is zero.

Before proceeding further with the analysis, it is convenient to non-dimensionalize the parameters for convenience in numerical solution. The dimensionless quantities are:

$$z^* - z/D_e$$

$$V^* - \dot{m}\lambda/Q_{nominal}$$

$$\mathscr{D}^* - M(c_{ev}\mathscr{D}_{ev}/D_e)A_v\lambda/Q_{nominal}$$

$$T_i^* - T_i/T_{ev}$$

$$T_w^* - T_w/T_{ev}$$

$$T_0^* - T_0/T_{ev}$$

$$T_s^* - T_s/T_{ev}$$

$$T_R^* - T_R/T_{ev}$$

$$Q_e^* - \frac{dQ^*}{dz^*} = S^* (T_w^* - T_s^*)$$

$$S^* - F^* (4\varepsilon\sigma T_i^{*3} + H^*)$$

$$F^* - \eta P D_e \sigma T_{ev}^4/Q_{nominal}$$

$$H^* - h/\sigma T_{ev}^3$$

$$C^* - CT_{ev}/D_e Q_{nominal}$$

where T_{ev} is the evaporator temperature which sets the total pressure in the system, and D_e is an equivalent diameter allowing for the presence of arteries within the pipe,

$$D_e = (4A_v/\pi)^{\frac{1}{2}} , \qquad (6\text{-}48)$$

where A_v is the cross-sectional area available for vapor flow. An exponent E is an empirical factor to account for the temperature variation of the mass diffusivity defined by

$$c\mathscr{D} = c_{ev}\,\mathscr{D}_{ev}(T_i/T_{ev})^E \tag{6-49}$$

Equations (6-38), (6-43), (6-44), and (6-40) written in dimensionless form become

$$C^* \frac{d^2T_w^*}{dz^{*2}} + K^*(T_i^* - T_w^*) - S^*(T_w^* - T_s^*) = 0 \tag{6-50}$$

$$\frac{d\phi}{dz^*} = \frac{V^*}{\mathscr{D}^* T_i^{*E}} \tag{6-51}$$

$$\frac{dV^*}{dz^*} = K^*(T_i^* - T_w^*) \tag{6-52}$$

$$1 - e^{-\phi} = e^{-T_0^*(1/T_i^*-1)} \tag{6-53}$$

Using the assumption of high radial wick conductance permits replacing $\frac{d^2T_w^*}{dz^{*2}}$ with $\frac{d^2T_i^*}{dz^{*2}}$, and Eq. (6-50) can be approximated as:

$$C^* \frac{d^2T_i^*}{dz^{*2}} + K^*(T_i^*-T_w^*) - S^*(T_w^*-T_s^*) = 0 \tag{6-54}$$

The simplifying feature of this approximation is that the second derivative in Eq. (6-54) can now be eliminated. Equation (6-53) is differentiated with respect to z^*, and Eq. (6-51) is used to eliminate $d\phi/dz^*$. The result multiplied by C^* is

$$C^* \frac{dT_i^*}{dz^*} = C^* \frac{e^{-\phi}\, T_i^{*2-E}}{1-e^{-\phi}\mathscr{D}^* T_0^*}\, V^* \tag{6-55}$$

Equation (6-55) is differentiated again with respect to z^*, Eq. (6-51) is used again to eliminate $d\phi/dz^*$, and Eq. (6-55) itself is used to eliminate dT_i^*/dz^*.

$$C^* \frac{d^2T_i^*}{dz^{*2}} = \Phi_1 \frac{dV^*}{dz^*} - \Phi_1\,\Phi_2\,\Phi_3 \tag{6-56}$$

where the functions Φ_1, Φ_2, Φ_3 are

$$\Phi_1(\phi) = C^* \frac{e^{-\phi}}{(1-e^{-\phi})} \frac{T_i^{*2-E}}{\mathscr{P}^* T_0^*} \tag{6-57}$$

$$\Phi_2(\phi) = 1 - (2-E)(T_i^*/T_0^*)e^{-\phi} \tag{6-58}$$

$$\Phi_3(\phi, V^*) = V^{*2}/ (1-e^{-\phi})\mathscr{P}^* T_i^{*E} \tag{6-59}$$

Equation (6-54) together with Eqs. (6-52) and (6-56) now can be written

$$\frac{dV^*}{dz^*} = Q_e^* - \Phi_1 \Phi_4 \tag{6-60}$$

where

$$\Phi_4(\phi, V^*) = \frac{Q_e^*(\phi) - \Phi_2(\phi)\Phi_3(\phi, V^*)}{1 + \Phi_1(\phi)} \tag{6-61}$$

Equations (6-51) and (6-60) together with (6-53) and the definitions of Φ_j in Eqs. (6-57), (6-58), (6-59) and (6-61) form a set of two simultaneous non-linear first order ordinary differential equations which are amenable to numerical solution. The initial conditions are $V^* = 0$ and $\phi = \phi_0$ at $z = 0$. Values of n and Q for a pipe with condenser length L_c can be obtained versus ϕ_0 for a given set of parameters and an evaporator temperature T_{ev}. An iterative routine can be used to find ϕ_0 for a prescribed value of either n or Q.

A review of the features of the analysis and assumptions made are as follows:

1. Radiation and convection from a finned pipe is considered. Absorbed radiation from the surrounds is included.
2. The condenser wall temperature T_w is assumed close to the wick interface temperature T_i. The first and second

derivatives of T_w and T_i with respect to z are assumed equal, respectively. In essence high wick conductance is assumed.

3. Axial conduction of heat in the pipe wall and fin and one-dimensional axial diffusion of the condensible species, which carries latent heat, is accounted for.
4. Vapor pressure drop in the pipe is neglected. In calculating the shape of the wall temperature and wick temperature distributions, an approximate vapor pressure law derived from Clausius-Clapeyron is used. But in calculating the pressure in the pipe and the amount of non-condensible present a more accurate expression is used.
5. The condition of zero wall temperature gradient is met at z = 0. Either the total number of moles of non-condensible present in the pipe or the total heat rejected by the pipe is specified.

6.3.2 TRW Gaspipe Computer Program

The equations resulting from the analysis of section 6.3.1 have been programmed for solution on a digital computer. In the numerical solution of these equations, an initial value of T_i slightly in excess of the sink temperature is used to fix $\phi(0)$, and a fourth order Runge-Kutta routine is used to solve for $\phi(z)$ and $V^*(z)$. Either the amount of gas in the pipe or the total heat rejection is then compared with the input value, and an iterative routine followed until agreement is reached within one-tenth of one percent.

The program has been generalized to increase its usefulness to the heat pipe engineer. Although the equations were derived for the model shown in Fig. 6-20, the program is not limited to this geometry. Non-circular and non-axisymmetric configurations can also be studied by calculating equivalent diameters, thicknesses, etc. consistent with the formulation of the equations.

In its current form it allows one to:

- Calculate the wall temperature profile along a gas loaded heat pipe.
- Calculate the gas inventory necessary to obtain a desired evaporator temperature at a desired heat load.
- Calculate the heat and mass transfer along the pipe, including the vapor-gas front region.
- Calculate the heat leak when the condenser is filled with gas.
- Calculate whether or not freezing occurs in the condenser and, if so, at what rate.
- Determine the information required to size the gas reservoir for variable conductance heat pipes.

The program contains numerous reservoir options which allow it to be used for hot or cold reservoir passive control, as well as heated reservoir feedback control heat pipes. Additional input options permit its convenient use for parametric studies and off-design performance predictions as well as heat pipe design. Provision is also made for two condenser sections with a step change in the condenser/fin properties or environmental conditions. Thus, it can accommodate cold traps or adiabatic sections in addition to the primary condenser.

The program requires the following input information:

Fluid Characteristics;

Vapor pressure law constants, molecular weight of condensible, binary mass diffusivity of non-condensible into condensible, temperature exponent of diffusivity and latent heat of vaporization.

Vapor Flow, Pipe and Wick Characteristics:

Outside diameter, wall thickness and thermal conductivity of pipe; thickness and effective thermal conductivity of wick; diameter of internal artery, reservoir or reservoir feed tube, if any.

Condenser Characteristics for Each of Two Condenser Sections:

Perimeter, length, effectiveness, heat transfer coefficients, emissivity, thickness and effective axial conductivity of the fin; ambient fluid temperature and power per unit area absorbed on the heat transfer surface.

Operating Conditions:

(a) Evaporator temperature and total heat dissipated, or

(b) Evaporator temperature and moles of gas present in the pipe (in this case a nominal estimate of Q ($Q_{nominal}$) must be input because it is used in non-dimensionalizing the equations.

The program output consists of profiles of x_i, T_i, T_w, $\dot{m}$ and Q(z) vs. z. In addition, the missing value of n for case (a) above or a correct value of $Q(L_c)$ for case (b) is obtained.

A description of the actual program is beyond the scope of this report. However, a document is available which presents a listing and flow charts of the program, instructions on its use and a sample run, as well as the analysis upon which it is based. This report, entitled "User's Manual for the TRW Gaspipe Program", was prepared under this contract and is available upon request (reference V15).

6.3.3 Experimental Verification of TRW Gaspipe Program

A series of measurements were made with a laboratory gas-loaded heat pipe to provide a basis for testing the predictive capability of the TRW Gaspipe Program. The design details of the heat pipe are presented in Figure 6-21 and Table 6-2.

The heat pipe was instrumented with 24 chromel-alumel thermocouples, 23 on the outside wall and one within the vapor core in the evaporator. In addition, a strain gage pressure transducer was attached to the fill tube. Heat input to the 12 inch evaporator was supplied with glass-insulated Nichrome heating wire close-wound around the pipe wall. The

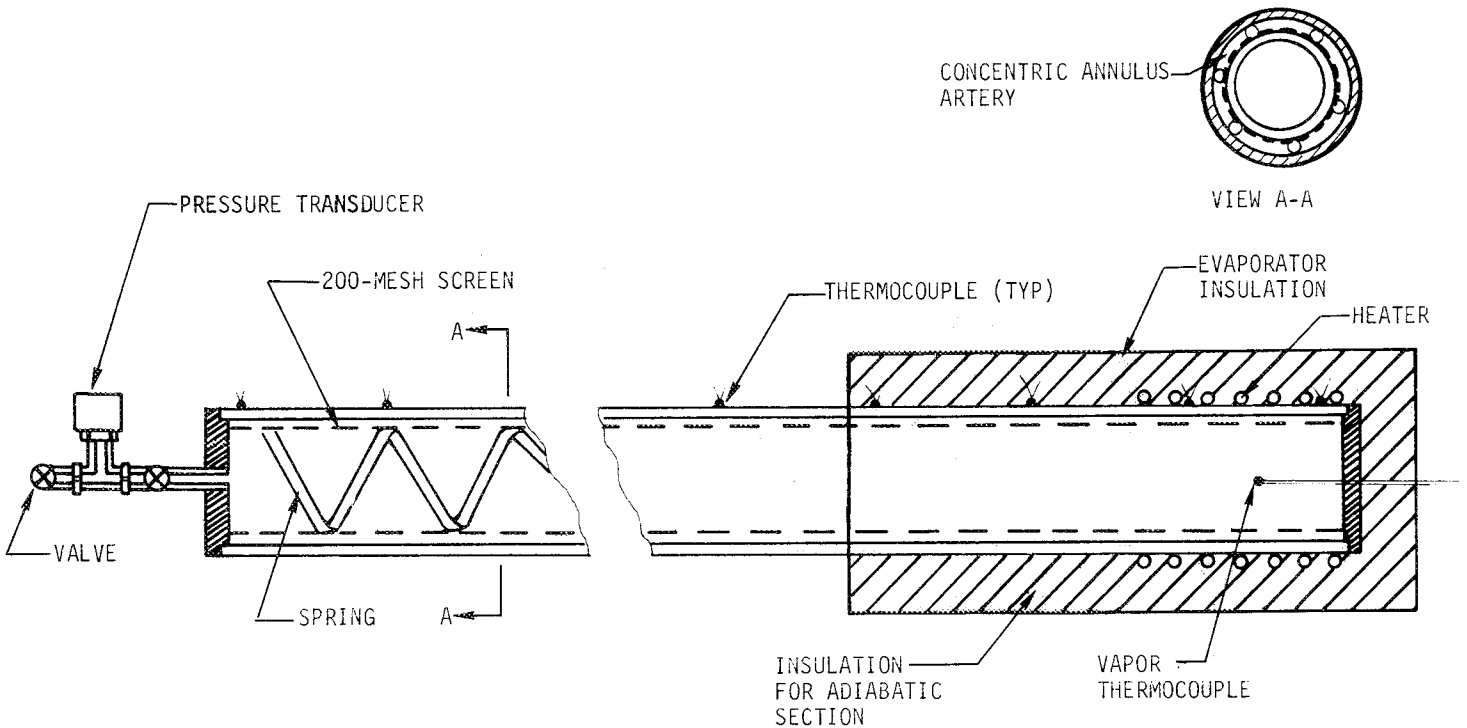

FIGURE 6-21. Schematic Diagram of Experimental Gas-Loaded Heat Pipe

TABLE 6-2

EXPERIMENTAL HEAT PIPE DESIGN DETAILS

Working Fluid:	Water	
Inert Gas:	Air (2.67×10^{-6} $\pm 5\%$ lb-moles)	
Pipe:	Material:	Stainless steel
	Outside Diameter:	0.565 in.
	Wall Thickness:	0.036 in.
	Overall Length:	54.75 in.
	Condenser Length:	30.25 in.
	Evaporator Heat Input Length:	12.5 in.
	Adiabatic Section Length:	12.0 in.
Wick Structure:		
	Material:	200 mesh stainless steel screen
	Description:	Concentric annulus artery (0.015 in. gap width) with two wraps of screen held in place by a spring.

evaporator and adiabatic sections were insulated with 2 inches of polyurethane foam. Heat transfer from the condenser was by radiation and natural convection to ambient.

Additional instrumentation included an ammeter and voltmeter for power measurements, a multipoint recorder and a hand balanced potentiometer for temperature measurements, a digital voltmeter and transducer power supply for pressure measurements, and a precision thermometer and barometer for measuring ambient conditions.

The experimental procedure involved simply setting a fixed power input to the heater, allowing the system to equilibrate (using the multipoint recorder as an indicator), and then recording the appropriate data (using the potentiometer for accurate temperature measurements). Five runs were made in total, such that the vapor-gas interface traversed the entire condenser.

The non-condensible gas inventory was determined using the pressure transducer attached to the fill tube. The procedure was to turn off the power to the heaters and allow at least twelve hours for the pipe to equilibrate. This rather lengthy equilibration period was required for the vapor and gas to thoroughly diffuse yielding a uniform mixture. The internal total pressure was then measured. The partial pressure of gas was determined by subtracting the vapor pressure of water at measured ambient temperature from the total pressure as measured by the transducer. The molar inventory of gas was then calculated from the perfect gas law since the total void volume of the pipe and the gas temperature were also known. Such measurements were made at the beginning of the test program, midway through it and at the end. All measurements yielded the same gas inventory indicating that no leakage or gas generation occurred during the test program.

The TRW Gaspipe Program was then utilized to obtain performance predictions for each of the test runs. The required input data for the program were listed earlier. All but one of the required inputs are either known

properties of the materials or directly measured quantities. The exception is the coefficient of heat transfer - h. Since the predicted heat dissipation for a given temperature distribution is quite sensitive to the assumed value of h, this value was determined for each test run by using Newton's cooling law, $q = h\Delta T$, in conjunction with the measured power and temperature distribution. The calculated values of h represent both radiative and natural convection heat transfer. They are of appropriate magnitude for such a heat transfer mode.

Figure 6-22 presents both the measured and predicted temperature profiles. As is apparent, the computer program predicts the position of the gas front quite well. This is particularly true in view of the sensitivity of the system to gas inventory and evaporator temperature. The shaded band around one curve on Fig. 6-22 represents the predicted front positions for a $\pm 5\%$ variation in gas inventory. This is about the limit of accuracy estimated for this measurement. The effect of a $\pm 2°F$ measurement error in evaporator temperature is shown as a shaded band on the second curve. Again, this represents the limit of accuracy estimated for absolute temperature measurements with the system used.

The program also does a credible job in predicting the shape of the temperature profile, particularly at the low temperature end. At the high end, the predicted profile rises somewhat more steeply than the measured data. This is due to the approximate method used to account for the radial wick resistance. The analysis allows a somewhat higher condensation rate in this region then actually occurs, leading to a slightly sharper gas front.

Also of interest is the ability of the analysis and computer program to predict the heat rejection vs. evaporator temperature characteristic of the heat pipe. This characteristic describes the steady-state performance of gas loaded heat pipes from a system design point of view. Figure 6-23 shows the comparison between measured data and the computer predictions. Very good agreement is evidenced between measured and predicted results.

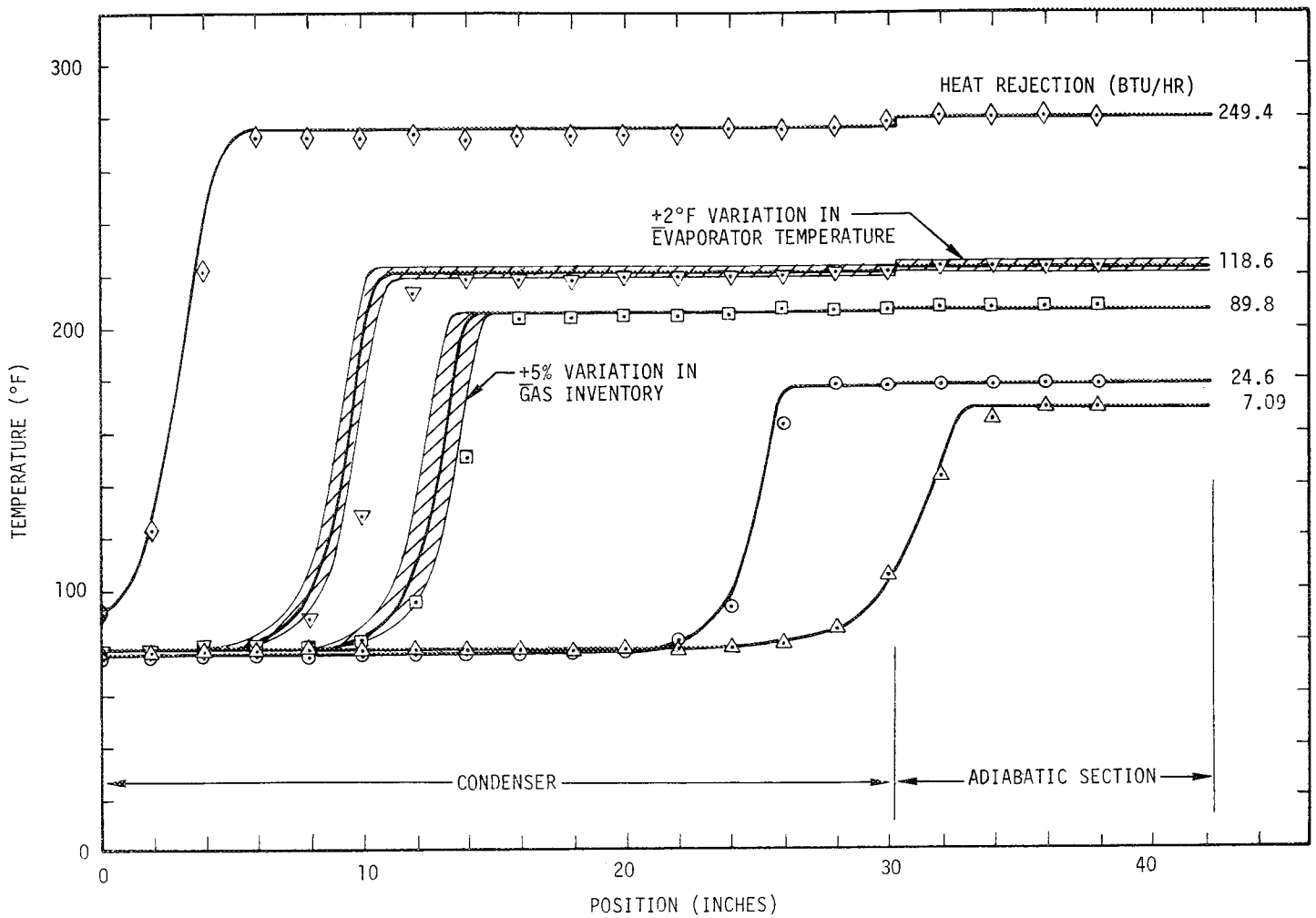

FIGURE 6-22. Comparison of Measured and Predicted Temperature Profiles for a Gas Loaded Heat Pipe

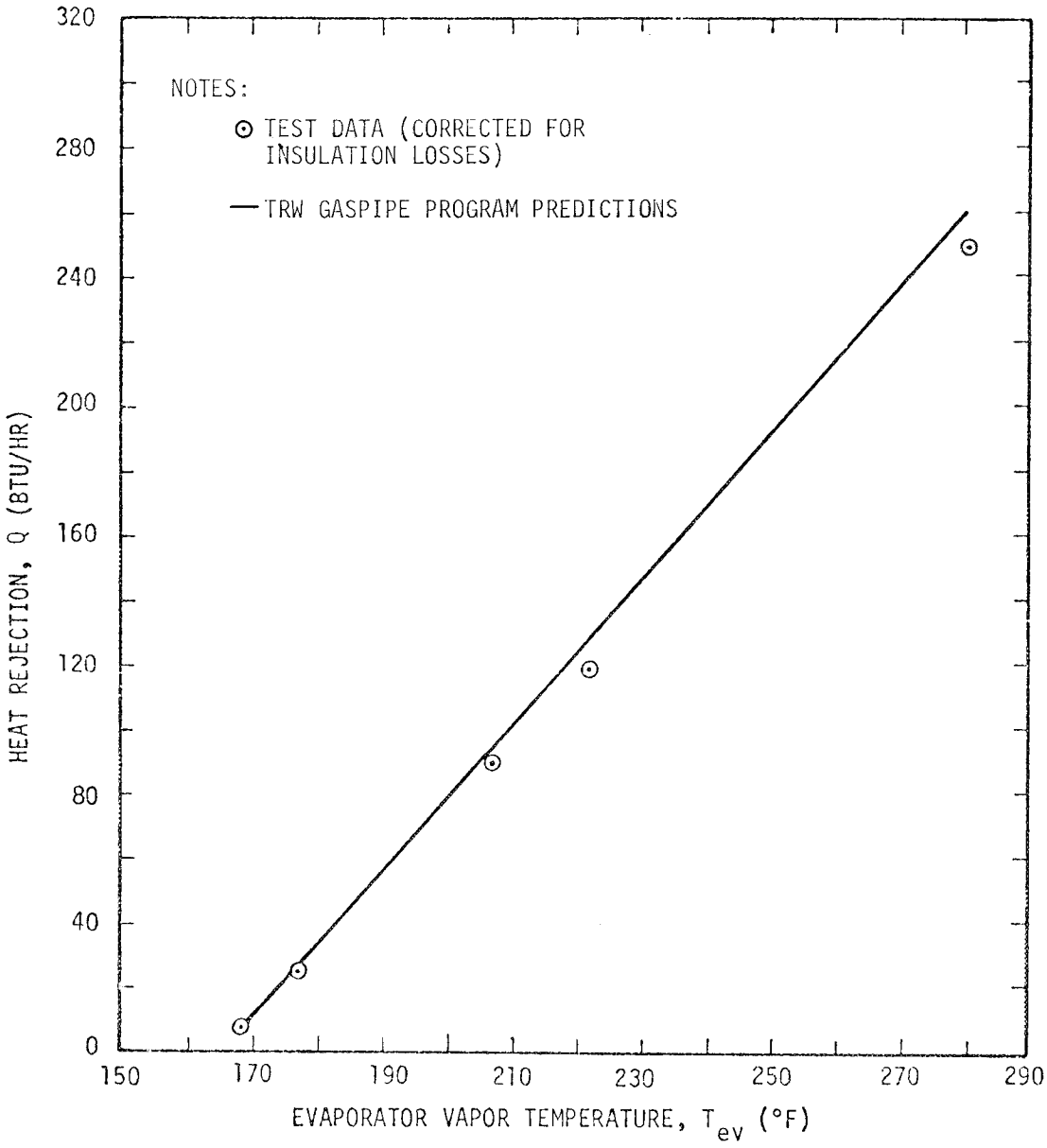

FIGURE 6-23. Comparison of Predicted and Observed Heat Transfer Rates as a Function of Heat Pipe Evaporator Temperature

6.3.4 Parametric Study of Gas Front Behavior

With the analysis and computer program experimentally verified, a series of computations were performed to examine the influence of pertinent variables on the nature of the vapor-gas front. Several of the most important results, showing the influence of working fluid, axial wall conductivity and operating (evaporator) temperature are presented here.

A single geometry was used for all calculations so as to isolate the effect of the variables under study. This consisted of a five foot tubular condenser section which was assumed to radiate heat from its surface to an arbitrary heat sink.

The parameters defining the cases studied are presented in Table 6-3. All are self-explanatory except for the "Nominal Gas Length". An input option in the computer program allows one to specify the gas inventory either as the number of moles present or the length of condenser which the gas would occupy based on flat front theory. Using the latter option it was possible to position the fronts approximately midway up the condenser for all cases without tedious calculation of appropriate molar inventories. This permitted a clear comparison of the profiles when comparing different fluids or operating temperatures (and pressures).

6.3.4.1 Effect of Wall Conductivity

It was expected that axial conduction in the pipe wall and radiator fins (if any) would play a substantial role in defining the vapor-gas interface. To examine the magnitude of this effect, calculations were performed for titanium, stainless steel, nickel and aluminum heat pipes with methanol and ammonia as the working fluids.*

*The known chemical incompatibility of aluminum and methanol was not of concern in this study.

TABLE 6-3
SUMMARY OF CASES STUDIED

Common Variables:

Condenser length	5 feet
Outside diameter	0.5 inches
Wall thickness	0.022 inches
Wick thickness	0.020 inches
Surface emissivity	0.8
Non-condensible gas	nitrogen
Nominal gas length	2.5 feet

Variable Matrix:

Run	Fluid	Material	Evaporator Temp. (°R)	Effective Sink Temp (°R)
1	Methanol	Titanium	550	350
2	Methanol	Stainless Steel	550	350
3	Methanol	Nickel	550	350
4	Methanol	Aluminum	550	350
5	Ammonia	Titanium	550	300
6	Ammonia	Stainless Steel	550	300
7	Ammonia	Nickel	550	300
8	Ammonia	Aluminum	550	300
9	Ammonia	Stainless Steel	550	350
10	Water	Stainless Steel	550	350
11	Ammonia	Stainless Steel	500	300
12	Ammonia	Stainless Steel	450	300
13	Methanol	Stainless Steel	550	300
14	Methanol	Stainless Steel	500	300
15	Methanol	Stainless Steel	450	300

The calculated temperature profiles along the condenser for methanol are shown on Fig. 6-24. One clearly sees that wall conductance tends to spread the front over the condenser, and that this can be a very large effect with high conductivity materials like aluminum. Diffuse vapor-gas fronts are undesirable in gas-controlled heat pipes. They tend to decrease control sensitivity.

The calculations also yielded the heat transfer from that portion of the condenser which is downstream of the point at which T_i has risen 99% of the way from the sink temperature to the evaporator temperature. This transfer represents the minimum power required to keep the gas blocked zone from entering the evaporator (or adiabatic section if there is one) to any appreciable extent. The results, which are presented in Table 6-4 clearly show that this value is also sensitive to wall conductance, increasing with increasing k. A large Q_{min} is also undesirable in gas-controlled heat pipes in that it decreases the variable conductance ratio.

The computer program also yields the axial mass transport at any position along the condenser. This quantity at the position where the wick reaches the freezing point of the fluid yields the rate at which diffusing vapor freezes and is lost to the system. This "diffusion freezeout rate" is also tabulated in Table 6-4. There are no results shown for the runs corresponding to Fig. 6-24 because the sink temperature (350°R) was above the freezing point of methanol (322.7°R). However, the ammonia results with a sink temperature below the freezing point show that the freezeout rate increases with decreasing conductivity. This behavior is not surprising in that one expects the diffusion rate to vary with the temperature gradient. Sharp fronts represent high temperature gradients and thus high diffusion rates. Thus, one must examine the magnitude of the diffusion freezeout rate in a given application and, if of consequence, trade this off against the advantages of sharp fronts (lower Q_{min}, better temperature control) in establishing the axial conductance.

6.3.4.2 Effect of Working Fluid

The effect of working fluid is shown on Fig. 6-25 for water, methanol and ammonia in a stainless steel heat pipe. The results are

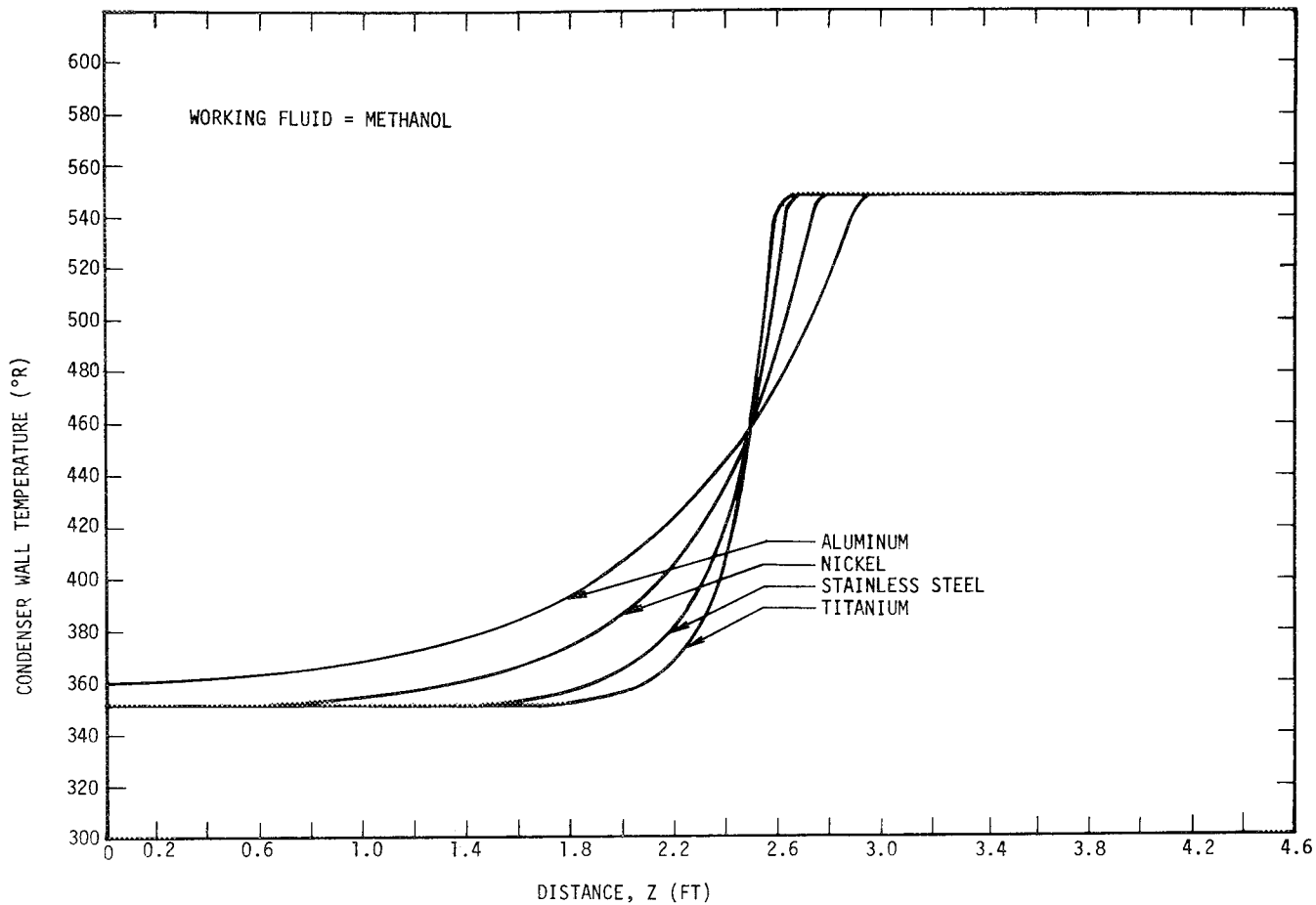

FIGURE 6-24. Effect of Axial Wall Conduction on the Condenser Temperature Profile

TABLE 6-4

Results of Calculations: Diffusion Freezeout Rate, Minimum Power and Total Power

Run	Freezeout Rate (cc/hr)	Minimum Power (Btu/hr)	Total Power (Btu/hr)
Effect of wall material:	Methanol		
1 (titanium)	-	1.9	34.1
2 (stainless)	-	2.5	34.2
3 (nickel)	-	4.2	34.5
4 (aluminum)	-	7.1	35.0
Effect of wall material:	Ammonia		
5 (titanium)	10.0×10^{-4}	2.1	36.7
6 (stainless)	6.7×10^{-4}	2.7	36.5
7 (nickel)	3.6×10^{-4}	4.7	35.9
8 (aluminum)	2.0×10^{-4}	7.9	35.2
Effect of fluid:			
2 (methanol)	-	2.5	34.2
9 (ammonia)	3.0×10^{-5}	2.5	34.1
10 (water)	6.4×10^{-2}	2.8	34.6
Effect of operating temp.:	Ammonia		
6 (550°R)	6.7×10^{-4}	2.7	36.5
11 (500°R)	1.6×10^{-3}	2.1	24.2
12 (450°R)	5.0×10^{-3}	1.6	14.9
Effect of operating temp.:	Methanol		
13 (550°R)	9.0×10^{-7}	2.7	36.5
14 (500°R)	4.1×10^{-6}	2.0	24.3
15 (450°R)	2.8×10^{-5}	1.4	15.0

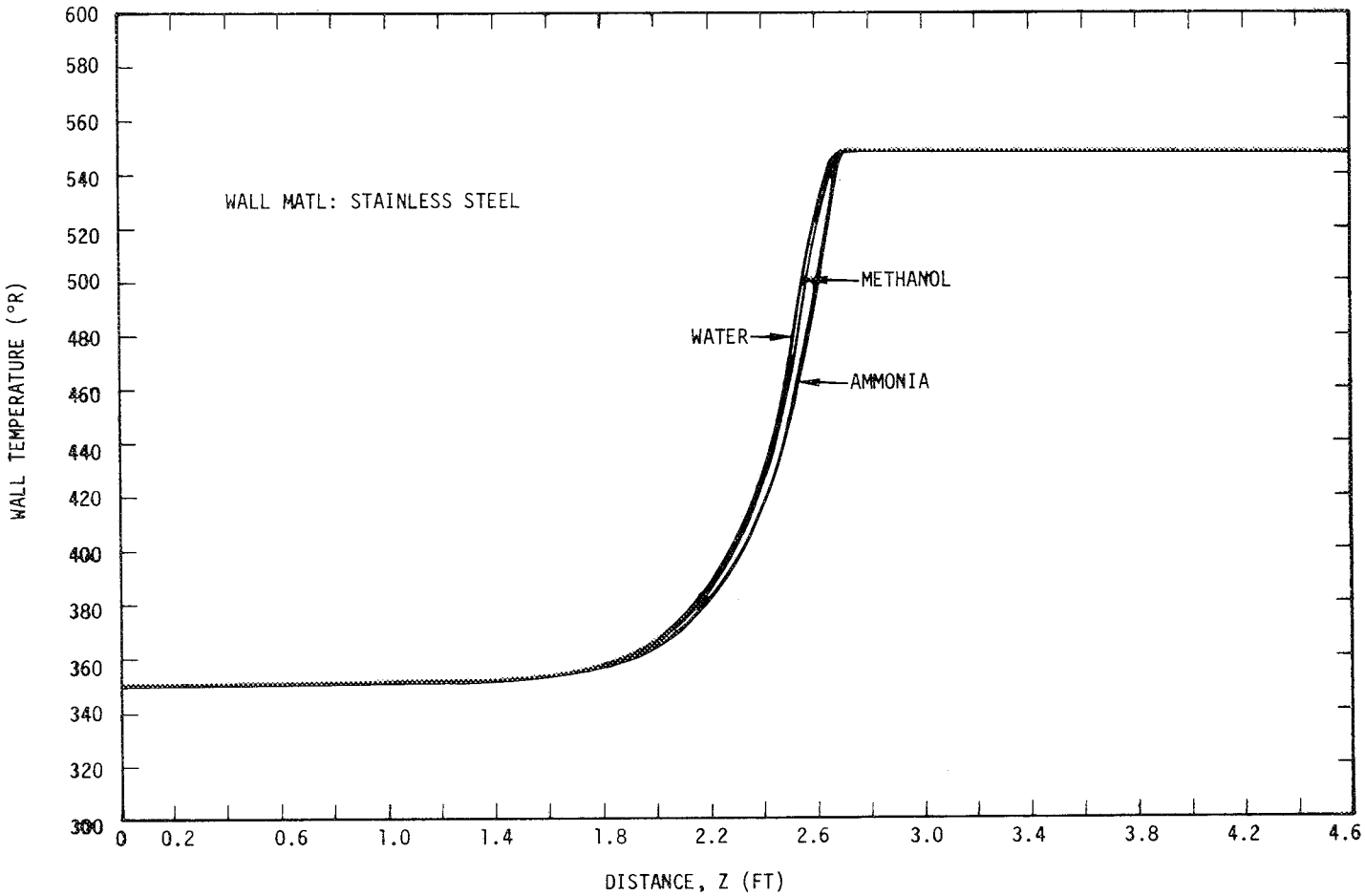

FIGURE 6-25. Effect of Working Fluid on the Condenser Temperature Profile

quite significant. One sees that the profiles are very similar, indicating a relative lack of fluid influence. Such behavior suggests that heat transport by mass diffusion is minimal and axial conduction dominates. This observation is substantiated by the minimum power predictions, which are also nearly equal for the three fluids (Table 6-4).

Although axial mass diffusion does not appear to significantly affect the wall temperature profile, it is both finite and important, for it is the mechanism behind the diffusion freezeout phenomenon. In this regard, Table 6-4 indicates substantially different values of predicted diffusion freezeout rates for the three fluids. This variance is due to a combination of factors including differences in vapor-gas diffusivity, total pipe pressure, and freezing point. Thus, in situations where diffusion freeze-out is of potential concern, the choice of working fluid can be of principal importance.

6.3.4.3 Effect of Operating Temperature

The primary influence of operating temperature (evaporator temperature) is to alter the pressure in the system. Thus, in view of the previous discussion, one would expect similar temperature profiles as T_{ev} is varied. This is clearly seen in Fig. 6-26 for ammonia. Varying the operating temperature from 450°R to 550°R has little effect on the shape of the profile. In each case the curves exhibit the characteristic conduction-dominated shape.

Although the effect of pressure on axial diffusion is not reflected in the conduction dominated temperature profiles, it is obvious when one examines the predicted diffusion freezeout rates. Table 6-4 shows that for both methanol and ammonia, the diffusion freezeout rate increases as the operating temperature and, hence, total pressure is lowered.

6.3.5 Summary and Conclusions

A study was performed on the heat and mass transfer characteristics of heat pipes containing non-condensible gases. An analysis was formulated based on a one-dimensional model which included (1) simultaneous radiation

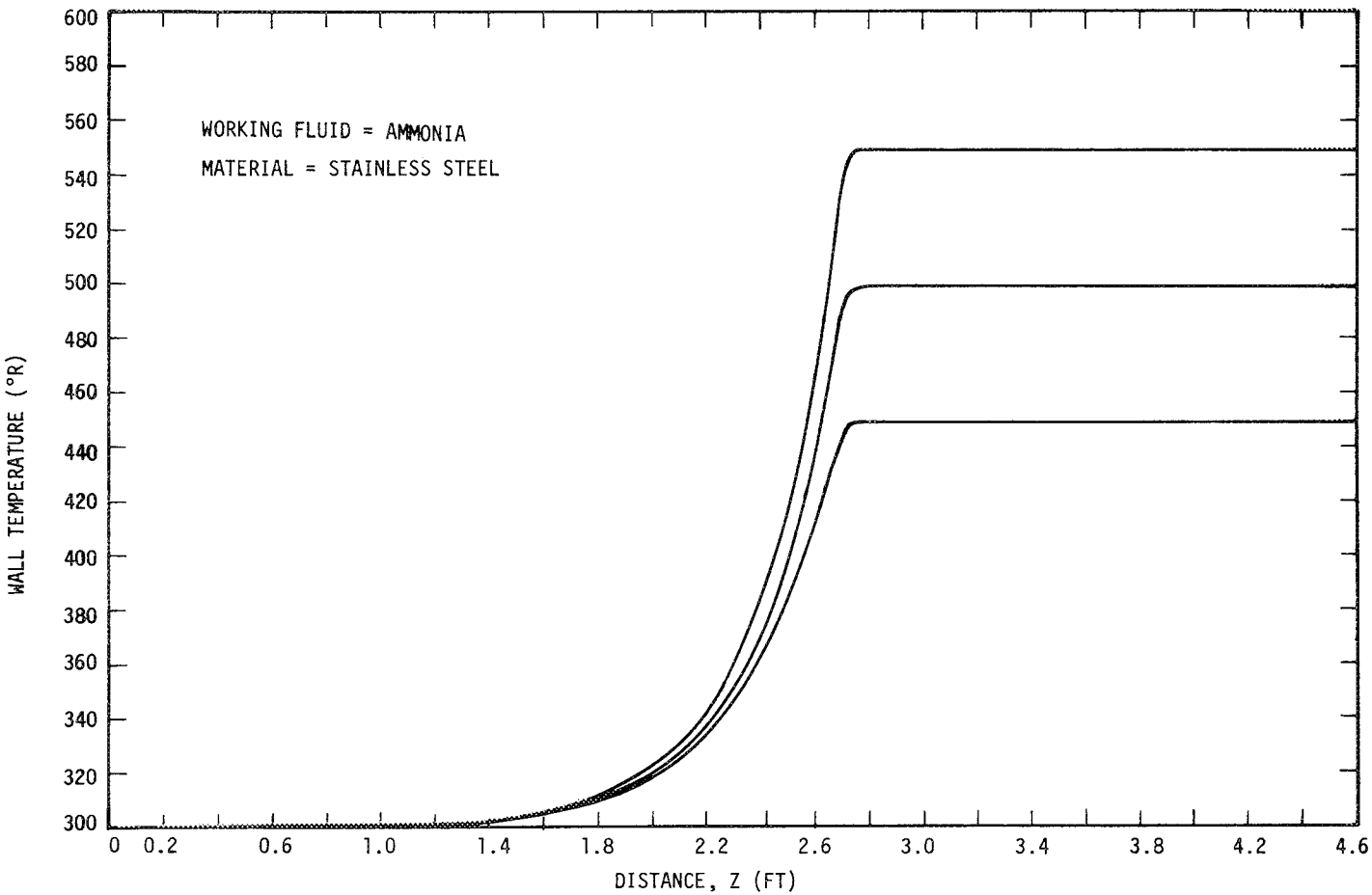

FIGURE 6-26. Effect of Operating Temperature on the Condenser Temperature Profile

and convection from a finned condenser, (2) axial conduction in the walls, fins and wicks, (3) binary mass diffusion between the vapor and gas, and (4) an approximate treatment of wick resistance which is accurate for high conductance wicks. The governing equations were programmed for numerical solution on a digital computer such that the program can be used for heat pipe design or performance prediction calculations.

Parametric calculations showed an important influence of axial conductance upon the behavior of gas loaded heat pipes. In fact, over the range of variables considered, axial diffusion had negligible impact on the shape of the wall temperature profiles compared with the conduction effect. Thus, the choice of working fluid had little effect on the temperature profiles. Axial diffusion is, however, important in establishing the diffusion freezeout rate for conditions under which this occurs. The freezeout rate varies widely with working fluid and, for a given fluid, increases with decreasing operating temperature (total pressure).

Experimental measurements made with a laboratory heat pipe were in excellent agreement with calculated performance. In particular, the temperature profiles along the pipe wall and the operating characteristic for the pipe (heat rejection vs. evaporator temperature) were correctly predicted.

The experimental verification of the analysis and associated computer program suggests that these may be useful tools for designing gas loaded heat pipes.

6.4 Transient Performance of Gas-Controlled Heat Pipes

All of the material heretofore discussed relates to the steady-state performance of gas-controlled heat pipes (except for diffusion freeze-out which is treated as a quasi-steady-state process). It is necessary, however, from a system design point of view, to also understand and be able to predict their transient performance. This includes their response to start-up, shut-down, and changes in input, reservoir or sink conditions.

As one might imagine, seeking an accurate predictive capability for heat pipe transient behavior is a substantially more ambitious task than the development of steady-state theory. This is particularly true if the internal liquid and vapor dynamics play a significant role in the transient. Such is the case, for example, in the start-up of liquid metal pipes where the vapor pressures are so low and vapor velocities so high that one must account for compressibility, recovery, sonic flow, etc. in the vapor phase.

Such phenomena may also be of importance with ordinary working fluids in conventional heat pipes if they experience very low temperatures and pressures at some point in the transient.

Fortunately, though, gas-controlled variable conductance heat pipes which use working fluids of interest in spacecraft thermal control are generally not subject to these phenomena. The presence of the non-condensible gas, at pressures corresponding to the relevant range in operating temperature, maintains the total system pressure high enough such that vapor dynamics do not contribute appreciably to transient behavior.* In fact, it is generally true for these systems that the steady state vapor flow losses have little impact on performance. As a consequence, the transient response of such heat pipes is primarily controlled by sensible heat transfer (i.e., the thermal capacity of the system's elements) and/or vapor-gas diffusion effects.

In treating this subject, it is convenient to separate gas controlled heat pipes into two classes; depending on whether the gas storage reservoir is wicked or non-wicked.

6.4.1 Wicked Reservoir Heat Pipes

In wicked reservoir heat pipes, the partial pressure of vapor everywhere in the system tends towards equilibrium with the local

---

*Except for diffusion between vapor and gas.

temperature of the wick surface. As a consequence, diffusion effects between the vapor and gas are minimal. The diffusion lengths involved correspond to the distance of a given point in the vapor core or reservoir from the nearest wick surface, and these tend to be very small.

If one also neglects the internal liquid and vapor dynamics, the thermal response of the system simply corresponds to changes in sensible heat storage of its various elements. Consequently, ordinary thermal modeling techniques can be used to predict transient behavior.

TRW Systems has performed such thermal modeling studies, although not as part of this contract. However, for completeness, an outline of the approach and a comparison with experimental data will be presented. Details of the modeling technique can be found in reference [V11].

6.4.1.1 Nodal Model

The first step is to generate a nodal model of the system such as shown in Fig. 6-27. The active portion of the heat pipe (evaporator, adiabatic section and active condenser length) is assumed to be at uniform temperature. Variable conductors between the heat pipe vapor and heat pipe wall nodes simulate the variable position of the vapor-gas interface. The position of the vapor-gas interface can be obtained from an analysis similar to the diffuse-front theory presented in section 6.3. However, the parametric analysis of diffuse fronts (section 6.3.4) showed that the wall temperature profile is conduction dominated and diffusion can be neglected. Thus, it is generally adequate to locate the gas front using a technique similar to that in section 6.1. That is, calculating L_a/L_c by integrating the molar inventory of gas in the heat pipe (integrating Eq. 6-2 along the reservoir and condenser). Note that this does not imply using the flat-front theory in its entirety. The wall temperature in the gas-blocked portion of the pipe is not set equal to the sink temperature, but is calculated. It is only assumed that, within the vapor core, condensation becomes negligible at the start of the vapor-gas front. Parametric studies with the TRW Gaspipe Program have shown this to be an excellent assumption.

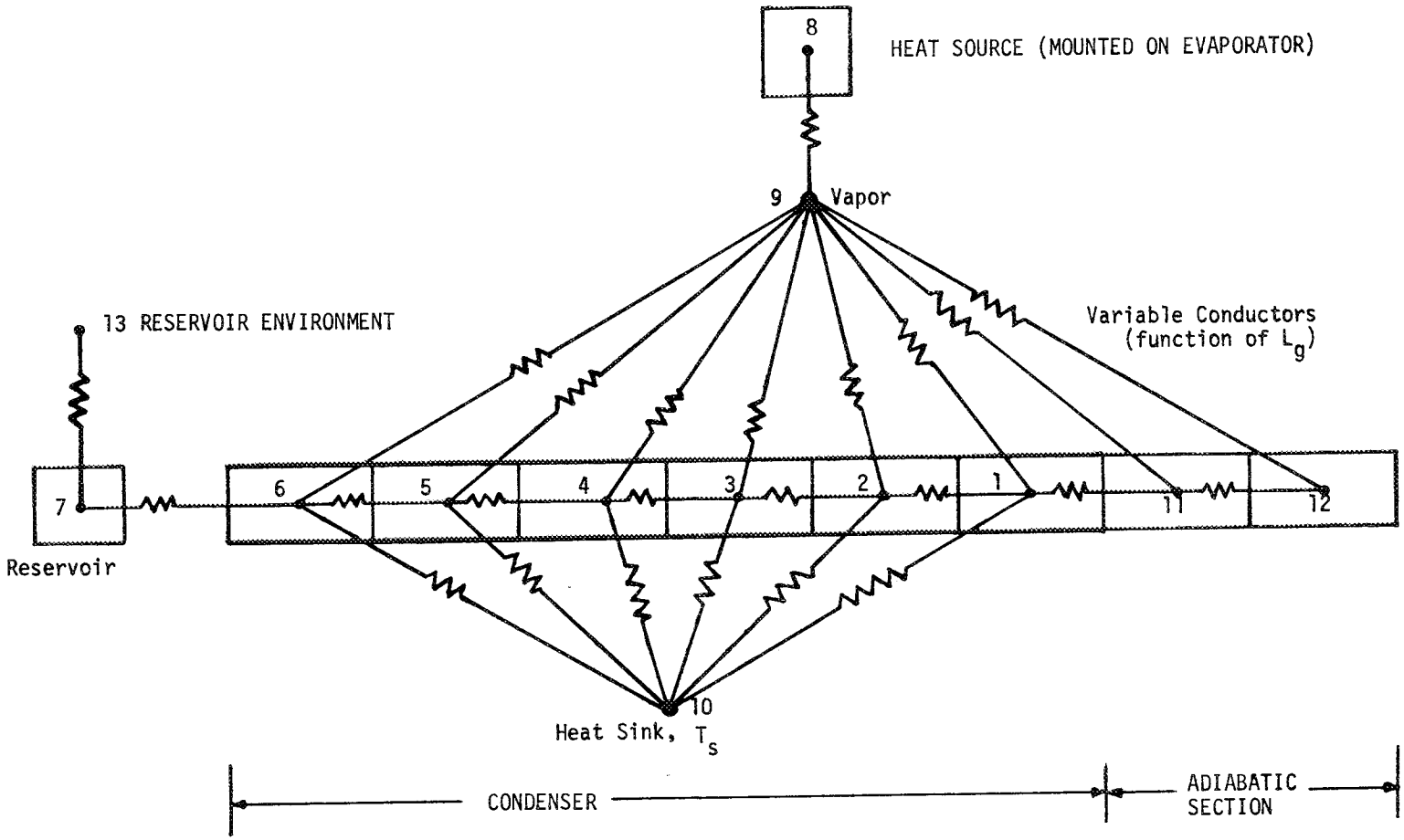

FIGURE 6-27. Heat Pipe Nodal Model

Thus, if a node is totally blocked by gas, the variable conductor is set equal to zero. For partially blocked nodes, the ratio of the blocked to total node length is multiplied by the conductance of a fully active node.

6.4.1.2 Solution Technique

The appropriate solution technique depends on the thermal analyzer program used. At TRW Systems, the model has been solved using the SINDA forward differencing routine CNFRWD and taking advantage of the fact that this routine can be integrated with Fortran routines and statements written for this specific problem. Details of this technique can be found in reference [V11].

6.4.1.3 Experimental Verification

The transient thermal model and solution technique described are applicable to all wicked reservoir systems. If the reservoir sees a different environment than the condenser, the appropriate reservoir sink temperature is assigned to node 13 on Fig. 6-27. If the reservoir is controlled at a fixed temperature (e.g., thermostatic heater), that temperature is assigned to node 7. If the system involves feedback control of a reservoir heater, this is input based on the temperature of the reference point; e.g., the source temperature-node 8.

To demonstrate the predictive capability of this modeling technique, results for a feedback controlled heat pipe will be presented. A schematic of the experimental system is shown on Fig. 6-28. It consists of an aluminum-ammonia-neon heat pipe with a heated wicked reservoir. Electrical heat is supplied to a large thermal mass (copper block) mounted on the evaporator. Condenser heat rejection is by conduction through a thin gas layer between the condenser wall and a cooled copper sleeve. Further details can be found in reference [V11].

This system has been tested with both an electronic proportional feedback controller (as shown in Fig. 6-28) and a bi-metal thermostat controller mounted on the thermal mass. In the latter case, the reservoir heater operates in an on-off mode and, thus, the system is never in thermal equilibrium. This provides the ultimate test of a transient thermal model.

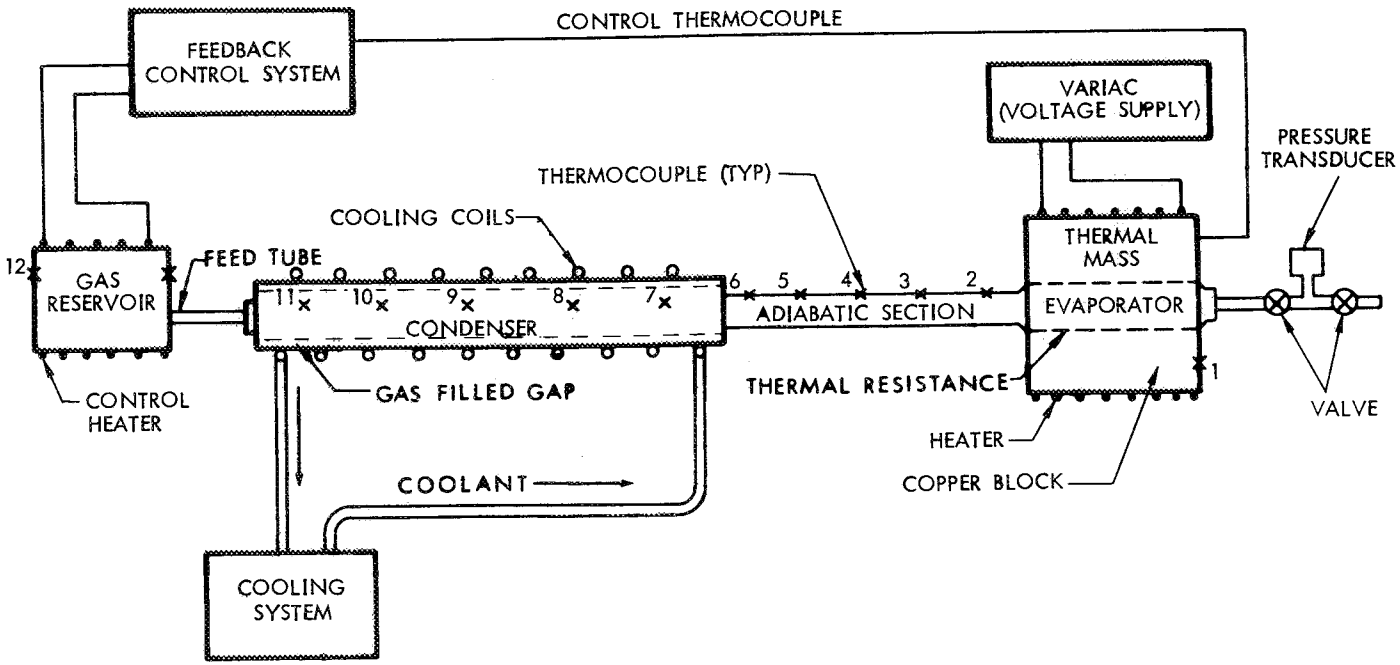

FIGURE 6-28. Feedback Controlled Heat Pipe Test Setup

A sample comparison of measured and predicted transient behavior for the thermal mass (heat source) is presented on Fig. 6-29. The curves depict the oscillatory behavior characteristic of the on-off power to the reservoir control heater at constant source power input. They also depict the system response to a temporary increase in source input of such magnitude as to exceed the control range and overdrive the pipe. That is, the entire condenser becomes active whereupon the pipe rises in temperature as would a non-controllable heat pipe.

The results are impressive, indicating that the assumptions made in the analysis are reasonable, and the thermal model adequate.

6.4.2 Non-Wicked Reservoir Heat Pipes

The transient behavior of non-wicked reservoir heat pipes differs from that of wicked reservoir systems in one all-important respect. The partial pressure of vapor within the reservoir of non-wicked systems is established by diffusion of vapor to and from the end of the condenser rather than the reservoir walls. As opposed to wicked reservoir systems, the diffusion paths are no longer small. Thus, diffusion rates have a substantial impact, and often dominate the transient behavior of these systems.

Not only must diffusion serve to regulate the partial pressure of vapor within the reservoir, it may also have to provide a mechanism for removal of liquid. It is quite possible that circumstances might arise (e.g., adverse body forces or vibration during launch) such that liquid is forced from the wicks into the reservoir. Under such conditions, when the heat pipe is started up the liquid in the reservoir will vaporize, establishing a vapor pressure corresponding to the reservoir temperature rather than that at the end of the condenser. Since the reservoir temperature must be higher than the sink temperature T_s (see section 6.1.4.3) and may even equal the evaporator vapor temperature - T_{va} (see Fig. 6-8), the reservoir vapor pressure will be excessive, forcing gas out, and resulting in an operating temperature and pressure considerably higher than design conditions. These conditions will prevail until the liquid is removed

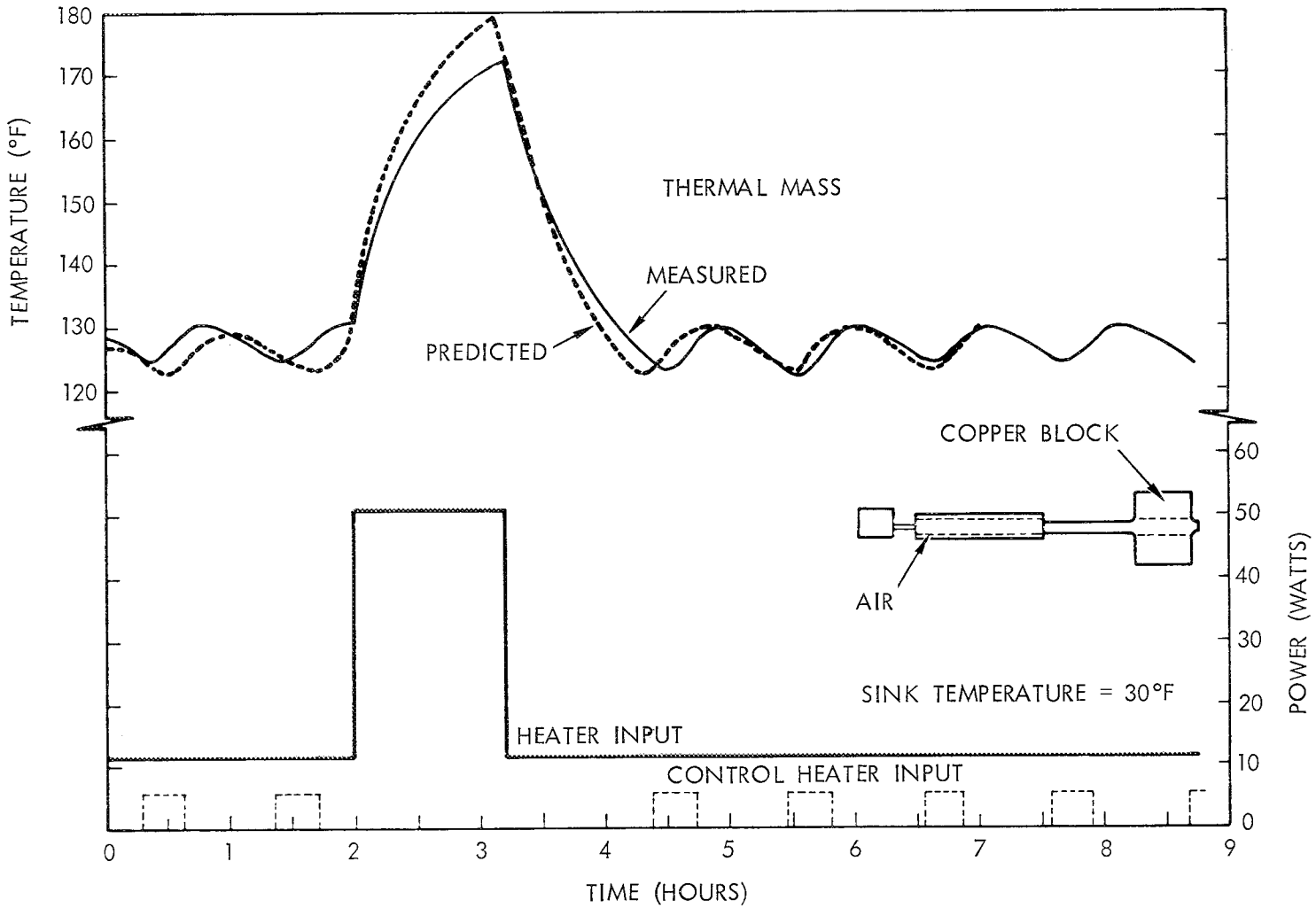

FIGURE 6-29. Comparison of Measured and Predicted Transient Heat Pipe Behavior

from the reservoir by diffusion to the end of the condenser where it is re-captured by the wick structure.

6.4.2.1 Experimental Observations

Several laboratory experiments were performed to demonstrate the phenomena described above. Two internal reservoir heat pipes as shown in Fig. 6-16 were used. The design details were presented in Table 6-1. Both heat pipes were identically fabricated and processed except that pipe no. 2 had a perforated Teflon plug blocking the opening of the reservoir. The purpose of the Teflon plug was to prevent liquid from entering the reservoir while permitting the gas to pass through. The instrumentation was described in section 6.2.2.

Liquid Penetration Experiments:

Figure 6-30 shows the results of several transient experiments with pipe no. 1 (without the Teflon plug). Two pressure-time histories are shown--one for a start-up with the reservoir free of working fluid and one for which the pipe was vigorously shaken to assure its presence. (Pressure is used as the ordinate rather than temperature, for it is a much more sensitive variable. The solid lines represent smoothed continuous data taken with a strip chart recorder). The dry-reservoir run was made in the heat pipe mode (evaporator elevated) and its start-up transient came directly to operating conditions and remained there (slight variations with time represent changes in ambient temperature).

The wet reservoir run was initially started in the reflux mode (condenser elevated) to prevent the liquid from running out by gravity. In this case the start-up transient came up to a pressure (and temperature) considerably above design conditions and remained there. If undisturbed, it would have remained at this condition until all the liquid in the reservoir vaporized and diffused out. Instead, after a period of time the pipe was simply tipped to the heat pipe mode allowing the liquid to run out by gravity. After a short pulse due to excess fluid moving from the hot to the cold end, the pipe exhibited a slow recovery transient as vapor remaining in the reservoir diffused out. Ultimately, the pipe reached equilibrium at

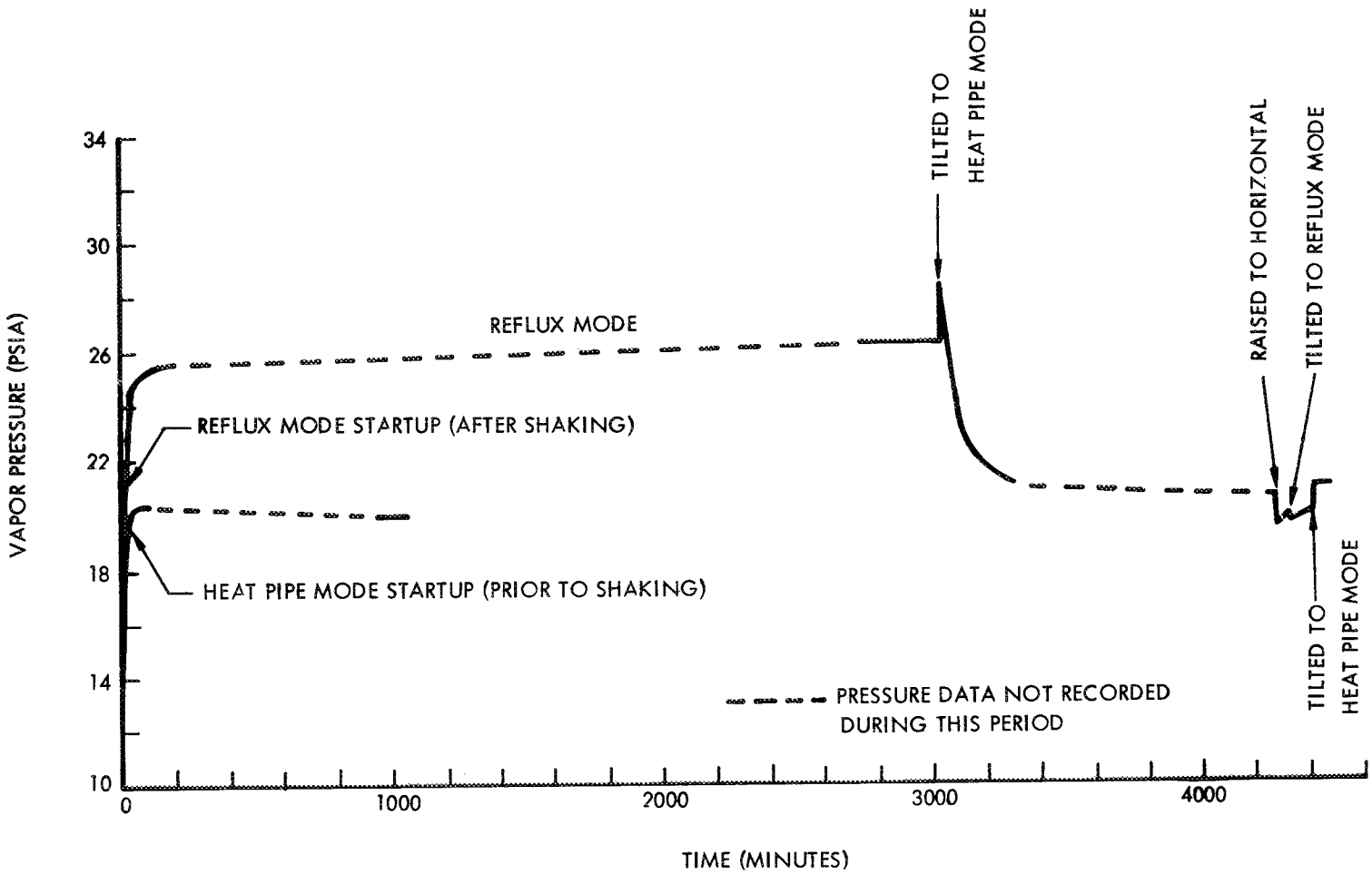

FIGURE 6-30. Transient Start-up Test Results for Internal Reservoir Gas Controlled Heat Pipe without Teflon Plug (Pipe No. 1)

conditions similar to those reached directly in the dry-reservoir start-up. Once at this condition, subsequently tipping the pipe mode had no effect other than to generate the short thermal transients caused by the slight excess fluid moving from the cold to the hot end and vice versa.

When heat pipe no. 2 was tested in a similar way, no such temperature or pressure excesses were observed (Fig. 6-31). The Teflon plug apparently prevented liquid from entering the reservoir when the pipe was shaken, for both start-up transients came directly to design operating conditions, and tipping the pipe back and forth between the reflux and heat pipe modes had no effect other than that due to excess fluid.

These results clearly demonstrated that the presence of liquid in the reservoir gave rise to high operating pressures and temperatures, as hypothesized, and that a perforated Teflon plug is apparently an effective method of impeding the mechanical insertion of liquid into the reservoir.

Vapor Penetration Experiments:

Although the perforated Teflon plug apparently prevented the passage of liquid, it certainly does not prevent the flow of vapor. In fact, the theory of non-wicked reservoir heat pipes, as presented in section 6.1.4.3, is based on diffusion equilibrium between the reservoir and the end of the condenser. However, if one is to design for such diffusion equilibrium, it is important to appreciate the transient response rates involved. For example, if conditions are temporarily such that a large quantity of vapor is driven into the reservoir, a subsequent return to normal operating conditions will be characterized by a relatively long diffusion transient as the vapor comes back out. This is clearly seen in Figure 6-32 which shows three pressure and temperature histories measured with heat pipe no. 2.

The top curves show the result of overdriving the pipe, that is, raising the power beyond the control range so that it operates as an ordinary heat pipe. Under such conditions, the active zone of the condenser extends to the reservoir entrance, allowing vapor penetration. Given sufficient

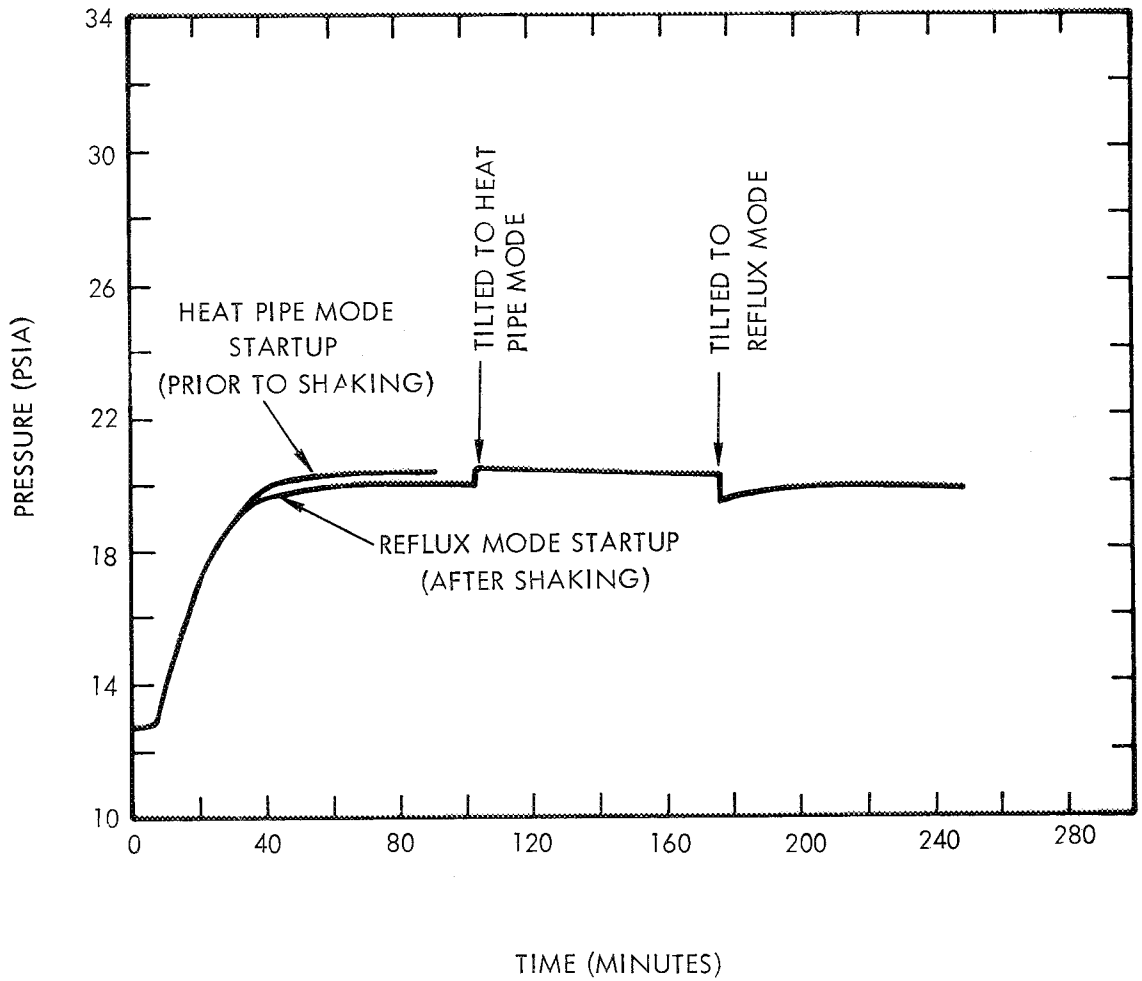

FIGURE 6-31. Transient Start-up Test Results for Internal Reservoir Gas Controlled Heat Pipe with Teflon Plug (Pipe No. 2)

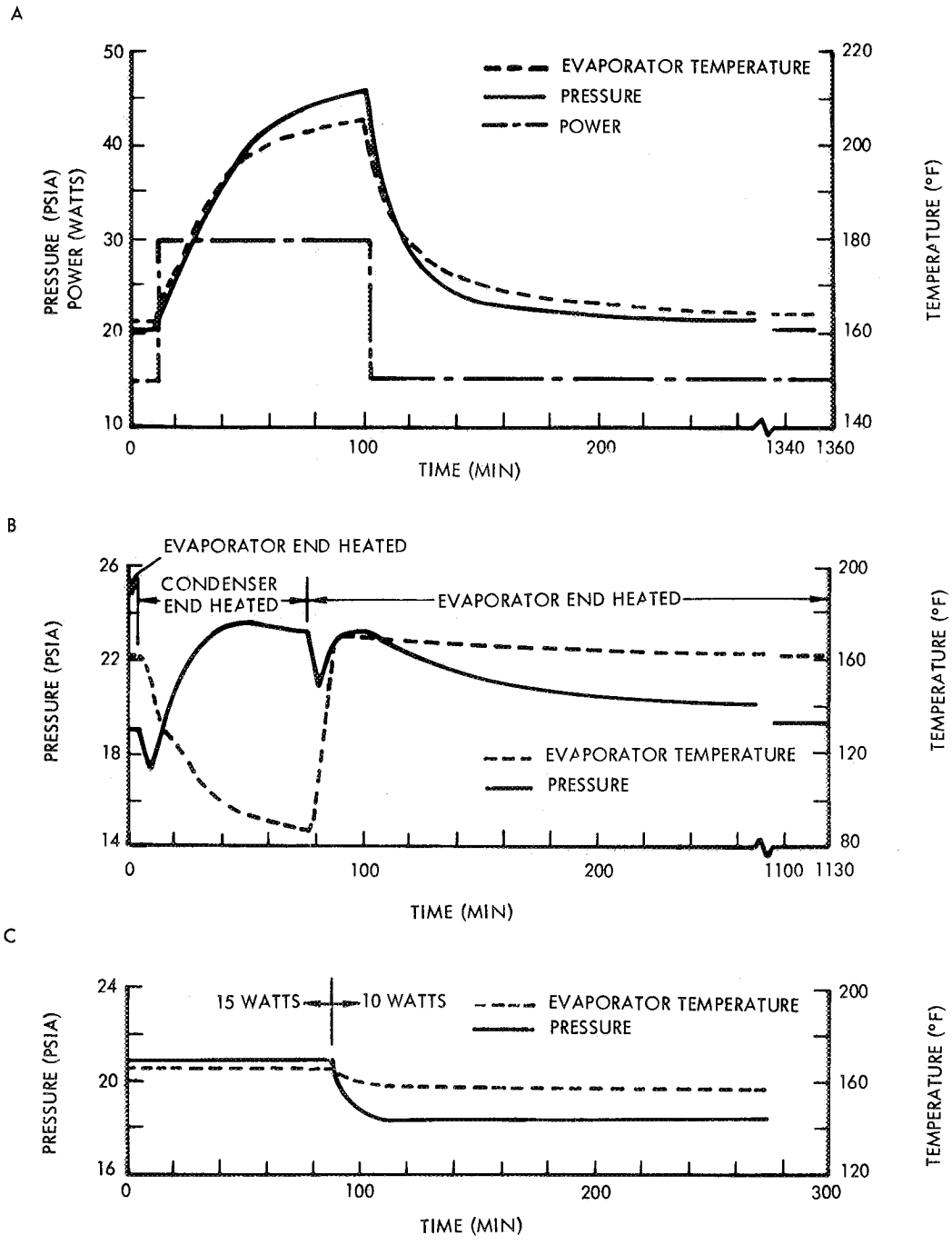

FIGURE 6-32. Transient Test Results of Vapor Penetration Experiments (Heat Pipe No. 2)

time under such circumstances, vapor will continue to diffuse into the reservoir, displacing gas, until the vapor pressure in the reservoir equals that at its entrance. When the power was returned to its starting value, the pressure and temperature did too, but with the slow transient characteristic of the diffusion process necessary to rid the reservoir of the vapor which had occupied it.

The second history shows the result of operating the pipe backwards for a period of time. This was accomplished by placing a heater at the condenser end as well as the evaporator end and simply reversing heaters while maintaining power constant. Once again, when the heat supply was returned to normal, the pressure and temperature recovery of the heat pipe showed the now familiar diffusion characteristic. The initial dip in pressure observed each time the heated end was reversed is a reflection of the thermal capacity of the heat pipe. The previously cold end had to be heated while the previously hot end cooled. This gave rise to a temporary situation in which all portions of the pipe were cooler than the evaporator prior to switching heaters, which resulted in a lower pressure.

The third history is shown for comparison and represents a simple step change in power while the pipe was functioning within its control range. In this case the transient is an ordinary thermal one involving no diffusion and consequently is much more rapid.

6.4.2.2 Theoretical Considerations

The dynamic behavior of non-wicked reservoir heat pipes is considerably more difficult to model than wicked reservoir systems because of the influence of diffusion. It is necessary to simultaneously solve the coupled diffusion and heat transfer equations for the entire heat pipe system.

This is a task on which TRW is currently working. The analysis has been formulated and a computer program written. However, the program is not yet operational and thus the analysis not yet verified. It is therefore premature to present it here. It will be presented as part of a future report on this program.

In the absence of a detailed thermal modeling capability, it is still possible to obtain order-of-magnitude estimates of transient thermal response for the conditions of primary concern. This refers to conditions where diffusion dominates the transient. That is, the diffusion time constant is so large with respect to the thermal time constant that the thermal aspects of the problem can be neglected. The problem can then be reduced to modeling the diffusion process between the reservoir and the end of the condenser.

Even in this case the problem is complex, for there exists a temperature gradient across the reservoir feed tube through which the vapor diffuses, and the temperature, total pressure and gradient in partial pressure of vapor are changing with time.

However, to obtain order-of-magnitude results, one can make further simplifications.

6.4.2.2.1 Lumped-Parameter, Quasi-Steady-State Diffusion Model

The following assumptions are made:

1. The system geometry is as shown in Figs. 6-7 or 6-8.
2. Conditions in the reservoir are uniform (lumped parameter reservoir).
3. A one-dimensional diffusion model through the reservoir feed tube adequately represents the process.
4. The transient can be treated as a quasi-steady state process at constant temperature and pressure for each instant of time.
5. Thermal diffusion can be neglected (see section 6.1.4.3.1).

To describe the diffusion process through the reservoir feed tube, assumptions 3 and 4 imply that Fick's first law applies in the following form:

$$\rho_v V = -\mathscr{D}\frac{d\rho_v}{dz} \qquad (6\text{-}62)$$

where:

ρ_v - density of vapor
V - velocity of vapor
$\mathscr{D}$ - mass diffusivity for vapor-gas pair

For a quasi-steady-state process, the density gradient across the reservoir feed tube is linear. Thus, the vapor flow rate through the feed tube is given by:

$$\rho_v V A_F = - A_F \mathscr{D} \left(\frac{\rho_{vR} - \rho_{vs'}}{L_F}\right) \tag{6-63}$$

where:

A_F - flow area of feed tube
L_F - length of feed tube
ρ_{vR} - vapor density at reservoir and of feed tube
$\rho_{vs'}$ - vapor density at condenser end of feed tube (at temperature - $T_{s'}$).

In view of assumption 2, the mass of vapor within the reservoir is simply $m = \rho_{vR} V_R$, where V_R is the reservoir volume. The mass flow rate into or out of the reservoir can thus be written $\dot{m} = \dot{\rho}_{vR} V_R$. Equating this to Eq. (6-63) for the feed tube yields:

$$\dot{\rho}_{vR} V_R = -A_F \mathscr{D} \left(\frac{\rho_{vR} - \rho_{vs'}}{L_F}\right) \tag{6-64}$$

Assuming $\mathscr{D}$ constant, equation (6-64) is simply a first order, linear differential equation with constant coefficients which describes the response of the reservoir (ρ_{vR}) to changes in conditions at the end of the condenser - ($\rho_{vs'}$). It yields an exponential solution:

$$\left(\frac{\rho_{vR} - \rho_{vs'}}{\rho_{vRo} - \rho_{vs'}}\right) = \exp\left(- \frac{A_F \mathscr{D}}{L_F V_R} t\right) \tag{6-65}$$

where: ρ_{vRo} - initial reservoir condition.

Equation (6-65) is, of course, only a highly simplified approximation to the transient behavior of non-wicked reservoir heat pipes. However, it yields an expression for the relaxation time constant,

$$\tau_{\mathcal{D}} = \frac{L_F V_R}{A_F \mathcal{D}} \qquad (6\text{-}66)$$

which is useful in identifying the key parameters controlling the diffusion process.

For the heat pipes discussed in section 6.4.2.1, Eq. (6-66) yields $\tau_{\mathcal{D}} \approx$ 250 minutes. Comparing this with the diffusion transients of Fig. 6-30 and Fig. 6-32a & b, we see that Eq. (6-66) does give order-of-magnitude agreement with experimental results.

6.4.2.2.2 Start-up With Liquid in the Reservoir

The experiments described in section 6.4.2.1 demonstrated two important characteristics of non-wicked reservoir heat pipes: (1) they can be subject to relatively long, diffusion-dominated transients when conditions at the end of the condenser ($T_{s'}$) are altered, and (2) they can experience substantially higher temperatures and pressures than those corresponding to steady state conditions if liquid should penetrate the reservoir and if the reservoir is maintained at a temperature significantly higher than T_s.

In the absence of a detailed thermal modeling capability, Eqs. (6-65) and (6-66) provide a criterion for estimating diffusion-dominated transient response. Clearly, a similar criterion is needed to estimate the maximum pressure the system might experience should liquid penetrate the reservoir. Although the liquid will automatically be purged from the reservoir, it is necessary to design the heat pipe to withstand the temporary high pressures it would experience.

Such a criterion can be simply obtained, for an upper bound to the pressure corresponds to a quasi-steady-state situation where the reservoir vapor pressure is that corresponding to its own temperature - T_R, rather than that at the entrance to the feed tube - $T_{s'}$.

The best approach to calculating this value is to use the TRW Gaspipe Program. However, an estimate can also be achieved using the flat-front

theory of section 6.1. It was shown in section 6.1.4 that the characteristic equation for a reservoir heat pipe where P_{vR} corresponds to T_R is given by Eq. (6-15), and for one where P_{vR} corresponds to T_s^* is given by Eq. (6-17). Thus, Eq. (6-15) will provide an upper bound for the pressure and temperature of a non-wicked reservoir heat pipe with liquid in the reservoir, and for which Eq. (6-17) has been used to size the reservoir volume - V_R and the molar gas inventory - n.

To appreciate the potential magnitude of the over-pressure problem, consider the case where reservoir temperature equals the evaporator temperature (e.g., an internal reservoir as shown in Fig. 6-8). Also, for simplicity, assume that $P_{vs} << P_{va}$.

An expression for n can be obtained from Eq. (6-17) by considering that, at the maximum end of the control range, $L_a = L_c$ and,

$$\frac{V_R\, T_s}{A_v\, T_{vamax}} = \frac{nR_u T_s}{A_v\,(P_{vamax}-P_{vs})} \qquad (6\text{-}67)$$

where: $P_{vamax} = P_{va}$ at maximum steady state conditions (no liquid in reservoir).

Solving Eq. (6-67) for n, substituting into Eq. (6-15) with $T_R = T_{va}$ yields:

$$Q = hA'\,(T_{va}-T_s)\left[L_c - \frac{V_R}{A_v}\frac{T_s}{T_{va}}\frac{P_{vamax}}{P_{va}}\right] \qquad (6\text{-}68)$$

A little further algebra and substituting $V_c = L_c A_v$ yields an expression for P_{va}/P_{vamax}, the system overpressure ratio, as a function of the power throughput.

$$\frac{P_{va}}{P_{vamax}} = \frac{V_R}{V_c}\frac{T_s}{T_{va}}\left[\frac{1}{1-\dfrac{Q}{hA'\,L_c(T_{va}-T_s)}}\right] \qquad (6\text{-}69)$$

*$T_{s'} = T_s$ when using flat-front theory

Equation (6-69) is very revealing. At low values of Q, the term in brackets approaches unity. Under these conditions, the system pressure will exceed the maximum steady-state design pressure by a factor of $\frac{V_R}{V_c}\frac{T_s}{T_{va}}$. Since V_R/V_c ratios are generally large ($\approx$5 - 20) to achieve good control sensitivity, and T_s/T_{va} ratios are generally not very small ($\approx$0.5 - 0.9), this suggests that the factor $\frac{V_R}{V_c}\frac{T_s}{T_{va}}$ is typically of order 10.

Furthermore, as Q increases the term in brackets increases, yielding even greater (P_{va}/P_{vamax}) ratios, the maximum corresponding to the maximum design heat rejection rate - $Q_{max} = hA' L_c(T_{vamax}-T_s)$.

Obviously, the potential for transient overpressures on the order of 10 times the nominal design pressure is an important consideration in designing non-wicked reservoir heat pipes. With low pressure fluids like methanol ($\approx$2 psia at 70°F), the potential overpressures pose little problem. However, this phenomenon would certainly be troublesome with an ammonia heat pipe (vapor pressure $\approx$130 psia at 70°F).

6.5 Designing Gas-Controlled Heat Pipes for Spacecraft Thermal Control

6.5.1 Summary of Control Schemes

The purpose of gas controlled heat pipes is to control the operating temperature of a component, platform or any other heat source against variations in heat dissipation and/or environmental conditions. Under certain conditions extremely close temperature control is possible. However, as we have seen, the degree of control which can be achieved is a strong function of the operating temperature and the thermal boundary conditions involved in a given application.

For applications to spacecraft thermal control, the limiting factor in controllability is generally the magnitude and degree of variation in the thermal environment of the condenser and non-condensible gas reservoir. Variations in the non-condensible gas temperature and the partial pressure of vapor within the condenser and gas reservoir impact the total pressure

and, hence, the operating temperature of these devices. In spacecraft applications, it is not unusual for the effective absolute sink temperature to vary by nearly a factor of two (leading to large variations in the reservoir partial pressure of gas), and for its upper bound to approach within 50 - 60°R of the heat pipe operating temperature (leading to large variations in the reservoir partial pressure of vapor). Such adverse boundary conditions require special techniques to achieve close temperature control limits.

Cold Reservoir Heat Pipes:

The simplest gas-controlled heat pipe utilizes a wicked, cold reservoir as shown on Fig. 6-33a. This device is simplest and least costly to fabricate and integrate into the spacecraft design. It also provides the ultimate in transient response and reliability. However, because the gas reservoir is exposed to the same environment as the condenser, this type of heat pipe is most sensitive to environmental variations and, thus, offers the poorest control capability.

Hot Reservoir Heat Pipes:

If the cold wicked reservoir design cannot offer sufficient temperature control for a particular application, this can be improved by utilizing a hot non-wicked reservoir thermally coupled to the evaporator.* This configuration, shown in Fig. 6-33b, minimizes the effects of gas temperature variations, and provides for closer control ranges.

The hot non-wicked reservoir heat pipe minimizes gas temperature (and, hence gas pressure) variations. It does not prevent variations in partial pressure of vapor within the reservoir, but rather alters its dependence from the reservoir temperature to that of the condenser at the reservoir entrance (the closest point to the reservoir where there

---

*Or any other convenient, relatively constant temperature point where $T_R > T_{s/max}$.

exists liquid). Because of this, the partial pressure of vapor within the reservoir is controlled by diffusion to and from the condenser. This gives rise to diffusion-controlled transient phenomena and causes the heat pipe to respond more slowly to changes in environmental conditions, as discussed in section 6.4.2.

Active Control Heat Pipes:
The hot and cold reservoir heat pipes reviewed so far are passive devices. They have no moving parts and require no power to operate. Consequently, they promise very high reliability. However, as pointed out, their controllability is limited when used in applications involving widely varying thermal environments.

Under such circumstances, or whenever very close temperature control is required, one can employ heaters for reservoir temperature control. These are modifications of the cold wicked reservoir system in that the reservoir is provided with a heater and control circuit (or thermostat) which is activated in accordance with a reference temperature signal. The reference point can be the reservoir itself, in which case T_R is held constant. Alternately, it can be the temperature of the evaporator heat source, in which case the reservoir temperature is actually varied to provide closer control over the source temperature. The latter scheme, known as feedback control, is depicted in Fig. 6-33c.

Active reservoir temperature control (i.e., the use of heaters) offers closest source temperature control in most applications. However, it represents a more complex system with a related decrease in reliability, and it introduces a requirement for heater power.

6.5.2 Design Approach

The first and most important step in designing a gas-controlled, variable conductance heat pipe is to realistically define the thermal control problem. This, of course, includes the range in heat rejection required (Q_{max} and Q_{min}) as well as the range in effective sink temperatures anticipated (T_{smax} and T_{smin}). But, most important, one

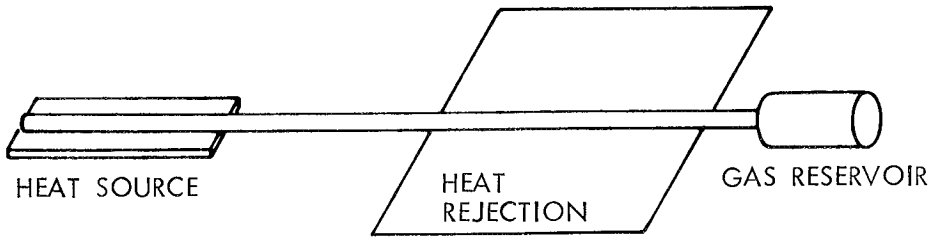

A) COLD WICKED RESERVOIR

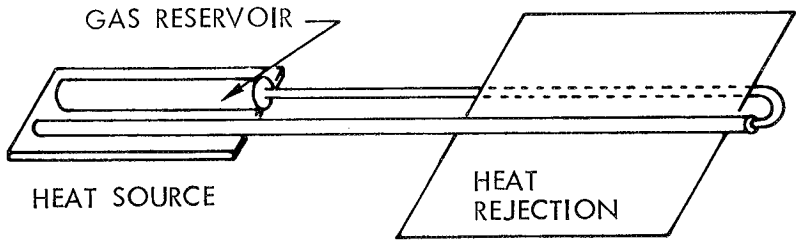

B) HOT NON-WICKED RESERVOIR

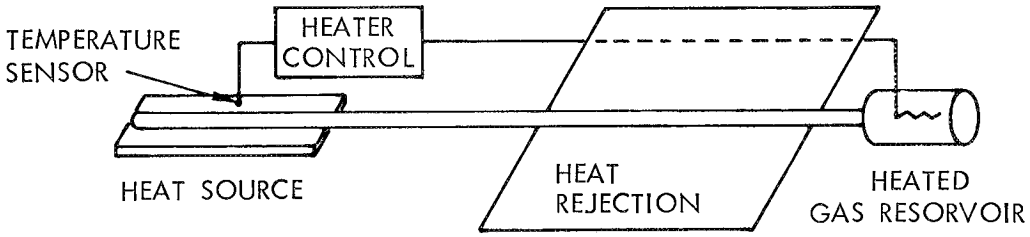

C) HEATED RESERVOIR ACTIVE FEEDBACK SYSTEM

FIGURE 6-33. Schematic Diagrams of Various Gas Controlled Heat Pipe Reservoir Configurations

must define the necessary control range (T_{vamax} and T_{vamin}). This is emphasized because, as shown previously, the degree of control which can be achieved for a given range in Q and T_s varies considerably with the working fluid and reservoir system chosen. As it happens, improved controllability is accompanied by increased system complexity. Thus, one should not specify a control range any smaller than is actually required, if this would require choosing a more complex system over a simpler one.

It is recommended that the preliminary control design calculations, leading to selection of the control technique, be performed using the flat-front theory of section 6.1. It is a relatively simple matter to generate parametric curves of V_R/V_c vs. ΔT_{va}, as shown on Figs. 6-9 and 6-10, for various working fluids and reservoir conditions (fixed or variable temperature, wicked or non-wicked). This will permit identification of the simplest control technique which will meet the requirements.

After a tentative control scheme and the general system configuration is established, the TRW Gaspipe Program can be used to refine the design, size the reservoir, determine the gas inventory, and examine heat pipe performance for both design and off-design conditions.

6.5.3 Design Considerations and Trade-offs

This section summarizes some of the specific parameters involved in the design of typical gas-controlled heat pipes and identifies trade-offs which must be made. The task is facilitated by separating the field into four categories; (1) passive wicked reservoir systems, (2) passive non-wicked reservoir systems, (3) heated reservoir systems - T_R constant, and (4) heated reservoir systems - feedback control.

6.5.3.1 Passive Wicked Reservoir Systems

Condenser Geometry: It is always desirable to minimize the condenser void volume - V_c, for this allows utilizing smaller reservoirs for a given temperature control range. Both the condenser length - L_c and the vapor core flow area can be minimized, consistent with heat

rejection area requirements and avoiding excessive vapor flow losses.

Working Fluid: Several factors enter into the selection of the working fluid in addition to those which are important in conventional heat pipes (compatibility, liquid transport factor, g-field factor, nucleation tolerance, etc.). Best control will be obtained using fluids with high Gas Control Sensitivity Factors (Fig. 6-3).

However, if the range in sink temperature falls below the freezing point of the fluid, one must also consider the diffusion freezeout phenomenon (section 6.3.4). If possible, it is preferable to utilize a fluid which does not freeze over the entire range in T_s. However, if this is not possible, the TRW Gaspipe Program should be used to assure that the diffusion freezeout rates are not problematic for any given fluid.

Note that these criteria often imply a trade-off against hydrodynamic capacity. For example, ammonia exhibits a higher liquid transport factor than methanol for operating temperatures of interest in spacecraft thermal control. However, methanol has both a higher Gas Control Sensitivity Factor (Fig. 6-3) and a lower freezing point (-137°F vs. -108°F) than ammonia.

Q_{min}: This parameter refers to the axial heat leak by conduction and diffusion when the condenser is fully turned off. In many cases, it is desirable to render this heat leak as small as possible; i.e., provide for a minimum heat pipe conductance approaching zero. The best approach to achieving a low Q_{min} is to (1) provide sufficient gas so that the front moves somewhat upstream of the condenser in the full-off condition, and (2) provide for a very low axial conductance in this region.

Cold Traps: Variations in reservoir temperature limit the degree of evaporator temperature control achievable, due both to variations in gas and vapor partial pressures. Fluctuations in T_R can be minimized by assuring that axial conduction does not cause T_R to increase above T_s under conditions of high condenser utilization. This can be done by

providing a low-axial conductivity region between the primary condenser and the reservoir to assure a fully-developed front at the reservoir entrance.

Materials of Construction: Aside from considerations common to conventional heat pipes (compatibility, fabricability, etc.), it is generally preferred to use materials with low thermal conductivity for the heat pipe tube and wicks. The basic principle of gas-controlled heat pipes rests on the generation of an axial temperature gradient along the condenser. Low k materials facilitate the generation of sharp gradients, helping to provide low Q_{min} values and more effective cold traps.

On the other hand, sharp temperature gradients increase the diffusion rate of vapor into the gas-blocked zone, and aggravate the diffusion freezeout problem if one exists. Thus, if T_{smin} falls below the freezing point of the working fluid, diffusion freezeout rates should be considered in establishing the axial conductance of the condenser.

Transient Performance:
The transient performance of a wicked reservoir heat pipe is primarily a function of the system thermal capacity. Diffusion effects are minimal, and the system responds rapidly to changing input or environmental conditions. The techniques of section 6.4.1 can be used to model transient behavior.

LSM Prototype Heat Pipe:
A prototype variable conductance heat pipe for temperature control of NASA's Lunar Surface Magnetometer (LSM) was designed and fabricated by TRW Systems as part of this program. The function of this heat pipe is to supplement heat rejection during the lunar day (preventing excessively high operating temperatures) while shutting off during the lunar night (to avoid excessively low operating temperatures). It is a passive gas controlled heat pipe utilizing a cold, wicked gas reservoir, and serves as a good example of the design technology discussed above. A schematic of the LSM heat pipe is shown on Fig. 6-34.

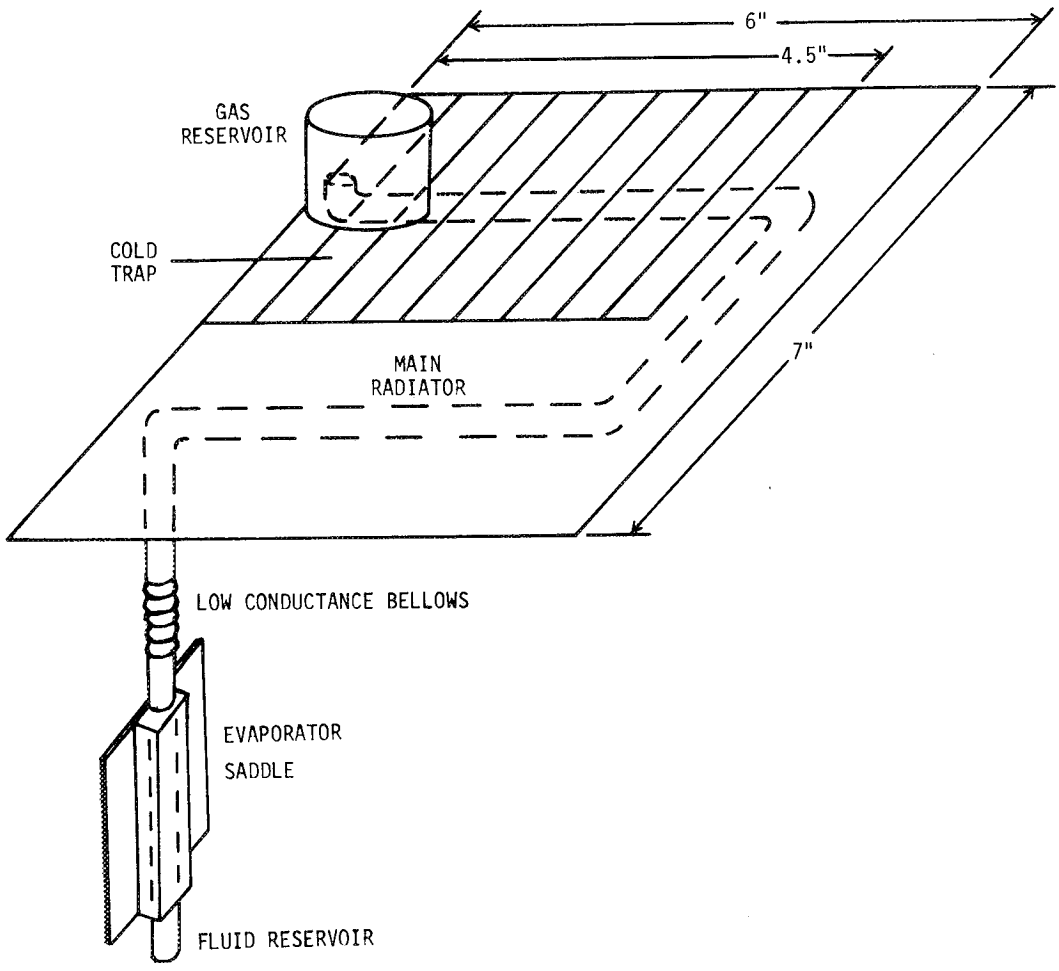

FIGURE 6-34. Schematic Diagram of Lunar Surface Magnetometer Heat Pipe

In order to help minimize the required reservoir volume, V_c was made small by using only 1/4 inch O.D. tubing. Methanol was selected as the working fluid in view of its low freezing point, smaller V_R/V_c requirement, low operating pressure,* and compatibility with the low conductivity stainless steel used for the tube and wicking. To reduce Q_{min}, a 5 mil wall bellows was placed between the evaporator and condenser, and the gas inventory adjusted so that the front moved upstream of the bellows under shut-down conditions. This bellows, in conjunction with a circumferential groove condenser wick design, provided the LSM heat pipe with a variable conductance ratio of 600:1 between full-on and full-off conditions.

Finally, the last 4 1/2 inches of aluminum fin were slotted to provide a low axial conductance cold trap which assured that the reservoir operated near sink temperature under "full-on" conditions.

6.5.3.2 Passive Non-Wicked Reservoir Systems

When dealing with hot non-wicked passive reservoirs, similar criteria apply with respect to condenser geometry, Q_{min}, and materials of construction as with wicked systems. Also, cold traps are again desired, but in this case to minimize fluctuations in the temperature at the end of the condenser (T_s) rather than the reservoir temperature itself (which is presumably relatively constant).

The principal difference in design technology has to do with the transient behavior of these systems. As shown in Section 6.4.2, non-wicked reservoir heat pipes are characterized by relatively slow diffusion-controlled transient response to changes in reservoir entrance conditions. Also, they are subject to considerable temporary overpressures if liquid should penetrate the hot reservoir.

Both of these factors dictate the use of low pressure working fluids such as methanol. Diffusion rates vary inversely with system pressure and

---

*This was required by the 5 mil wall bellows discussed below.

thus low pressure systems will exhibit faster response characteristics. Also, this constrains the maximum temporary overpressures to within tolerable limits (e.g., usually 10 - 30 psia with methanol) should liquid penetrate the reservoir.

Aside from using low pressure fluids, the system response characteristics can be maximized by utilizing short, large diameter reservoir feed tubes (Eq. 6-62). In this way, the Ames Heat Pipe Experiment on the OAO-C spacecraft* [V6] was designed with a diffusion time constant of only about two hours. A drawing of this system, showing the short, relatively large diameter reservoir feed tube between the non-wicked internal reservoir and the cold-trapped end of the condenser, is shown on Fig. 6-35.

It should be noted that Hinderman et. al. [V9] suggest an entirely different approach to the problem of diffusion into and out of non-wicked reservoirs. They suggest de-coupling the reservoir from conditions at its entrance by making $\tau_{\mathcal{D}'}$ extremely large (e.g., using very long, small diameter feed tubes). In this way, the partial pressure of vapor in the reservoir will seek a time-average value of conditions at its entrance and will not fluctuate with relatively short term changes.

Such an approach promises better control capability than allowing P_{VR} to fluctuate with $P_{VS'}$. However, there is a serious inherent danger with this approach. If conditions are temporarily such that (1) the condenser is overdriven and vapor is forced into the reservoir, or (2) liquid is forced into the reservoir, the very large value of $\tau_{\mathcal{D}'}$ will act to prevent the system from recovering to normal operating conditions for a very long time.

---

*Designed and fabricated as part of this program.

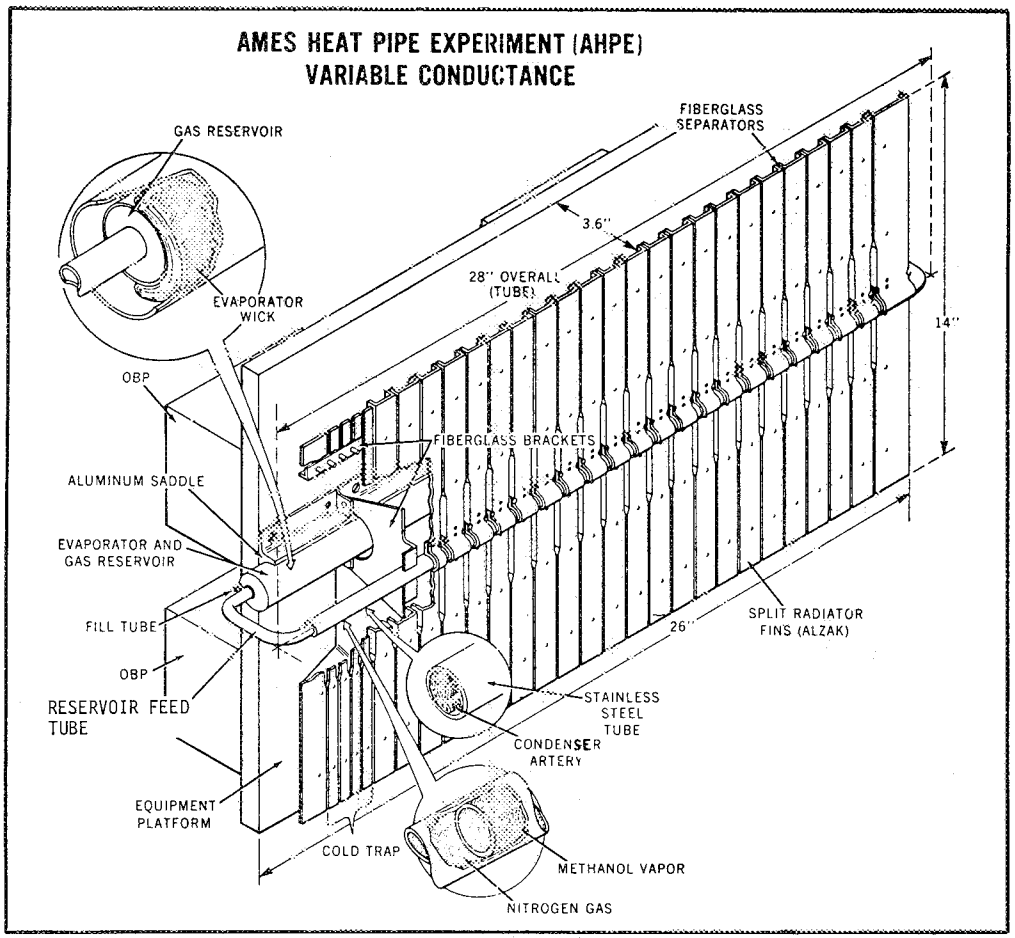

FIGURE 6-35. Schematic Diagram of the Ames Heat Pipe Experiment

6.5.3.3 Heated Reservoir Systems - T_R Constant

The design of active heated reservoir heat pipes where T_R is held constant is similar to that of passive systems except for the region of the reservoir. Because the reservoir is held at constant temperature, it is best that it be wicked since that provides control over both the gas temperature and the partial pressure of vapor within it. Thus, one achieves both better control and better transient behavior than with non-wicked systems.

To minimize heater power requirements, it is preferable to both insulate the reservoir and operate it at as low a temperature as possible. The required power then corresponds to insulation leakage, and conduction plus diffusion along the reservoir feed tube to the end of the condenser. This can be minimized by using long, thin-walled, low conductivity feed tubes.

Under such conditions, if T_R is to remain constant it must operate at a temperature exceeding the maximum temperature at the condenser end of the feed tube, since this point represents its heat sink. Also, as shown in section 6.1.4.2, T_R must be much lower than the minimum operating temperature. Thus, the reservoir should be designed to operate at: $T_{s'max} \leq T_R << T_{vamin}$.

Considerations pertaining to condenser geometry, working fluid, Q_{min}, materials of construction and transient behavior are the same as for wicked reservoir passive systems (section 6.5.3.1). In addition, cold traps are again desirable. However, in this case they serve to lower $T_{s'max}$ and thus T_R (and heater power) rather than to reduce fluctuations in T_R.

6.5.3.4 Heated Reservoir Systems - Feedback Control

This system is ostensibly similar to the previous one except that the reservoir heater is referenced to the source temperature rather than the reservoir temperature itself. However, this results in a completely different operating principle, as discussed in section 6.1.9. Rather than allowing reservoir temperature variations to degrade control, this system employs such variations to provide it.

The design of such heat pipes is somewhat more complex than those discussed previously, for it involves trading off steady-state versus transient performance. Because the transient response of this system is based on changes in reservoir temperature, it is subject to source temperature overshoots and undershoots depending on (1) the thermal capacities of its various elements, (2) the thermal coupling between the reservoir and its heat sink, and (3) the change in reservoir temperature required to accommodate changes in input or environmental conditions.

Thus, source temperature stability is improved by minimizing reservoir temperature change requirements. On the other hand, reservoir volume requirements are minimized by allowing T_R to vary over its maximum tolerable range.

It is TRW's experience that the design of such heat pipe systems is best performed on a transient basis using the modeling techniques discussed in section 6.4.1. A description of this design approach is beyond the scope of this report. However, certain design guidelines can be enumerated.

- As with constant temperature heated reservoir systems, heater power requirements are minimized if the reservoir is insulated and uses the condenser as its heat sink. However, the thermal coupling between the reservoir and condenser should not be minimized, but established to provide adequate reservoir cooling rates (high coupling) while avoiding excessive heater power requirements (low coupling). Thus, a trade-off is involved.
- The thermal capacity of the reservoir should be minimized to increase its thermal response characteristics.
- From a steady-state point of view, a minimum reservoir volume will result if the reservoir is allowed to vary between $T_{s/max}$ at full-on condenser conditions and T_{vamin} at full-off conditions.

- From a transient point of view (stability of the source temperature), it is preferred to use larger reservoirs and operate with a narrow range in T_R near T_{va}.
- As opposed to the previous systems discussed, the preferred working fluid has high rather than low values of P_{vR}/P_{va} for any given value of T_R below T_{va}. Thus, whereas ammonia offered the poorest control of the fluids considered for passive or constant T_R active systems (Fig. 6-4), it is the best for the feedback system.
- Considerations pertaining to condenser geometry, Q_{min} and materials of construction are similar to those for passive systems. However, cold traps may or may not be desirable depending on whether T_{smax} without a cold trap provides a sufficiently low temperature sink for the reservoir.

Further information on the design of heated reservoir feedback control systems can be found in the literature [V7, V8, V11, V13].

7.0 VARIABLE CONDUCTANCE THROUGH THE USE OF EXCESS WORKING FLUID

This control technique is closely related to non-condensible gas control. It utilizes the same fundamental control approach--that of passively varying the condenser area to accommodate changing heat rejection requirements. However, it differs from ordinary gas-control concepts in two principal ways. Rather than rely on the compressibility of a non-condensible gas to accommodate changes in the inactive volume of the condenser, this scheme utilizes a bellows (or bladder, etc.) containing a two-phase control fluid. Also, excess working fluid is used to block the condenser rather than a gas diffusion barrier. Such a system is schematically shown on Fig. 7-1.

Figure 7-2 shows the pressure-temperature diagram for this system. Since both the control and working fluids are two-phase systems, the P, T curves are unique for each of them. As long as the control fluid curve has a smaller slope at the point of intersection than that of the working fluid, the system will function properly; i.e., a drop in operating temperature will cause a decrease in condenser area and vice versa.

If the bellows containing the control fluid offers no resistance to displacement, the operating temperature will be at the point of intersection of the two curves (T_A). Thus, for a given set of working and control fluids, there exists only one operating temperature. Of course, the control fluid can be a mixture of several fluids and, hence, its P, T curve can be tailored to intersect the working fluid curve at any desired point.

In comparison with ordinary gas-controlled heat pipes, the use of a two-phase control fluid bellows to directly vary the inactive condenser volume permits using much smaller reservoirs for equivalent control.*

---

*The use of a control fluid to vary the reservoir volume in gas-controlled heat pipes, providing closer "feedback" control, has been suggested by Bienert [V7].

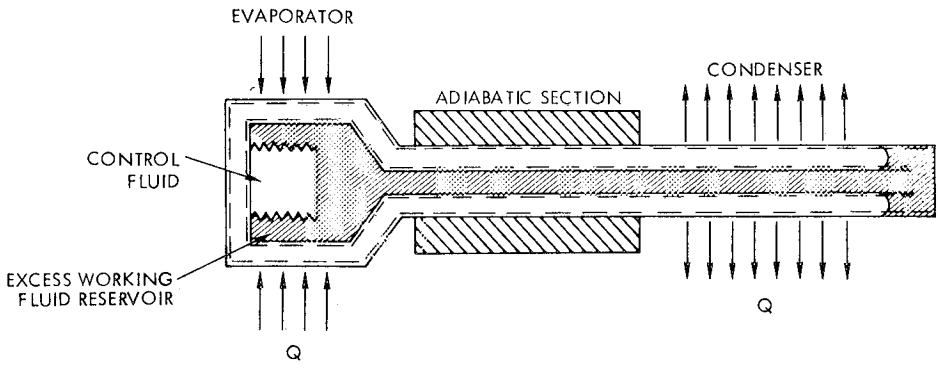

FIGURE 7-1. Schematic Diagram of an Excess Liquid Controlled Variable Conductance Heat Pipe

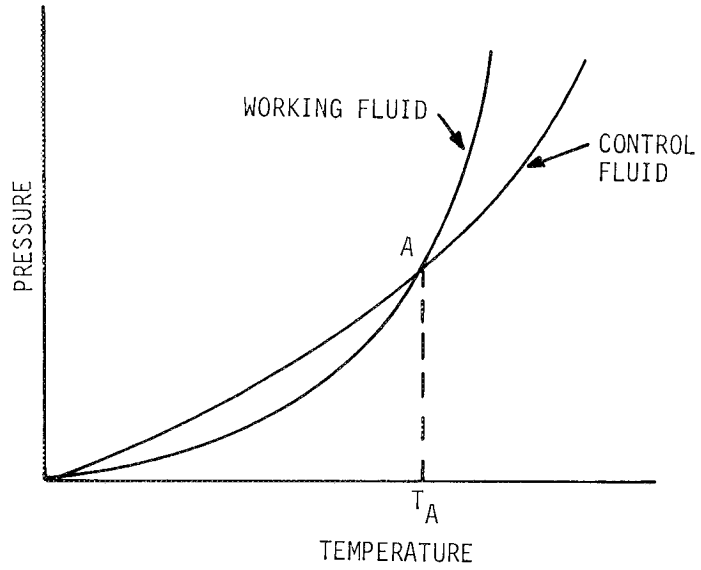

FIGURE 7-2. Pressure-Temperature Relationship for an Excess Liquid Controlled Variable Conductance Heat Pipe

In fact, if the bellows (or bladder) offered no resistance to displacement and could fill the reservoir, a reservoir to condenser volume ratio near unity would yield precise temperature control. In other words, the expandable two-phase control fluid reservoir potentially provides this scheme with a very high control sensitivity $(\frac{\partial Q}{\partial T}_{va})$.

However, the principal potential advantage of excess fluid control lies not in its high control sensitivity, but in its insensitivity to variations in sink conditions. As emphasized in section 6.0, one of the serious limitations on gas controlled heat pipes is their sensitivity to changes in sink temperature, which alters both the gas temperature and partial pressure of vapor within the gas-blocked region. This, in effect, alters the volume of the gas-blocked region for a given total system pressure. In contrast, the liquid used to block the condenser in the excess fluid control scheme is relatively incompressible, and changes in sink temperature do not appreciably alter its effective volume at constant pressure. Consequently, changes in sink temperature should not effect the control temperature of the device other than through changing heat rejection area requirements.

Another advantage of liquid condenser flooding is that it is not subject to diffusion effects between gas and vapor, since there is no gas in the system.

On the other hand, this technique also suffers some obvious disadvantages. It introduces difficulties in 1-g testing in that gravity tends to cause the excess fluid to puddle in the condenser rather than reside as shown in Fig. 7-1. To permit 1-g testing, it is therefore necessary to provide the heat pipe with an internal capillary structure to retain the fluid against gravitational forces.

Also, this approach is limited to applications where the effective sink temperature is above the freezing point of the working fluid. If the working fluid freezes in the "shut-off" end of the condenser, the reservoir is de-coupled from the operating portion of the pipe by the solid plug, causing a loss of control.

The excess fluid control technique is under continuing study as part of this program. System limitations, range of applicability, working fluids, control fluids, etc., are under consideration with respect to spacecraft thermal control applications. These studies, however, are incomplete and will be documented in a later report.

8.0 VARIABLE CONDUCTANCE THROUGH THE USE OF LIQUID FLOW CONTROL

Liquid flow control involves interrupting or impeding the condensate flow in the wick so as to starve the evaporator of working fluid. By somehow servoing the interruption or throttling mechanism to the evaporator temperature, this scheme could yield a variable conductance device which maintains the evaporator temperature within a prescribed control band. Furthermore, by utilizing either a two-phase control fluid bellows (as in section 7.0) or a bi-metallic element to actuate the control mechanism in reference to the evaporator temperature, the resultant device would offer passive control.

As pointed out in section 5.1, for dissipative heat sources, liquid flow control is limited to providing "on-off" thermal switching. A potential problem arises, however, in the event of a mismatch in the thermal response characteristics of the evaporator (and heat source) and the hydrodynamic response characteristics for resaturating the evaporator wick. Depending on the particular system, the thermal inertia may be so small in comparison with the hydrodynamics as to give rise to large amplitude fluctuations and non-uniformities in the evaporator for any reasonable on-off switching rate.

Additional disadvantages associated with this scheme include its requirement for moving parts and the design problems associated with providing high capacity wick systems with make-break or throttling mechanisms.

The obvious drawbacks of this control scheme, and the apparent lack of advantages when compared with other concepts has resulted in its receiving relatively little development effort. This author is not aware of any published work in liquid flow control other than Anand's experiments [V2] in which it was demonstrated that wick interruption leads to evaporator runaway. Additional work has also been performed by R. N. Schmidt, et. al., at Honeywell Systems and Research Center, who developed an on-off thermal switch using this principle.

9.0 VARIABLE CONDUCTANCE THROUGH THE USE OF VAPOR FLOW CONTROL

Interrupting or throttling the vapor flow between the evaporator and condenser sections of a heat pipe gives rise to a pressure differential between the two regions and, hence, a corresponding temperature difference. Using this principle, the over-all temperature drop can be varied for any given axial heat transfer rate; i.e., the heat pipe has a variable thermal conductance.

If the vapor flow path is interrupted, the evaporator temperature and pressure can increase and/or the condenser temperature and pressure can increase and/or the condenser temperature and pressure can decrease until the pressure differential across the pipe exceeds the "bubble point" pressure of the wick/fluid combination. At this point vapor will "blow through" the wick, short circuiting the vapor blockage, and interfere with the liquid flow so as to cause evaporator dryout. This phenomenon can be used to provide on-off control, similar to liquid flow interruption. Thermal switches based on this principle have been developed by TRW and reported in the literature [V1].

On the other hand, if the vapor flow is only throttled, one can continuously control the evaporator-condenser temperature differential. However, the range of continuous control is substantially limited by the fact that the evaporator-condenser pressure differential must not exceed the bubble point pressure of the wick fluid combination. Furthermore, whatever the magnitude of this pressure differential, it "comes off the top" of the available capillary head and reduces the hydrodynamic capacity of the heat pipe.

In spite of these limitations, vapor flow modulation is a promising control technique in that it offers several potential advantages over gas controlled heat pipes. Like the excess fluid control technique (section 7.0), it does not require bulky gas reservoirs. Also, the fact that the entire condenser is maintained at a nearly uniform temperature may represent a better thermal interface with the rest of the spacecraft. But, most important, this system offers close control under conditions where the sink temperature

varies and is not far below the evaporator temperature. High, variable sink temperature conditions seriously limit the control capabilities of passive gas-controlled heat pipes due to vapor pressure variations within the reservoir and gas blocked condenser region (section 6.0). The vapor modulation scheme does not suffer any equivalent limit for high sink temperature. In fact, performance improves as $T_s \rightarrow T_{ev}$ in that smaller evaporator-to-condenser pressure differentials are required.

To implement this control technique effectively, a promising approach is to passively actuate the throttling valve with the same type of two-phase control fluid bellows discussed in section 7.0. This is shown on Fig. 9-1.

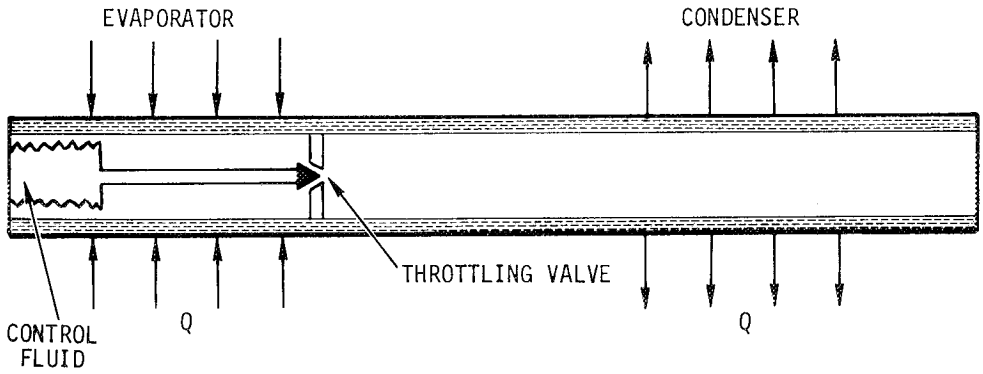

FIGURE 9-1. Schematic Diagram of a Vapor Modulated Variable Conductance Heat Pipe

If the evaporator temperature exceeds the control point, the bellows contracts, enlarging the valve orifice which increases the heat transfer rate and vice versa. By actuating the throttling valve in this manner, the P, T diagram shown on Fig. 7-2 characterizes this system in the same way as it does the excess liquid condenser flooding system.

9.1 Analytical Model

As with the flat-front theory for gas controlled heat pipes, a good deal of insight into the operational limitations of vapor modulated heat pipes can be gained with a very simple analytical model. We shall make the following assumptions:

(1) Steady-state conditions prevail
(2) Body forces can be neglected (e.g., 0-g)
(3) Axial conduction can be neglected
(4) Radial heat transfer is uniform over the evaporator condenser sections
(5) Fluid properties are constant along the entire pipe
(6) The vapor in both the evaporator and condenser is in thermodynamic equilibrium with the liquid in the wick
(7) The vapor pressure drop in the pipe is negligible when the throttling valve is fully open; i.e., the entire vapor pressure drop occurs across the valve
(8) The thermal resistance of the wick and wall can be neglected

With these assumptions, the hydrodynamic pressure balance for the vapor modulated heat pipe becomes:

$$\Delta P_c = \Delta P_\ell + \Delta P_{vt} \tag{9-1}$$

where:

ΔP_c - net capillary head
ΔP_ℓ - liquid pressure drop
ΔP_{vt} - vapor pressure drop across the throttling valve

The liquid pressure drop for the heat pipe is given by:

$$\Delta P_\ell = \frac{Q\,(L + L_a)\mu_\ell}{2\pi K \rho_\ell \lambda (R_w^2 - R_v^2)} \tag{9-2}$$

where:

Q - axial heat transport
L - length of heat pipe
L_a - length of adiabatic section
μ_ℓ - viscosity of liquid
K - wick permeability

ρ_ℓ - density of liquid
λ - latent heat of vaporization
R_w - outside radius of wick
R_v - radius of vapor core

Thus, Eq. (9-1) can be written:

$$Q = (\Delta P_c - \Delta P_{vt}) \left(\frac{2\pi K \rho_\ell \lambda (R_w^2 - R_v^2)}{(L + L_a)\, \mu_\ell} \right) \tag{9-3}$$

If one now writes Eq. (9-3) for the capillary pumping limit (maximum circulation rate) under conditions where the throttling valve is partially closed ($\Delta P_{vt} \neq 0$) and fully open ($\Delta P_{vt} = 0$), and then ratios the two, the following equation results:

$$\frac{Q_{CL}}{Q_{CLmax}} = \frac{\Delta P_{cmax} - \Delta P_{vt}}{\Delta P_{cmax}} = 1 - \frac{\Delta P_{vt}}{\Delta P_{cmax}} \tag{9-4}$$

where:

Q_{CL} - capillary pumping limit
Q_{CLmax} - capillary pumping limit with throttling valve fully open
ΔP_{cmax} - maximum capillary head for wick/fluid pair

Equation (9-4) describes the effect of vapor throttling on heat pipe hydrodynamic performance. When the valve is wide open and $\Delta P_{vt} = 0$, the heat pipe exhibits its maximum capacity. As the valve closes and ΔP_{vt} increases, less of the maximum capillary head is available for liquid pumping and the capacity decreases. When ΔP_{vt} equals ΔP_{cmax}, the capacity of the pipe goes to zero.

9.1.1 Blow Through Limits

The condition where $\Delta P_{vt} = \Delta P_{cmax}$ represents the "blow through" limit of the wick. For saturated wicks,* the maximum capillary head

*Partially desaturated wicks cannot sustain a vapor pressure differential across the throttling valve.

also represents the bubble point of the wick/fluid pair. If ΔP_{vt} were to exceed ΔP_{cmax}, vapor would blow through the wick from the evaporator to the condenser.

Thus, the evaporator-condenser temperature differential corresponding to $P_{ve} - P_{vc} = \Delta P_{vt} = \Delta P_{cmax}$ represents an upper bound for continuous vapor-modulation control. To establish potential operating ranges for this control scheme, this temperature differential was calculated as a function of evaporator temperature for various wick pore sizes and working fluids. To perform these calculations the maximum capillary head was taken as $\frac{2\sigma}{r_e}$, where σ is the liquid surface tension and r_e is the effective pore radius.

Results for water, methanol and ammonia are shown on Figs. 9-2, 9-3 and 9-4, respectively. Also shown on the curves are the freezing lines corresponding to the temperature differential which drives the condenser below the freezing point of the working fluid. This is an obvious constraint on the vapor modulation flow scheme since it would prevent liquid return to the evaporator.

The curves on Figs. 9-2, 9-3 and 9-4 represents the outer bounds of the performance maps for vapor modulation systems. For a given wick pore size and working fluid, the system can theoretically be operated below the blow through limit and to the right of the freezing limit. These maps are general, since there was no reference to a particular heat pipe configuration in the calculations. They can therefore be used in selecting a preferred working fluid and pore size for a given application.

For reference, the graphs also contain a table of wire spacing for several standard wire mesh screens. Taking the effective pore radius as half the wire spacing establishes a correspondence between several of the blow through limit curves and these screen mesh sizes.

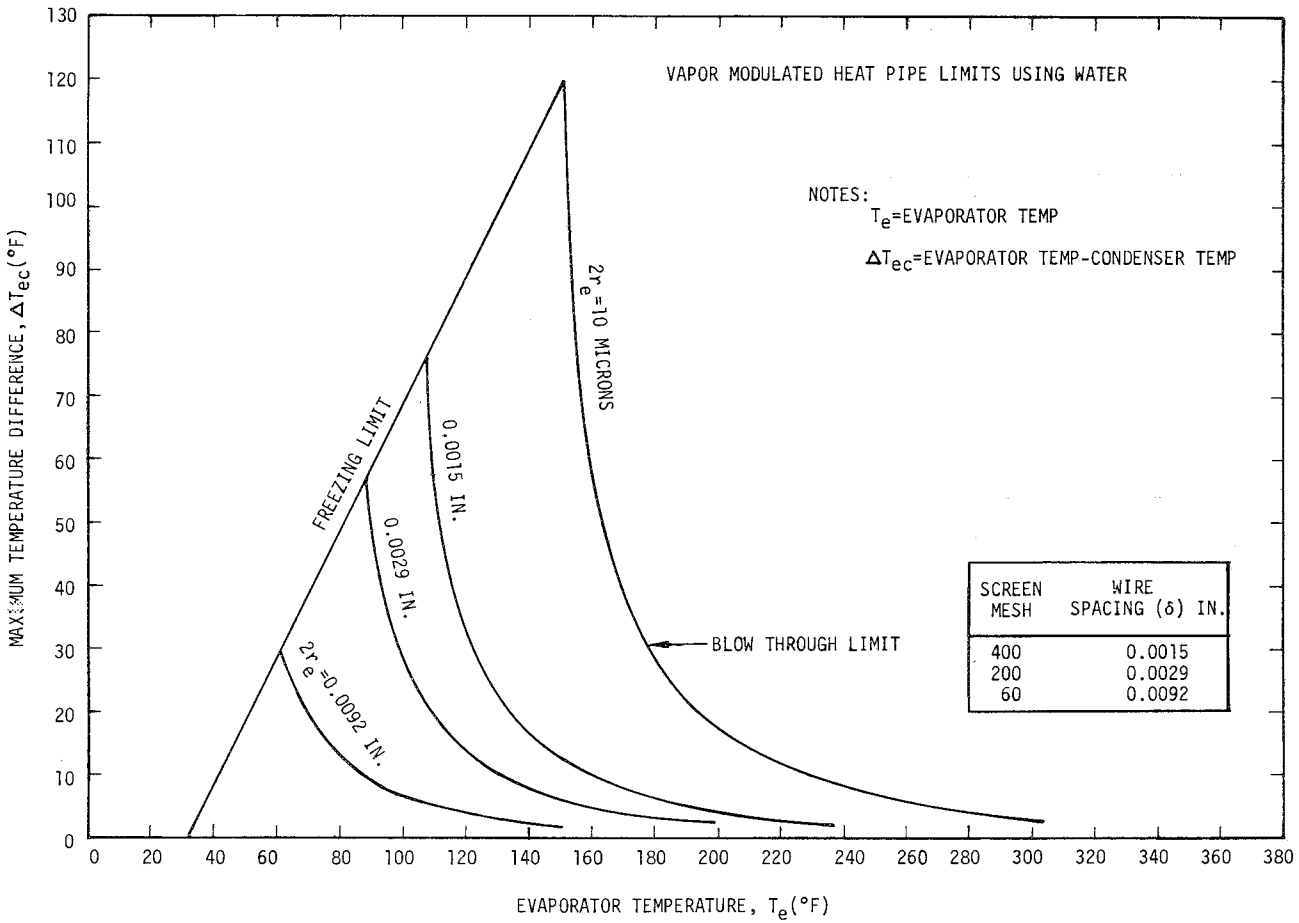

FIGURE 9-2. Vapor Modulated Heat Pipe Limits Using Water

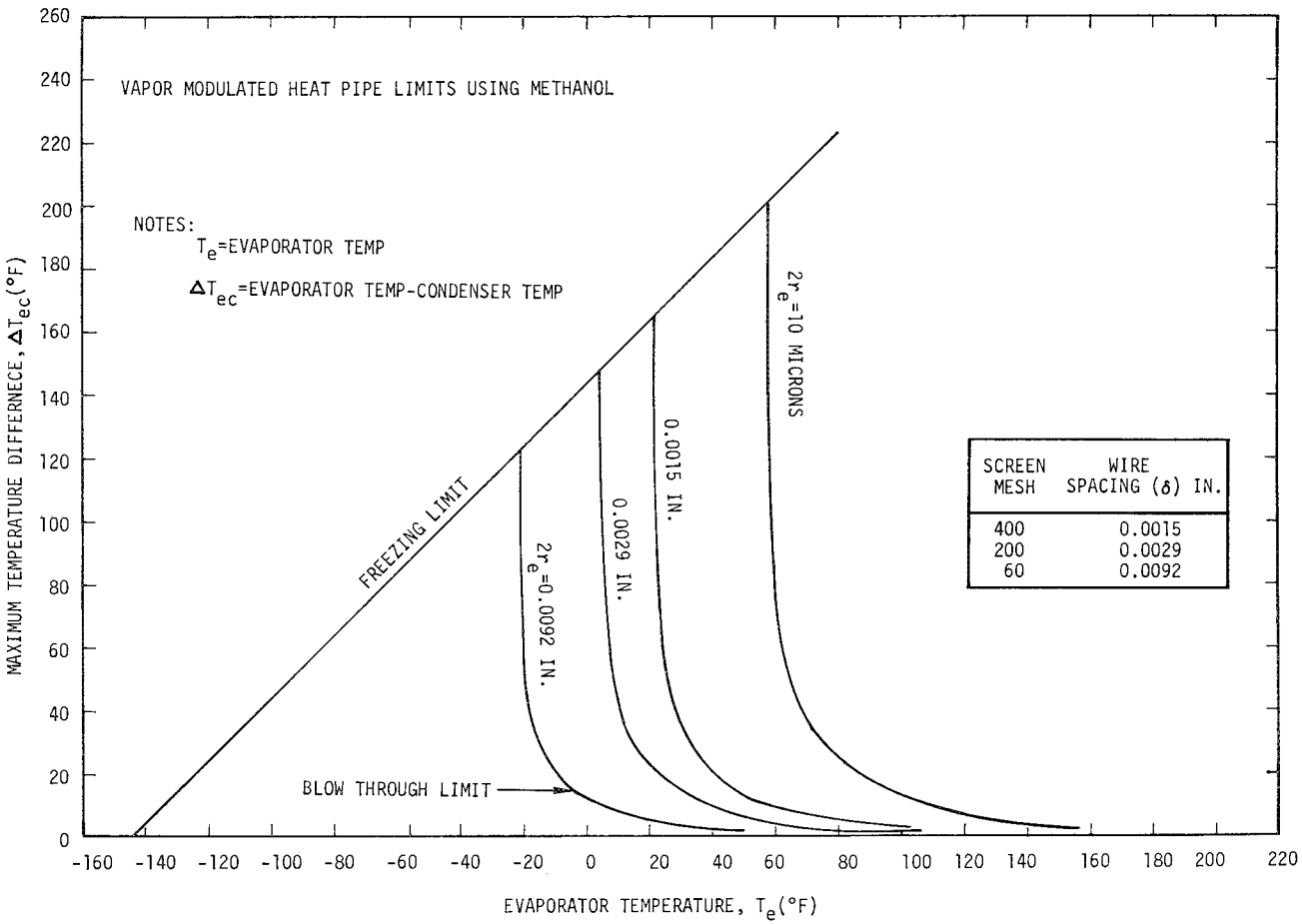

FIGURE 9-3. Vapor Modulated Heat Pipe Limits Using Methanol

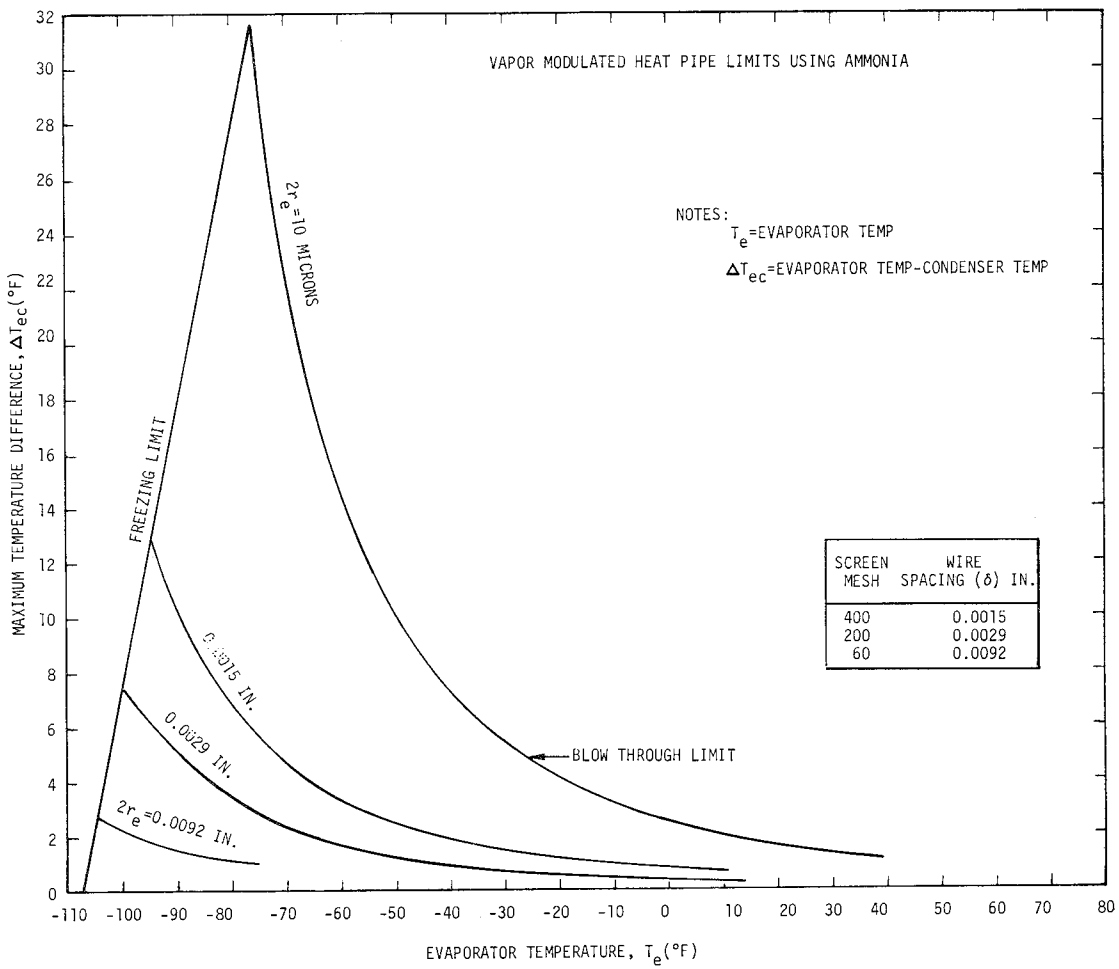

FIGURE 9-4. Vapor Modulated Heat Pipe Limits Using Ammonia

The physical significance of the curves on Fig. 9-2, 9-3 and 9-4 can be seen more clearly with reference to Fig. 9-5. This is a plot of Eq. (9-4) for water using a wick with an effective pore diameter of 0.0029 in. (200 mesh screen). For fixed evaporator temperatures (control set points), the curves show the effect of throttling the vapor (altering the difference between the evaporator and condenser temperatures) on the axial heat flow capacity - Q_{CL}/Q_{CLmax}.

The intersection of each of the fixed T_e curves on Fig. 9-5 with the abscissa ($Q_{CL} = 0$) represents the blow through limits for that particular value of T_e. Thus, the blow through limit curve of Fig. 9-2 for $2r_e$ = 0.0029 in. represents the locus of the points of intersection for all values of T_e.

Note that for $T_e = 70°F$, the performance curve of Fig. 9-5 does not intersect the abscissa. This corresponds to the situation where the absolute pressure corresponding to T_e is lower than the maximum capillary head generated by the wick/fluid pair. Under such circumstances, the condenser temperature and pressure can be lowered arbitrarily without reaching a blow through condition. Of course, the freezing limitation still exists as shown on the curve (F.P.).

9.1.2 Operating Characteristics

The curves of Figs. 9-2, 9-3, 9-4 and 9-5 represent operating limits for vapor modulation control heat pipes. The actual operating characteristic is determined by the heat rejection characteristics of the system.

If condenser heat rejection can be assumed proportional to the condenser-sink temperature differential, we can write:*

$$Q = hA' L_c (T_c - T_s) \qquad (9\text{-}5)$$

*For radiation heat transfer, Eq. (9-5) is replaced by an appropriate radiation equation as discussed in section 6.1.

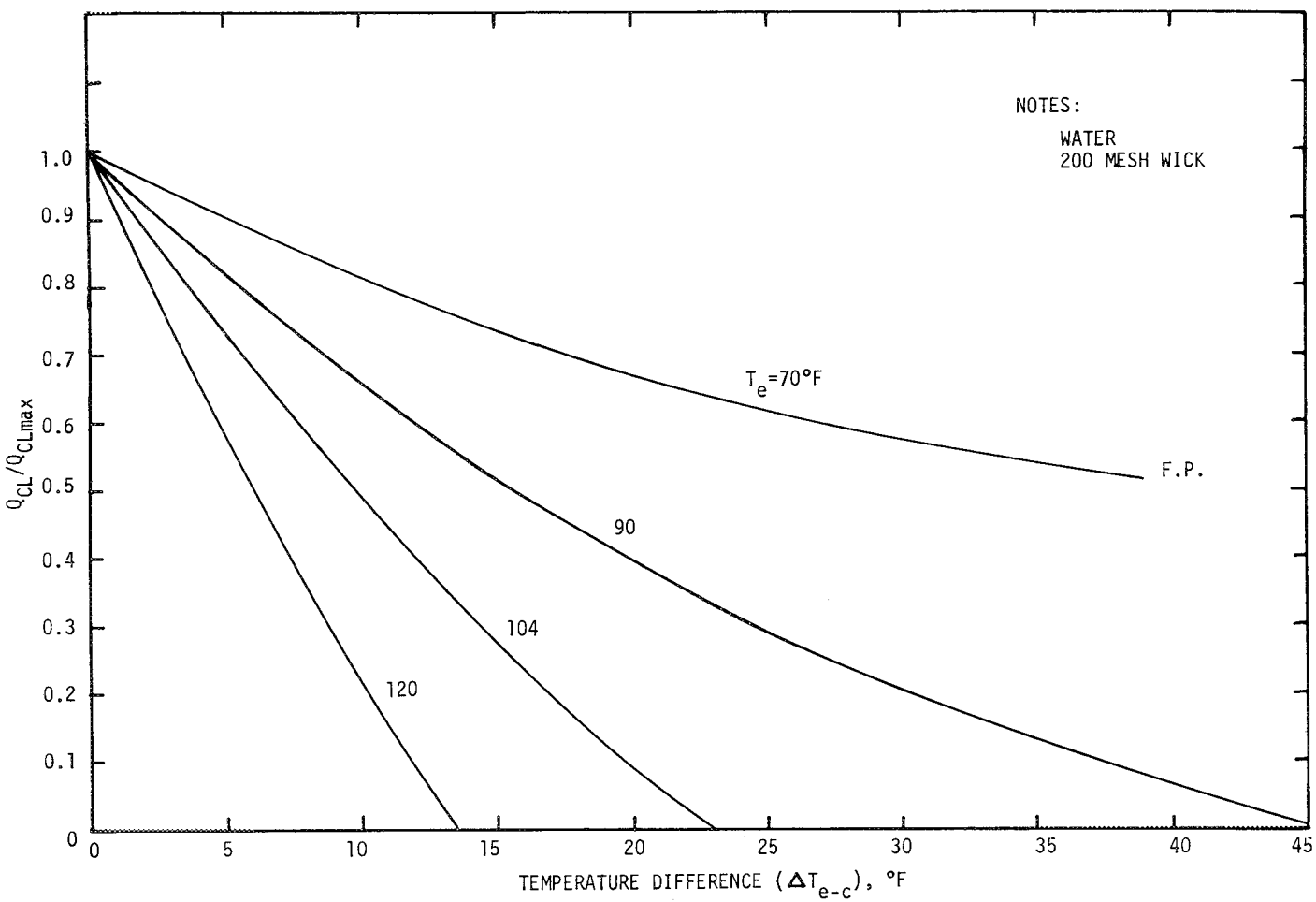

FIGURE 9-5. Effect of Vapor Throttling on Axial Heat Transfer Capacity - Water

where:

h - heat transfer coefficient

A' - heat rejection area per unit length of condenser

L_c - condenser length

T_c - condenser temperature

T_s - sink temperature

Defining the maximum heat rejection rate (when the throttling valve is wide open and $T_c = T_e$) as Q_{max}, Eq. (9-5) can be normalized as follows:

$$\frac{Q}{Q_{max}} = \frac{(T_c - T_s)}{(T_e - T_s)} \tag{9-6}$$

For a given evaporator set point, one can now compare the heat rejection characteristic with the heat pipe capacity by plotting both Eq. (9-6) and (9-4) on a single graph. However, in terms of design requirements, the graph can be made more informative by first defining a hydrodynamic safety factor as the ratio of the maximum capillary limit to the maximum heat rejection requirements:

$$Q_{CLmax} = SF \times Q_{max} \tag{9-7}$$

Now Eq. (9-4) can be written:

$$\frac{Q_{CL}}{Q_{max}} = SF \left(1 - \frac{\Delta P_{vt}}{\Delta P_{cmax}}\right) \tag{9-8}$$

Figure 9-6 shows Q_{CL}/Q_{max} from Eq. (9-8) and Q/Q_{max} from Eq. (9-6) plotted against condenser temperature for water with a 200 mesh screen wick and an evaporator temperature of 90°F. Curves of Q_{CL}/Q_{max} are shown for safety factors of 1, 2 and 3. Curves of Q/Q_{max} are shown for sink temperatures of 50°F and 40°F.

This example serves to illustrate several of the design requirements for vapor-modulated heat pipes. The operating range of such a heat pipe corresponds to those conditions for which the axial heat transfer capacity exceeds the heat rejection requirements. Comparing the heat rejection

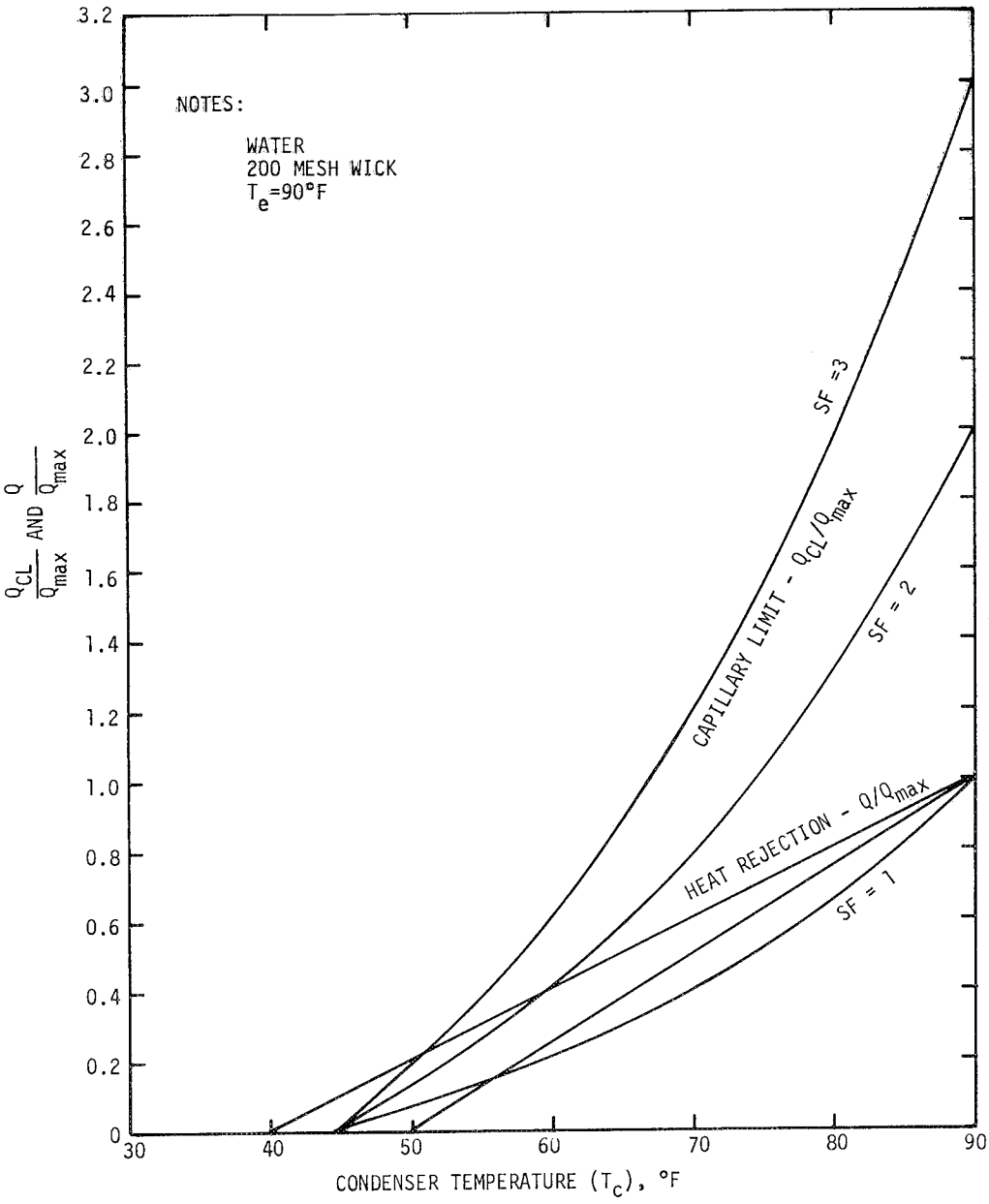

FIGURE 9-6. Operating Range of Vapor Modulated Heat Pipe - Water

curve for a 50°F sink with the SF = 1 curve for axial capacity (capillary pumping limit), one sees that the pipe cannot operate over most of the potential range of condenser temperatures (50 - 90°F). This is because the axial heat transport capacity falls off more rapidly with T_c than does the condenser heat rejection as T_c is lowered from T_e. Thus, it is necessary to design the heat pipe so that, with the throttling valve fully open, the maximum axial capacity is somewhat greater than the maximum heat rejection requirement. As shown in Fig. 9-6, a safety factor of 2 is more than sufficient for this case.

Note, however, that if the sink temperature is 40°F, the pipe cannot operate over the entire range in condenser temperature regardless of the safety factor. This is because the ΔP_{vt} required to sustain the evaporator at 90°F with the condenser at 40°F exceeds the bubble point pressure; that is, exceeds the blow through limit. Thus, for the heat pipe of this example with T_s = 40°F, the continuous control range would not extend down to shut-off conditions, but only to the intersection of the Q_{CL}/Q_{max} and Q/Q_{max} curves. As SF is increased, this intersection occurs at lower and lower temperatures and, in the limit of SF $\rightarrow \infty$, corresponds to the blow through limit (T_c = 45°F).

This is not to say that a vapor modulated heat pipe using water cannot be designed to operate with T_c = 40°F. To do so would simply require that a wick with a smaller pore size be used. From Fig. 9-2, it is seen that with a 400 mesh rather than a 200 mesh screen wick, the blow through limit exceeds the 50°F ΔT_{ec} requirement. On the other hand, the condenser can obviously not operate below 32°F, the freezing point of water, regardless of the blow through limit.

9.2 Summary

The simple analytical model presented in the last section is not very precise in view of the assumptions made. However, it does serve to scope the problem and point out several important design considerations.

Clearly, if one wishes a variable conductance heat pipe which can be nearly shut-off, the pipe must be able to function with $T_c = T_s$. Thus, one must select a working fluid which does not freeze at minimum sink conditions, and a working fluid-wick pore size combination which yields a blow through limit in excess of $T_e - T_s$.

The latter requirement is assured if the fluid vapor pressure at T_e is less than the maximum capillary head, although this is not absolutely necessary. However, it is generally the case that low pressure working fluids will be necessary to maintain continuous control over appreciable ranges in T_c.

Similar considerations suggest the use of very small pore wicks to achieve high capillary heads. Since small pores also lead to high flow resistance with homogeneous wicks, arterial wick structures are particularly attractive for these systems.

The vapor modulation control scheme is under continuing study by TRW as part of this program. Further results of these studies will be documented in a later report.

10.0 SELECTED BIBLIOGRAPHY PERTINENT TO SPACECRAFT THERMAL CONTROL

10.1 Hydrodynamics & Hydrostatics

H1 T. P. Cotter, "Theory of Heat Pipes", Los Alamos Scientific Laboratory, LA-3246-MS, March 1965.

H2 D. M. Ernst, "Evaluation of Theoretical Heat Pipe Performance", Thermionic Conversion Specialist Conference--Conference Record, pp. 349-354, Palo Alto, Calif., 30 Oct - 1 Nov 1967.

H3 C. L. Tien and K. H. Sun, "Minimum Meniscus Radius of Heat Pipe Wicking Materials", Int'l. Jour. Heat and Mass Trans., Vol. 14 pp. 1853-55, Nov. 1971.

H4 E. C. Phillips and J. D. Hinderman, "Determination of Properties of Capillary Media Useful in Heat Pipe Design", A.S.M.E. Paper No. 69-HT-18, 1969.

H5 R. A. Farran and K. E. Starner, "Determining Wicking Properties of Compressible Materials for Heat Pipe Applications", Proceedings of the Annual Aviation and Space Conference, Beverly Hills, Calif., pp. 659-670, 16-19 June 1968.

H6 C. A. Busse, "Pressure Drop in the Vapor Phase of Long Heat Pipes", Thermionic Conversion Specialist Conference--Conference Record, pp. 391-398, Palo Alto, Calif., 30 Oct - 1 Nov 1967.

H7 G. H. Parker and J. P. Hanson, "Heat Pipe Analysis", ASME-Advances in Energy Conversion Engineering, pp. 847-857, August 1967.

H8 G. A. Carlson and M. A. Hoffman, "Effect of Magnetic Fields on Heat Pipes", Space Systems and Thermal Technology for the 70s, A.S.M.E. Space Technology and Heat Transfer Conference, Los Angeles, 21-24 June 1970.

H9 J. E. Kemme, "High Performance Heat Pipes", Thermionic Conversion Specialist Conference--Conference Record, pp. 355-358, Palo Alto, Calif., 30 Oct - 1 Nov 1967.

H10 E. K. Levy, "Investigation of Heat Pipe Operating at Low Vapor Pressures", Proceedings of the Annual Aviation and Space Conference, Beverly Hills, Calif., pp. 671-676, 16-19 June 1968.

H11 R. A. Freggens, "Experimental Determination of Wick Properties for Heat Pipe Applications", RCA Electronic Components, Paper #699108, Proceedings of the Fourth Intersociety Energy Conversion Engineering Conference, Washington, D. C., 1969.

H12 L. S. Langston and H. R. Kunz, "Liquid Transport Properties of Some Heat Pipe Wicking Materials", ASME Paper No. 69-HT-17, 1969.

H13 T. I. Sweeney, "The Performance of a Sodium Heat Pipe", A.I.Ch.E. Preprint No. 7, A.I.Ch.E.-A.S.M.E. Heat Transfer Conference, Minneapolis, 1969.

H14 J. Bohdansky, H. Strub, and Evan Andel, "Heat Transfer Measurements Using a Sodium Heat Pipe Working at Low Vapor Pressure", Thermionic Conversion Specialist Conference--Conference Record, pp. 144-148, 1966.

H15 J. E. Kemme, "Heat Pipe Capability Experiments", Los Alamos Scientific Laboratory, LA-3585-MS, August 22, 1966.

H16 A. Carnesale, J. H. Cosgrove, J. K. Ferrel, "Operating Limits of the Heat Pipe", Proceedings of the Joint Atomic Energy Commission--Sandia Laboratories Heat Pipe Conference, Vol I, Sandia Corporation Report SC-M-66-623, Albuquerque, New Mexico, pp. 30-44, October 1966.

H17 S. Frank, J. T. Smith, K. M. Taylor and W. J. Levedahl, "Heat Pipe Design Manual", Martin Nuclear Report MND-3288, Martin Marietta Corp., Baltimore, Md., February 1967.

H18 A. E. Scheidegger, The Physics of Flow Through Porous Media, The Macmillan Co., pp. 68-90, 1960.

H19 Sidney Frank, "Optimization of a Grooved Heat Pipe", ASME-Advances in Energy Conversion Engineering, pp. 833-846, August 1967.

H20 F. J. Stenger, "Experimental Feasibility Study of Water-Filled Capillary-Pumped Heat-Transfer Loops", NASA-Lewis Research Center Report No. NASA TM X-1310, November 1966.

H21 W. L. Haskin, "Cryogenic Heat Pipe", Technical Report AFFDL-TR-66-228, June 1967.

H22 T. P. Cotter, "Heat Pipe Start-up Dynamics", Presented at the 1967 Thermionic Conversion Specialist Conference, Palo Alto, Calif., 30 Oct - 1 Nov 1967.

H23 J. E. Deverall, "The Effect of Vibration on Heat Pipe Performance", LASL Report LA-3798, Oct 1967.

H24 J. E. Deverall, et al, "Heat Pipe Performance in a Zero Gravity Field", J. Spacecraft Rockets, Vol. 4, No. 11, pp. 1556-1557, Nov 1967.

H25 T. P. Cotter, "Status of the Engineering Theory of Heat Pipes", Proceedings of Joint Atomic Energy Commission/Sandia Laboratories Heat Pipe Conference, Vol. 1, NASA N67-26791, Rpt. No. SC-M-66-623 CONF-660645, Oct 1966.

H26 J. E. Deverall and E. W. Salmi, "Heat Pipe Performance in a Space Environment", Thermionic Conversion Specialist Conference --Conference Record, pp. 359-362, Palo Alto, Calif., 30 Oct - 1 Nov 1967.

H27 Johns Hopkins University, "The GEOS-2 Heat Pipe System and its Performance in Test and in Orbit", Report No. S2P-3-25, NASA CR-94585, NASA N68-23540, 29 April 1968.

H28 J. K. Ferrell, "A Study of the Operating Characteristics of the Heat Pipe", Report No. ORO 3411-9, NASA N68-23098, 1 Nov 1967.

H29 J. K. Ferrell and E. M. Schoenborn, "A Study of the Operating Characteristics of the Heat Pipe: Capillarity in Porous Media", Report No. ORO-3411-10, NASA N68-23099, 20 Feb 1968.

H30 W. Bienert, et al, "Application of Heat Pipes to SNAP-29", Proceedings of Intersociety Energy Conversion Engineering Conference, Boulder, Colorado, pp. 477-486, 1968.

H31 F. W. Holm, P. L. Miller, "Thermal Scale Modeling of a Heat Pipe", Texas A&M Univ., ASME Paper No. 70-HT/SpT-14, 1970.

H32 M. Green, "An Improved Method of Calculating Frictional Pressure Losses Along Grooved Heat Pipes", Grumman Aircraft Engineering Corp., Bethpage, N.Y. Report No. ADN-04-02-69.1, June 1969.

H33 J. W. Richardson, et al, "The Effect of Longitudinal Vibration on Heat Pipe Performance, J. Astronaut. Sci., V. 17, no. 5, Mar-Apr 70, p. 249-266.

10.2 Heat Transfer

T1 A. E. Bergles and W. M. Rohsenow, A.S.M.E. Transactions, Journ. of Heat Transfer, August 1964.

T2 D. W. Green and R. H. Perry, "Heat Transfer with a Flowing Fluid through Porous Media", Chem. Engr. Progress Symp. Series, Heat Transfer, Buffalo

T3 R. L. Goring and S. W. Churchill, "Thermoconductivity of Heterogeneous Materials", Chemical Engineering Progress, Vol. 57, No. 7, pp. 53-59, July 1961.

T4 M. M. Soliman, D. W. Grauman, P. J. Berenson, "Effective Thermal Conductivity of Saturated Wicks", AiResearch Manufacturing Co., ASME Paper No. 70-HT/SpT-40, 1970.

T5 W. D. Allingham and J. A. McEntire, "Determination of Boiling Film Coefficient for a Heated Horizontal Tube in Water-Saturated Wick Material", J. Heat Transfer, pp. 71-76, Feb 1961.

T6 C. P. Costello and E. R. Redeker, "Boiling Heat Transfer and Maximum Heat Flux for a Surface with Coolant Supplied by Capillary Wicking", Chem. Engr. Progress Symp. Series, No. 41, 59, pp. 104-113, 1963.

T7 C. P. Costello and W. J. Frea, "The Role of Capillary Wicking and Surface Deposits in the Attainment of High Pool Boiling Burnout Heat Fluxes", AIChE Journal, 10, pp. 393-368, May 1964.

T8 P. J. Marto and W. L. Mosteller, "Effect of Nucleate Boiling on the Operation of Low Temperature Heat Pipes", A.S.M.E. Paper No. 69-HT-24, 1969.

T9 J. K. Ferrell, H. R. Johnson, "The Mechanism of Heat Transfer in the Evaporator Zone of a Heat Pipe", North Carolina State University, A.S.M.E. Paper No. 70-HT/SpT-12, 1970.

T10 J. K. Ferrell and J. Alleavitch, "Vaporization Heat Transfer in Capillary Wick Structures", Chem. Eng. Prog. Symp. Ser. Vol. 66, 1970.

T11 J. K. Ferrell and J. Alleavitch, "A Study of the Operating Characteristics of the Heat Pipe, Part III: Vaporization Heat Transfer From Flooded Wick Covered Surfaces", North Carolina State University Final Report No. ORO-3411-12, 158 p., 30 April 1969.

T12 J. K. Ferrell and H. R. Johnson, "A Study of the Operating Characteristics of the Heat Pipe, Part IV: Heat Transfer in the Evaporator Zone of a Heat Pipe", North Carolina State University Final Report No. ORO 3411-12, 150 p., April 1969.

10.3 Materials Compatibility

M1 J. Schwartz, "Performance Map of the Water Heat Pipe and the Phenomenon of Non-Condensible Gas Generation", ASME Paper No. 69-HT-15, 1969.

M2 E. D. Waters and P. O. King, "Compatibility Evaluation of an Ammonia-Aluminum-Stainless Steel Heat Pipe", ASME Paper No. 70-HT/SpT-15, 1970.

M3 A. Basiulis and M. Filler, "Operating Characteristics and Long Life Capabilities of Organic Fluid Heat Pipes", AIAA Paper No. 71-408, AIAA 6th Thermophysics Conf., 1971.

M4 A. P. Shlosinger, Materials Research Report, TRW Systems No. 06462-6003-RO-00, NASA CR 73169, September 1967.

M5 W. Woo, "Study of Passive Temperature and Humidity Control Systems for Advanced Space Suits - Material Research Report", 1 July 1967 - 1 Sep. 1968, TRW Systems Report No. 06462-6007-RO-00, NASA CR-73271, November 1968.

10.4 Variable Conductance Techniques

V1 A. P. Shlosinger, "Heat Pipes for Space Suit Temperature Control", Proc. ASME Aviation and Space Conference, Beverly Hills, Calif., 1968.

V2 D. K. Anand and R. B. Hester, "Heat Pipe Application for Spacecraft Thermal Control", A.P.L., Johns Hopkins Univ., Tech Memo DDC AD-662241, NASA N68-15338, 1967.

V3 W. Bienert, "Heat Pipes for Temperature Control", Proc. 4th Intersociety Energy Conversion Engineering Conference, Washington, D.C., 1969.

V4 R. C. Turner, "The Constant Temperature Heat Pipe--A Unique Device for the Thermal Control of Spacecraft Components", AIAA Paper No. 69-632, AIAA 4th Thermophysics Conference, 1969.

V5 B. D. Marcus and G. L. Fleischman, "Steady-State and Transient Performance of Hot Reservoir Gas-Controlled Heat Pipes", ASME Paper No. 70-HT/SpT-11, 1970.

V6 J. P. Kirkpatrick and B. D. Marcus, "A Variable Conductance Heat Pipe Flight Experiment", AIAA Paper No. 71-411, AIAA 6th Thermophysics Conference, 1971.

V7 W. B. Bienert and P. J. Brennan, "Study to Evaluate the Feasibility of a Feedback Controlled Variable Conductance Heat Pipe", NASA CR 73475, 1970

V8 W. B. Bienert, P. J. Brennen, and J. P. Kirkpatrick, "Feedback Controlled Variable Conductance Heat Pipes", AIAA Paper No. 71-421, AIAA 6th Thermophysics Conference, 1971.

V9 J. D. Hinderman and E. D. Waters, "Design and Performance of Non-condensible Gas Controlled Heat Pipes", AIAA Paper No. 71-420, AIAA 6th Thermophysics Conference, 1971.

V10 F. Edelstein and R. J. Hemback, "The Design, Fabrication and Testing of a Variable Conductance Heat Pipe for Equipment Thermal Control", AIAA Paper No. 71-422, AIAA 6th Thermophysics Conference, 1971.

V11 G. L. Fleischman and D. J. Wanous, "Subscale Temperature Control Tests: Heat Rejection Heat Pipe System for 1 kw Battery - AFAPL," TRW Report No. 16459-6009-RO-00, Feb 1971.

V12 T. Wyatt, "Controllable Heat Pipe", U.S. Patent No. 3,517,730, June 30, 1970.

V13 W. Bienert and P. Brennan, "Transient Performance of Electrical Feedback Controlled Variable Conductance Heat Pipes", ASME Paper No. 71-Av-27, July 1971.

V14 D. K. Edwards and B. D. Marcus, "Heat and Mass Transfer in the Vicinity of the Vapor-Gas Front in a Gas Loaded Heat Pipe", submitted to Journal of Heat Transfer.

V15 D. K. Edwards, G. L. Fleischman and B. D. Marcus, "User's Manual for the TRW Gaspipe Program", NASA CR-114306, April 1971.

10.5 General

G1 G. M. Grover, T. P. Cotter and G. F. Erickson, "Structures of Very High Thermal Conductance", J. Appl. Phys. 35, 1990, 1964.

G2 B. D. Marcus, "On the Operation of Heat Pipes", TRW Report 9895-6001-TU-000, May 1965.

G3 L. S. Langston, et al, "Vapor-Chamber Fin Studies", Pratt & Whitney Aircraft, Final Report, NASA CR-812, June 1967.

G4 ICICLE Feasibility Study, Final Report, NASA Contract NAS 5-21039, RCA-Defense Electronic Products, Camden, New Jersey, NASA-CR-112308.

G5 S. Katzoff, "Heat Pipes and Vapor Chambers for Thermal Control of Spacecraft", Paper No. 67-310, AIAA Thermophysics Specialist Conference, New Orleans, April 1967.

G6 C. A. Busse, "Heat Pipe Thermionic Converter Research in Europe", Paper #699105, Proc. Fourth Intersociety Energy Conversion Engineering Conf., Washington, D. C., 1969.

G7 O. W. Clausen, B. D. Marcus, W. E. Piske and R. C. Turner, "Circumferential Heat Pipe System for Large Structures", Final Report, NASA Contract NAS 9-10299, NASA CR-114783, 1970.

G8 J. D. Hinderman, J. Madsen and E. D. Waters, "An ATS-E Solar Cell Space Radiator Utilizing Heat Pipes", AIAA 4th Thermophysics Conference, San Francisco, Paper No. 69-630, 1969.

G9 P. E. Eggers and A. W. Serkiz, "Development of Cryogenic Heat Pipes", ASME Paper No. 70-WA/Ener-1, 1970.

G10 A Luikov, Heat and Mass Transfer in Capillary-Porous Bodies, 1st Ed. Pergamon Press, New York, 1966.

G11 E. Schmidt, Contribution a l'Etude des Calodues , Ph.D. Thesis, Univ of Grenoble, France, 1968.

G12 W. M. Kays, Convective Heat and Mass Transfer, McGraw Hill, 1966.

G13 R. Bird, W. Stewart and E. Lightfoot, Transport Phenomena, John Wiley & Sons, New York, 1960.

G14 E. C. Phillips, "Low-Temperature Heat Pipe Research Program", NASA Report No. NASA CR-66792.

G15 B. G. McKinney, "An Experimental and Analytical Study of Water Heat Pipes for Moderate Temperature Ranges", NASA Technical Memorandum Report No. 53849, June 6, 1969.

G16 W. B. Bienert, "Fabrication and Evaluation of Aluminum Heat Pipes", Technical Summary Report, DTM-70-2, NASA Contract No. NAS5-11271.

G17 E. E. Gerrels and J. W. Larson, "Brayton Cycle Vapor Chamber (Heat Pipe) Radiator Study", NASA CR-1677, 1971.

G18 J. A. Bilenas, W. Harwell, "Orbiting Astronautical Observatory Heat Pipes--Design, Analysis and Testing", ASME Paper No. 70-HT/SpT-9, 1970.

G19 K. T. Feldman and G. L. Whitlow, "Experiments with a Two-Fluid Heat Pipe", Proc. 4th Intersociety Energy Conversion Engineering Conf., Washington, D. C. Paper No. G99127, 1969.

G20 F. E. Bliss, E. G. Clark, B. Stein, "Constructure and Test of a Flexible Heat Pipe", ASME Paper No. 70-HT/SpT-13, 1970.

G21 S. W. Chi, T. A. Cygnarowicz, "Theoretical Analyses of Cryogenic Heat Pipes", Catholic Univ. of America, ASME Paper No. 70-HT/SpT-6, 1970.

G22 A. Basiulis and J. C. Dixon, "Heat Pipe Design for Electron Tube Cooling", ASME Paper No. 69-HT-25, 1969.

G23 C. L. Tien, "Two-Component Heat Pipes", AIAA Paper No. 69-631, AIAA 4th Thermophysics Conference, 1969.

G24 H. Cheung, "A Critical Review of Heat Pipe Theory and Applications", Lawrence Radiation Lab, Calif. Univ. Livermore, Report No. UCRL 50453, July 1968, NASA N69-22519, 70 p.

G25 J. E. Kemme, "Ultimate Heat Pipe Performance", Thermionic Conversion Specialist Conference-Conference Record, pp. 266-271, October 1968.

G26 J. K. Ferrell, et al, "A Study of the Operating Characteristics of the Heat Pipe, Part I: An Analytical Model for the Prediction of Operating Limits of Heat Pipes, Part II: Capillarity in Porous Media", North Carolina State Univ. Final Report No. ORO 3411-12, 50 p., 30 April 1969.

G27 E. van Andel, "Heat Pipe Design Theory", International Conference on Thermionic Electrical Power Generation, 2nd Proceedings, (Stresa, Italy, 27-31 May 1968), Luxembourg, EURATOM Center for Information and Documentation, (EUR no. 4210 f, e), 1969, 1438 p.

G28 J. L. Thurman and S. Mei, "Application of Heat Pipes to Spacecraft Thermal Control Problems" Brown Engineering Co., Inc., Huntsville, Ala., Report No. TN-AST-275, July 1968, 102 p., NASA CR 109991, NASA N70-34436.

G29 A. Basiulis, "Unidirectional Heat Pipes to Control TWT Temperature in Synchronous Orbit, p. 165-173, Thermodynamics and Thermophysics of Space Flight, Proceedings of the Symposium, Palo Alto, Calif., 23-25 March 1970, Sunnyvale, Calif., Lockheed Missiles and Space Co., 1970, 269 p.

11.0 NOMENCLATURE

A, A_w	-	Wick cross-sectional area
A'	-	Heat rejection area per unit length of condenser
A_c	-	Cross sectional area
A_F	-	Flow area of groove channel, etc.; flow area of reservoir feed tube
A_v	-	Flow area of vapor core
C	-	Axial conductivity-area product
D	-	Diameter
D_A	-	Artery diameter
D_e	-	Effective pore diameter for axial flow
D_s	-	Diameter of spheres in packed sphere bed
D_w	-	Wick diameter
$\mathscr{D}$	-	Mass diffusion coefficient
E	-	Empirical constant for temperature dependence of $\mathscr{D}$
F	-	Crimping factor for screens
F^*	-	Non-dimensional quantity defined in section 6.3.1
F_b	-	Body force
H	-	Irradiation onto condenser surface
J	-	Mechanical equivalent of heat
K	-	Permeability; radial wick conductance
L	-	Length; length of heat pipe
L_a	-	Length of adiabatic section; length of active zone
L_e, L_c	-	Length of evaporator and condenser
L_{ex}	-	Length of excess fluid slug in condenser
L_F	-	Length of reservoir feed tube
M	-	Mesh size for screen-wires per inch; molecular weight
P	-	Pressure; heat transfer perimeter of fin
P_w	-	Wetted perimeter of groove, channel, etc.
Q	-	Heat transfer rate; total axial heat transport
Q'	-	Radial heat transport per unit length
Q_{CL}	-	Axial heat transport at capillary pumping limit
Q_e	-	Axial heat transport at entrainment
Q_s	-	Axial heat transport at sonic limit
Q_{BL}	-	Axial heat transport at boiling limit

Q_e^* - Non-dimensional quantity defined in section 6.3.1

R - Gas constant

R, R_1, R_2 - Meniscus radii of curvature

Re - Reynolds number

R_o - Outside radius of pipe

R_u - Universal gas constant

R_v - Radius of vapor core

R_w - Outside radius of wick

S - Shape factor; safety factor; radial conductance from condenser

T - Temperature

T_0 - Temperature at 100% theoretical fluid fill; characteristic temperature of fluid defined in section 6.3.1

T_{sat} - Saturation temperature

V - Volume; velocity of vapor

V_s - Sonic velocity of vapor

We - Weber number

b - Tortuosity factor

c - Molar concentration

d - Wire or fiber diameter

f - Effective pore size factor - parallel wire wick

g - Magnitude of acceleration field

h - Coefficient of heat transfer

k - Ratio of specific heats; thermal conductivity

k_{eff} - Effective thermal conductivity of saturated wick

k_s - Thermal conductivity of solid wick material

k_T - Thermal diffusion coefficient

m - Mass, mass of fluid in heat pipe

$\dot{m}$ - Mass flow rate

n - Molar inventory of non-condensible gas

q - Heat flux

q''_r - Radial heat flux at evaporator

r_e, r_{eA}; r_{eB} - Effective pore size for capillary pumping

r_h - Hydraulic radius

r_n - Effective radius of nucleation cavity

r_p - Radius of cylindrical pore; effective pore radius for axial flow

r_s - Radius of spheres in packed sphere bed

$v_{\ell g}$ - Difference in specific volume between vapor and liquid

v_o - Average liquid velocity

w - Groove width - axial rectangular grooves

x - Mole fraction

z - Axial position; characteristic dimension for entrainment

dV - Volume element

ΔP_b - Body force head

$\Delta P_{b_\parallel}$, $\Delta P_{b_\perp}$ - Components of body force head parallel and perpendicular to heat pipe axis

ΔP_c - Net capillary head

ΔP_i - Interfacial pressure difference

ΔP_ℓ - Liquid pressure drop

ΔP_o - Wick "loading" - defined by Eq. (4-31)

ΔP_v - Vapor pressure drop

ΔP_{vt} - Vapor pressure drop across throttling valve

ΔT - Temperature difference

ΔT_{crit} - Critical evaporator ΔT for nucleation

α - Absorptance of condenser surface

β - Circumferential angle around pipe or wire

δ - Wick thickness; wire spacing; gap width

ε - Total hemispherical emittance of condenser surface

η - Effectiveness of condenser fin

θ - Angle of heat pipe axis with respect to acceleration field vector

λ - Latent heat of vaporization

μ - Viscosity

ρ - Density

σ - Surface tension; Stefan-Boltzmann constant

ϕ - Dimensional variable defined in section 6.3.1; wick porosity

$\Phi_1, \Phi_2, \Phi_3, \Phi_4$ - Dimensionless groupings defined in section 6.3.1

ψ - Wetting angle

Subscripts (except when defined otherwise above):

a - Active zone

abs - Absorbed from surrounds

avail - Available

b - Bulk average (area-velocity weighted) value

c - Condenser

e - Effective or equivalent value

e, ev - Evaporator

f - External fluid conditions; friction

g - Gas

gi - Gas at temperature T_i

i - Wick surface conditions

ℓ - Liquid

m - Momentum

min - Minimum,

max - Maximum

nominal - Initialized value for numerical solution

n - Cross-sectional element of pipe

o - Initial conditions

opt - Optimum

p - Pipe

R - Reservoir

s - Effective sink conditions; spatial (area weighted) average

tot - Total

v - Vapor

w - Condenser wall conditions

Notes:

* - Superscript denotes non-dimensional variable

Multiple subscripts: T_{vamax} - Maximum vapor temperature within the active zone

"The aeronautical and space activities of the United States shall be conducted so as to contribute . . . to the expansion of human knowledge of phenomena in the atmosphere and space. The Administration shall provide for the widest practicable and appropriate dissemination of information concerning its activities and the results thereof."

—NATIONAL AERONAUTICS AND SPACE ACT OF 1958

NASA SCIENTIFIC AND TECHNICAL PUBLICATIONS

TECHNICAL REPORTS: Scientific and technical information considered important, complete, and a lasting contribution to existing knowledge.

TECHNICAL NOTES: Information less broad in scope but nevertheless of importance as a contribution to existing knowledge.

TECHNICAL MEMORANDUMS: Information receiving limited distribution because of preliminary data, security classification, or other reasons.

CONTRACTOR REPORTS: Scientific and technical information generated under a NASA contract or grant and considered an important contribution to existing knowledge.

TECHNICAL TRANSLATIONS: Information published in a foreign language considered to merit NASA distribution in English.

SPECIAL PUBLICATIONS: Information derived from or of value to NASA activities. Publications include conference proceedings, monographs, data compilations, handbooks, sourcebooks, and special bibliographies.

TECHNOLOGY UTILIZATION PUBLICATIONS: Information on technology used by NASA that may be of particular interest in commercial and other non-aerospace applications. Publications include Tech Briefs, Technology Utilization Reports and Technology Surveys.

Details on the availability of these publications may be obtained from:

SCIENTIFIC AND TECHNICAL INFORMATION OFFICE

NATIONAL AERONAUTICS AND SPACE ADMINISTRATION

Washington, D.C. 20546